Queen Mary
University of London

Can interface conditions be modified by support surfaces to minimise the risk of pressure ulcer development?

Chai, Chanyuan

For additional information about this publication click this link.
http://qmro.qmul.ac.uk/jspui/handle/123456789/1309

Can Interface Conditions be Modified by Support Surfaces to Minimise the Risk of Pressure Ulcer Development?

By: Chanyuan Chai

School of Engineering and Materials Science

Queen Mary University of London

May 2011

Abstract

The characteristics of a patient support interface can influence the susceptibility of subjects, particularly there who are immobilised and insensate, to pressure ulcer development. Accordingly, externally powered alternating pressure air mattresses (APAM) are utilised to produce intermittent pressure relief and control of the interface microclimate. These conditions will permit adequate blood and lymph flow within the soft tissues and favourable conditions at the loaded skin surface and thus minimise the risk of ulcer formation.

Two sets of measurements were performed. Tissue viability was estimated, from a measure of transcutaneous gas tensions and sweat content, from healthy volunteers subjected to various alternating pressure regimens. The latter was achieved by two different strategies a) a custom–made controller which imposes the pressure profile on the subject and b) a prototype APAMs incorporating a novel sensor, which adjusts the profile according to individual subject characteristics. The latter prototype was placed on an articulated hospital bed, with an adjustable Head of Bed (HOB) angle. The second set of measurements involved monitoring the microclimate, namely temperature and humidity, at the interface loaded with a human analogue model supported on an APAM system. The interface was saturated with moisture to simulate sweating.

The human studies, involving healthy subjects with BMI values ranging from 18.9 to 42.5 kg/m^2, revealed significant differences in soft tissue response under various support surface profile by both strategies. In many cases, the T_cPO_2 levels either remained fairly stable during the loaded period or fluctuated at a periodicity equivalent to the cycle period of the APAM system, with the corresponding T_cPCO_2 levels remaining within the normal basal range. These findings were associated with

maximum interface pressures generally not exceeding 50 mmHg (6.67 kPa). By contrast in some cases, there was a significant compromise to the T_cPO_2 levels during the loaded period, which was often associated with an increase in T_cPCO_2 levels. These cases generally corresponded with the internal pressures in the mattress prescribed at a maximum amplitude of 100 / 0 mmHg or when the Head of Bed angle was raised to 45 °or above.

Changes in prototype covering sheet and air flow rates of the APAM system were found to influence both interface temperature and humidity. These results revealed enhanced levels of humidity often reaching 100% RH at the high simulated sweat rates. By contrast, at the lower sweat rate of 1.5 ml/min, the nature of the prototype covering sheets had an effect on the interface humidity profile, with values considerably reduced in the latter stages of the monitoring period. These results were compared with a compartmental model, which predicted the transport of moisture and heat using various mattress support systems.

The results offer the potential for the development of intelligent APAM systems, whose characteristics can be adjusted to an individual morphology. These systems will need to be designed to ensure adequate tissue viability and maintain appropriate microclimate at the loaded interface. Such an approach will be directed at those subjects considered to be at high/medium risk of developing pressure ulcers.

Acknowledgements

Table of Contents

List of Figures

List of Tables

List of Acronyms

AP: Alternating pressure

APAM: Alternating pressure air mattress

ATP: Adenosine Triphosphate

BGP: Bisphospoglycate

BMI: Body Mass Index

BPMS^{TM}: Body Pressure Measurement System

CLP: Continuous Low Pressure

CP: Continuous pressure

DTI: Deep Tissue Injury

GAGs: Glycosaminoglycan

HOB: Head of Bed

I/R: Ischaemia – Reperfusion

LAL: Low Air Loss Mattress

LDF: Laser Doppler Flowmetry

MDA: Malonyldialdehyde

MEC: Mattress Environment Chamber

MPO: Myeloperoxidase

NIR: Near Infra-Red

OFRs: Oxygen Free Radicals

OPM: Oxford Pressure Monitor

PRD: Product Requirement Document

PRI: Pressure Relief Index

RH: Relative Humidity

SAALP^{TM}: Self-Adjusting Alternating Low pressure sensor

SBF: Skin Blood Flow

TPM: Talley Pressure Monitor

TRS: Tissue Reflectance Spectroscopy

Chapter 1

Characterisation of Healthy Soft Tissues

Pressure ulcers represent localised areas of soft tissue damage caused primarily by prolonged mechanical loading of the skin and underlying tissues. The skin and subcutaneous soft tissues perform important functions including maintaining body homeostasis, providing an effective barrier against injury and a supporting surface for the underlying body structures. The different soft tissues represent living organs, and as such, require a balance between nutrient supply and waste product removal to ensure their viability. A compromise to their viability may lead to the development of soft tissue breakdown, resulting in several conditions including pressure ulcers. In order to investigate the pathophysiology of tissue breakdown it is important to understand the anatomy and function of healthy skin and soft tissue. A cross-section of the former is illustrated in Figure 1-1.

1.1 Anatomy and Function of Healthy Skin and Soft Tissue

1.1.1 Skin

Human skin is a dynamic structure in which the cellular replacement and any modification in response to local needs are continuous processes, which occur throughout life. The skin acts as a protective barrier that is relatively resistant to water, chemicals and bacteria and provides some protection for the body against chemical agents. Its critical functions include the maintenance of core body temperature, the transmission of sensory information from the environment and an active role in the immune system to protect against disease (Kumar and Clark, 2002). The skin is the

largest organ of the human body, providing approximately 10% of the body mass covering an area of approximately 1.8 m^2 in a standard human adult. Skin is formed by the intimate association between three distinct layers, the epidermis, dermis, and subcutaneous tissue.
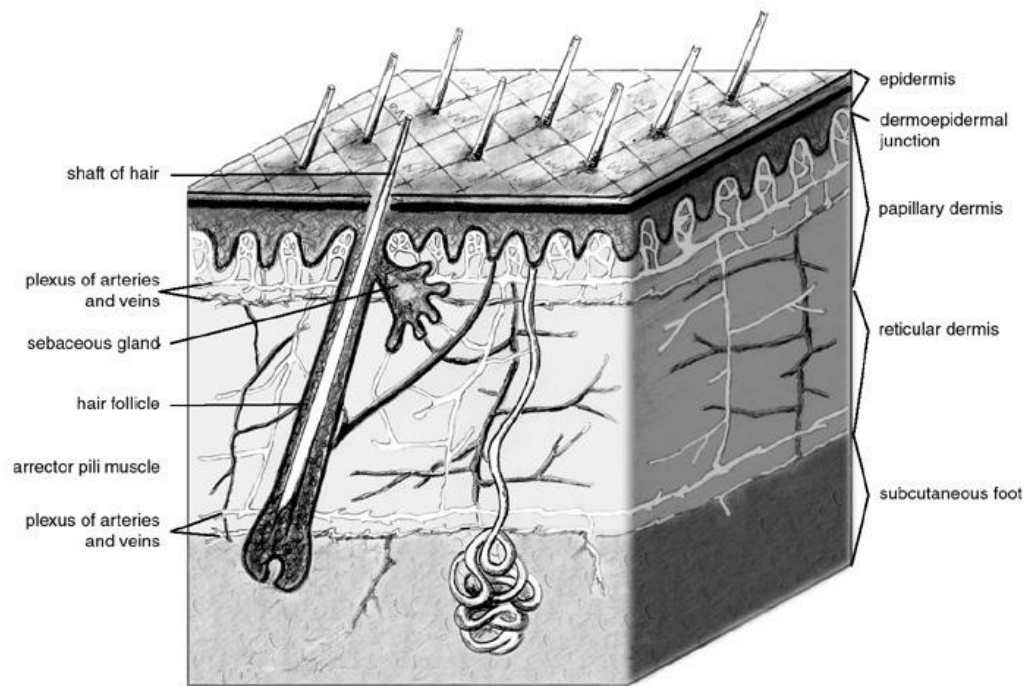
Figure 1 - 1 Cross section through the skin and subcutaneous tissues, illustrating adnexal structures.

i. Epidermis is the outermost layer of skin. Epidermal thickness is location dependent, varying between 60 μm and 100 μm in most areas, but attaining over 600 μm in the plantar surface of the foot and palms of the hands (Rushmer et al., 1966). The epidermis represents a complex multilayered membrane compressed of five histological distinct layers which, from the inside to the outside, are the stratum basale, stratum spinosum, stratum granulosum, stratum lucidum and the stratum corneum.

Keratinocytes are the epidermal cells responsible for the production of the fibrous protein keratinis which is produced in the stratum basale. These cells migrate towards the skin surface until, at the stratum corneum; die and are regularly sloughed away.

Other epidermal cells include *melanocytes*, responsible for skin pigmentation, touch sensitive *Merkel cells* and *Langerhan cells*, which contribute to the immune response against microrganisms.

The epidermal layer has various functions. It organises cell content, synthesises vitamin D and cytokines, enables division and mobilisation of cells, and maintains contact with the dermis, via the epidermal-dermal junction.

ii. Dermis is the connective tissue matrix of the skin. The general functions of the dermis are to act as a support structure with inherent mechanical integrity, supply nutrition, resist shear forces, maintain body temperature, perceive external stimuli, evoke an inflammatory response, and interact with the epidermis.

The dermis layer consists of two layers, the papillary dermis and the reticular dermis. It also contains a network of nerve endings, blood vessels including capillaries and venules, lymphatic vessels, sweat glands, sebaceous glands and hair follicles (Figure 1-1). The reticular layer contains bundles of collagen and elastin fibres, which have a preferred fibre orientation along the line of greatest applied force. This can be represented by the characteristic Langers lines at the surface of the skin. The papillary layer, which provides oxygen and nutrition to the epidermis and the reticular layer are of great importance in maintaining the integrity of the skin and protecting the body from external stimuli. There are differences with body sites. For example, the papillary layer is thinner in the sacral skin than in the skin at the ischium for aged individuals, as measured at post mortem (Hagiswa et al., 2001). This suggests that the blood supply and nutritional transport in the sacral skin may be impaired when exposed to applied loads sufficient to cause collapse of vessels.

The epidermal-dermal junction is an undulating interface between the epidermis and the dermis composed of a basement membrane. It has three major functions (Sanders et al., 1995):

3

- it provides a permeable barrier between the vascular dermis and avascular epidermis,

- it influences the epidermal cells during their differentiation, growth; and repair,

- it provides adherence of the epidermis to the underlying tissues.

In addition, the structure of the epidermal-dermal junction may greatly affect the tissue integrity. Indeed the skin capillaries vessels are situated just under the reticulin sheet of the papillary layer of the dermis, providing support to maintain normal expend in epidermis. Thus, if the junction becomes flattened, there is an associated decrease in capillary density and thus a compromise to the overall skin viability (Hagisawa et al., 2005).

iii. Subcutaneous tissue (hypodermis), is composed of adipose tissue and connective tissue, fascia. The adipose tissue, containing adipocytes which store triglycerides, is highly vascular containing major blood vessels and has a well supplied nervous system. It acts as a thermal insulator by storing calories in a form of heat energy, controls body shape and acts as a mechanical shock absorber. This layer is usually characterised by a pale yellow-like appearance, although a darker appearance can indicate dehydration of the tissue. The fascia tissue separates and surrounds the structures and facilitates movement between the adjacent structures, including muscle, tendon and bone. Lymphatic vessels are located within the subcutaneous layer.

STRUCTURAL COMPONENTS

COLLAGEN

Collagen is a fibrous protein that provides the skin form with stiffness and strength. As indicated in the schematic Figure 1-2, it holds together all the various structural components of skin and gives it plumpness and firmness. The collagen protein is

composed of linear, un-branching sequences of 20 or more naturally occurring amino acids. The sequence along the polypeptide chains, known as α-chains, is – [Gly-X-Y]$_n$, where glycine, the smallest amino acid occurs every third amino acid and X and Y, are commonly proline and hydroxyproline, respectively. The basic unit of collagen is a triple helix comprising of three α-chains configured in a left hand helix, which are wound around each other forming a right hand super-helix. The high strength and stability of collagen is attributed to the covalent cross-links occurring both within and between adjacent molecules. The destruction and/or degradation of these cross-links will diminish the integrity of the collagen fibre structure.
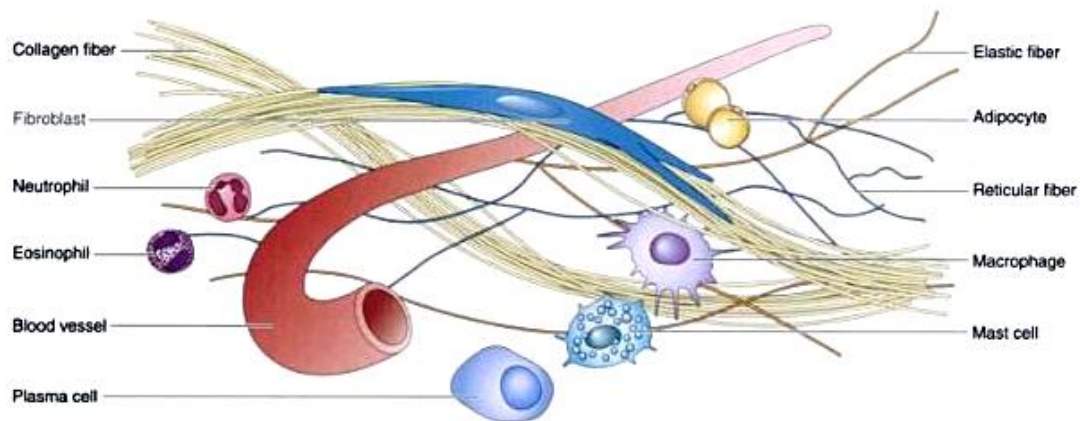
Figure 1 - 2 Cellular and Structural Components of Fibrous Connective Tissue (Premkumar, 2004).

The collagen fibres are secreted by fibroblasts, the predominant cell types in the dermis, into the ground substance. Indeed fibroblasts are relatively large, star-shaped cells representing the most common resident cells in connective tissues. They secrete both collagen and elastin fibres into the matrix, providing skin with its strength, suppleness and elasticity. When tissues are damaged, fibroblasts in the affected areas multiply rapidly and secrete large amounts of collagen and other macromolecules that help to seal the wound.

ELASTIN

In common with collagen, elastin is a protein which contains hydroxyproline. The highly cross-linked polypeptide molecules containing a high proportion of non-polar amino acids form rubber-like, elastic fibres. Elastin is interwoven with the collagen fibers to form elastic tissue in skin. This gives the skin its flexibility and elasticity, which enables it to resume its shape after expanding or stretching. This is particularly important for skin covering flexible joints.

PROTEOGLYCANS

Proteoglycans consist of unbranching chains of disaccharides, called glycosaminoglycan (GAGs), which includes hyaluronan (formerly termed hyaluronic acid), heparan sulphate and dermatan sulphate. These latter two GAGs, with their sulphate groups, may be electrostatically attached to the positive groups associated with the collagen and elastin fibres in the matrix, as well as the hydrogen atoms of water molecules. Thus proteoglycans have a high affinity for water and constitute a natural hydrogel.

1.1.2 Skeletal Muscle

Skeletal muscle is a form of striated muscle tissue existing under control of the somatic nervous system. It is one of three major muscle types, the others being cardiac and smooth muscle. A schematic diagram of human skeletal muscle fibres is shown in Figure 1-3. Skeletal muscle is made up of individual components known as muscle fibres, which are long, cylindrical, multinucleated cells composed of actin and myosin myofibrils repeated within a sarcomere. This functional unit is responsible for the striated appearance of skeletal muscle and constitutes the basic machinery necessary for muscle contraction.
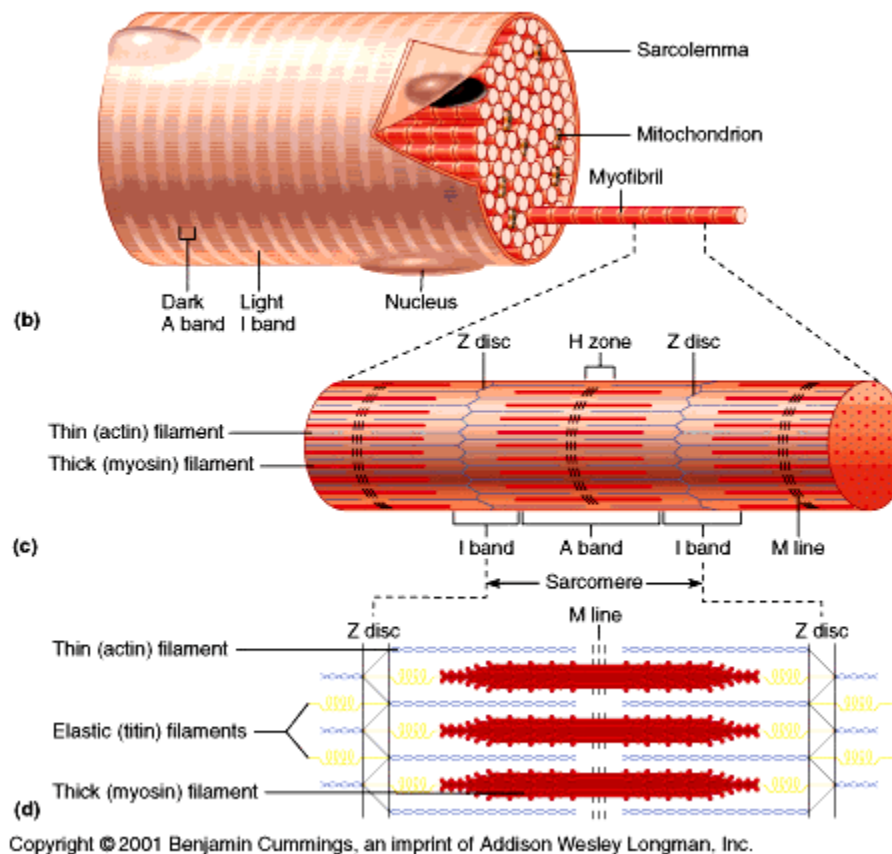
Figure 1 - 3 The anatomy of a muscle fiber is illustrated on top and in the center the composition of a myofihril is shown with its characteristic bands. On the bottom, a single sarcomere is depicted with a description of its components (Adapted from Benjamin Cummings 2001).

Muscle cells are formed by fusion of the muscle precursor cells, termed myoblasts, during myogenesis. In vitro, mononucleated myoblasts can be induced to fuse into myotubes, an immature muscle fibre, as illustrated in Figure 1-4. Depending on the source of the myoblasts namely, primary isolated cells or foetal-derived cells, a stage of maturation beyond the myotube stage can be achieved.
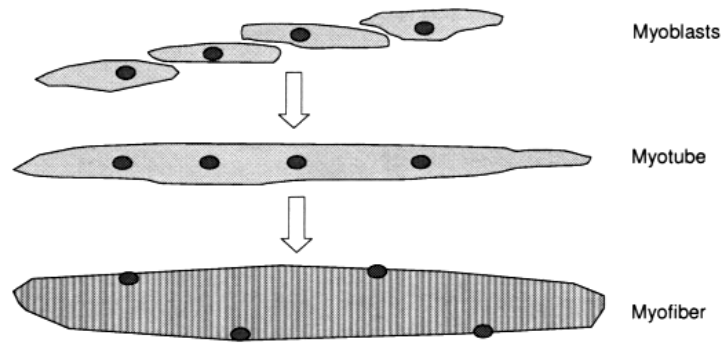
Figure 1 - 4 A schematic representation of the formation of a muscle cell. Myoblasts fuse into miiltinucleated myotubes and if their maturation continues, this results in cross-striated myofibers with peripherally located nuclei (dark dots).

1.1.3 Blood Vessels

Blood vessels in the skin form a complex network with plexi at two levels, as indicated in Figure 1-5.
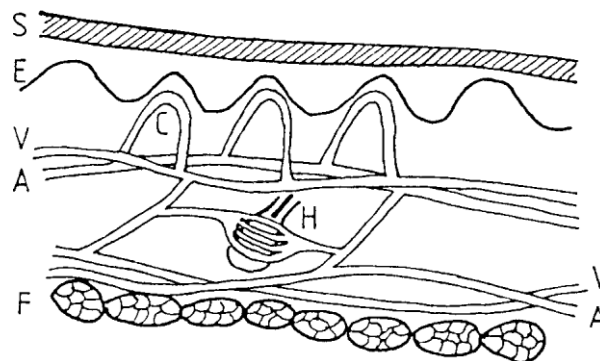
Figure 1 - 5 Blood vessels in the skin. The diagram shows the arrangement of blood vessels in the skin. (S) stratum corneum, (E) epidermis. (V) venule. (A) arteriole, (C) capillary, (H) hair follicle, (F) subcutaneous fat (Shakespeare and Swain, 1985).

There is an upper plexus in the subpapillary dermis and a lower plexus in the loose connective tissue adjacent to the subcutaneous fat and fascia (Bravemann, 1983), with conducting vessels running in both directions between these two plexi. Between these conducting vessels run horizontal capillary bundles supplying the deep structures, such as hair follicles, sweat and sebaceous glands. The upper plexus of arterioles, venules and anastomosing vessels is the source of the upward-rising capillaries that supply the papillary dermis. These upper capillaries can be clearly observed through the surface of the skin, using a stereomicroscope, partially in the presence of a layer of

8

paraffin or clear nail-varnish, which clarifies the upper layers of the skin (Shakespeare and Swain, 1985).

1.1.4 Cutaneous Microcirculation

The cutaneous microcirculation has a unique anatomical arrangement that accommodates different, often conflicting, functions including the supply of nutrients, clearance of waste products and control of heat exchange (Wheater et al., 1979). The smallest vessels in the circulatory system form the crucial connection between the arterial and venous blood supply systems, as they are required to exchange water, gas and solutes between blood and tissues. The distribution of blood capillaries vessels in the papillary dermis depends upon the local tissue metabolic requirements and thus differs according to site on the body, age and usage (Pasyk et al., 1989).

The micro-circulatory system is divided by a number of vessels, the diameters and functions of which are detailed in Table 1-1. The function of these vessels can be divided into three, namely, resistance vessels for control of flow, exchange vessels for respiration and reservoir vessels to store blood. The low velocity of blood flow within the capillaries allows adequate time for exchange of gases, nutrients and waste products between blood and tissues. The blood flow within the capillaries is not always constant due to the contraction of muscle fibres in the arterioles and pre-capillaries. This results in an intermittent flow, known as vasomotion, which is controlled by local oxygen concentration in the tissues (Campbell et al., 1974).

Table 1 - 1 Characterstics of vessels in the microcirculatory system.

Vessel	Diameter	Form	Innervations
Terminal arteries	$> 50\,\mu m$	Endothelium, internal elastic lamina, 2 rings of vascular smooth muscle	Sympathetic & circulating vasodilators and constrictors
Arterioles	20-50 μm	As above but a single layer of smooth muscle	Sympathetic & circulating vasodilators and constrictors
Metarterioles	8-15 μm	Endothelium with intermittent smooth muscle	Sympathetic & circulating vasodilators and constrictors
Pre-capillary sphincters		Cuff of smooth muscle	Vasoactive substances only
Arterial capillaries	4-5 μm	Endothelial cells with 10 nm holes	passive
Venous capillaries	7-10 μm	Endothelial cells with 10 nm holes	passive
Venules	10-15 μm	Endothelium, connective tissue and basal lamina	Not innervated or affected by vasoactive substances
Muscular venules	$> 50\,\mu m$	Similar to terminal arterioles	Sympathetic and vasoactive substances to a lesser extent than arterioles

1.1.5 Lymphatic Vessels

The lymphatic system comprises a network of vessels which convey proteins, large waste particles, and excess fluids, in the form of lymph, from tissue fluids to the blood stream. Most studies on pressure ulcers have been traditionally focused on blood flow, although the removal of waste products by the lymphatics is arguably of equal importance.

The lymphatic vessels originate as microscopic vessels in the spaces between cells. These so called terminal lymphatics are very delicate with a single layer of endothelial cells with no associated smooth muscular or contractile elements, distributed in the dermis. Several lymphatics join to form collecting vessels under the dermis which, in turn, join to form larger transporting lymphatics. Some of the terminal lymphatics are collapsed in the normal state and are connected to tissue fibres via anchoring filaments (Shimada, 1991) In contrast, the transporting lymph vessels have smooth muscle, which can contract and thereby control fluid transport.

1.1.6 Sweat Glands

Sweat glands are simple tubular glands and widely distributed over the skin with a total number of between 2 and 4 million. The aggregate weight of all sweat glands has been estimated as approximately 0.1 kg, equivalent to the weight of a kidney. The densities of sweat gland in different regions of the body vary as summarised in Table 1-2. The sweat glands produce sweat in response to heat and stress. Sweat is composed of water, salt, and other chemicals. As sweat evaporates off the skin, it helps cool the body. Thus, the amount of sweat is regulated as a function of body temperature.

Table 1 - 2 Sweat gland density in different regions of the body (Sato, 1977)

Region of the body	Density gland / cm^2
Back	64
Forearms	108
Forehead	181
Palmar and plantar regions	600-700

There are two types of sweat glands, eccrine sweat glands and apocrine sweat glands. Both types of glands are controlled by the sympathetic nervous system, which controls many of the involuntary actions of the body including breathing, regulation of heart beating and sweating.

Apocrine sweat glands, as shown diagrammatically in Figure 1-6 have the same structure as the hair follicle and sebaceous glands. They produce a highly individual scent, the production of which is dependent on the presence of sex hormones. Thus, apocrine glands 'sweat' is relative thick and viscous with a milky consistency due to its higher content of fatty acids and other compounds, including cholesterol, squalene, triglycerides, androgens, ammonia, sugars and traces of ferric iron *etc*. The apocrine glands are active with the onset of puberty. They are found particularly in the armpit and the genital area. The breasts are modified apocrine sweat glands. Human apocrine glands are not responsive to heat, although psycho-emotional stimuli are implicated in stimulating secretory activity (Desmond, 2006).
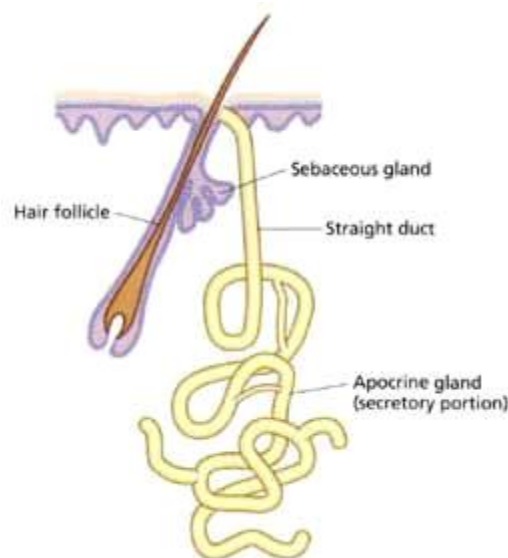
Figure 1 - 6 An apocrine gland, which produces little sweat, but is responsible for the body's natural scent.

Eccrine sweat glands, as shown diagrammatically in Figure 1-7 are distributed over the entire body surface but are particularly abundant on the palms of hands, soles of feet, and on the forehead. These produce sweat that is composed primarily of water with various salts. These glands are used for body temperature regulation.

Eccrine sweat glands are coiled tubular glands derived from the outer layer of skin but extending into the inner layer. Eccrine sweat glands are controlled by sympathetic cholinergic nerves, which are controlled by a centre in the hypothalamus. The

hypothalamus senses core temperature directly, and also has input from temperature receptors in the skin and modifies the sweat output, along with other thermoregulatory processes.
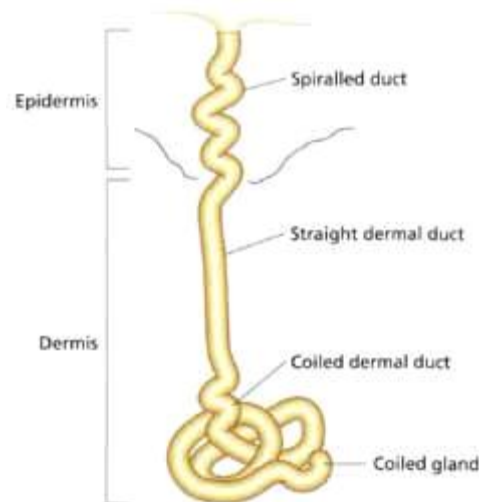
Figure 1 - 7 An eccrine sweat gland, which produces most of the body's sweat.

1.2 Physiology of Skin and Subcutaneous Tissues

1.2.1 Micro-circulation

Capillaries are formed by thin flattened nucleated polygonal cells which are joined together by a cementing agent. The caliber and tone of the capillary can be changed independently of arterioles and venules in response to a number of stimuli, even in the absence of muscle fibres. For example, when capillary tone is high they can resist the distending force of raised venous or arteriolar pressure, but when the tone is low they tend to passively follow pressure changes in arteries and veins.

The capillary tone is controlled by local physical and chemical condition in addition to vasoactive substances (Table 1-1). The former, including acetylcholine, adrenaline, angiotensin and bradykinin, cause a narrowing of the blood vessels and a resulting decrease in flow volume. Vasodilators include raised CO_2 tension, increase in H^+

concentration, histamine and various non-acidic dilator substances which are released during activity. During ischaemia locally acting dilator substances accumulate, leading to an increased blood flow and/or hyperaemia during reperfusion. The duration of occlusion determines the degree of resulting hyperaemia which is characterised by dilation of capillaries and arterioles, leading to perfusion, increased blood flow and pulsatile volume.

1.2.2 Internal Respiration

Internal respiration is the exchange via diffusion of carbon dioxide and oxygen in the cells of the body tissues. Red blood cells carry the oxygen to the body, and bring back the carbon dioxide to the lungs. Oxygenated blood enters the capillaries with an oxygen tension or partial pressure (pO_2) of about 105 mmHg (14 kPa), whereas cells in the tissues have an average pO_2 of 40 mmHg (5.3 kPa). This difference in tension leads to the diffusion of oxygen from the capillaries into the tissues. The partial pressure or tension of carbon dioxide (pCO_2) of cells in tissues is 45 mmHg (6.0 kPa) compared to the pCO_2 of capillary oxygenated blood of 40 mmHg (5.3 kPa). This difference leads to a diffusion of carbon dioxide from the tissue to the capillary blood.

Transportation of Oxygen

Oxygen does not easily dissolve in water so only a small proportion is transported in the blood plasma, with the remainder being transported with haemoglobin in red blood cells. Indeed each 100 ml of oxygenated blood contains about 20 ml of oxygen, of which 19.7 ml (97%) combined with the haemoglobin (Hb) present in red blood cells and only 0.3 ml (3%) dissolved in the plasma (Tortora and Grabowski, 1996). Oxygen and haemoglobin combine in a reversible reaction to form oxyhaemoglobin (HbO_2):

$$Hb \ + \ O_2 \ <=> \ HbO_2 \qquad \qquad \textit{Equation 1-1}$$
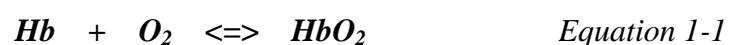
Haemoglobin consists of four iron-containing pigments called haems and a protein called globin. Each iron atom can combine reversibly with one molecule of oxygen.

In the loading and unloading of oxygen, there is cooperation between these four haem groups. When oxygen binds to one of the groups, the others change shape slightly and increase their attraction to oxygen. Thus the loading of the first oxygen results in the rapid loading of the next three forming oxyhaemoglobin. By contrast, when one group unloads its oxygen, the other three also rapidly unload as their groups change shape again this time with less attraction for oxygen. This method of cooperative binding and release can be seen in the dissociation curve for haemoglobin (Figure 1-8).
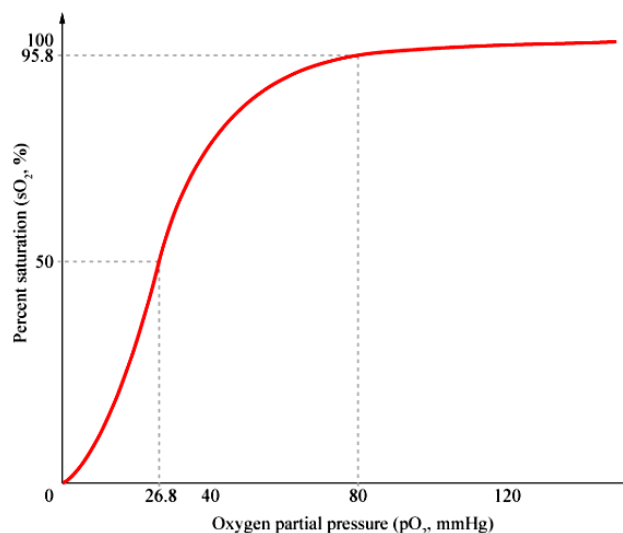
Figure 1 - 8 Oxygen- haemoglobin dissociation curves. The curve reveals a low binding stage when oxygen partial pressure values are below 26.8 mmHg. Above this value, there is an increased affinity for O_2 up to 80 mmHg, beyond which the curves reach a saturation stage.

The curve indicates that the relationship between partial pressures and haemoglobin saturation have an "S" shape. When pO_2 is high, haemoglobin binds with large amounts of oxygen and is almost completely saturated. When pO_2 is low, haemoglobin is only partially saturated and oxygen is released from oxyhaemoglobin. At these low levels of pO_2, the oxygen release is sensitive to small changes in pO_2.

Other factors influence the affinity of the haemoglobin for oxygen, these include:

1. The pH of the blood - at higher levels of acidity haemoglobin has less affinity for oxygen,

2. The partial pressure of carbon dioxide in the blood – at higher pCO_2 oxygen is released by haemoglobin more readily,

3. The temperature of the blood – at higher temperatures the oxygen dissociates with the haemoglobin more readily,

4. The amount of 2, 3-bisphospoglycate (BGP) in the blood – the higher the levels of this substance the greater the dissociation of oxygen.

Adequate perfusion leads to an increase in the tissue oxygen tension, whilst a reduction in perfusion leads to the release of more oxygen by the haemoglobin. The use of tissue oxygen is constant and as the volume of consumption is quite small, it is recommended to measure the partial pressure of tissue oxygen (PO_2), because it is a sensitive indicator of small changes in local blood flow. Indeed oxygen and perfusion are intricately linked and thus oxygen is often used as an alternative measure for perfusion (Hampton and Collins, 2004).

Transportation of Carbon Dioxide

Carbon dioxide is carried to the lung by blood flowing through the skin, the muscles and other tissues. As with oxygen, one of the way it is transported is dissolved in blood plasma. Carbon dioxide is much more soluble in blood than oxygen, and about 7% of carbon dioxide is transported unchanged, simply dissolved in the plasma. A large proportion of the CO_2 diffuses into the red blood cells. Carbon dioxide combines reversible with haemoglobin to form carbaminohaemoglobin and the process involves the reation:

$$Hb \; + \; CO_2 \; <=> \; HbCO_2 \qquad\qquad Equation\ 1\text{-}2$$

In this case, carbon dioxide combines chemically with the amino groups on the polypeptide chains of haemoglobin. It also binds to amino groups on the polypeptide chains of plasma proteins. About 23% of carbon dioxide is transported to the multiple amino groups of haemoglobin (Carboxyhaemoglobin).

An alternative transport mechanism for about 70% of the carbon dioxide is transport in the form of bicarbonate ions, indicated as:

$$H_2O \quad + \quad CO_2 \quad <=> \quad H_2CO_3 \quad <=> H^+ + HCO_3^- \qquad Equation\ 1\text{-}3$$
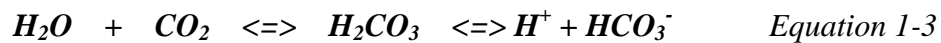
Carbon dioxide enters red blood cells in the tissue capillaries where it combines with water to form carbonic acid (H_2CO_3). This reaction is catalysed by the enzyme carbonic anhydrase which is found in the red blood cells. Carbonic acid then dissociates to form bicarbonate ions (HCO_3^-) and hydrogen ions (H^+).

The changes in concentration of CO_2 or HCO_3^- ion can induce slight pH changes in the blood even though it is buffered. At the same time, the concentration of H^+ ions will influence the concentrations of CO_2 and HCO_3^- ions.

1.2.3 Skeletal Muscle

In addition to actin and myosin components that constitute the sarcomere, skeletal muscle fibres contain two other important regulatory proteins troponin and tropomyosin that are necessary for muscle contraction to occur. These proteins are associated with actin and they cooperate to prevent its interaction with myosin. Skeletal muscle cells are excitable and are subject to depolarisation by the action of the neurotransmitter, acetylcholine, which is released at the neuromuscular junction by motor neurons (Costabzo, 2002). Once the cell is sufficiently stimulated, the sarcoplasmic reticulum releases calcium ions (Ca^{2+}) which interacts with the regulatory protein troponin. Calcium bound troponin undergoes a conformational change that leads to the movement of tropomyosin, subsequently exposing the myosin-binding sites on actin. This allows for myosin and actin ATP (adenosine

triphosphate) -dependent cross-bridge cycling and shortening of the muscle.

The inorganic phosphate that is released during the contraction can be dissociated from ATP, such as muscle contraction. ATP provides the energy for tissue reactions, and is obtained from glucose, preferably by aerobic metabolism. However, when muscle cells are deprived of oxygen and all available energy stores are depleted, anaerobic metabolism is used to produce ATP. The latter pathway results in an accumulation of lactic acid, which subseqeuntly diffuses into the extracellular space. If anaerobic metabolism persists for an extended period of time without reperfusion, cellular acidification within the tissues may occur.

1.2.4 Sweat Production and Composition

Sweat is a true secretion, but not simply a filtrate. It is controlled and managed by mechanisms that are present in almost all levels of the nervous system. The hypothalamus is the major centre for the temperature regulation of the body (Johnson, 1991). However, there is strong evidence that local cutaneous thermoreceptors are the initial reflex response to exercise and may trigger the hypothalamus to act on the pituitary glands which, in turn, stimulate the sweat glands (Polliack et al., 1993).

Sweat can be collected at the skin surface and, therefore, it can affect the microenvironment of skin. However, the microenvironment of the support interface greatly affects the likelihood of tissue breakdown leading to the formation of a pressure ulcer. High moisture levels at the interface can be produced by incontinence or perspiration on impermeable cushion covers. This excess moisture could lead to the maceration of the epidermis, a precursor of tissue breakdown which is accelerated by an alkaline environment (Polliack et al., 1993).

During normal metabolism, oxidative phosphorylation is the main metabolic pathway of the eccrine sweat gland (Sato, 1977). However, under conditions of ischaemia

and/or in anaerobic conditions, glycolysis becomes the main metabolic pathway resulting in the formation of lactate. This explains the elevated lactate concentrations observed in the sweat collected from the bony prominence during ischaemia (Sato and Dobson, 1973). It is interesting to note that lactate concentration has an inverse relationship with sweat rate, with highest lactate concentrations at lowest sweat rates (Heyningen and Weiner, 1952; Polliack et al., 1993).

The production of sweat takes place following stimulation by neuronal impulses; the diagram in Figure 1-9 shows the stages of sweat production in the human eccrine sweat gland.

Secreted acetylcholine (ACh) enters sweat gland through basal lamina and intercellular channels, where clear cells are depolarized

⇩

Na^+ ions and interstitial fluid from dilated blood vessels flows into cell

⇩

Osmotic balance between clear cell and intercellular channels

⇩

Na^+ pumped across luminal cytomembrane followed by interstitial fluid and lactate and glycolysis products

⇩

Precursor sweat expands lumen of secretory segment and myoepithelial cells contract to propel fluid

⇩

Isotonic precursor fluid is reabsorbed in coiled duct by dark and myoepithelial cells

⇩

Hypotonic sweat reaches the skin surface

Figure 1 - 9 Flow diagram indicating the stages of sweat production.

Sweat is a hypotonic solution of sodium and chloride ions in water, as well as other constituents including lactate, urea, and potassium. The presence of these metabolites accounts for about 95 percent of the osmotically active substances in sweat (Heyningen and Weiner, 1952). The concentration of these chemicals in sweat is affected by a number of factors, including sweat rate and the metabolism of the sweat gland. Table 1-3 outlines the major components of human eccrine sweat. These metabolites can be transferred via the sweat glands and can be collected at the skin surface.

Table 1 - 3 Components of sweat and their composition. (Lentner, 1981)

Component	Concentration mmol/L unless where stated (age)	Comments
Sodium	46.8 (17-50 years) 60 (>50 years)	Increases with sweat rate and age. Affected by sodium intake in diet.
Potassium	8.6 (17-50 years)	Increases with both heat and pharmacological stimulation.
Chloride	29.7 (17-50 years) 38.9 (>50 years)	Concentration changes are similar to those in sodium concentration.
Urea	19.6	At low sweat rates the concentration is 4 times that in serum but, at higher rates, sweat concentrations are closer to those in serum.
Uric Acid	12 umol/L	---
Lactic Acid	6.84	The concentration can be 4-40 times greater than that in serum and decreases with increasing sweat rate.

Sweat urea is believed to be derived mainly from serum urea by the passive diffusion across the glandular wall and cell membrane, although it is still unknown whether it is also produced by the sweat gland (Sato and Dobson, 1973). Sweat urea levels are therefore expected to be similar to levels within the blood, particularly at high sweat

rates (Whitehouse, 1935). However, it has been proposed that water reabsorption is responsible for sweat to plasma urea ratios greater than unity (Schwartz et al., 1955). Low sweat rates have been found to result in elevated sweat urea concentrations during ischaemia (Komives et al., 1966).

Urea is the main product of protein metabolism and can thus be an indicator of tissue damage if elevated levels are found in bodily fluids, such as urine or blood. Prolonged periods of ischaemia can lead to muscle damage, resulting in an increased serum urea level which, in turn, can result in enhanced concentrations of sweat urea (Sato and Glucose, 1973).

1.3 Biomechanics Skin and Subcutaneous Tissue

Unlike engineering materials, the responses of soft biological tissues to mechanical loading are complex. For example, they exhibit self-adapting and self-repairing characteristics, adapting to the changing in vivo mechanical demands. Their mechanical properties will change with both age and some connective tissue diseases. In addition, soft tissues can be considered to be composite materials with non-homogeneous and anisotropic properties, and are viscoelastic in nature.

In vivo and in vitro studies on skin and soft tissues have led to a greater understanding of their mechanical properties. The relationship between the properties of tissue elements, their structure and chemical bonding, has also increased the understanding of the mechanical behaviour of these tissues.

1.3.1 Mechanics Properties of Structural Components

The behaviour of the structural components which make up soft tissues, and thus the nature of the recovery, will depend on the rate and time of loading, as well as its magnitude. Short-term loading generally produces elastic deformation with minimum creep and rapid elastic recovery, whereas long-term loading results in marked creep

and requires significant time for complete tissue recovery.

When the force is applied, initially elastic fibres are thought to be stretched, while collagen fibres change their geometrical configuration before they play a part in load resistance and increased forces. If the force applied is extensive, the collagen fibres will not return to their original alignment even after the force is removed (Gibson et al., 1965).

Collagen fibres

The collagen fibres consist of bundles of fibrils, 0.6-1.8 µmin diameter in the papillary layer, and 6-10 µm in the reticular layer, that are responsible for preventing tensile and shear failure.

The collagen fibrils in the skin are composed primarily of collagen types I and III. The diameter of collagen type I, 80-120 nm, is greater than that of type III, 40-60 nm. The most superficial surface of the papillary layer is made up of a continuous thin sheet of reticulin fibrils (type III), showing finger-like configuration, a delicate network and regular arrangement of the dermal papillae. The reticulin fibrils are interwoven in slightly loose networks with 30 to 60 nm spaces through which the tissue fluid and other substances pass (Arao et al., 1998). This space plays an important role in maintaining viability of the tissues by enabling exchange nutrients and metabolites.

Collagen fibril diameter distribution is a function of both the applied load and its duration. The mechanical properties of a connective tissue are strongly correlated with the collagen fibril diameter distribution (Parry et al., 1978).

Elastic fibres

The mechanical properties of elastic fibres can be compared to that of rubber. The

ultimate tensile stress of elastic fibres amounts to only several percent of that of collagen fibres (Silver, 2002). Therefore, elastic fibres are weaker, softer, and more extensible than collagen fibres.

The diameter of elastic fibres is approximately 1-10 μm; each fibre is made up of microfibrils of 10-12 nm in diameter. The fibres are connected via cross links, similar to collagen. The distribution of elastic fibres in the areas of the skin prone to pressure ulcers has been examined microscopically by Hagisawa et al., (2001). Thick elastic fibres (5-10 μm) are densely distributed in the ischial skin, where extension of the skin is needed in association with various body movements, in contrast to the case of sacral skin with thinner and less dense elastic fibres (2-3 μm). This difference may greatly contribute to tissue recovery from deformation in the ischial skin, in which the blood restoration may also be facilitated following ischaemia.

Proteoglycans

Proteoglycans consist of a protein core to which glycosaminoglycan side chains are attached, composing bulk of the interfibrillar matrix, including hyaluronic acid, chondroitin sulphate and dermatan sulphate. Proteoglycans are involved in resisting compressive forces and facilitation of the response to stress at the fibrillar level (Canning et al., 1992).

Collagen, elastic fibres and proteoglycans play a key role in determining the mechanical properties of the skin. They are important in maintaining tissue shape, transmiting/absorbing loads, and recovering from deformation.

1.3.2 Tensile Properties of Skin and Soft Tissue

Simple tensile tests on specimens of skin and soft tissue yield a characteristic non-linear relationship between stress and strain. The characteristic form shows two distinct regions, one occurring at low strain and the other at high strain. The low strain

region is linear up to strains of 40% and exhibits a modulus of 5 kPa, 100 times less than that of soft rubber or elastin (Daly, 1982). Within this region of the curve, the tissue exhibits elastic behaviour and the properties are thought to be influenced by elastin and proteoglycan content (Nola, 1980) rather than collagen. The elastin fibres act as an elastomeric material and provide a spring return mechanism for the collagen network. Tensile testing of skin tissues also reveals directional variations, namely anisotropy, with sample properties highly dependent on the orientation of the local collagen fibres in the dermis.

1.3.3 Compressive Properties of Skin and Soft Tissue

Skin and soft tissue are predominantly subjected to compressive loading when they come into contact with any supporting surface, such as a mattress, wheelchair or seating device. Therefore the compressive properties of skin and soft tissue have more relevance to physiological loading conditions than tensile properties.

There are a limited number of studies over the years, which have examined the compressive properties of soft tissues, either using *in vitro,* and to a lesser extent *in vivo* approaches (Kirk and Kvorning, 1949; Barbanel et al., 1972; Cow and Odell 1978; Daly, 1982; Bader and Bowker, 1983; Bader, 1990). Similar to the response in tension, compressive stress-strain curves are also non-linear and the soft tissues exhibit viscoelastic behaviour. Most of the associated models are based on the movement of fluid away from the compressed tissue. There is a continuing debate as to whether tissue is incompressible due to the large water content or whether fluid transport is one of the mechanisms of tissue deformation.

1.3.4 Viscoelastic Properties of Skin and Soft Tissue

A number of different techniques have been employed to measure viscoelastic

properties of soft tissues. For example, indenters have been used to measure uniaxial creep (Zhang and Robert, 1993) and torsional creep (Barbanel et al., 1972) *in vivo.* By contrast, wave propagation techniques have also been used to investigate the frequency response of soft tissues *in vivo* (Potts et al., 1993; Pereira et al., 1991). Results indicated that at frequencies of up to 500 Hz, the viscoelastic behaviour was highly influenced by the epidermis, whereas at higher frequencies the properties appeared to be more dependent on the proteoglycan component of the soft tissue. Manschot and colleagues (Manschot 1986) suggested that the time-dependent recovery after load removal was influenced by the elastin content of the dermal layers.

A number of phenomenological and constitutive models have been used to charcterise the viscoelastic behaviour of skin and soft tissues. For example, Maxwell and Voigt models, involving a series of springs (to represent the elastic component) and dashpots (to represent the viscous component) in different arrangements, have been used to model experimental data from different materials including soft tissue. If successful, these models can provide a number of selected parameters, which can be compared for variations in structural tissue properties involving, for example, disease and ageing.

Chapter 2

Soft Tissue Breakdown

Pressure ulcers are localised areas of soft tissue damage that adversely affect the quality of the victim's life. These can occur in a number of different physiological situations, but most commonly at the interface between the skin and a supporting surface. It is particularly common among individuals, who have impaired mobility and are normally bedridden or wheelchair-bound. Initial symptoms include the presence of an area of hyperemia, as evidenced by reddened skin. If the conditions progresses a blister appears, which may lead to the development of an open ulcer, resembling a crater. The problem of soft tissue breakdown has taken on new importance in the last decade in a society where health care litigation is becoming more commonplace and the cost of health care more accountable. In addition, the presence of pressure ulcers has become an indicator of poor quality of care in many countries.

2.1 Aetiology

Although there are several factors implicated in the aetiology of tissue breakdown, the common factor is accepted to be prolonged pressure applied to the tissues. Mechanical loading applied to the skin can take the form of compression, shear, frictional forces or their combination. These forces can occur due to the interaction between the tissues and a supporting surface, such as a mattress, chair cushion or external orthosis or prosthesis.

As mentioned in the previous chapter, normal cell metabolism is dependent upon the delicate balance between the delivery of nutrients via a healthy blood supply and

removal of waste products via the lymph system. When prolonged pressure is applied to the skin, the underlying blood vessels may be partially or totally occluded, creating an ischaemic environment and, as a result, oxygen and other nutrients are not delivered at a rate sufficient to satisfy the metabolic demands of the cells and the soft tissues. The lymphatic and venous drainage will also be impaired and thus the breakdown products of metabolism accumulate within both the interstitial spaces and in the vicinity of the cells (Krouskop et al., 1978). Lymph propulsion is largely dependent upon lymphatic smooth muscle contractions and the motility of these vessels is very sensitive to distension, hypoxia and circulating hormones, such as histamine, serotonin and prostaglandins. Lymphoedema, an accumulation of lymph, results in tissue necrosis which is very similar to the tissue breakdown evident in pressure ulcers. As energy stores diminish there is an increasing possibility of failure of some of the cellular processes and dissipation of ionic gradients across cellular membranes (Bouten et al., 2001). These events can potentially interact to lead to tissue breakdown as summarized in Figure 2-1.

```
                    ┌─────────────────────────┐
                    │      EXTERNAL LOAD      │
                    └─────────────────────────┘
                      ↙                   ↘
    ┌──────────────────────┐      ┌──────────────────────┐
    │ Squeeze out of       │      │ Blood vessel          │
    │ interstitial fluid   │      │ occlusion –           │
    │                      │      │ state of ischaemia    │
    └──────────────────────┘      └──────────────────────┘
               │                            │
    ┌──────────────────────┐      ┌──────────────────────┐
    │ Capillary Bursting   │      │ Release of hormones   │
    │ on removal of load   │      │                       │
    └──────────────────────┘      └──────────────────────┘
               │                            │
    ┌──────────────────────┐      ┌──────────────────────┐
    │ Interstitial         │      │ Lymphatic smooth      │
    │ flooding             │      │ muscle damage         │
    └──────────────────────┘      └──────────────────────┘
                                            │
                                  ┌──────────────────────┐
                                  │ Accumulation of       │
                                  │ metabolic waste       │
                                  └──────────────────────┘
               ↘                    ↙
              ┌─────────────────────────┐
              │    TISSUE BREAKDOWN     │
              └─────────────────────────┘
```
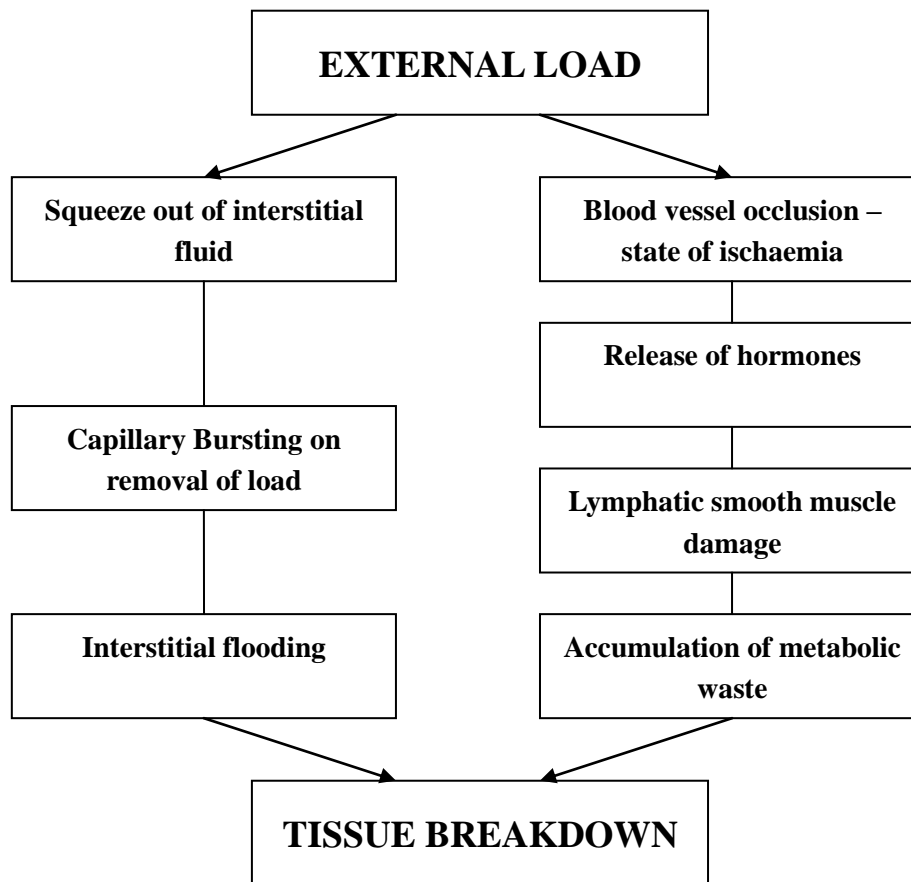
Figure 2 - 1 Proposed mechanism involving lymphatic system for soft tissue breakdown (Based on Krouskop, 1983).

Most of the research into the aetiology of pressure ulcers has focused on damage caused by ischaemia and neglected the roles of other mechanisms, such as impaired interstitial fluid transport, ischaemia-reperfusion injury and cell deformation (Bouten et al., 2003). As an example, injury due to ischaemia-reperfusion can occur following the reperfusion of blood to previously ischaemic tissue (Pretto, 1991). In the process in which blood supply is restored to the tissue and oxygen debt (describe in Figure 5-6) is recovered, there is a possible build up of oxygen free radicals, also known as reactive oxygen species, which are highly toxic to the local cells within the tissue. The ability of an area of tissue to recover from a period of pressure-induced ischaemia may be an important factor in the susceptibility to develop subsequent tissue breakdown (McCord, 1985).

```
I
S
C
H        ATP                    Xanthine Dehydrogenase
A
E        Inosine                          ↓
M                                  Xanthine Oxidase        Xanthine
I        Hypoxanthine  ──────────────────────────────→        +
A                              + O₂ during reperfusion     Superoxide
                                                              Radical
```
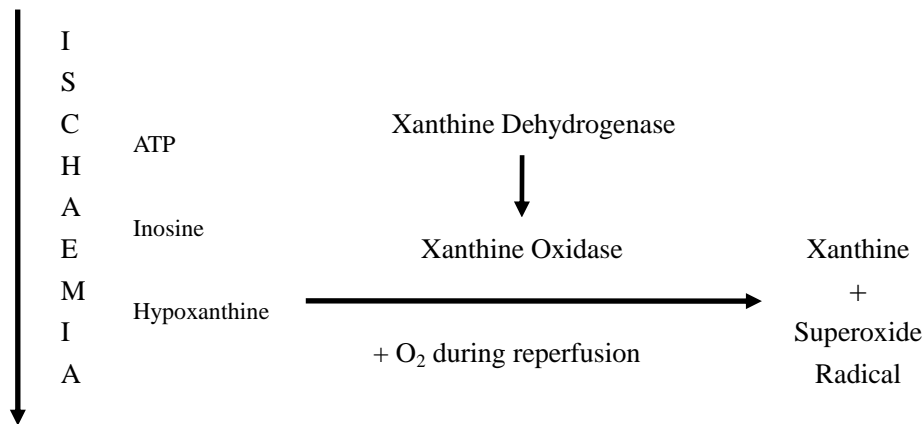
Figure 2 - 2 Purine metabolism during ischaemia-reperfusion (Taylor and James, 2005).

Recently research has shown purine metabolism plays an important role in tissue breakdown during both ischaemia and reperfusion (Taylor and James, 2005), as indicated schematically in Figure 2-2. Terminal products of purine metabolism produced during these periods, may directly produce cell injury (Fox et al., 1987). In a recent research, Bader (Bader et al., 2005) collected sweat from loaded tissues of normal volunteers and measured the associated concentrations of lactate, uric acid, hypoxanthine and xanthine. Results indicated that it took a significant period of reperfusion to restore the concentrations of lactate and the three purines back to baseline unloaded levels.

2.2 Risk Factors

Although tissue breakdown will not occur in the absence of pressure, pressure may not be solely responsible, as indeed some individuals can tolerate high pressures without tissue damage. There appears to be many other factors, both extrinsic and intrinsic in nature, which predispose tissue to compromise both its biochemical and structural integrity. Extrinsic factors are generally the result of the external

environment and can therefore potentially be controlled, whilst intrinsic factors are inherent to the individual.

2.2.1 Extrinsic Factors

Pressure and Time

Pressure applied to soft tissues is undoubtedly one of the major causes of tissue breakdown. Indeed in 1841, Hunter stated that 'pressure external to the body stimulates and gives signs of increased strength with increases in thickening of the skin'. However, if the pressure exceeds the stimulus of thickening, then the pressure becomes an irritant. Indeed, it is well established that there is a pressure and time threshold above which ulceration is more likely, and below which skin adaptation has been observed (Sanders et al., 1998). It is generally accepted that a combination of the loading conditions results in an increase in the occurrence of ulceration (Crenshaw and Vistnes, 1989). Tangential shear forces act in a direction parallel to the supporting interface and are often coupled with normal pressures which act perpendicular to the tissue surface, as indicated in Figure 2-3. These external conditions will establish internal stresses and strains, the absolute levels of which depend on the mechanical characteristics of the various soft tissue layers, in particular the relative mechanical stiffness and thickness.
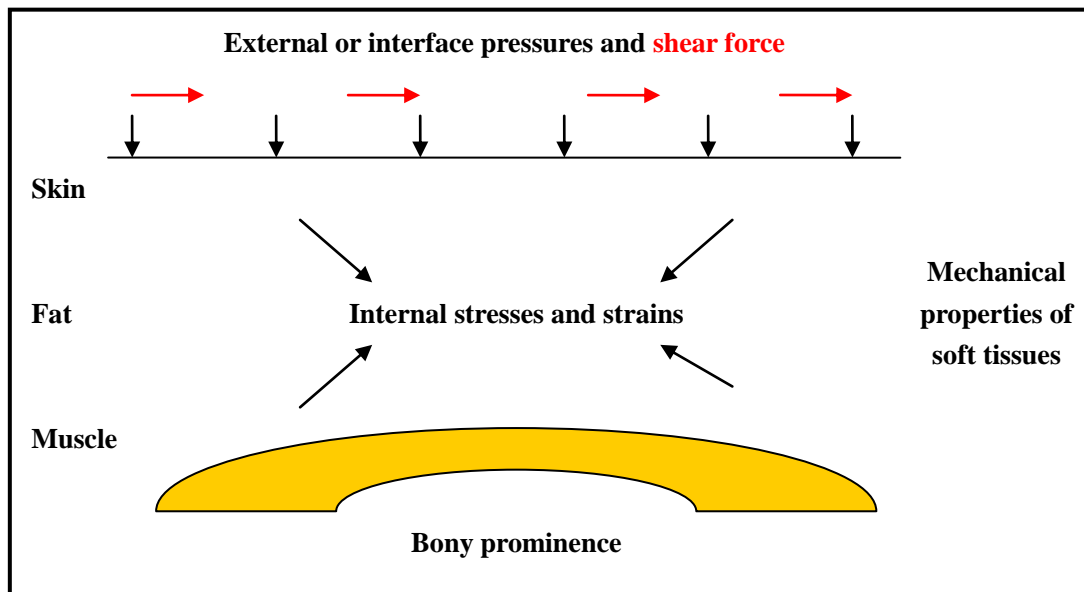
Figure 2 - 3 Schematic representation of the development of internal mechanical conditions in the various soft tissue layers overlying a bony prominences, resulting from external pressure and shear forces. (adapted from Bader, 2004).

Traditional literature has proposed that externally applied pressures, in excess of the capillary perfusion pressure, will cause capillary closure. Indeed it was shown many decades ago that pressures above 32 mmHg (4.26 kPa) were sufficient to close the capillaries of the nail bed (Landis, 1930), and this value is often misleadingly quoted as a safe maximum pressure which tissues can tolerate. However, this measurement was made in a nail fold capillary and performed at heart level. This situation is completely different to that in which external pressures created at the body support surface interfaces can occlude blood flow in capillaries in soft tissues overlying bony prominences. Indeed, to date, no safe threshold value for externally applied pressures has been proposed based on either clinical or scientific studies.

The importance of the pressure/time relationship was reported by Reswick and Rogers (1976), as a retrospective analysis of patients in a hospital setting. This yielded curves with a hyperbolic form, as indicated in Figure 2-4 (a). They suggest that the combination of either high pressures for short time periods or lower pressure prolonged over a number of hours are both potentially damaging to tissues as

indicated by the "unacceptable domain" in the figure. Conversely combinations of pressure-time within the "acceptable" domain, would not normally lead to pressure-induced damage.

a)   b)
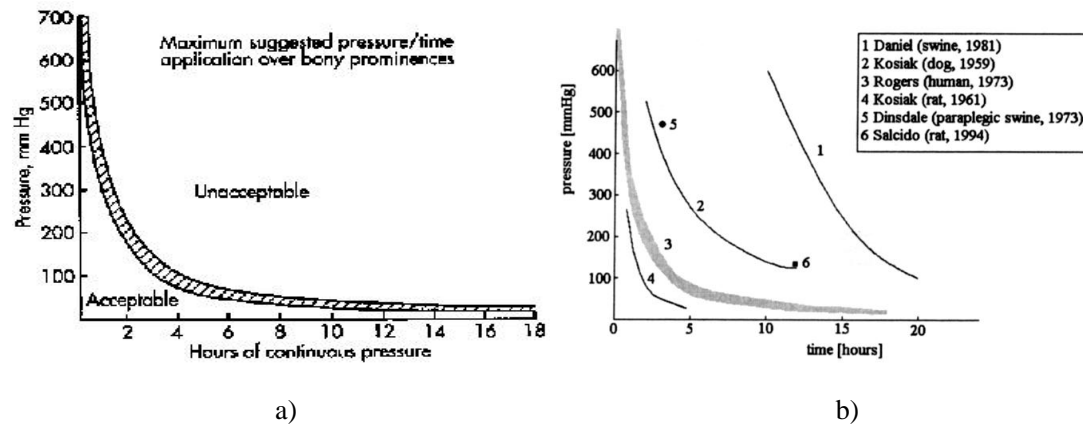
Figure 2 - 4 The relationship between pressure and time (a) In a clinical study (Based on Reswick and Rogers, 1976) and (b) in a range of animal studies (Based on Stekelenburg et al., 2005).

The trends of these risk curves have also been demonstrated by several animal studies (Figure 2–4 b). For example, Kosiak (1959) applied pressures of different intensities for various durations over the femoral trochanter and ischial tuberosity in a canine model. In a later study using a rat model, Kosiak (1961) applied a constant load and equal amounts of intermittent loads and reported a higher susceptibility of tissue to the constant load. In 1981, Daniel and colleagues (1981) experimentally produced pressure ulcers in swine over the greater femoral trochanter. The animals were subjected to localised pressures ranging from 30 mmHg to 1000 mmHg (4.0 - 133.3 kPa) for periods between 2 hours and 18 hours, and results show, the investigators were also able to plot a critical pressure/time curve for pressure ulcers in swine. In a more recent rat model, (Salcido et al., 1994) applied pressure for a 6 hours period on each of two consecutive days. This resulted in tissue damage at a pressure of 145 mmHg (19.3 kPa). The hyperbolic form of these curves (Figure 2-4) has been recently challenged by the work of several authors. In particular Gefen and colleagues (2007) have shown that even at relatively low pressures for short periods of time, both cells and tissues may be susceptible to damage.

Shear and friction

Shear forces, such as stretching and pulling on the skin, damage the perforating vessels to the skin causing thrombosis of the vessels (Hunter et al., 1974). Their presence represents one of the most dangerous problems affecting semi-recumbent patients (Figure 2-4) or those in chairs, or whenever soft tissues are being dragged along the surface of a bed, such as when patients are being transferred between support surfaces or when the head of the bed is lifted (Fowler's position) (Versluysen, 1986; Waterlow, 1988). Shear forces can only occur in the presence of normal pressures, which makes it particularly challenging to estimate the level of shear alone acting at the skin surface (Lowthian, 1997). Although the role of shear in the formation of pressure ulcers is still unclear, its importance cannot be underestimated. One theory is that shear stress causes a decrease in fibrinolytic activity, which is believed to be associated with tissue necrosis (Crenshaw, 1989).

The importance of shearing force as a factor in the development of ischemic ulcers was first reported by Reichel (1958). Although his work was primarily a clinical study, it clearly showed that shearing and stretching of internal structures, such as blood vessels, tended to compound the ischemic changes produced by external pressure (Figure 2-5), thereby increasing the rate of tissue breakdown. Bader et al., (1986) investigated the effects of shear force on healthy skin of the volar aspect of the forearm. Skin was stretched between two points and the tissue vasculature was monitored. It was found that there was an increase in the number of vertical and horizontal blood vessels in the skin that collapsed with increase in shear applied to the skin. Similarly, other authors (Bennett et al., 1979 and 1988; Dinsdale, 1974) showed that at a sufficiently high level of shear, the pressure necessary to occlude vessels was almost half that when the shear was absent.
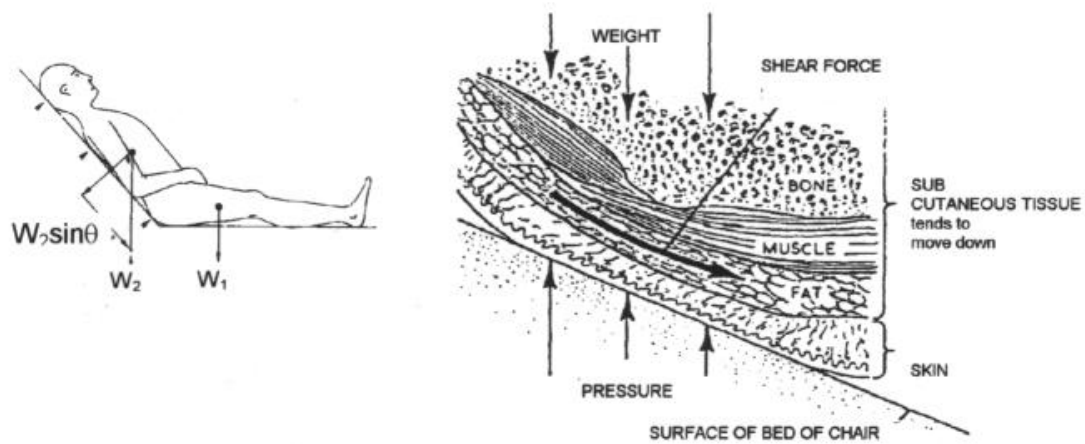
Figure 2 - 5 Effect of shear Forces on soft tissue, resulting from body posture (Bogie, 1992).

Frictional forces occur when there is a physical interaction between two surfaces exposed to normal forces. The tendency of one surface to slide with respect to the other is dependent on the coefficient of friction. The value of this parameter is higher prior to relative movement between the surfaces (known as static friction), but reduces when relative movement occurs (known as dynamic friction).

Friction occurring, for example, when a patient is pulled across a bed sheet, this can result in a loss of epidermal cells, intra-epidermal blistering and, ultimately superficial ulcers (Hunter et al., 1974). A number of authors have demonstrated that the application of pressure and friction increased the susceptibility of the skin to ulceration (Dinsdale, 1974; Waterlow, 1988; Dealey, 1993).

Temperature

Raising tissue temperature increases both cell and tissue metabolism and, therefore, increases the risk of ischemic necrosis. Indeed there is an estimated 13 per cent increase in metabolic rate for every 1 ℃ rise in skin temperature (Fisher and Kosiak, 1979). If the interface temperature increases, the supply of nutrients via blood to the cells will need to be more efficient. This situation will be compromised in the presence of interface pressures leading to reduced blood flow and an associated reduction of delivery of vital nutrients. It is important to note that local temperature

also increases with either pressure (Mahanty and Roemer, 1979) or when and if the support mattresses and cushions act as thermal insulators (Fisher et al., 1978). This poses an additional risk factor in the formation of pressure ulcers.

Moisture

It has been reported that 400 grams of insensible moisture vapour flows through the skin per day (Flam, 1987). Moist tissue is weaker and is susceptible to both increased maceration and excoriation. Moisture can increase the friction between skin surfaces and bed sheet, and tends to produce their most damaging effects when coupled with excessive pressure. This situation can be exacerbated by patients who are incontinent, a situation often found with the elderly in extended care settings. It is important to understand that moist skin is more easily abraded, more permeable and more readily colonised by micro-organisms than healthy skin. It is also less resistant to infection than dry skin.

2.2.2 Intrinsic Factors

Nutrition

Inadequate nutrition can increase both the risk of developing pressure ulcers and the delay of the healing process. Thus nutritional status is considered to be critical in both the prevention and management of pressure ulcers, as indicated in the schematic in Figure 2-6. Malnutrition leads to reduction of both fat and muscle tissue, the natural cushioning materials of the body which minimises the stresses transferred to the underlying bony prominences. It is therefore surprising that relatively little evidence-based research has been published to inform practice in the area of nutritional support related to pressure ulcers. Nonetheless, Allman et al., (1986) did report an association of hypoalbuminemia due to malnutrition to the development of pressure ulcers in a cross-sectional survey of 634 hospitalised adult patients.

Hypoproteinemia, associated with inadequate intake or excess loss, causes interstitial oedema which, in itself, lowers resistance to pressure ulcer development. For an adequate metabolic response, it has been estimated that a patient with a pressure ulcer should have a protein intake of 80 - 100 gm each day (Michael, 1991). This usually requires high protein supplements in addition to the three daily meals. In addition ascorbic acid, in the form of vitamin C, may also provide an enhanced tissue resistance to damage. For example, Taylor et al., (1974) studied 20 surgical patients in a prospective double-blind controlled trial of ascorbic acid supplementation. They showed a significant difference in pressure areas after only one month of supplementation. Poor or low hydration can also affect body weight, albumin levels and overall patient heath. Thus it is very important that nutrition status is assessed with each patient, who may be at risk of developing pressure ulcers.
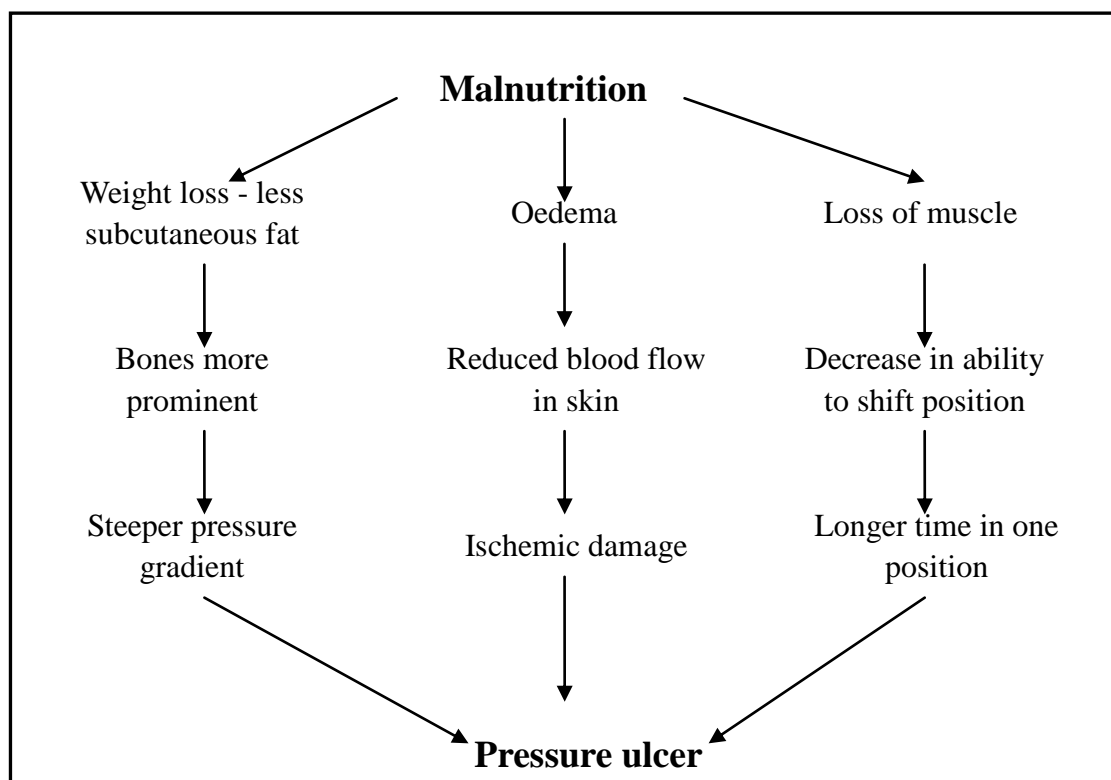
Figure 2 - 6 Schematic indicating the relationship between malnutrition and the development of a pressure ulcer.

Infection

Although infection will not cause a pressure ulcer, its presence can increase the susceptibility of ulcer formation. As an example, infections can cause fever that increases the metabolic rate of the entire body. This increases the demand for oxygen, further endangering the area of ischaemia. In addition, severe infection can cause nutritional disturbances and weaken the body's reserves. Localised bacteria can also increase the demands on local metabolism both by their own requirements and by the response of the immune system (Torrance, 1983). In addition septicaemia associated with deep Grade IV pressure ulcers can ultimately lead to death. This was the case with the "Superman" actor, Christopher Reeves, a high level spinal cord injured patient, who died from complications associated with infection of his deep pressure ulcer.

Body Type

An individual with a body type and/or morphology, in which the pressure is distributed fairly uniformly over areas adjacent to bony prominences, are generally less susceptible to pressure ulcer development. For example, a thin person with little subcutaneous fat and poor muscle bulk is particularly susceptibility to ulcer formation over the bony prominences. By contrast, bariatric subjects may exhibit excess soft tissues, which can provide uniform load distribution. However, damage may still occur due to contact between their substantial tissue folds and as a result of poorer internal circulation and impaired mobility. Thus, a morphological index of an individual, such as the Body Mass Index (BMI), in kg/m^2 (as determined by Weight / Square of the Height), is commonly employed to assess susceptibility for tissue damage.

Impaired Sensation

Individual who exhibit an impaired sensation and thus are unable to detect normal levels of pain, particularly during periods of pressure-induced ischaemia, have an

enhanced susceptibility to pressure ulcer formation. Accordingly, these individuals are unlikely to re-distribute their weight or reposition themselves following prolonged periods of pressure ischaemia. Those subjects particularly affected are some subjects with spinal cord injury, spina bifida, stroke, diabetes mellitus, full-thickness burns and peripheral neuropathy. Thus each condition is generally associated with an enhanced susceptibility to ulcer formation due to their impaired sensation.

Impaired Mobility

The ability of a patient to move freely, in order to re-distribute the forces over a larger area of soft tissue, is of significant importance in the maintenance of tissue viability. Indeed there is a direct correlation between pressure ulcers occurrence and impaired mobility, as healthy individuals consciously reposition themselves approximately every 15-20 minutes. It has also been reported that if individuals reposition themselves less than about 20 times during the night, they can increase the risk of ulcer development (Australian Wound Management Association, 2003). The ability to move is reduced in a number of patient groups including those suffering from paralysis, locomotor disorders or fractures, patients who are drowsy, in a stupor or, depressed state or those undergoing surgical procedures under general anaesthesia. Each of these conditions increases their susceptibility to developing tissue breakdown.

Aging

Age is just one of the many intrinsic risk factors for pressure ulcers, but it is not considered to be age, per se, but the associated problems of ageing that lead to the enhanced susceptibility. For example, there are several age-related structural changes in the dermis and epidermis including a decrease in elastin content, change in tissue stiffness and strength, loss of dermal vasculature, flattening of the epidermal-dermal junction and increased epidermal permeability. In addition, the potential of soft tissue remodelling decreases with age associated, in part, by the reduced cellular activity, and reduced ability to control infection, both of which can enhance the potential

development and severity of a pressure ulcer. Other reasons for the increased incidence of pressure ulcers with advancing age can be attributed to a greater lack of mobility, poorer state of nutrition, high incidence of complicating medical problems impairing cellular metabolism. All these factors increase incidence with age, for example, a study reported that over 50 percent of patients admitted with pressure ulcers were over 70 years of age (Hampton and Collins, 2004).

At the other end of the age scale, it is well known that both neonates and very young children are also susceptible to tissue breakdown, due to the inherent fragility of their soft tissues and their disproportionate head-to-body weight. It is interesting to note that this young group exhibits tissue breakdown at sites, less common than in adults. For example, there is greater risk of pressure damage to points on the back of the head, or from repeated heel pricks for blood monitoring in neonates, than in the sacrum or heel, common sites of pressure-induced injury in adults.

2.3 Pathophysiology of Tissue Breakdown

Tissue breakdown is generally considered to be the result of ischaemia developed in loaded tissues. Histological studies have shown that, after pressure has been applied for a period of time, there is dilation of capillaries and venules and an associated swelling of endothelial cells, changes in osmotic pressures and fibrinolytic activity (Crenshaw and Vistnes, 1989). A number of theories have been proposed to describe the consequence of this occlusion, many of which have been based on the results of pressure-induced damage in animal models.

In one of the earlier studies, Husain (1953) examined the effects of pressure on soft tissue and the development of tissue breakdown, using both rat and guinea pig models. Pressure was applied to the tails and legs using pressure cuffs. Varying magnitudes and durations of pressure were applied and some animals were transected at the spinal cord to model paraplegia. The findings strongly suggested that uniformly distributed

pressure was less damaging than localised or point pressures and that low pressures maintained for long periods of time produced more tissue damage than high pressures for short periods. The work suggested that pressure caused an increase in the permeability of capillaries producing oedema, whereby lymphatics and venous channels were obstructed. Pathological changes included loss of muscle striations, conversion of sarcoplasm into homogeneous material, fragmentation, granularity and necrosis of muscle fibres.

Other animal studies have investigated the effects of pressure on tissue perfusion and blood flow. For example, Herrman and colleagues (1999) applied step increases in pressures over the greater trochanter of fuzzy rats until capillary perfusion pressure reached an apparent minimum, as measured by laser Doppler flowmetry. It was reported that skin perfusion increased with low levels of surface pressure and then decreased at higher pressures. It is probable that the tissue was able to withstand the initial increases of surface pressure while maintaining good perfusion because of: (1) the inherent stiffness of the connective tissue; (2) the increased tissue internal pressure due to loss of water causing an increased proteoglycan concentration; and (3) vasodilation and recruitment of vessels. However, these mechanisms proved inadequate at elevated pressures. When an additional ischaemic period was applied to the same region for 5 hours followed by a 3 hours reperfusion period, the response of stressed skin was even more adversely affected. Findings, which suggested compromise to the vasodilatory mechanisms, included:

- a loss of the initial increase in perfusion with low levels of increasing pressure,
- a depression (45% lower than controls) in the hyperaemic response with delayed recovery time, and
- a decreased (54% lower than controls) amplitude of low-frequency rhythms in skin perfusion.

These data suggest that soft tissues needs sufficient time for recovery before returning to normal tissue behaviour.

The role of lymph flow and the associated fluid pressure is also potentially important in the development of some pressure ulcers. In one of the few related studies, Miller and Seale (1981) investigated lymph clearance during compressive loading on the hind limb of mongrel dogs. These authors reported that a pressure of 60 mmHg can initiate lymph vessel closure. They also suggested that it was more likely that the terminal lymph vessels would collapse before the collecting lymph vessels as they are smaller and closer to the site of pressure application. However, since that time, due to the complexity of the measurement, very few other studies have examined how the lymph flow affects the viability in the impending tissues with respect to pressure ulcer development.

By contrast, a number of studies have investigated the effects of repeated pressures on consecutive days. Nola and Vistnes (1980) compared the effects of 6 hours of pressure (100-110 mmHg) per day, over 4 days, on skin over bone and skin over muscle over bone. These authors reported that a pressure regimen which caused 100% skin ulceration over bone did not necessarily cause skin ulceration when muscle was present. These findings suggest different damage susceptibility of skin and muscle, and that the breakdown mechanisms associated with skin breakdown are different to those for deeper tissues.

It is inevitable that tissue compression will lead to a degree of tissue and cellular deformation and also to ischemia by mechanical closure of blood vessels. The relative effects will be influenced by the mechanical properties. If deformation exceeds a lower threshold (Figure 2-7), apoptosis may be enhanced in the cells but if a higher threshold is surpassed, cells will enter the pathway to necrosis. Ischemia compromises hypoxia, which will induce the cells to conform to lower oxygen tensions and thus down-regulate metabolic processes. Additionally, anaerobic metabolism will be adopted leading to increased glucose consumption and increased lactate production.

Lactate production will, however, further down-regulate metabolic processes, causing an inhibition of lactate production and glucose consumption (Figure 2-7, dashed lines). Once a lactic acid threshold is exceeded, the cells may become necrotic, possibly through apoptosis. In a comparable fashion, glucose deprivation will induce tissue necrosis (Gawlitta et al., 2007). Findings from these cell-based studies also revealed that increases in cell deformation caused proportional increases in apoptotic and necrotic cell death, while no apparent cell death was recorded in the presence of hypoxia within the relatively short culture period of 22 hours. This observation suggested an important role for deformation in the onset of apoptosis and eventual tissue breakdown.
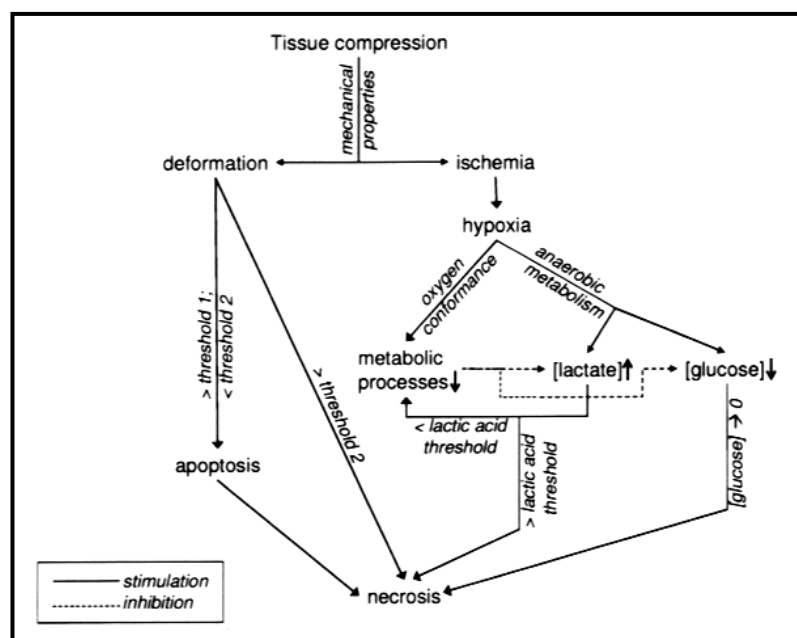
Figure 2 - 7 Schematic depicting the hypothesized order of events taking place during tissue compression (Based on Gawlitta, 2007).

Cell deformation triggers a variety of effects such as altered membrane stresses, volume changes and cytoskeletal reorganisation, which may be involved in early cell damage. It has been shown that the response of muscle cells to deformation during tensile or shear straining is crucial to cellular degeneration or adaptation (Vandenburgh et al., 1991; Cheng et al., 1993) and a comparable response was found

for compressive straining (Breuls et al., 2003; Wang and Vadgama, 2005). A summary of these findings is presented in Table 2-1.

Table 2 - 1 Summary of the major findings of selected 'in vitro' studies.

Author	Model	Time scale Compression	Main results
Peeters et al., 2003	Single myoblasts	seconds	◆ Stepwise strain > 50%: structural cell damage ◆ Strain > 60%: membrane bulging ◆ 72% strain: cells start to burst ◆ Dynamic straining: bulging at 40%, bursting at 54% ◆ Cells more sensitive to high frequency than low frequency
Bouten et al., 2001	Myoblasts and myotubes in agarose	1-24 hours	◆ Strain > 20%: bucking of myotubes ◆ Strain > 30-40%: bucking of myoblasts ◆ Increase in damage in cell after 1 hour of straning
Wang and Vadgama., 2005	Myoblasts and myotubes in agarose	1/2 – 12 hours	◆ At 10% strain: increase in damage after 4h compression ◆ At 20% strain: increase in damage after 1/2 hour compression ◆ 60-70% of cell death due to apoptosis ◆ Myotubes more sensitive to straining than myoblasts
Breuls et al., 2003	Myoblasts and myotubes in collagen matrigel mix	1-8 hours	◆ At 30% and 50% strain: immediate cell damage ◆ At 30% strain: 50% damaged at 8 hours ◆ At 50% strain: 80% damaged at 8 hours

2.4 Ischaemic-Reperfusion Tissue Injury

Ischaemia-Reperfusion (I/R) injury can be a factor in the formation of pressure ulcers. I/R injury can be defined as cellular injury resulting from the reperfusion of blood to

tissue areas, which had been previously exposed to an ischaemic insult. At a cellular level, tissue metabolism may be reduced after significant periods of ischaemia to preserve function. However, this inherent protective mechanism can evoke a cascade of detrimental effects within the tissue as the blood supply is restored (McCord, 1985). The sudden decrease in oxygen tension within the extracellular matrix and the cells themselves results in the activation of control mechanisms to maintain steady state, as energy metabolism transfers from oxidative phosphorylation to anaerobic glycolysis in cell mitochondria. This leads to the slowing down or ceasing of ATP generation, resulting in the inevitable down-regulation of various energy-requiring processes, such as protein synthesis and ion pumps action.

At reperfusion, under aerobic conditions, there is a potential formation of oxygen free radicals (OFRs) which can convert hypoxanthine, a product of energy ATP degradation, to uric acid (Vajo, 1996; Mondek et al., 2004), as indicated in Figure 2-2. Under normal circumstances oxygen free radicals are buffered by free radical scavengers, such as reduced glutathione. However, in tissues undergoing oxidative stress, there is a decrease in the levels of these enzymes. As a consequence, during reperfusion the oxygen free radicals are buffered to a lesser degree and this is reflected in an increase in concentration of hydrogen peroxide (McCord, 1985; Parks and Granger, 1988; Russell et al., 1989).

Production of oxygen free radicals may initiate a cascade of biochemical events that may significantly contribute to or result in the production of pressure ulcers (Houwing et al., 2000; Peirce et al., 2000). Of the few studies, Peirce and colleagues (2000) investigated the effects of I-R injury on skin ulceration in an animal model. The extent of the damage was indicated by an increase in both necrotic area and the degree of leucocyte extravasation. Their results indicated that five I-R cycles, equivalent to a total ischaemic period of 10 hours, were more damaging to the skin than one continuous compression-induced ischaemic period of 10 hours.

Several substances are thought to prevent free radical formation or to scavenge free radicals once they are formed. (Houwing et al., 2000) investigated the effect of one such scavenger, vitamin E. The study showed that pre-treatment with 500 mg of vitamin E prevented damage caused by pressure to a large degree. Although vitamin E does not prevent oxidative stress during the application of pressure, as reflected in reduced glutathione and total glutathione, it does prevent the excess production of oxygen free radicals and hydrogen peroxide during reperfusion.

Unal and colleagues (Unal et al., 2001) investigated the effect of gradual increase in blood flow on I-R injury of the skeletal muscle. They induced ischaemia by applying clamps to the femoral vessels of rats. Three groups of rats were used:

- A control group: no ischaemia was induced,
- A conventional clamp release group: 150 mins ischaemia was followed by immediate release of the clamps,
- A gradual clamp release group: 150 mins ischaemia was followed by gradual release of the clamps (blood flow velocity recovered in 120 seconds).

Tissue histology indicated inflammatory cell infiltration and loss of striation of the muscle, which was less noticeable in the gradual-reperfusion group than in the conventional reperfusion group. The tissue levels of malonyldialdehyde (MDA) and myeloperoxidase (MPO), markers of superoxide radicals, were also significantly greater in the conventional group. Thus this study demonstrated that gradual reperfusion decreases neutrophil accumulation, superoxide radical occurrence, and tissue infarction in the rat hind limb model.

2.5 Classification of Pressure Ulcer

Pressure ulcers are generally classified into four of five stages or grades, dependent on the extent of the soft tissue damage. These categories or stages, the term recently adopted by the combined NPUAP/EPUAP Guidelines (NPUAP-EPUAP Pressure Ulcer Classification System, 2009), will inevitably have variable healing rates and prognoses, and these will inevitably inform planning strategies for effective treatment.

Stage I

This stage, as shown in Figure 2-8, is characterised by a non-blanchable discoloration of the skin. The skin is unbroken and the wound is superficial. This condition is equivalent to light sunburn or a first-degree burn as well as a beginning of a pressure ulcer. The burn heals spontaneously or the discolouration rapidly fades when pressure is relieved on the area.

Figure 2 - 8 Features of Stage I pressure ulcer (Based on NPUAP-EPUAP Pressure Ulcer Classification System, 2009).

Stage II

This stage as indicated in Figure 2-9 is characterized by a blister, either broken or unbroken. Skin tissue breakdown with loss of epidermis is limited to the demarcation between the dermis and subcutaneous tissue. It is characterised by irregular edges, shallow ulcers with subcutaneous fat at the base and can involve both oedema and pain. Such an ulcer might be associated with infection and this would certainly delay healing for several weeks after the relief of pressure.
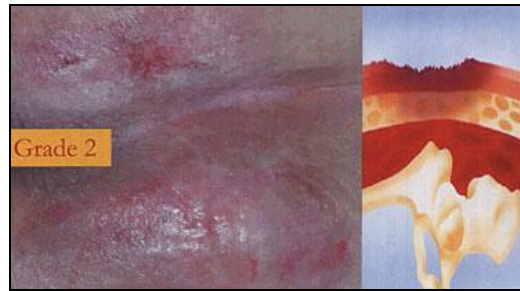
Figure 2 - 9 Features of Stage II pressure ulcer (Based on NPUAP-EPUAP Pressure Ulcer Classification System, 2009).

Stage III

This stage, illustrated in Figure 2-10, can be characterised as a full thickness ulcer involving the epidermis, dermis, subcutaneous tissue and, possibly, extending to the fascia. It is generally not painful but may have a foul-smelling drainage. It the ulcer is associated with infection, it will take several months to heal following pressure relief.

Figure 2 - 10 Features of Stage III pressure ulcer (Based on NPUAP-EPUAP Pressure Ulcer Classification System, 2009).

Stage IV

A Stage IV ulcer, as indicated in Figure 2-11, extends through the skin and can involve underlying muscle, tendons, bone, and joints. The wound may appear small at the surface but have extensive tunnelling underneath and also have foul-smelling discharge. Such a stage IV ulcer can take months or years to heal.

Figure 2 - 11 Features of Stage IV pressure ulcer (Based on NPUAP-EPUAP Pressure Ulcer Classification System, 2009).

These stages do not always predict or account for some forms of tissue breakdown. For example, deep tissue injury (DTI) represents damage which originates deep within the tissue leading to an extensive area of subcutaneous damage. At a later stage damage is identified by involvement of the superficial skin layers. The "bottom-to-top" hypothesis is supported by the fact that skeletal muscle tissue is highly susceptible to sustained deformation, potentially leading to tissue breakdown in the form of deep pressure ulcers (Nola and Vistnes, 1980; Daniel et al., 1981). Thus, deep pressure ulcers can originate within the skin or muscle tissue layers.

Table 2 - 2 Critical tissue ischemic times (Steinau, 1988)

Tissue	Time
Muscle	4 hours
Nerve	8 hours
Fat	13 hours
Skin	24 hours
Bone	4 days

A relative estimate of the times to ischaemia for a range of tissues was made by Steinau (1988). The values will also inevitably depend on ambient temperature, and tissue mass. Nonetheless, muscle generally appears tolerant of ischemia for up to 4 hours, nerve changes remain reversible up to 8 hours, fat up to 13 hours, skin up to 24 hours, and bone up to four days at normothermia (Table 2-2). A separate study noted that the extent of necrosis in muscle after 3, 4, and 5 hours of ischemia was 2%, 30%, and 90%, respectively (Labbe and Walker, 1987). The authors also noted that the

muscle necrosis was greater in the central portion of the muscle and observed that external evaluation of the degree of ischemic damage was clinically unreliable.

Although skeletal muscle tissues are very susceptible to damage development due to compression, deep pressure ulcers represent the smaller proportion of ulcers in the general patient population in hospitals and nursing homes. They have 2.2-6.4% for grades III and IV only, as compared to 13.2 - 32.4% for all pressure ulcers (Bours et al., 2002).

The importance of distinguishing deep tissue injury (DTI) in addition to the other four types of pressure ulcers has been recognized by the NPUAP and EPUAP. They are defined as pressure-related injuries under intact skin (Ankrom et al., 2005). There is still much debate as to how DTI can be classified and whether an extension of the traditional staging of ulcers is required.

2.6 Occurrence of Pressure Ulcer

While prevalence surveys can provide useful immediate baseline data, incidence studies are considered to represent a more accurate assessment of pressure ulcer development (Dealey, 1993). Studies over the last decade, undertaken in a variety of different UK health care settings have reported pressure ulcer prevalence ranging from 7% to 33%, as summarised in Table 2-3. This variation is, in part, due to use of different assessment tools, patient groups, health care settings and data collection methods. This precludes direct comparisons between different health care settings. Such values are equivalent to similar findings obtained from surveys in the US, Europe and Australia.

Pressure ulcers that develop in hospitalised patients typically occur in patients older than 70 years (Allman, 1989). However, they may also occur with a higher frequency in neurologically impaired young patients, who are particular susceptible due to their

limited mobility and lack of sensation. For example, within five years of injury, spinal cord subjects exhibit an incidence of up to 26% (European Pressure Ulcers Advisory Panel, 2001).

Table 2 - 3 Pressure ulcer prevalence in different health care setting

Setting	Reported Prevalence	
Acute hospitals	7%-19%	(Dealey, 1993)
Nursing home	7.5%	(Roberts, 1994)
Community	0-15%	(Hanson, 1997)
Hospice	21-33%	(Chaplin, 1999)
Long-term care	7-23%	(Smith et al., 1999)
Spinal cord injury at		
Quadriplegia	15-26%	(Smith et al., 1999)
1 year after injury	12%	(Chen et al., 2005)
15 year after injury	21%	(Chen et al., 2005)

2.7 Localisation of Pressure Ulcer

Pressure ulcers are commonly located over bony prominences. In most stationary positions, mainly seating and supine positions, the likely affected areas include the sacrum, as the skin over the sacral bone is almost devoid of muscle padding. This factor, in combination with the sacral bone having an extremely high radius of curvature causes pressure ulcers to develop there most often when an individual is positioned in the supine position (Stahelin, 1986).

Patients in chairs or wheelchairs are at risk of developing pressure ulcers over the ischial tuberosities, greater trochanters, knees, ankles, shoulder blades, back of the head, and the spine. These areas are generally devoid of thick layers of adipose tissue which can cushion or protect the blood and lymph vessels. Other areas where pressure ulcers are common include the perineum, particularly in incontinent subjects, which is continually moist and difficult to keep clean, and the heels often in bed-bound geriatric subjects. Figure 2-12 shows common sites of the body in adults, which is most affected by tissue breakdown.
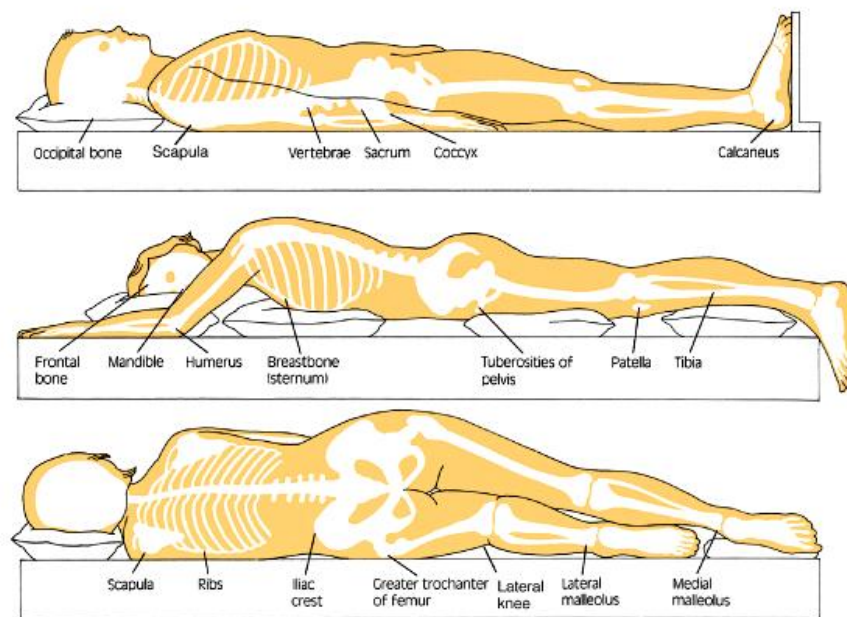
Common sites for development of pressure ulcers.

Figure 2 - 12 Common sites for development of pressure ulcers for adults (Williams and Wilkins, 2005).

2.8 Cost of Pressure Ulcer

Pressure ulcers negatively affect the health and morale of the patient and their carer, and place an immense burden on a healthcare system as a whole. There have been various attempts to estimate the financial burden. As an example, a report commissioned by the Department of Health and carried out by a major accounting company, Touche Ross (1993), estimated the treatment costs of pressure ulcers to range from £180 million to £321 million, or 0.4 - 0.8% of the annual healthcare spending in the UK. In a more recent study, Dealy and colleagues (2004), estimated the relative costs of a stage 1 to stage 4 pressure ulcer as £1,064 and £10,551, respectively. Indeed in the UK, the government dedicates the NHS 4% of its annual spending (£1.4 - £2.1 billion) on the treatment of pressure ulcers alone, representing an expensive health problem. Indeed treatment costs escalate due to the extended length of hospital stay, nursing time, and cost of dressings and the possible requirement of surgery. Such financial considerations can not quantify the pain and psychological cost in suffering to the patient with a pressure ulcer and their cares.

The major legal change in the US in 2009 involves penalising individual healthcare centres in which a hospital-acquired pressure ulcer occurred during medical treatment, in those individual not deemed to be at high risk on entry to the hospital. In such cases, the medical insurance schemes will now not be liable to recompense the hospital for any of its treatment costs. Such legislation has elevated the topic of pressure ulcer prevention, a measure of quality of care, considerably in terms of the priorities of US hospitals.

2.9 Treatment and Management

The conventional treatment of pressure ulcers, particularly those designated as Stages III and IV and DTI, is almost always problematic. In particular, deeper ulcers have variable prognosis, and even the most successful treatments take many months to heal. During this period, the condition is often physically and mentally stressful for patients who are hospitalised, bedridden, or wheelchair bound to decrease pressure on the affected and surrounding tissue areas.

Conventional treatment of pressure ulcers incorporates three main strategies:

(1) Local treatment of the wound using dressings and other topical applications,

(2) Treating concurrent conditions that may delay healing, such as poor nutrition, infection,

(3) Pressure relief strategies using beds, mattresses or cushions, or by regular repositioning of the patient, to off-load the affected areas. The wound is assessed and then must be cleaned and dressed in an appropriate manner. Surgery may be needed to close and speed the healing of large pressure ulcers. If one course of treatment does not work, alternative treatments must be attempted. Figure 2-13 presents a flow chart of some of the processes, which can be used to treat a pressure ulcer.

Healing ulcers and surgical wounds should be monitored regularly to ensure continued progress toward the goal of complete healing. The frequency of monitoring should be determined by the clinician based on the condition of the patient, the condition of the ulcer, the rate of healing, and the type of health care setting. If progress in healing cannot be demonstrated, the treatment plan must be reassessed and the level of adherence to that plan evaluated. The plan and implementation strategy should be modified as necessary.

2.10 Prevention

Prevention of pressure ulcer must represent the ultimate goal of healthcare. This should involve monitoring the important risk factors and addressing them in an appropriate manner. An effective pressure ulcer prevention program will require a co-ordinated multi-disciplinary approach to patient care involving the patient, the caregiver, physician, nurses, nutrition services and other disciplines.

Identification and Assessment

Remove pressure

Treat predisposing factors

Clean and debride the wound

Dress the wound

Continued assessment and treatment

Normal Healing — NO — Surgery possible? — NO — Alternative treatments

YES

YES

Complete healing?

NO

Surgical closure

YES

Treatment complete
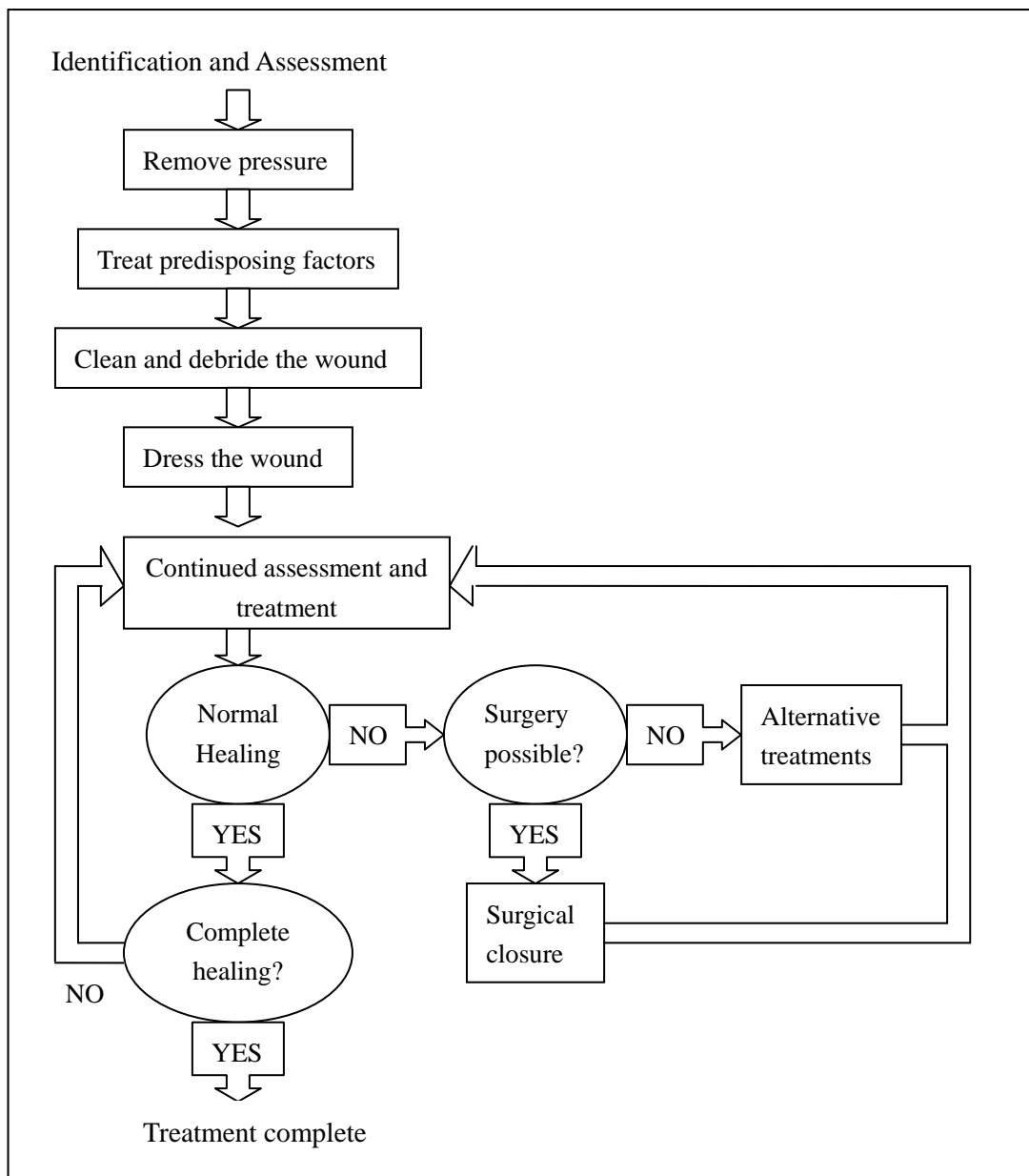
Figure 2 - 13 The treatment strategies of pressure sores presented as a flow chart. (Based on Webster, 1999).

Chapter 3

Measurement of the Soft Tissues Status under External Loading

This chapter describes a range of measurement techniques at the patient-support interface, which have been used to monitor the effect of factors implicated in tissue breakdown. These include the measurement of interface pressure and the assessment of tissue viability or status, using both physical and biochemical approaches. In addition, this chapter includes some discussion on the nature of the support surfaces with particular reference to their ability to control the micro-environment at their interface with the body.

3.1 Measurement of Interface Pressure in Soft Tissues

3.1.1 Design Features of an Interface Pressure Monitoring System

In the clinical environment, interface pressure measurements have important ramifications in the design of patient support systems, which aim to prevent tissue breakdown. As highlighted in section 2.2.1, high pressures can be experienced over the sites adjacent to bony prominences, such as the sacrum, heel, ischial tuberosities and trochanters. These sites represent the common site of tissue breakdown. Indeed, a series of reports by Swain and colleagues (1993; 1994 and 1995) have revealed the range of interface pressures at these sites on a group of elderly ambulant volunteers. The results as indicated in Table 3-1, reveal highest pressures recorded under the heel and sacrum.

Table 3 - 1 Range of interface pressures measured at critical sites on a group of elderly volunteers lying on a standard King's Fund mattress (Data summarised from UK Department of Health Evaluation Reports (Swain et al., 1993; 1994 and 1995).

Loading Location	Interface Pressures
Sacrum when semi-recumbent, backrest at 45°	62 – 107 mmHg (8.3-14.3 kPa)
Trochanter, side lying, hips and knees at 60°	6 – 156 mmHg (8.1-20.8 kPa)
Heels	107 – 213 mmHg (14.3-28.4 kPa)
Ischial tuberosities when sitting on 3-in stand cushion	60 - 146 mmHg (8-19.5 kPa)

It is clear that the measurement of interface pressures can identify sites exposed to high pressures, which might be reduced by strategies involving modifications of support surfaces and/or postures. Interface pressure measurement is also important within the stump socket interface associated with lower limb prosthesis, an area not generally associated with supporting high pressures. Each of these different types of patient support interfaces will experience a wide range of physical conditions. Thus physical measurement systems, such as interface pressure transducers must be based on individual design specifications.

3.1.2 Design Features of an Interface Pressure Measurement Systems

The ideal technique for the measurement of interface pressures would involve a method which is continuous, non-invasive and causes minimal distortion of the interface between the patient and the support surface (Ferguson-Pell et al., 1976). Accordingly, sensors must be sufficiently compliant, flexible, thin and small enough to measure local pressures. For the interfaces involving sitting on a cushion or lying on a mattress, the sensor must provide a reliable, and preferably linear, output over the range 10 - 250 mmHg (1.3 to 33.33 kPa), as illustrated in Table 3-1, with negligible hysteresis. Its data acquisition rate should be approximately 1 Hz. Time dependence

must be minimal or at least well defined and repeatable, and the sensor must be smaller than the radius of curvature of the body area under investigation. Finally, a calibration method must consider a number of factors (Swain, 2005) including:

- the thickness and flexibility of the transducer,
- the compliance of the loading interfaces and,
- the possibility of the sensitivity of the transducer to forces other than those in the normal direction.

Over the last 40 years, there has been a diverse range of systems, which have been proposed to measure interface pressures in both the research environment and the clinical setting. These systems have incorporated sensors based on a number of physical principles. For example, a selection of devices consisted of thin sheets of various materials treated with inks or chemicals (Ferguson-Pell et al., 1976). These devices have the advantage of providing a map of the pressure distribution, but are difficult to quantify, subject to in-plane forces and also sensitive to rate of loading and temperature. Other measurement principles, as shown in the schematic in Figure 3-1, utilise air- or fluid-filled cells. The cells which are either in a single unit or array form are located under specific body sites to be measured. They are inflated, or pressurised in the case of fluid-filled cells, until the pressure is equivalent to and starts to exceed the applied interface pressure (Figure 3-2). However, in practice, the sensors which incorporated electrical contacts (Figure 3-1, middle), such as the Talley SA500 Pressure Evaluator with both the 28-mm and 100-mm sensor pads, often failed due to the fragility of the constructs. Accordingly, a more sophisticated pneumatic system was introduced, the principles of which are illustrated in Figure 3-2. This commercial system was first developed with a 12-cell array, which was later extended to a 96-cell array covering the entire mattress surface (Models Oxford Pressure Monitor (OPM) Mk II and Talley Pressure Monitor (TPM) Mk III, respectively, both manufactured by Talley Medical, Romsey, UK).
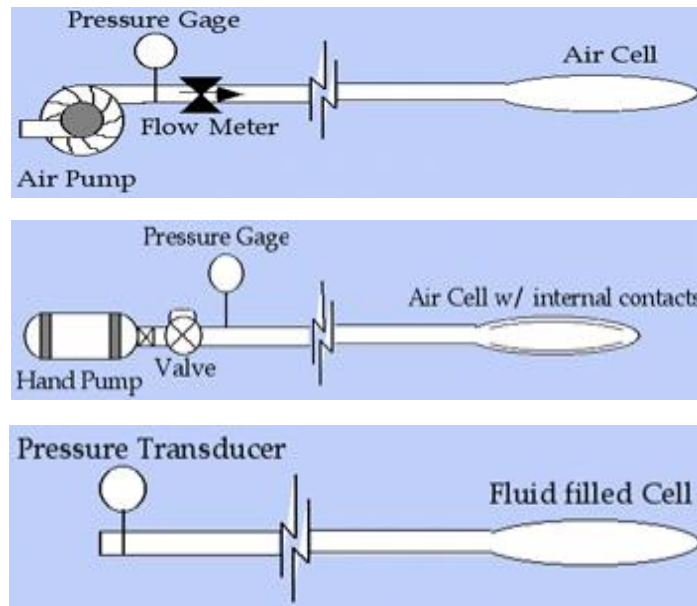
Figure 3 - 1 Show principle for Pneumatic bladder (above), electropneumatic bladder (middle), and fluid filled bladder (below), (Hobson, 2001).
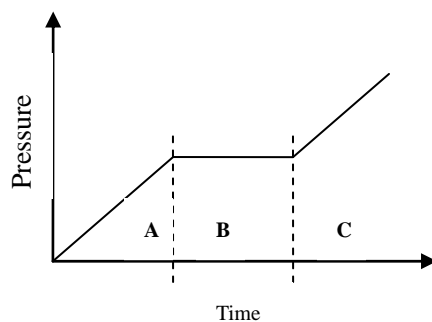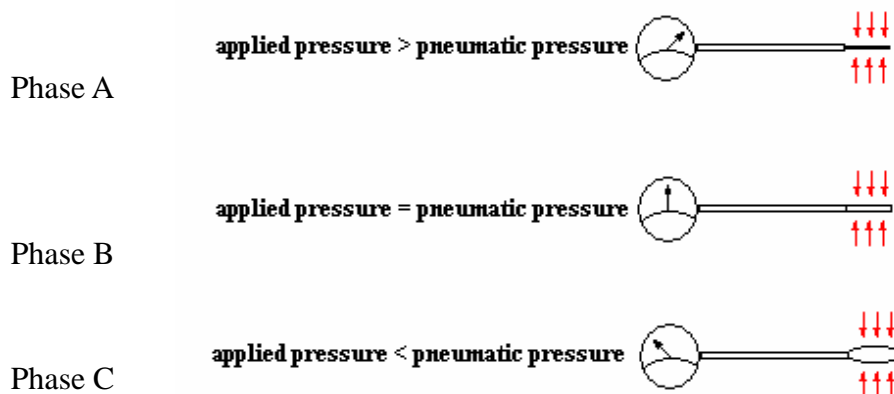
Figure 3 - 2 Schematic indicating that an increase in I pneumatic pressure within bladders will lead to an opening of the air bladder, when the applied pressure is exceeded. This manifests as a change in pressure-time profile as indicated by a change from Phase A to B (Based on Bader, 1982).
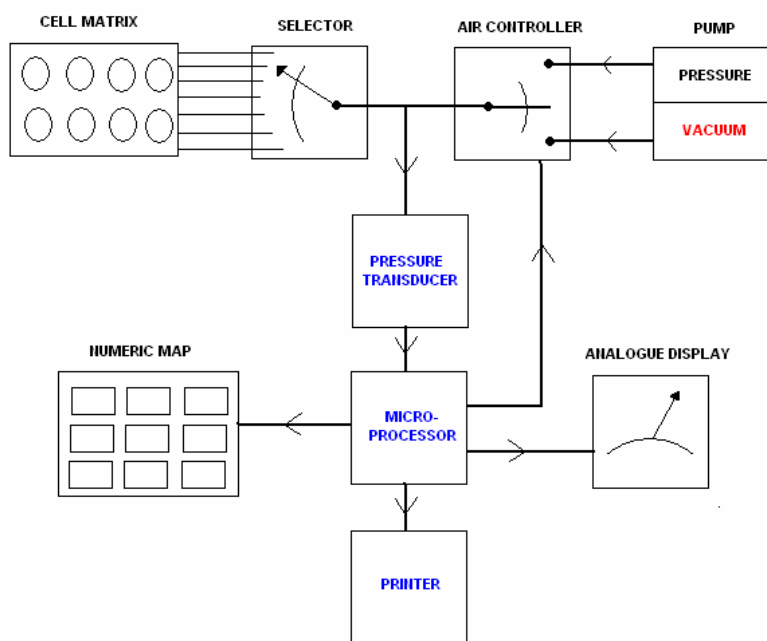
Figure 3 - 3 A block diagram of the pneumatic bladder system (adapted from Bader et al., 1986).

This system, as illustrated in Figure 3-4, has been largely consigned to research laboratories to be replaced by systems incorporating thin capacitive, resistive or inductive materials. These systems have been developed into a number of commercial products, consisting of an extensive array of sensors with associated elegant software to display pressure data, for both research and clinical use. One such system, commercially available as Tekscan®, incorporates an array of over 1000 sensing elements, whose electrical resistance changes in response to an applied pressure. This principle has been produced in forms for use at a variety of patients support interfaces, including the seating interface and for use in shoe sensors under the foot.

Figure 3 - 4 Talley Pressure Monitor and Matrix of pneumatic cells (Apatsidis et al., 2002).

As an example, BPMS™ (Body Pressure Measurement System) is one of the recent systems developed by Tekscan as a tool for the measurement and location of peak interface pressures. This system also allows the dynamic 2D and 3D display of real time analysis and locates centre of force. An example of a typical read-out for a seated subject is shown in Figure 3-5. The sensors have a pressure range of 0 - 200 kPa (1500 mmHg) with varying levels of sensitivity. Calibration involving such an extensive array can prove to be problematic.

There have been a few reported comparisons of different pressure measuring systems. Allen et al., (1993) looked at the repeatability and accuracy of the Talley SA500 Pressure Evaluator (Talley Medical, Romsey, Hants, UK). They reported the highest accuracy associated with the 28mm sensor when compared with both the 100 mm version and another commercial system (Model DIPE, Next Generation, CA, USA). Ferguson-Pell and Cardi (1993) compared three arrays, the Force Sensing Array (FSA), with 225 sensors (Vista Medical, Winnipeg, Canada) and the Tekscan, with 2064 sensors, and the TPM with 96 sensors (Talley Medical). The TPM differs from the other two, consisting of small arrays of sensors as well as individual sensors which can be directly located on the skin surface. By contrast the FSA and Tekscan are large arrays, typically 500 x 500 mm, which cover the whole area of interest. The authors

found that the TPM was the most accurate, stable and reproducible of the systems tested but was limited in its ease of use, speed and data presentation (Ferguson-Pell and Cardi, 1993). It should be noted, however, that as of today there is still no single system that meets all the requirements, which could be used for both research and clinical applications (Ferguson-Pell and Cardi, 1993; Bader et al., 1982). In addition, it has been well reported in many studies that interface pressures alone are not sufficient to alert the clinician to potential areas of tissue breakdown (Swain and Bader, 2002; Swain, 2005). What is more appropriate is to examine the effects of pressure and other interface parameters, such as shear and temperature, on the status of the soft tissues under the skin down to those adjacent to the bony prominences.
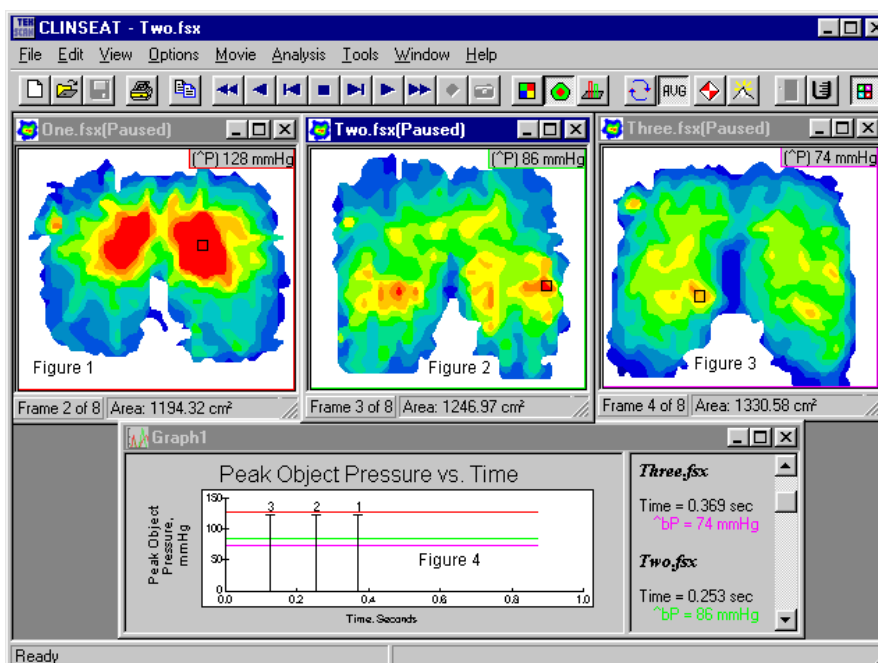
Figure 3 - 5 A typical read-out using Tekscan BPMS™ for a seated subject. In below graph, the peak object pressure range is between 0-150mmHg.

3.2 Assessment of Tissue Viability using Physical Sensors

Although it is convenient to measure parameters at the interface, what is of most relevance is to interrogate the internal status of the tissue under load. Over the last two decades, there have been a number of discrete sensing systems which have been proposed to indicate the viability, or status, of soft tissue subjected to periods of

loading. These techniques have been largely restricted to examining the response of skin layers to mechanical loading, and include measurements of blood flow using laser Doppler flowmetry (LDF) (Schubert and Fagtell, 1991; Sliver, 2002) and reflective spectrophotometry (Hagisawa et al., 1994; Sprigle et al., 2003). The most popular of these techniques, however, has been to measure transcutaneous gas tensions (T_cPO_2, and T_cPCO_2) at elevated skin temperatures. This technique is continuous and non-invasive and therefore fulfils many of the requirements of the ideal tissue status transducer (Ferguson et al., 1988). In all cases these physical systems measure physiological changes in tissues associated with either the application of load-induced ischaemia and/or the reperfusion response when the load is removed.

Given the many limitations of pressure mapping, interest has been directed towards the use of physiological monitoring where the body's response to a support system is used to indicate its suitability. A number of discrete sensing systems have been used for this purpose, including transcutaneous measurements of the partial pressure of oxygen in the tissues (Bader, 1990), tissue reflectance spectroscopy (TRS) (Hagisawa et al., 1994; Sprigle et al., 2003) and laser Doppler flowmetry (LDF) (Silver, 2002).

3.2.1 Techniques for Measuring Tissue Micro-Circulation

Laser Doppler Flowmetry imaging uses a stable monochromatic laser light source directed through a fibre optic to illuminate the tissue. Backscattered light is collected using a second fibre optic placed close to the source (approximately 1.5 mm centres). The frequency of the backscattered light will be shifted slightly if the scattering medium, namely blood, is moving either towards (blue shift) or away from (red shift) the point of measurement. The net effect is for the bandwidth of the frequency spectrum of the backscattered light to be broadened by an amount proportional to the average velocity of the scattering medium. The tissue thickness sampled is typically 1

mm, the capillary diameters 10 um and the velocity spectrum measurement 0.01-10 mm/s (Ferguson-Pell, 2005).

Transcutaneous Gas Tension Measurements involve the diffusion of oxygen across the skin to an electrochemical electrode attached to the skin surface. In order to measure the partial pressure of oxygen in the tissue the electrode is heated to 42-44 ℃. This induces maximal vasodilation, so that the oxygen diffusing through the skin is equilibrated closely with arterial oxygen tension. There are four factors which affect the measurements, namely:

- Rightward shift of oxygen-haemoglobin curve due to heating,
- Resistance of skin to O_2 permeability,
- Metabolic consumption of O_2 in skin,
- Effective rate of cutaneous blood flow.

Transcutaneous carbon dioxide tensions are not affected to such an extent by the above factors, due to the fact that there is only a small difference between arterial and venous pCO_2, and CO_2 can diffuse much faster through tissues than O_2. However, during periods of low blood flow, there is likely to be an increase in carbon dioxide and values will deviate from arterial pCO_2 (Spence et al., 1985).

Tissue Reflectance Spectroscopy has been adopted to use the absorption spectrum of light in the visible region to characterise the blood content and oxygenation of the superficial vasculature of the skin. Oxy- and deoxyhaemoglobin have distinctly different absorption spectra, particularly in the green and red regions of the spectrum as well as in the near infra-red (NIR) region of between 700 and 850 nm. Advances in this technique have enabled distinct absorption spectra to be identified for oxygenated and deoxygenated blood in skin (Ferguson and Hagisawa, 1995).

Combined Sensors - A recent study has employed a sensor which uses both LDF and diffuse reflectance spectroscopy for non-invasive determination of oxygen supply in tissue diffused with blood (Renalda et al., 2009 (a) and (b)). The system purports to measure oxygenation up to a depth of 8 mm. Results from a small number of spinal cord injured subjects suggested that by imposing dynamic sitting patterns, higher values of both cutaneous and subcutaneous oxygenation levels were recorded compared with those in the reference static sitting posture (Reenalda et al., 2009 (a)). In another recent study, a combined probe incorporating LDF and photoplethysmography was employed to assess the status of loaded sacral tissues using an elderly group of volunteers (Bergstrand et al., 2009). These authors reported differences in the response of tissues at different depths. In particular, the statuses of superficial skin layers were most readily compromised by external loading.

There are advantages and disadvantages in all the above systems, the most important factor in using a system for measuring tissue status is the understanding of the parameter being measured. The most accurate measurement technique would combine a number of different methods in order to elucidate as much information as possible.

3.2.2 Review of Transcutaneous Gas Tension Monitoring

The occlusion of blood flow to specific areas of tissue and the resultant ischaemia caused by the application of prolonged or excessive loads has been identified as one of the major contributing factors to the development of tissue breakdown. Thus, research has been carried out to determine the levels and duration of loading which may be detrimental to tissue status. The desired outcome of these researches is to identify threshold levels of load magnitude and duration below which the status of soft tissues is not compromised.

The initial studies were aimed at investigating the effect of loading at different locations with respect to the proximity of the bony prominences. (Seiler and Stahelin, 1979) and (Sangeorzan et al., 1989) used transcutaneous gas tension monitoring to examine blood flow over loaded areas of the trochanter and quadriceps, and tibia and tibialis major respectively. Their results clearly showed a linear relationship between T_cPO_2 and load. The response was most marked over bony sites with limited soft tissue covering. Thus total anoxia, where T_cPO_2 tended to 0 mmHg, was demonstrated for pressure of 150 mmHg (19.6kPa) and 525 mmHg (68.7kPa), over bony sites and soft tissue sites, respectively.

In a separate study, loads were applied at tissue sites using a flat indenter, into which a transcutaneous oxygen probe was mounted (Newson et al., 1981). Loads were applied incrementally for short periods of time at various tissue sites until a cut-off load was reached with the T_cPO_2 levels falling to zero. The repeatability of this procedure was estimated from separate measurement sessions, producing a standard deviation of 5% from the mean cut off load.

A later study employed an assessment criterion for tissue viability at which the T_cPO_2 and T_cPCO_2 values were within acceptable levels (Bogie et al., 1995). Clear relationships were indicated between depressed levels of T_cPO_2 and elevated levels of T_cPCO_2, the latter parameter at associated high values of interface pressure on spinal cord injured subjects. The work suggests that T_cPCO_2 provides useful additional information on the nutritional status of the tissue and the effect of pressure on micro-circulation. However, related studies yielded no clear guidelines as to the precise relationship between compromised tissue gas levels for a set time period and the onset of progressive tissue breakdown that will ultimately result in a pressure ulcer.

Bader (1990) investigated cyclic loading of sacral tissue of normal and debilitated subjects using T_cPO_2 measurement. It was found that the T_cPO_2 levels in all of the healthy subjects and some of the debilitated subjects showed complete recovery from the load within a short period of time. However, a significant proportion of the debilitated subjects demonstrated a delayed recovery to the cyclic loading, as indicated in Figure 3-6.
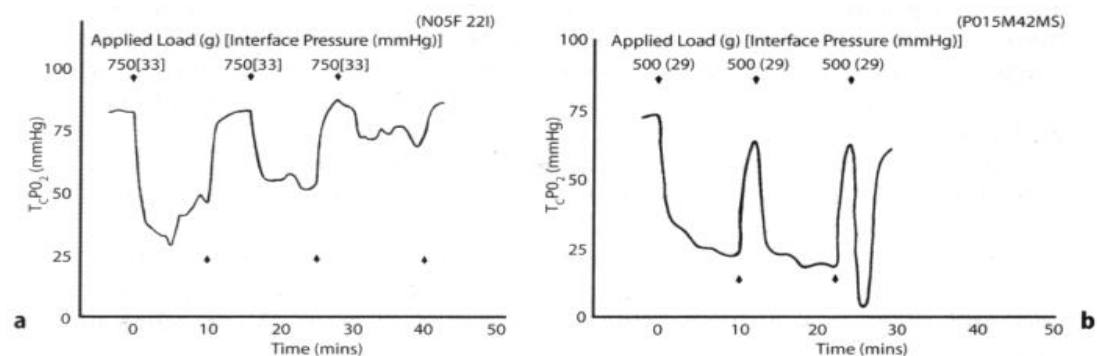
Figure 3 - 6 Tissue response to repeated loading at the sacrum showing a) normal response; b) impaired response. Adapted from Bader, 1990.

There are clearly differences in the reperfusion characteristics of blood flow to tissue after a period of pressure-induced ischaemia in different patient groups. This may explain why some patients are more susceptible to tissue breakdown than other, even with the same medical condition. It was proposed that such an approach could lead to predictive screening techniques to identify those patients with specific high risk of developing tissue breakdown.

3.3 Tissue Viability Assessment using Biochemical Methods

An alternative to measure interface conditions using physical sensors, is the potential of interrogating the internal status of the tissues under load using biochemical methods. One such opportunity involves the determination of the metabolite levels in sweat, transported via the sweat glands, and collected at the skin surface. Sweat analysis has traditionally been employed in assessing tissue status, following periods of exercise, as well as for specific medical conditions, such as cystic fibrosis (Gibson and Cooke, 1959).

3.3.1 Techniques for Collection and Analysis of Sweat

A number of different techniques have been developed for the collection of sweat from the skin surface, as summarised in Table 3-2. Some of these methods have been developed to obtain quantitative measures of sweat rate, while others have been designed in order to determine the biochemical composition of the sweat. Methods should ideally offer critical design features, such as minimal contamination and evaporation and a thin and flexible method of collection, such that its physical presence will not distort the local tissue support interface. In addition a device to collect sweat from tissues areas must not contain any chemical products, which could either react with moist skin or contain any chemicals found in sweat, thus it should not disturb the local microenvironment at the interface. Accordingly the use of thin paper − like collection pads provides an attractive solution for sweat collection as it will retain maximum volumes of sweat (Polliack, 1994). Two types of paper were made from cellulose and glass microfibre papers are available for this purpose (Whatman Paper Ltd., Special Products Division, Maidstone, U.K.).

Table 3 - 2 Techniques for sweat collection

Referece	Technique	Comments
Van Heyningen and Weiner, 1952	Oilskin arm bags	Not site Specific, difficult to work out dilution
Ferguson-Pell et al., 1988	Macroduct	Bulky, requires iontophoresis
Mitsubayashi et al., 1994	Direct drippage into tube	Losses due to evaporation
Polliack et al., 1993	Filter paper	Liable to saturation
Tanaka et al., 1990	Washdown	Evaporation, contamination
Fukumoto et al., 1988	Body weight change	Non-quantitative
Boisvert et al., 1993	Encapsulating chamber	Not applicable for loading

The latter inorganic material containing borosilicate glass presents risk associated with skin irritation and the possibility of minute amounts of carcinogens in the microfibre papers. By contrast, the alternative cellulose-based chromatography paper is considered inert. In addition, Cellulose (1 Chr) chromatographic paper is light, weighing 87 g/m^2 with a small thickness of 175 um. It has a water absorption capacity of 16 mg/cm^2. This type of filter paper is made from 100 per cent cotton linter and has been designed specifically for clinical applications (Polliack, 1994).

In order to analyse the composition of sweat a number of different analysis techniques have been described in the literature, as summarised in Table 3-3.

Table 3 - 3 Techniques for analyzing sweat composition

Reference	Biochemical Marker	Method	Quantitative
Laccoureye et al., 1993	1-Lactate	Enzymatic electrode, 1-lactate oxidase + O_2 -›Pyruvate	Yes
Higo et al., 1994	Lactic acid	Inelastic tunneling spectroscopy	NO
Omokhodion and Howard 1994	Trace elements Zn, Cu, Mu, Ni, Cd, Al	Atomic absorption spectroscpy	Yes
Hannon et al., 1984	Lactate	Fluorescence microscopy	Yes
Faridnia et al., 1993	Lactate	Amperometric biosensor	Yes
Kondoh et al., 1992	d-lactate, Creatinine	HPLC (Jaffes method)	Yes
Verde et al., 1982	Na^+, K^+ Ca^{++}, Mg^{++} Cl^-	Flame emission photometer Atomic absorption spectroscopy Titration	Yes
Taylor et al., 1994	Lactate, Urea, Urate Chloride	Fluorescence spectroscopy	Yes
Mitsubayashi et al., 1994	Glucose, uric acid Na^+, Cl^-	Amperometric biosensor Ion selective electrodes	Yes

3.3.2 Review of Sweat Measurement

Investigations have generally been focused on the sacrum, which is often loaded during supine lying, thus has a high susceptibility to pressure ulcer formation. In addition, the relatively high density of sweat glands found at the sacrum, which leads to a high sweat rate, is of particular pertinence to the present technique. The relatively few studies focused on analysing sweat from the soft tissues under direct mechanical loading are summarised in Table 3-4.

Table 3 - 4 A review of the studies performed on the effects of arterial occlusion on the sweat composition.

Author	Type	Time of loading	Sweat collection area	Comments
Randall, 1947	Tourniquet ischaemia	20-30 mins	Forearm	Sweat rate decreased with increasing tourniquet ischaemia as a result of failure of neurotransmitter, and not as a result of exhaustion of the sweat glands per se.
Van Heyningen and Weliner, 1952	Tourniquet ischaemia	25 mins	Whole arm	Ischaemia resulted in a decrease in sweat rate and increase in lactate returning to basal levels during reperfusion.
Collines et al., 1959	Tourniquet ischaemia	30 mins	Whole arm	Ischaemia resulted in decreased sweat gland activity, even in the pressure of neurotransmitter drugs, and an increase in body temperature. Diminished sweat gland activity is due to a loss of responsiveness of the sweat gland cells to the neurotransmitter.
Elizondo et al., 1972 (a)	Tourniquet ischaemia	10-15 mins	Volar aspect of the forearm	Arterial occlusion resulted in lower sweat rates which were partially reversed with heating. Decreased sweat rate resulted in decreased sodium and chloride concentrations increased potassium and osmolar concentrations.
Sato and Dobson, 1973	Tourniquet ischaemia	10 mins	Volar aspect of the forearm	Sweat rate decreased with tourniquet ischaemia. During tourniquet ischaemia, sodium decreased lactate and potassium increased.
Elizondo et al., 1972 (b)	Tourniquet ischaemia	4-19 mins	Volar aspect of the forearm	Localized heating during tourniquet ischaemia had little effect on sweat gland stimulation,

				although they were stimulated by the neurotransmitters, pilocarpine and mecholyl and by iontophoresis of physostigmine during tourniquet ischaemia. This suggests that the local heating response and sweat gland activity occurs at the level of the neuroglandular junction.
Ferguson-Pell et al., 1988	Indenter ischaemia	30 mins	Volar aspect of the forearm	Lactate and sodium levels measured. Ischaemia resulted in a decreased sweat rate and a significant increase in lactate returning to basal levels during reperfusion.
Polliack, 1994	Sitting and lying	9-16 hours	Sacrum of healthy volunteers	Lactate, chloride, sodium, potassium, urea and urate levels measured. Results indicated that tissues subjected to pressure ischemia produced a general increase in concentrations of lactate, chloride, urea, and urate associated with a decreased sweat rate. In the reperfusion phase, some of these metabolites returned to unloaded levels.
Polliack and Bader., 1997	Sitting and lying	10 hours	Sacrum of 11 debilitated subjects	Elevated levels of lactate and urea, 39% and 28% respectively. Small variations in metabolites over repeated measurements with time for a single individual.
Knight et al., 1997	Indenter	30-60 mins	Sacrum	Lactate, urea T_cpO_2 and T_cpCO_2 levels measured. Ratios of concentrations at experimental to control sites used. Loading resulted in reduction in tissue oxygen and increase in lactate and urea levels.
Bader et al., 2005	Indenter	60 mins loading followed by 60 mins unloading.	Sacrum of normal volunteers	Results indicated that all the median ratios of lactate and three purines remained at an elevated level during the ischaemic period. During the first reperfusion period (30 min.), the ratios for lactate and xanthinedecreased, but the ratios for both hypoxanthine and, in particular, uric acid remained significantly above unity (loaded/unloaded). The ratios for all the metabolites decreased during the second 30 minutes reperfusion period to values approximating to or below unity.

The above table illustrates that most of the work has concentrated on the response of forearm and sacral tissues under load. The studies generally indicate a decrease in the sweat gland activity, as measured from sweat rate of the ischemic tissues. However, the mechanism by which the sudomotor function results in a decreased output of sweat in the presence of applied loading has remained an issue of debate.

A combined approach using the electrode and the measurement of sweat metabolites examined the effects of loading at the sacral tissues of normal volunteers (Knight et al., 2001). Results indicated that T_cPO_2 was lowered at increasing levels of pressures, and at pressures exceeding 120 mmHg (16.0 kPa) there was an associated increase in T_cPCO_2 levels, above the normal basal values of 45 mmHg (6 kPa). In addition there was some correlation between T_cPO_2/T_cPCO_2 levels and the loaded/unloaded concentration ratios for both sweat lactate and urea. Indeed a threshold value of T_cPO_2 was identified, representing a 60% reduction from unloading basal values, above which the rates of sweat metabolites increased significantly (Knight et al., 2001). These parameters may prove useful in identifying those subjects whose soft tissue may be compromised during periods of pressure ischemia. By comparing selected parameters, a threshold value for loaded T_cPO_2 could be identified, representing a reduction of approximately 60% from unloaded values, as indicated in Figure 3-7.
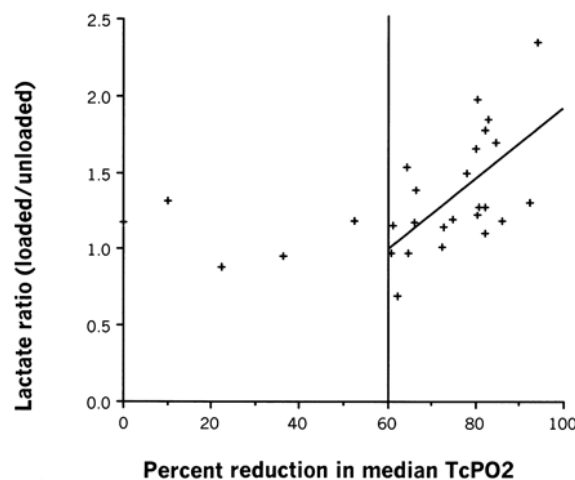
Figure 3 - 7 Relationship between ratio of sweat lactate concentration and percentage reduction in median transcutaneous oxygen levels, as a result of sacral loading on healthy subjects (Knight et al., 2001).

Above this threshold level there was a significant relationship between this parameter and the loaded/unloaded concentration ratios for both sweat lactate and urea (Knight et al., 2001). This degree of reduction (60% in median oxygen tension) may represent a critical level for the development of tissue damage. The study also related the lactate ratio to the percentage time at which T_cPCO_2 exceeded 50 mmHg. Thus, under conditions of mild ischaemia elevated levels of tissue carbon dioxide may be released from loaded areas in a normal manner, resulting in T_cPCO_2 values below 50 mmHg, whereas in severe conditions, both sweat lactate and T_cPCO_2 will be elevated as indicated in Figure 3-8.
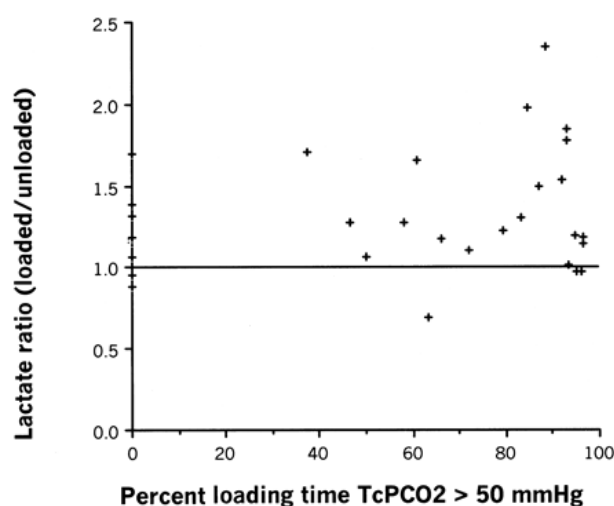
Figure 3 - 8 Relationship between ratio of sweat lactate concentration and percentage of time for which transcutaneous carbon dioxide levels exceeded 50 mmHg, as a result of sacral loading on healthy subjects (Knight et al., 2001).

3.4 Interface Climate Assessment

As discussed in Section 2.2.1, specific environmental factors at the interface, such as temperature and humidity, are also important if tissue breakdown is to be avoided at the patient support interface. For example, elevated temperatures produce sweat, thereby developing an excessively moist environment at the patient support interface, exacerbating the effects of pressure, friction, and shear, increasing the susceptibility to

tissue breakdown (KoKate et al., 1995). Indeed prolonged exposure to moisture can lead to tissue maceration and decreased ability of skin to resist shear forces and pressure, thus making it more susceptible to breakdown in the form of pressure ulcers.

3.4.1 Review for Influence of Temperature

The role of temperature in the causation of pressure ulcers has only been examined in a few studies. It is widely accepted that an increase of 1 ℃ in skin temperature results in an approximately 13% increase in tissue metabolic requirements (Fisher and Kosiak, 1979). However, in the presence of tissue compression, this relationship will clearly be changed.

A clinical study, conducted by Mahanty and colleagues (1981), compared the skin temperature response of normal and paraplegic skin to the application of localised pressure. It was suggested that if pressure is released following a period (t_p) of applied pressure (P_{app}), there will be a transient increase in skin temperature (T_{max}) , followed by a decline to basal levels for both paraplegic and non-paralysed skin. Furthermore, these authors proposed that the peak skin temperature was proportional to both the magnitude and duration of the applied pressure.

$$T_{\max} \; \propto \; k + \left| P_{app} \right| + t_p \qquad\qquad Equation\ 3\ \text{-}1$$

where, k is representative of a series of variables including the metabolic rate, ambient temperature and moisture concentrations. This trend was found to be appropriate for combinations of pressure and time, which were below the critical values for the development of pressure ulcers, as indicated in Figure 3-6.

Kokate et al., (1995) described a porcine model for the evaluation of temperature-modulated pressure-induced damage to tissues. Tests were performed with an applied pressure of 100 mmHg (13.3 kPa) for 5 hours, at temperatures of 25, 35, 40 and 45° C. The latter temperature represented a commonly accepted upper limit

for thermal therapies applied to skin, such as water beds. Results, in the form of histological assessment, indicated:

1. No damage at 25 °C,

2. Moderate muscle damage at 35 °C,

3. Partial epidermal necrosis and moderate muscle damage at 40° C,

4. Full-thickness epidermal necrosis, moderate dermal and subdermal damage and severe muscle damage at 45 °C.

These results indicated that the extent of tissue damage was exacerbated by elevated temperatures and strongly inferred that an applied temperature of 25 °C could be protective to the soft tissue area. In addition, the authors reported a change in the deformation characteristics of the soft tissues with temperature. In particular, heating tissue resulted in an increased resistance to applied pressure.

In a subsequent study, Patel and colleagues (1998) examined the combined effect of increased temperature and surface pressure on tissue perfusion and deformation. A heater, designed to raise the skin surface temperature locally, was attached to a pressure applicator. A range of pressures between 3.7 and 73 mmHg (0.5 and 9.7 kPa) were applied at two different temperatures, 28 °C and 36 °C. The study confirmed that there was a significant increase in perfusion, measured by a laser Doppler flowmeter, with increased temperature at surface pressures below 18 mmHg (2.4 kPa), probably due to local auto-regulatory mechanisms as illustrated in Figure 3-9. No corresponding increase in perfusion was reported at higher pressures, most likely because of mechanical occlusion of vessels induced by high surface pressure.
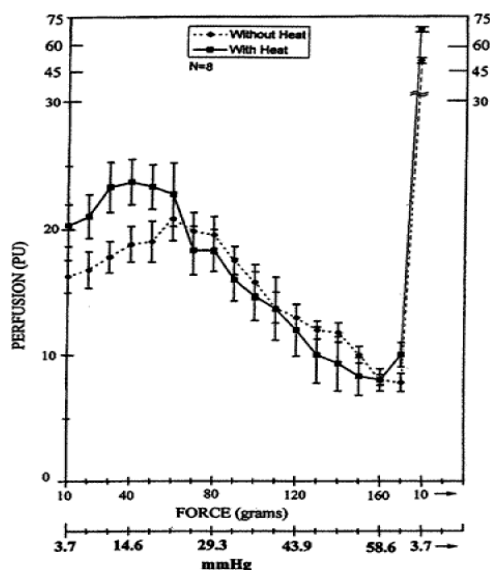
Figure 3 - 9 Changes in skin perfusion with an increase in skin surface pressure at 36 ℃ (with heat) and at 28 ℃ (without heat). It can be observed that the mean perfusion at the elevated temperature was only significantly greater for surface pressures in below of 18 mmHg (Patel et al., 1998).

Studies indicating an increase in local skin temperature caused by both pressure application (Mhanty and Romer, 1979) and the insulating effect of specific foam cushions and mattresses (Fisher et al., 1978) appear to confirm temperature as an important factor in pressure ulcer development. As an example, Figure 3-10 reveals that the nature of the support surface materials can influence the temporal changes of the interface temperatures. Cushioning materials which exhibit good thermal conductivity, such as water and gel, tend to dissipate heat, whereas materials exhibiting thermal insulation, such as foam, create a reservoir of heat energy leading to an elevated interface temperature (Ferguson-Pell et al., 1985). However, the data suggests that if continuously loading was extended beyond 2 hours, the temperature would increase for all interface materials.
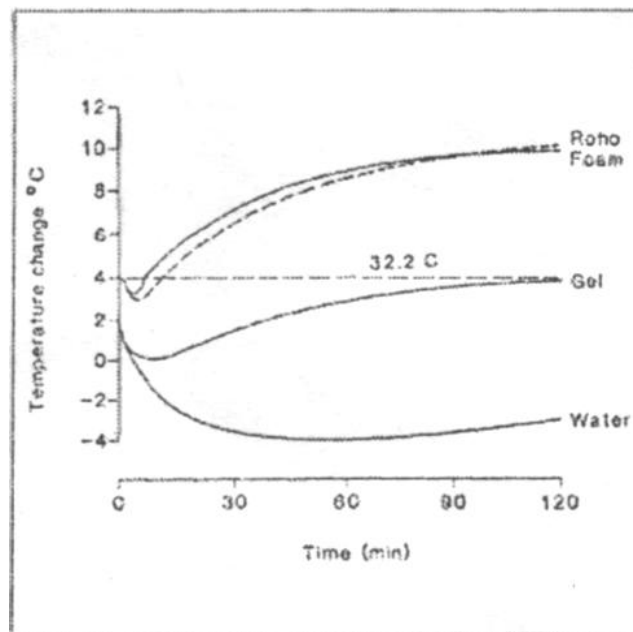
Figure 3 - 10 Changes in skin temperature at the interface of the ischium of able-bodied subjects
and various support surface materials for 2 hours (Ferguson-Pell et al., 1985).

3.4.2 Review of Influence of Moisture

As discussed in section 2.2.1, moisture is another extrinsic factor in the aetiology of
pressure ulcers which is important to regulate at the interface climate between the
patient and the support surface. The two main sources of moisture from the skin arise
from sweating and the other trans-epidermal processes, particularly water loss.
Altogether, moisture can have various implications on the integrity of implicated
tissues.

The excess moisture can lead to maceration of the epidermis, a precursor of tissue
breakdown, which is accelerated by an alkaline environment. Over hydration of the
skin due to the accumulation of moisture alters its properties. To quantify this
phenomenon, an in vitro experiment examined the response of isolated human
cadaveric stratum corneum specimens, from subjects aged between 78 and 88 years,
to differing humidity levels (Wua et al., 2006). This study reports that at 100%
relative humidity (RH) the energy to delaminate the stratum corneum is considerably
reduced to that estimated at 45% RH, particularly at a normal body temperature of

76

37 °C. This data is shown in Figure 3-11, which also indicates a reduction in peak stress in specimens tested at elevated humidity levels and temperature.
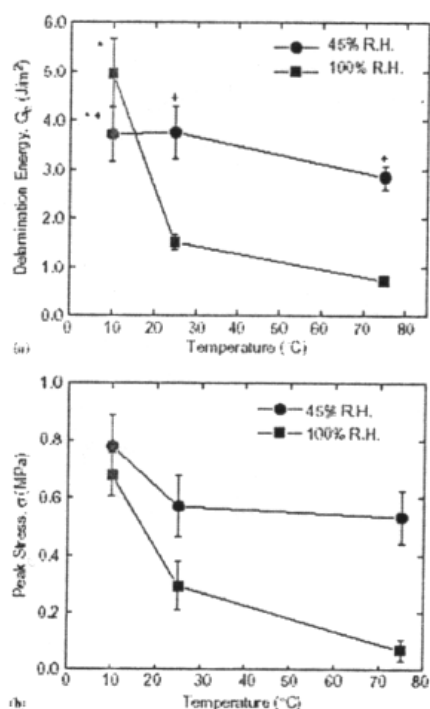
Figure 3 - 11 The effect of relative humidity with temperature on the a) delamination energy and b) peak stress for cadaveric stratum corneal specimens (Wua et al., 2006).

The presence of moisture on the interface can also increase the coefficient of friction between the patient and the support surface, which can effectively contribute towards the adhesion of the skin to the support surface. When this effect is coupled with prolonged pressure, it can cause intra-epidermal blisters and ultimately, superficial erosions (Dinsdale, 1974). The build up of moisture can also effect the surface environment of skin, which reduces the antibacterial properties of the epidermal layers and thus, can increase microbiological activity and the risk of infection in lesions (Sugarman, 1985).

3.4.3 Sweat and Evaporation

Moisture also affects the temperature at the interface which may, in turn, have subsequent effects within the tissue in terms of pressure ulcer risk. In one report, the

effects of different relative humidity on cooling were compared in Table 3-5.

Table 3 - 5 The effects of relative humidity on human body cooling in two separate scenarios (Berglund, 1998).

		Subject 1	Subject 2
Conditions	Relative Humidity of Atmosphere	50%	20%
	Atmospheric Temperature	24 ℃	24 ℃
	Body Clothing	0.6 (Clo *) (wearing trousers + long sleeve shirt)	0.6 (Clo *) (wearing trousers + long sleeve shirt)
	Resulting Evaporative Heat Loss	21 W	26 W

* Clo is a measure of thermal insulation of clothing material, where 1 Clo = 0.155 m^2kW (representing a subject wearing a business suit, whereas a. zero value for Clo corresponds to a naked person).

For general thermal comfort, example criteria for relative humidity is assumed to be 60% for "summer" and 40 % for "winter", and the acceptable range of operative temperature is in typical summer (cooling season) clothing (~ 0.5 clo) and typical winter (heating season) clothing (~ 1.0 clo) (ASHRAE Standard 55-92).

This effect basically exemplifies the phenomenon of evaporative heat loss from sweat evaporation. It can be assumed that decreasing the humidity promotes evaporation, resulting in a reduction on the temperature at the skin surface. This can be further quantified in the following equation (based on Johnson, 1991):

$$q_{evap} = h_d A (\omega_{sat} - \omega_a) H \qquad \text{Equation 3-2}$$

where: q_{evap} = evaporative heat loss, Nm/s

h_d = convection vapour transfer coefficient, kg/(m^2s)

This can be determined from:

$$Le = \frac{h_c}{h_d c} \qquad \text{Equation 3-3}$$

where: Le   = Lewis number, which is a dimensionless constant.

         h_c = heat conductivity, $Nm/(m^2s^oC)$

         C   = specific heat capactity of air at constant pressure, $Nm/(kg\ ^oC)$,

derived from:

$$c = 1000 + 1880 \left(\frac{\omega_{sat} + \omega_a}{2} \right) \qquad \text{Equation 3-4}$$

where: A   = body surface area, m^3

         ω_{sat} = humidity ratio of air saturated at body temperature

         ω_a = humidity ratio of surrounding air, kg H_2O / kg dry air

         H   = latent heat of vaporization of water at body surface temperature,

             Nm / kg, determined from:

$$H = 2.502 \text{ x } 10^6 - 2.376 \text{ x } 10^3 \theta \qquad \text{Equation 3-5}$$

This relationship applies for temperatures between 0° C and 50° C.

Alternatively the following hybrid relationship for evaporative heat loss can be employed

$$q_{evap} = h_v A (p_{sat} - p_a) \qquad \text{Equation 3-6}$$

Where, the additional parameters represent

         p_{sat} = partial pressure of water vapour at the skin surface, N / m^2

         P_a = partial pressure of water vapour in the surrounding air, N / m^2

         h_v = heat transfer coefficient for evaporation, m / s

3.5 Solutions for Support Surfaces

In chapter 2, several parameters were highlighted which have been implicated in the development of soft tissue breakdown. The most important factor was identified as the application of forces to the soft tissues which can lead to occlusion of the blood vessels causing ischaemia, reduction in available oxygen and an accumulation of

waste products.

To prevent pressure ulcers and allow the healing process to begin, pressure must be removed from the wound site to permit local tissue perfusion and oxygenation to occur (Seiler and Stahelin, 1986). Pressures can be relieved by regular turning of the patient by nursing staff. However, this is a very time consuming and intensive use of valuable nursing resources, which may not always be available. An efficient way to prevent or manage ulcers is to provide specialised pressure reducing or relieving beds, mattresses, pads, chairs and cushions, collectively termed and known together as Patient Support Systems, that limit the mechanical effect of soft tissue distortion (Bain et al., 1999).

Pressure air mattress systems have been used for the treatment and prevention of pressure ulcers for many years. For example, the low-air-loss mattress system was first described in the medical literature nearly 40 years ago (Scales, 1971). The authors described the system incorporating a series of interconnected air chambers with a flexible, vapor-permeable film between the skin and the supported air. The principle of this system was to minimise the volume of air and the size of the inflation air pump compared to high-air-loss surfaces, thereby, achieving uniform load distribution to accommodate a range of body morphologies.

Since that time, there have been a large number of systems which have reached the market place, each with their own specific characteristics and construction methods. In general terms, a support surface can operate in two distinct ways in order to reduce the probability of developing a pressure ulcer. These are shown diagrammatically in Figure 3-12. Static systems are designed to minimise the interface pressure by increasing the contact area. Accordingly, continuous low pressure systems are designed to mould around the patient such that their weight is distributed to distribute their weight over a larger area (Cullum et al., 2001). This redistribution of pressure is

the aim of placing a patient on a special support surface which can mimic the action of hydrostatic pressure as the interface surface will 'flow' around the hard bony prominences. Alternatively, dynamic systems includs alternating air pressure systems includes alternating temporal profile of periods of high pressure followed by periods of low pressure. Such systems are designed to enable the return of blood flow (Swain and Bader, 2002). If pressure is redistributed over an extensive area of the body, the patient is less likely to develop ulcers.
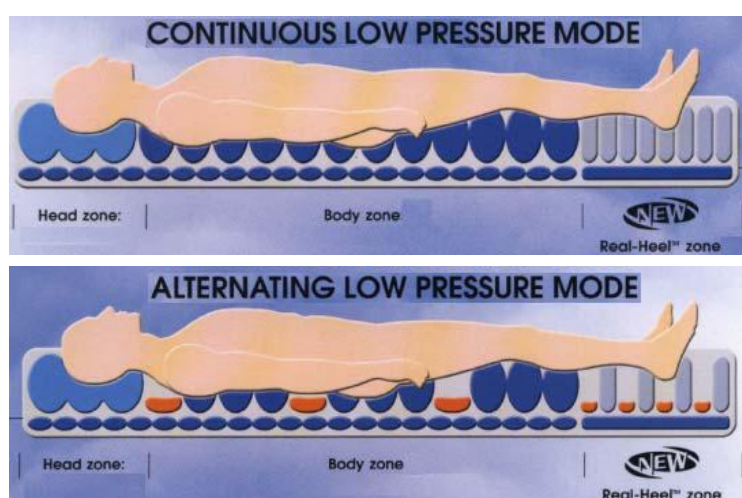
Figure 3 - 12 Schematic indicating Continuous Pressure Air Mattresses (above) and Alternating Pressure Air Mattresses (below) (Hill-Rom, Product Brochures, 2004).

3.5.1 Review of Alternating Pressure Air Mattress

There have been a significant number of studies which have utilised bioengineering measurement tools to assess normal volunteers and/or patients on wheelchair cushions. By contrast only a few corresponding studies have examined the effectiveness of mattress support systems.

The use of alternating pressure air mattress (APAM) to minimise the developmental risk of pressure ulcers is based on the premise that such systems, which are used in both hospital and community settings, reduce the effects of prolonged load bearing ischaemia on soft tissues. Indeed one large cohort study indicated that fewer patients

developed heel pressure ulcers on a commercial APAM compared to a control group on a viscoelastic foam mattress (Vanderwee et al., 2005). However, objective scientific evidence of their effectiveness is sparse in the literature. As a consequence, the design and manufacture of APAM have been influenced by practical issues, such as characteristics of the incorporated pumps, as opposed to considerations related to tissue viability or status. Of the few relevant studies, Rithalia and Gonsalkorale (2000) showed that with a group of normal volunteers a low profile APAM system retained transcutaneous oxygen levels closer to unloaded basal values, in conjunction with interface pressures which were generally maintained below 30 mmHg. In addition, the T_cPCO_2 levels were between 35-45 mmHg (4.7 − 6.0 kPa) throughout the mattress cycles which are values considered to be within the normal range (Bogie et al., 1995; Knight et al., 2001). In a separate study, the effects of full pressure relief compared to partial relief were evaluated by monitoring skin blood perfusion in the heel of normal volunteers supported by an air cell of an experimental mattress (Mayrovitz et al., 2002). Their findings revealed that with normal healthy subjects the degree of pressure relief was important in determining the level of skin perfusion. As an example, mean perfusion levels were enhanced with full pressure relief at the heel, as illustrated in Figure 3-13. However, the authors suggest that the impact of pressure-relief cycles may be different for patients with diminished hyperemic reserve. Another study was also carried out to determine the effects of pressure-relieving characteristics of two different designs of APAM system using both transcutaneous gas tension and laser Doppler flow-metry on the sacrum, heels, trochanters and buttock (Rithalia, 2004). This study found during the deflation phase of the cycle, contact pressures on the heel was significantly lower on the device whose inflation pressure was significantly higher. The result suggests that it is important to recognise that low APs are not necessarily associated with reduced IPs under the heel. Subsequently, Goossens and Rithalia (Goossens and Rithalia, 2008) investigated the performance of three APAM using pressure relief index (PRI) and blood perfusion measurements for subjects with a range of variously varying morphologies, as

measured by their Body Mass Index (BMI). Their findings report a statistically significant change in minimum interface pressure, pressure relief index and cycle time in dynamic mattress, but no statistically significant difference in maximum interface pressure for the three mattresses.

In a recent study (Liao et al., 2010), it was noted that using LDF the characteristic non-linear properties of blood flow oscillations may prove useful as an index for assessing risk of pressure-induced damage. The authors observed some decrease in these properties as measured at the sacrum in the elderly subjects with well established vascular impairment. Jan et al., (2011) also exammed on sacral skin perfusion under alternating or constant pressures profile in people with SCI. The results showed that pressure pattern affects skin perfusion responses in weight-bearing tissues. In particular, there was an increase in skin perfusion with alternating pressure when compared with SCI patients supported at constant pressure. Additionally there was no overall difference in the skin perfusion responses of patients with SCI as compared with non-SCI patients. This finding supports the concept of using alternating pressure technology to enhance skin perfusion, which may reduce the risk for pressure ulcers.
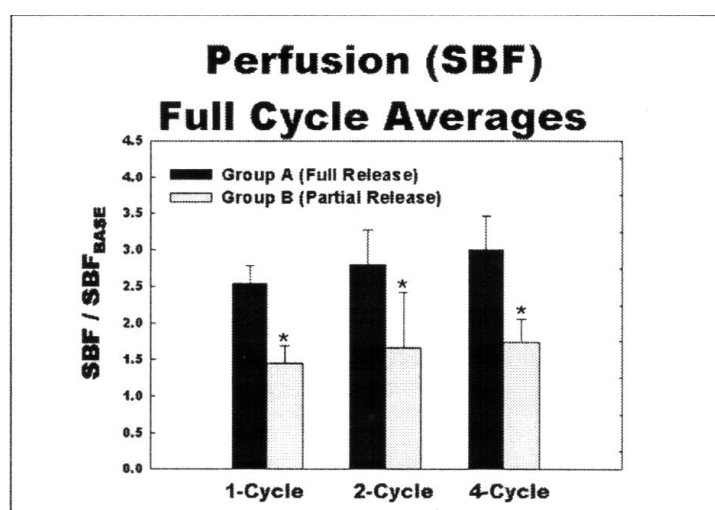
Figure 3 - 13 Tissue response, in terms of the ratio of skin blood flow (SBF) normalised to basal levels, as a result of full pressurisation and pressure-relief cycles at the heel (Mayrovitz et al., 2002).

3.6 Aim and Objectives

Aim

Early detection and prevention of pressure ulcers in patients at risk is acknowledged as a significant clinical and technical challenge. As discussed in the literature review, specialised support surfaces generically provide pressure reduction either, by distributing body interface pressure over a larger area, or pressure relief via the redistribution of pressure for prescribed periods of time, in order to minimise the risk of developing pressure ulcers.

The aim of this thesis was to examine the ability of APAM systems to control the loaded microclimate and to maintain the tissue viability in the sacrum of normal healthy volunteers supported in a supine position for prolonged periods.

Objectives

- To develop a range of measurement techniques to monitor interface temperature, humidity, pressure and tissue viability at the loaded support surface,

- To develop a system to control the internal alternating pressure to a set of prescribed values,

- To evaluate an in-built sensor which controls the internal pressures based on subject morphology,

- To monitor the microclimate at a loaded interface of a body analogue following the inclusion of different levels of moisture as created by simulated sweat rates,

- To develop a simple computational model, based on moisture vapour and heat transport, to predict the temporal profiles of temperature and humidity at the loaded interface,

- To evaluate research findings in the light of preventative strategies for those individuals at risk of developing pressure ulcer.

Chapter 4

System design and measurements at the loaded support interface

Before describing the individual studies, a number of measurement systems needed to be developed. These included a system which would control the pressure profiles within an APAM system, as well as an array of sensors which can monitor the microclimate at the loaded support surface. The development and performance of these systems are discussed in the present chapter.

4.1 Pneumatic Manager

4.1.1 Requirements of the Test Rig

The current commercial mattresses systems only offer a simple alternative air pressure signatory. This has provided motivation for the present work designed to manipulate the pressure signature within a support surface. Hence, a product requirement document (PRD) was established (Table 4-1) in order to identify the features which are necessary in the final design.

4.1.2 Concept Generation and Evaluation

4.1.2.1 Concept Generation Phase

The general concept involved a manipulative system, which interlinked each cushion of the support surface to four individual groups with a single air line supplied by an

Table 4 - 1 Product requirements document (PRD) for the pressure manipulation device.

Requirement	High Priority	Low Priority	Default
The device must be able to regulate pressure			X
The device must be fully manipulative to allow for the following			
Cycle profile (1:2, 1:4 alternating profiles), as show in Table 5-2	X		
Pressure difference (100/0, 60/40, 30/20), as show in Table 5-2	X		
Cycle period (3, 9, 15 min cycles), as show in Table 5-2	X		
Variation in the speed of inflation		X	
Variation in the speed of deflation		X	
Achieve various continuous low pressure modes		X	
Other functional requirements:			
The system must connect with other devices such as a computer, data logger	X		
The device should allow the monitoring of cushion pressure	X		
Cushion pressure measurements should be in real time		X	
The device should allow the monitoring of T_cPO_2 & T_cPCO_2	X		
T_cPO_2 & T_cPCO_2 measurement should be in real time		X	
The system should allow for an accuracy of 1mmHg		X	
The device should be easy to calibrate	X		
The device should ensure repeatability of tests	X		
The device shall operate on a standard AC supply			X
The device must be functional for at least 8000 cycles	X		
Manufacturing requirements:			
The device should cost no more than £1000 to construct	X		
The device should weigh no more than 10kg		X	
The device should be easy to manufacture		X	
End user requirements:			
The device shall conform to the UK Health and Safety legislations			X
The device should be easy to operate		X	
The device should be aesthetically plausible		X	
The device should be self contained		X	
The device shall be not pose a risk to the patient, operator and environment			X

air pump/compressor as the source. This will allow a minimum of 1:4 pressure cycle to be achieved where the length of cell inflation and deflation is controlled by timing switches, which regulate solenoid valves. Four other interconnections will extend from this supply line using a "T" junction. The pressure will be regulated using two pressure regulators, one situated on the supply line and the other incorporated into the common exhaust. The cell on/off will be controlled by the use of solenoid valves, which are to be programmed with the desired pressure cycle e.g. a 1:2 or a 1:4. The cycle period and profile can be controlled via the use of a logic controller. The speeds of both inflation and deflation phases can be set with the use of regulators.

4.1.2.2 Evaluation

The concept described in the above section is based on the use of a single air supply, as available on all support surfaces, which reduces the overall costs. In addition, it allows interface with other peripheral devices, such as the transcutaneous gas electrodes, intended for use in the subsequent study. This concept also has the potential of offering a continuous low pressure mode, which can prove useful when comparing with different commercial support systems incorporating a range of cushion geometries. The concept also provides a simple calibration system.

4.1.3 Final Concept Refinement

The concept refinement process specifically involved further detailing of the specific requirements. Most of the calculated and derived quantities were taken as benchmark values during component selection. In addition to the definition of these physical specifications, product costs and lead times were generated for projections, such as risk assessment.

4.1.3.1 Controller Characteristics

<u>Resolution</u>

It was important that the controller provides a fine regulation of pressures within the support surfaces. Commercial regulators generally provide a regulation of pounds per square inch (equivalent to approximately 50 mmHg). By contrast, the resolution for pressure regulation in the present system was required to be as low as 2 mmHg.

<u>Life time</u>

The controller was required to alternate pressure during normal operation. Accordingly its lifetime, in terms of cycles, was expected to reflect at least the number of cycles experienced during a series of experiments. This cycle life was calculated as follows:

Quantity of experiments per person = 20

Number of test subjects = 5

Running time = 1 hour

Fastest cycle time = 3 mins

Multiplication factor to accommodate trials, calibration and demonstrations = 4

$\therefore$ The # of cycles per hour = 60 mins / 3 mins = 20 cycles per hour

Also, the predicted minimum number of cycles

= 20 cycles/hour x 5 subjects x 20 experiments per person x 4 = 8000 cycles

This translates to a lifetime requirement on any of the regulators to be a minimum of 8000 cycles.

<u>Pressure range</u>

The pressure range manipulated by the regulators is dependent on the maximum and

minimum predicted values within the air cushions, which is, in part, influenced by the weight of the subject. As stated in the requirement (Table 4-1), the range of manipulation was expected to be at least from 0 - 100 mmHg. Additionally, the prescribed mattress pressures within the existing APAM was between 0 and 40 mmHg. Consequently, a pressure range between at least 0 to 100 mmHg satisfied both requirements.

Flow rates requirements

The requirements also specified the need to control the speeds of inflation / deflation which should, at the least, be equivalent to those available in commercial APAM systems. These minimum flow rates could be derived from the following calculations:
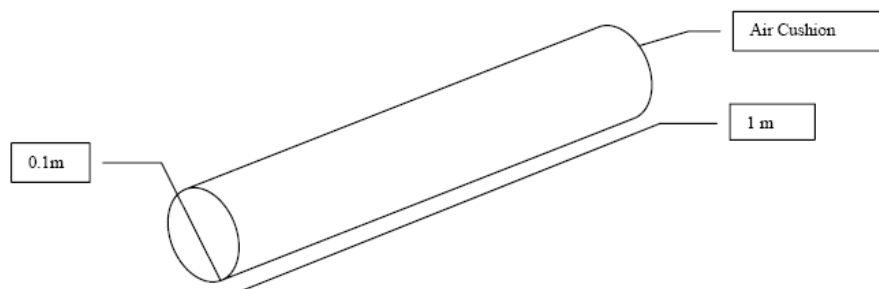
Figure 4 - 1 Dimensions of air cushion

With reference to the approximate dimensions of one of the air cushions shown in Figure 4 - 1, the maximum volume of the cell can be calculated as follows:

$$V \ = \ \pi r^2 h$$
$$= \ \pi \ x \ (0.05)^2 \ x \ 1 \ .0$$
$$= 0.01 m^3$$

Since there are a maximum of 3 air cushions in one state per group of 4

$\therefore$ the gross amount of air required to be exhausted or taken in

$$= 3 \ x \ V$$
$$= 0.03 m^3$$

Assuming a normal profile in which one of four cushions is deflated per cycle, termed 1/4 and a normal cycle time of 9 minutes

∴ Deflation time

$$= 1/4 \text{ x } 9 \text{ mins} = 2.25 \text{ mins} = 135 \text{ seconds}$$

∴ For the mattress to match this deflation time it should have at least a flow rate of at least

$$3V / 135 = 0.03 \text{ m}^3 / 135 \text{ sec} = 2.22 \text{ x } 10^{-4} \text{ m}^3/\text{second}$$

$$= 2.22 \text{ x } 10^{-4} \text{ m}^3/\text{second x } 3600\text{second/hour}$$

$$= 0.8 \text{ m}^3/\text{hr}$$

To accommodate a safety factor of 3.75, this translates to a minimum flow rate of the order of 3 m^3/hour. This flow rate will determine the selection of both the air supply and the pneumatic components, such as regulators, hoses, fittings etc.

Time resolution

The time switches are required to change between "on" and "off" states and vice versa at preset times determined by the cycle requirements. For the most part, a time resolution of 60 seconds would seem to be appropriate. Furthermore there is an implied requirement for total synchronization switching between time switches.

4.1.3.2 Data Logger – Sampling Rates

The sampling rates of a chosen data logger system are required to be sufficiently high to ensure the acquisition of uniformly spaced samples to show real trends in data as detailed in Table 4-1. Thus the sampling rate must accommodate the variations within the recorded data.

Pressure sensors

Maximum predicted rate of change of pressure = 100 mmHg in 20 seconds*

*where 20 seconds is the predicted time to achieve the maximum rate of deflation / inflation.

To represent this inflation / deflation profile, a minimum of 5 data points is required.

Thus the required data acquisition rate = 5 data points / 20 seconds or 0.25 Hz

Transcutaneous gas tensions

Assuming transcutaneous oxygen and carbon dioxide levels generally follow the support pressure profile, a similar acquisition rate of 0.25 Hz is required.
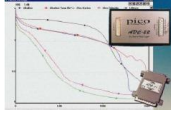
Input channels

It is required for the data logger to synchronize data from the 4 cushion pressure sensors, as well as the transcutaneous gas monitor. This required the device to have a minimum of 6 input channels for capturing data.

4.1.3.3 Individual Components

The process of selection of components and materials relative to the optimally derived specifications was performed in a systematic manner. Each of the components which met the required specifications are listed and briefly detailed in Table 4-2.

Table 4 - 2 Regulator for inflation / deflation of air pressure in mattress

Components		Description
Pressure regulator for inflation / deflation of mattress		Provides a quoted sensitivity of 6.3 mm water (equivalent to 0.463 mmHg) and an ability to maintain constant pressure at varying flow rates. (Control air Type 700 pressure regulator, hycontrol Ltd, Worcestershire, UK)
Solenoid Valves		Compatible with the pressure regulators. (Series 141, hycontrol Ltd, Worcestershire, UK)
Time switches		Provides automatic synchronization, unlimited variability in cycle period and profile (½ or ¼). The programmable unit minimizes experimental setup time and offers variation in experimental configuration. (Crouzet Millennium 2 plus, RS Components Ltd, Northants, UK)
Data logger		Matches the minimum requirements of sampling rates. (Model: ADC 11/10, Pico Technology Ltd, Cambridge shire, UK)
Pressure sensors		It offers better accuracy and "out of the box" usage with its conditioning circuit pre installed and verified. (Honeywell, 40PC Series, RS Components Ltd, Northants, UK)

4.1.4 System Design

4.1.4.1 Program Detail

Pneumatic circuit

The Pneumatic Circuit of the Pneumatic Manager as illustrated in Figure 4-2 was designed to interlink each air cell of the APAM support surface with a single air supply. This will allow a minimum of 1:4 pressure cycles to be achieved, where the length of cell inflation and deflation is controlled by timing switches which regulates

the solenoid valves. Additionally, there was a common exhaust line with a regulator linking all cells together and thus controlling the deflation pressure of the cushions.
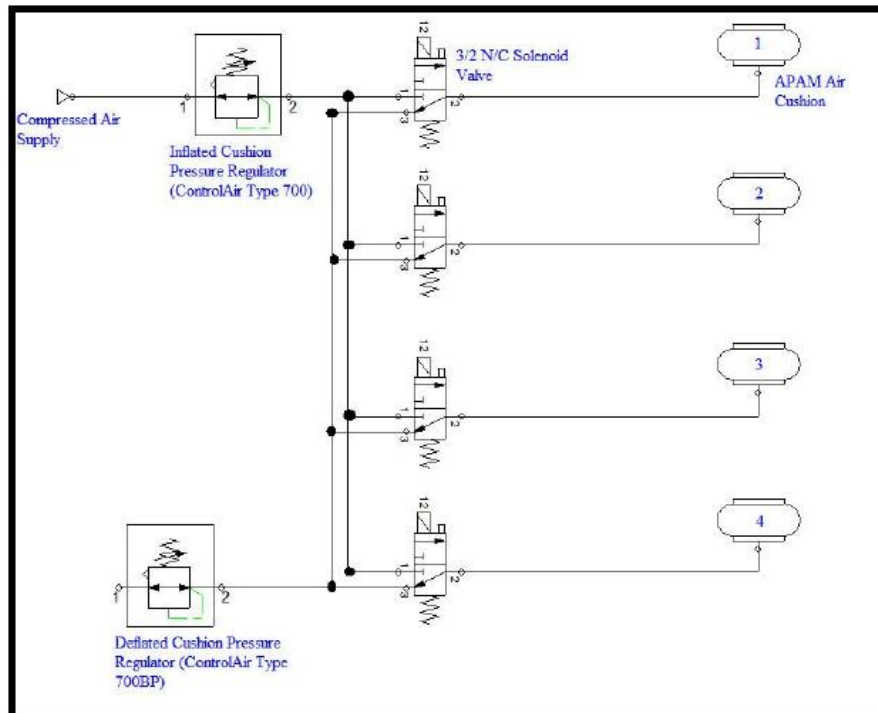
Figure 4 - 2 Pneumatic Circuit of the Pneumatic manager. A single air source supplying the cushions of the support surface with a common exhaust line, logic controller and four solenoid valves allows variation pressure configurations.

Logic controller

The logic controller contained both a cyclic timer block function (indicated in orange in Figure 4-3 and Figure 4-4) and a cam block function (indicated in blue). The former program prescribes the period at which a particular cam stage is maintained, where the latter details the profile (1:2 or 1:4) arrangement for each stage for the solenoid valves. Overall, the timer function block advances the cam one stage at a time coincident with the elapse of the presented deflation period. Each change in the cam stage brings about a new array of states for the solenoids. Consequently, depending on the states at each solenoid, the respective air cushions can be deflated (deactivated state) or inflated (activated state).
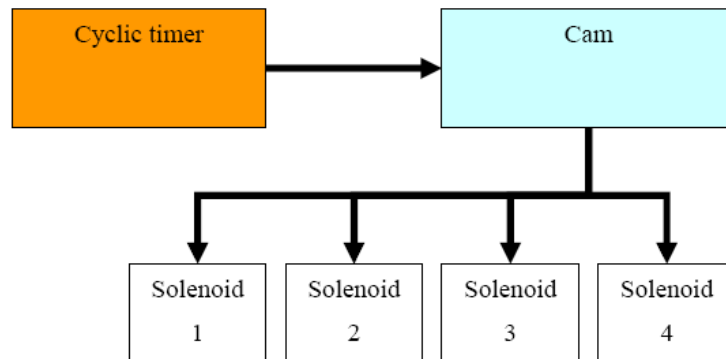
Figure 4 - 3 Layout of the Logic controller function for the Pneumatic manager.
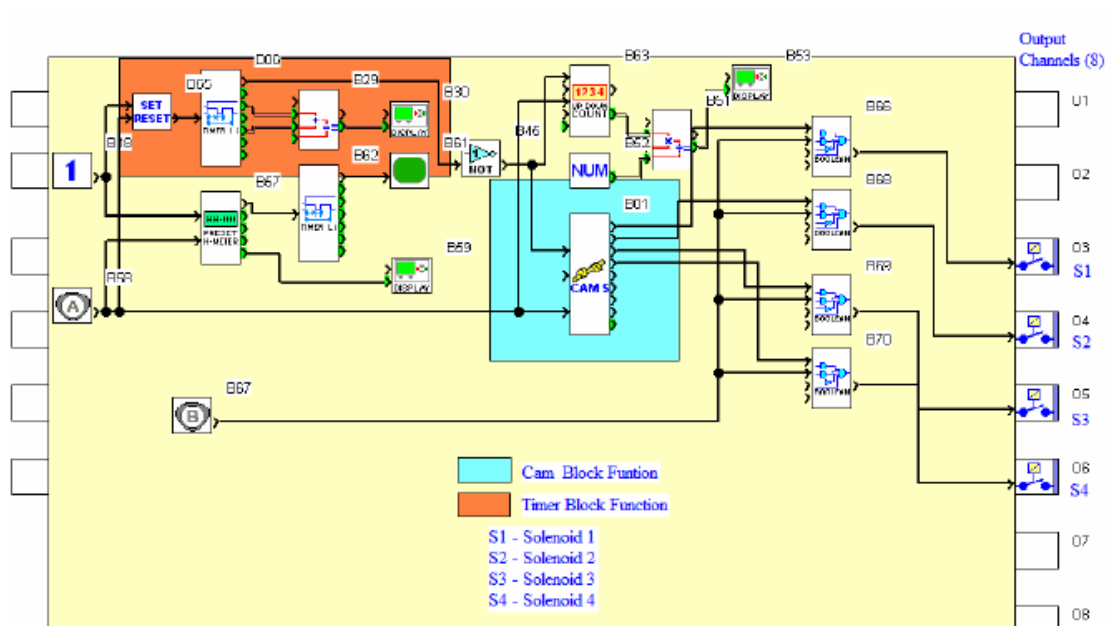
Figure 4 - 4 Actual logic controller program layout for the Pneumatic manager via the Crouzet's proprietary interface.

4.1.4.2 Hardware

1. After the main parts were acquired, manufacture of the controller commenced. This was initiated by the preparation of a standard 30 x 30 cm electrical controller box with some standard circular holes drilling for placement of parts.

2. Subsequently, the controller was assembled as illustrated in Figure 4-5. This involved mainly part fitting and making connections with pneumatic hose and fittings. The Pneumatic circuit was configured as shown in Figure 4-2.

3. Electrical circuits for the controller were designed by Olav Sadoo a medical engineering student in the host department. After assembly, the electrical circuitry was configured as shown in Appendix A (Figure A-1 and A-2). The controller was subsequently certified to the necessary standards (*PAT1000S* tested as prescribed by the *UK Electricity at Work Regulations 1989*) by a certified technician (Danny Nightingale, Department of Engineering).
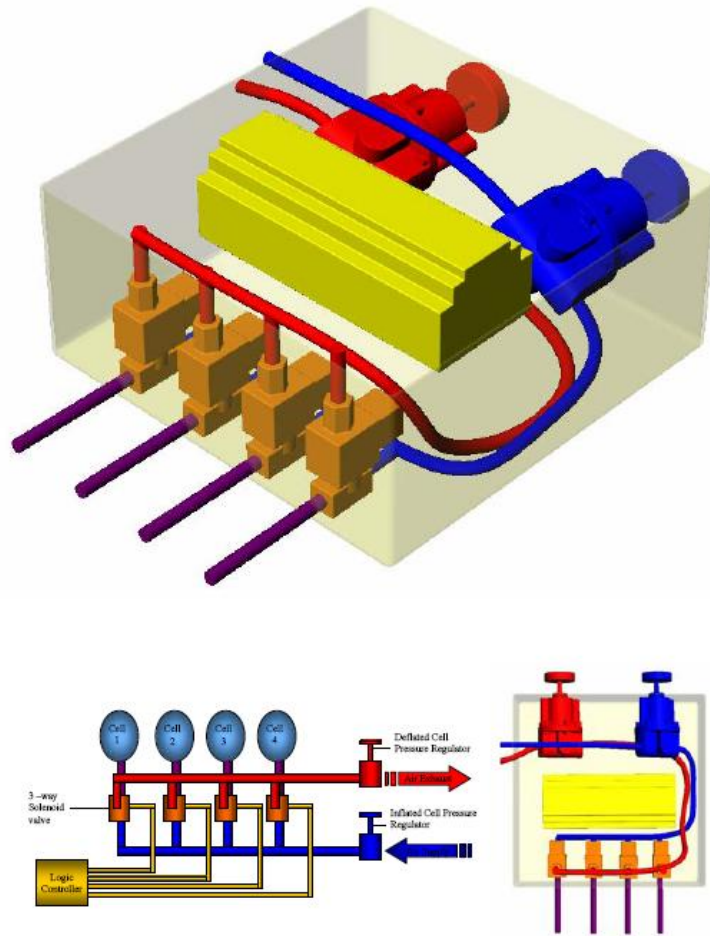
Figure 4 - 5 General assembly of the Pneumatic Manager for APAM.

4.1.4.3 Software

The function of the controller required a program to be viable. Through this program, the controller was required to manipulate the following:

1. Activation and deactivation time periods of the pneumatic solenoid valves as described in the PRD in Table 4-1. Practically in the program, this was achieved through the use of a functional block which starts with a timer function which operated by switching its outputs between on and off and vice versa at user-defined time intervals. The time intervals were chosen to match the period of deflation associated with the prescribed cycle configuration. This is shown graphically in Figure 4-6.
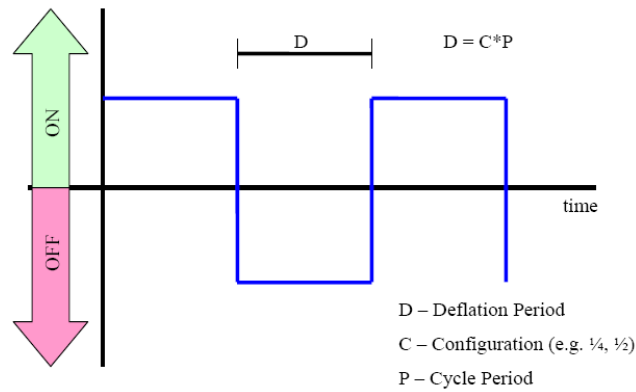
Figure 4 - 6 timer Function Block: Produces output (on/off) at time intervals of D (user defined).

2. Synchronization of the individual activation and deactivation cycles of the solenoid valves. i.e. manipulating either of the two profiles, 1:4 and 1:2. Practically, this was achieved through a cam function which operated by changing the cam stage when its input switches between "on" and "off" states. At each cam stage, the specific output for each individual solenoid was specified. The cam settings were defined as follows for both a 1:4 and a 1:2 profile (Table 4-3). Furthermore, a reset function after stage 4 of the cam was employed to simulate cyclic conditions of the APAM.

Table 4 - 3 Cam settings for the 1 : 4 and a 1 : 2 profile configuration.

Cam Stage	Output 1 : 4				Output 1 : 2			
	Solenoid 1	Solenoid 2	Solenoid 3	Solenoid 4	Solenoid 1	Solenoid 2	Solenoid 3	Solenoid 4
1	0	1	1	1	0	1	0	1
2	1	0	1	1	1	0	1	0
3	1	1	0	1	0	1	0	1
4	1	1	1	0	1	0	1	0

Key	Deactivated	0
	Activated	1

4.1.5 Functional and Performance Testing

Subsequent to the completion of the manufacture of the Pneumatic Manager, the system needed to undergo further performance tests to check its electrical connection and output. The following two tests were performed.

I. Calibration Tests

The transducers were linked with the data logger to a PC, which allowed real time monitoring of pressure. The voltage output of the each transducer was calibrated with known pressure readings through the use of a sphygmomanometer, for pressures ranging from 0-120 mmHg, to accommodate the working range of the APAM system. Results, as illustrated in Figure 4-7, showed significant linearity for each of the four pressure transducers.
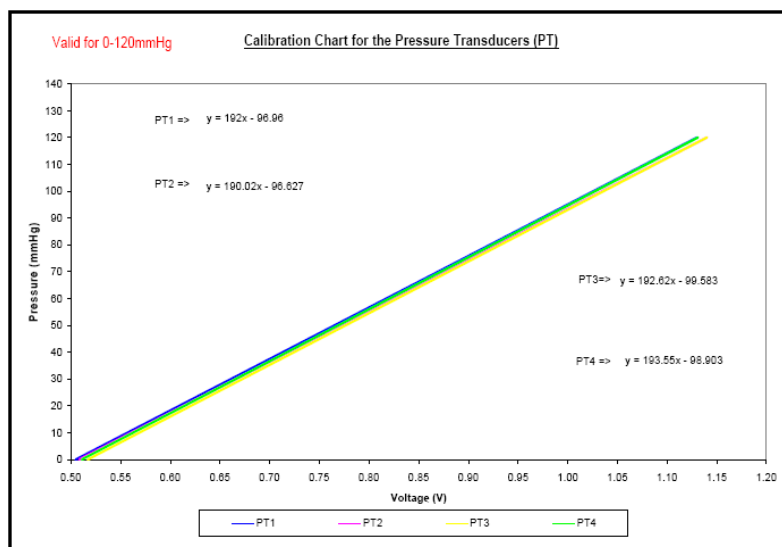
Figure 4 - 7 Calibration chart for the four pressure transducers which, allows conversion of voltage into pressure. This chart is valid for a pressure range of 0-120 mmHg.

II. Operational and Pressure Leak Testing

The controller, Pneumatic Manager, was tested for functionality by running the device under full operational conditions. The device was programmed to run on two default pressure profiles namely 1:4 and 1:2. The data as illustrated in Figure 4-8 revealed some perturbations when the pressure amplitude was at a maximum of 100/0 mmHg. In particular for both pressure profiles, the low pressure phase included some transients about a mean pressure of approximately 2 mmHg. In addition with the pressure profile of 1:4 only, there are two periodic transient decreases of approximately 30% from the maximum pressure of 100 mmHg. These represent a consistent feature of the Pneumatic manager system.
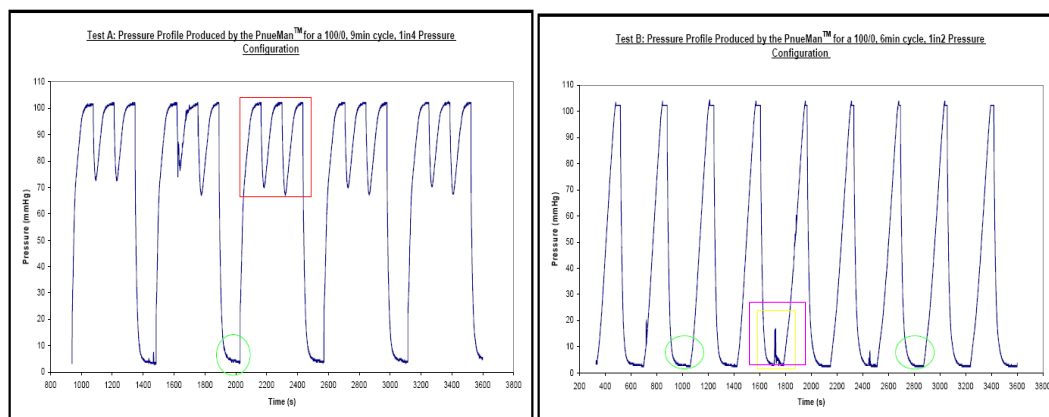
Figure 4 - 8 General pressure profile observed in a 1:4 (left) and 1:2 (right) alternating sequence of a support surface at pressure amplitude of 100/0 mmHg.

> The red square highlights the equilibration period of the system, which starts as soon as a cell deflates.
> The green circle indicates some pressure still remains once a cell becomes completed deflated, which is expected.
> The purple box highlights an area of sudden fluctuation which is a result of movement on the support surface.

4.2 Interface Humidity and Temperature Measurements

4.2.1 Requirements of the Test Rig

There was also a requirement for monitoring the microclimate at the loaded support interface. In particular, products requirements for the measurement of both temperature and humidity in the form of a product requirement document, summarized in Table 4-4.

4.2.2 Data Logger

The outputs from each of the temperature and humidity sensors, in synchronised form, would be connected by cable to a data logger. The data would then be displayed on a computer screen.

The sampling rates of a chosen data logger system are required to be adequately sensitive to the trends in the data. This translates into a sampling rate, which is dependent on the frequency of variation of the recorded data and necessarily the appropriate storage space. Although the duration of any experiment can extend to 2 hours, it is conceivable that humidity levels can increase from basal levels to saturation values of 100% RH in 30 minutes. Thus it is assumed that a minimum of 60 data points is required to adequately represent this variation, then the required sensitivity is as follows:

$$60 \text{ data points}/ 30 \text{ mins} = 1 \text{ data point every 30 seconds}$$
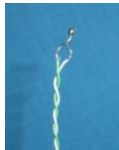
Table 4 - 4 Product requirements document (PRD) for humidity and temperature sensors to be used at a loaded support interface.

Requirement	High Priority	Low Priority	Default
The sensor must be able to obtain humidity & temperature value			X
The sensor functional requirements:			
The system must connect with other devices such as a data logger and a computer	X		
The sensor should allow the monitoring interface humidity & temperature	X		
Interface humidity & temperature measurements should be in real time		X	
The sensor should allow for a accuracy of pressure as 1mmHg		X	
The device should be easy to calibrate	X		
The device should allow for repeatability of tests	X		
The device shall operate on a standard AC supply			X
The device must include a minimum of 4 humidity and 4 temperature sensors	X		
Manufacturing requirements:			
The device should cost no more than £500 to construct	X		
The device should weigh no more than 10 kg		X	
The device should be easy to manufacture		X	
End user requirements:			
The device shall conform to the UK Health and Safety legislations			X
The device should be easy to operate		X	
The device should be aesthetically plausible		X	
The device should be self contained		X	
The device shall be not pose any risk to the patient, operator and environment			X

4.2.3 Individual Components

Individual components were sourced and selected dependent on the PRD form. A summary of these components is presented in Table 4-5, which also provides a brief description of each.

Table 4 - 5 Regulators for interface humidity and temperature sensor

Materials		Description
Humidity probes		Absorption-based humidity sensors provide %RH (Relative Humidity) outputs. Sensor laser trimming offers +5% RH accuracy and achieves 2%RH accuracy with calibration. (Honeywell, part no. HIH-4000-001, RS Components Ltd, Northants, UK)
Temperature Probes		The temperature sensor has special shape because made by thermocouples. The size of the sensor is 8mm (length), 3.5 mm (width), and diameter for head of thermocouple is 1.5 mm. (Manufacturer by technician at QMUL)
Humidity data logger		Accuracy: 0.1% ($\pm$39 mV to 1250 mV range), 0.2% ($\pm$2500 mV range) (Model: ADC-24, Pico Technology Ltd, Cambridgeshire, UK)
Temperature data logger		Conversion time: 100 ms (thermocouple and cold junction compensation) Temperature accuracy: Sum of ±0.2 % of reading and ±0.5 ℃ (TC-08 Thermocouple Data Logger, Pico Technology Ltd, Cambridgeshire, UK)

4.2.4 Manufacture of Integrated Components

The humidity probe was created by housing the specified humidity sensors in perforated stainless steel cages, as indicated in Figure 4-9. These cages provided a buffer environment within which the sensor can operate, as well as providing

structural protection for the fragile chip type humidity probes. The protective cage, which also contained a thermocouple for real-time temperature measurements, was of dimensions 40 x 10 x 5 mm. The real time temperature measurements facilitated the correction of humidity readings, based on a calculation of temperature compensation, as dictated by the manufacturers.
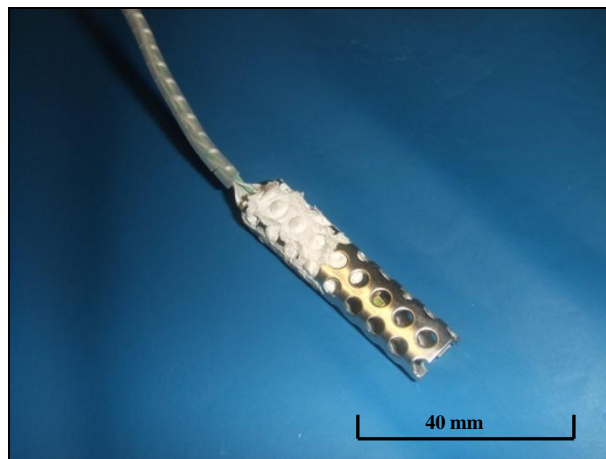
Figure 4 - 9 Photo of the specified humidity and temperature sensors in perforated stainless steel cages

All results from the humidity sensors were captured by the Pico Data Logger (Model ADC - 24). To accommodate the output range of the humidity sensors powered with 5V a potential divider was used to scale down output voltage to within the "±2.5 V" input range of the data logger, as indicated in Table 4-5. Potential divider employed for scaling the analogue output of each humidity sensor to the data logger, which was illustrated in Figure 4-10. Therefore, an the equation to calculate Relative Humidity is given as

$$V_{out} = \frac{56+10}{10} \times V_{reading} = 6.6 \times V_{read}$$

And each humidity sensor was calibration before use, so individual sensor calibration data was available.

i.e. sensor 1 calculated valued at 5V: V_{out} at 0%=0.801   at 75.3%=3.083

So $$RH\%(sensor"1") = \frac{0.753 \times (6.6 \times \frac{V_{reading}}{1000})}{3.083}$$
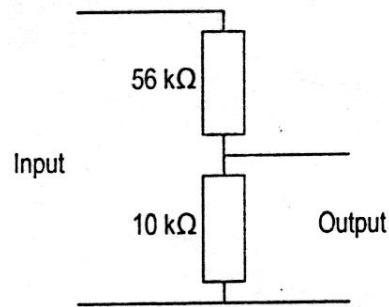
Figure 4 - 10 Potential divider employed for scaling the analogue output of each humidity sensor to the data logger.

4.2.5 Functional and Performance Test

Both the humidity and temperature sensors needed to be calibrated for each experimental test. This was accomplished by comparing the experimental humidity/temperature reading over time with a standard available in the market. A secondary humidity/temperature sensor (hygrometer) was used to compare the environment humidity and temperature to ensure consistency. The test arrangement included:

- RS 3-display indoor/outdoor thermometer clock
- Type-LCD triple display
- Max/Min temperature measurement   +70 / -50 ℃

A simple method was utilised. Both the digital sensor, test sensor and a graduated beaker were placed in a sealed transparent container with two temperature sensors placed outside the beaker and two humidity sensors placed on the beaker at same level, as indicated in Figure 4-11. During the calibration, the beaker was filled with 100 ml of water at different temperature ranging between 20° C to 45° C in 5° C increments.

Reading was taken and a mean value estimated for a repeat of six measurements. Figure 4-12 presents the individual findings for temperature and humidity sensors over the same time period. For each pair of sensors the variability of measurement was relatively small. For corresponding water temperature, the design sensors for both temperature and humidity were slightly higher than the control sensors. For example at a water temperature of 35°C, the design sensor recorded a RH of 53%, and the control sensor recorded 51% RH, as highlighted in Figure 4-12 (right). Nonetheless, uniform trends were observed between both sets of sensors with temperature.

In addition, the standard deviation show high stability for both temperature and humidity sensor. Thereby the calibration of the manufacturing sensor can be determined to be relatively reliable.
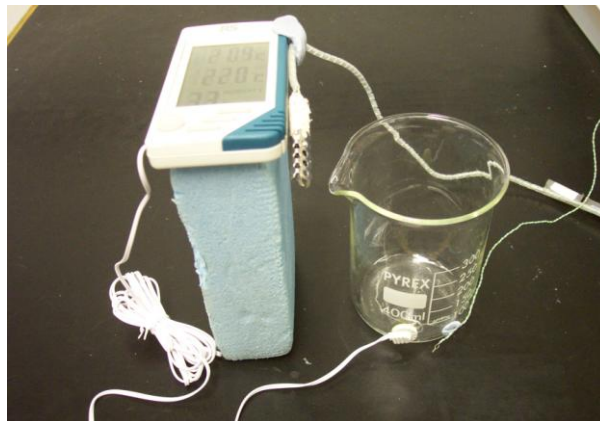
Figure 4 - 11 Photo of calibrate the humidity and temperature sensors.
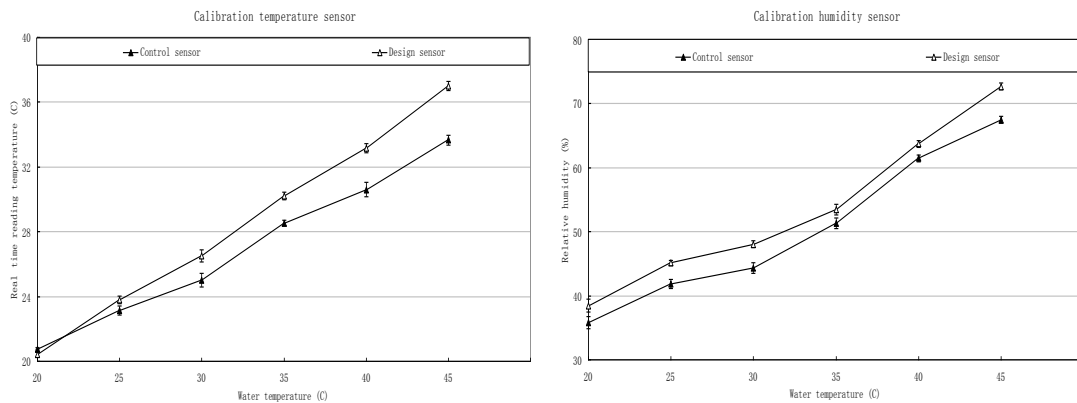
Figure 4 - 12 Calibration temperature (left) and humidity (right) sensor graph. Values represent mean $\pm$ SD.

Chapter 5

Physiological Response of Soft Tissues to a Variety of Controlled Pressure Profiles using an APAM Support Surface

There is considerable variation in the pressure profiles adopted by companies, who had developed APAM systems. These are often determined by practical issues, such as the characteristics of the incorporated pumps, as opposed to considerations related to maintaining tissue viability or status of the supported individual. Indeed only a few studies have evaluated the various components which determine the appropriate pressure signature associated with APAM systems. These have been described in section 3.5.1. This paucity of literature provides motivation for the present study, which addresses the important question whether there is an optimal internal pressure signature, which maintains tissue viability/status of subjects supported on an APAM system. To address this a number of objectives need to be fulfilled including:

i)   The design of a versatile controller for a commercial APAM system (Model Duo 2, HillRom, France). This process has been fully detailed in Chapter 4,

ii)   The design of an experimental matrix, which enables a comparison of range of pressure profiles imposed on a small group of young healthy volunteers,

iii)   Utilize a range of established non-invasive techniques to determine the viability/status of soft tissues subjected to alternating pressure. These all represent established techniques, which have been detailed in Chapter 3.

5.1 Experimental Techniques

5.1.1 Interface Pressure Measurement

A description of the various commercial interface pressure monitoring systems, whose mode of operation was associated with a range of physical principles, was provided in Section 3.1. The commercial pneumatic system (TPM MK111, Talley Research, Romsey, UK) was employed in the present study. Its mode of operation and a physical image are illustrated in Figures 3-2; 3-3 and 3-4, respectively. A 96 cells matrix was used with individual cells, each of 20 mm diameter, spaced uniformly within a flexible PVC sheet, which was placed over each of the test surfaces. For the measurement of heel pressures, a single 3 x 4 matrix was used. During monitoring, results are displayed on a computer screen by special software, which was designated "Pressure Data Manager".

5.1.2 Sweat Measurement

As described in section 3.4, a number of researchers have analysed the content of metabolites and ionic substances in sweat, as a reflection of the biochemical processes in the underlying tissue, with the aim of providing markers of tissue status or viability. One of the most important features of the sweat collection technique is its use of a thin filter paper, as had been previously employed in the host laboratory (Polliack et al., 1993; Knight et al., 2001), which provides non-invasive collection with minimal distortion of the loaded body-support interface.

The sweat was collected using pure cellulose Whatman (1 Chr) chromatography paper (Whatman Paper Ltd., Maidstone, Kent, U.K.), which is 100 per cent cotton and has been specifically designed for clinical applications. The water retention per unit area of the paper was estimated to be 245.87 $\pm$ 5.2 g/m^2 (Polliack, 1994). This value is equivalent to a maximum retention of 391 mg for circular sweat pads of 45 mm diameter.

Two different shapes of sweat pad were employed (Figure 5-1). Either individual pads of 45 mm diameter, or annuli with inner and outer diameters of 16 and 45 mm, the latter shape to be used in concert with a transutaneous gas electrode, in an arrangement previously reported (Knight et al., 2001), as indicated in Figure 5-2 (top). Both pads were stored in 30 ml labelled screw-capped "Universal" conical bottomed tubes (cat.no 1288, Bibby Sterilin Ltd., Stone, U.K). The conical bottomed tubes also contained removable separators resting at the top of the conical portion, as illustrated in Figure 5-1. The plastic container has the benefits of transparency, impermeability to moisture and tight sealing. The separators consisted of caps from plastic tubes (cat. no. 71060, LIP Equipment and Services Ltd., Shipley, U.K.), through which seven 2 mm diameter holes were drilled (Figure 5-1). This arrangement was designed to separate the sweat pad from the eluted sweat.

Figure 5 - 1 Image of the materials used to collect and store sweat. From left to right, the screw-capped plastic 30 mL conical bottomed tube, separators with drilled holes, and both circular and annular shapes of sweat collection pad and polypropylene plastic film over the top during the measurement.

5.1.3 Interface Climate Assessment

Sensors were used for microclimate measurements at the subject-support interface, whose design, manufacture and performance are described in section 4.2. To review briefly, the humidity and temperature sensors were incorporated in two perforated

stainless steel cages, as illustrated in Figure 4-9; one was applied at the sacrum and the other at the heel, the latter of which is illustrated in Figure 5-2 (below). Outputs from the sensors were recorded by the data logger and displayed on a computer screen using special software namely "Picolog Recorder".
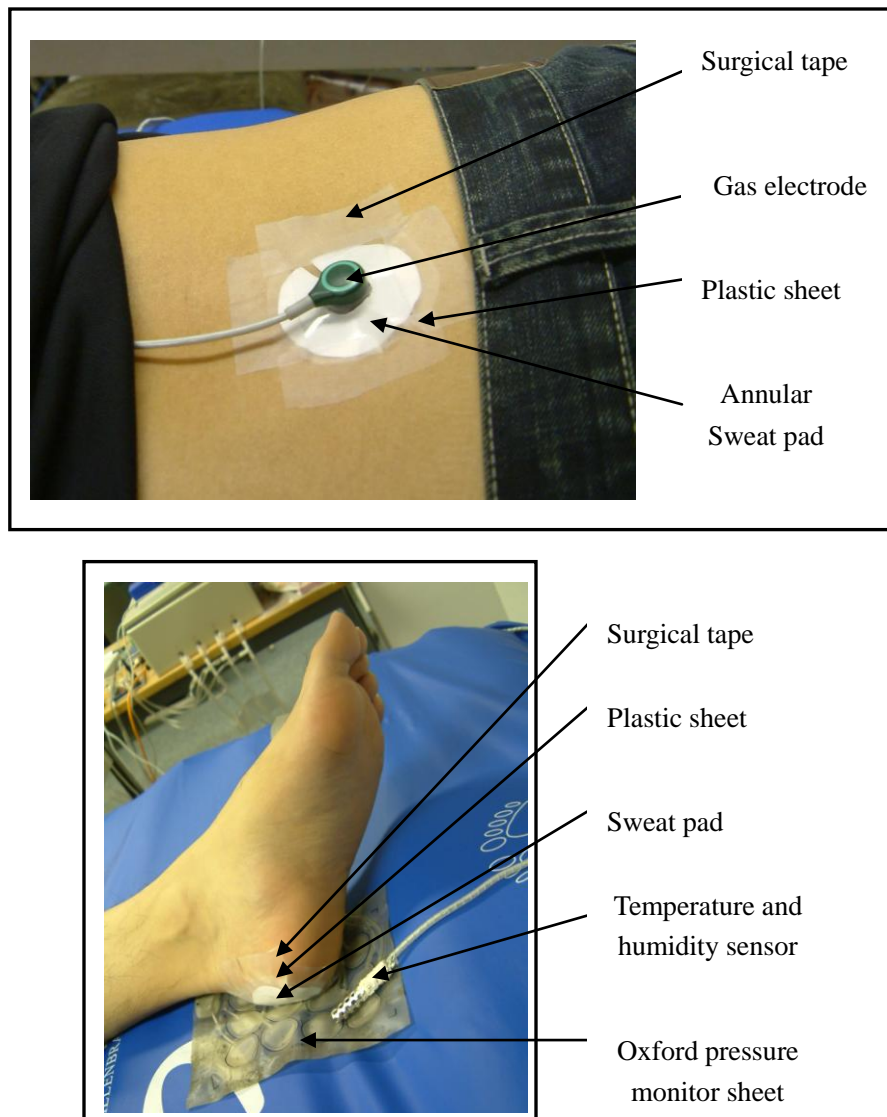
Figure 5 - 2 Images of location of sweat pads and gas sensor on sacrum (top) and sweat pads and humidity sensor on heel (below).

5.1.4 Transcutaneous Gas Tension Measurements

As discussed in section 3.2, transcutaneous monitoring of O_2 and CO_2 tension has been validated as a method of investigating tissue status both experimentally with

able-bodied subjects (Bader, 1990) and with at risk subjects (Bogie et al., 1992 and 1995). The technique is continuous and non-invasive and therefore fulfils some of the requirements of the ideal transducer at the loaded interface (Ferguson-Pell et al., 1988).

A combined oxygen and carbon dioxide electrode (Model D481) was used in conjunction with a transcutaneous blood gas tension monitor (Model TINA, Radiometer AS, Copenhagen, Denmark). This electrochemical method has been used in previous work in the host and other laboratories, to assess tissue viability or status in loaded soft tissues (Bader, 1990; Knight et al., 2001). These studies have reported that an electrode temperature of 44°C is generally considered to be adequate to produce maximal vasodilation in adults and hence provides a relative measure of oxygen and carbon dioxide tensions in skin tissues. Calibration of the system, using a standard gas composed of 5% CO_2 and 20.9% O_2 was undertaken before each measurement session, according to the guidelines prescribed by the manufacturer. The attachment site was cleaned, where the sensor was applied, and dried. The electrode is inserted onto a fixation ring, containing a volume of electrolyte, which is attached to the skin surface with double-sided tape (Figure 5-2). Once in position, an equilibration period is required to attain a steady state or basal value of both transcutaneous gases, typically between 60-80 mmHg for oxygen and 35-50 mmHg for carbon dioxide.

5.1.5 Support Surfaces

The alternating pressure air mattress (APAM) used in this study was a commercial system, Model Duo 2, loaned by the Research and Development Department of the manufacturer (HillRom, France). The system has a default operation in which the two distinct sets of cells along the long axis of the mattress are alternatively inflated and deflated. As a comparison a Continuous Low Pressure (CLP) air mattress (Primo [TM], HillRom, France) was tested. This system was designed to incorporate a low volume

of air uniformly filled in each cell of the mattress, which was maintained throughout the test. Both air mattresses were also compared with a standard King's Fund NHS foam mattress.
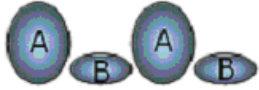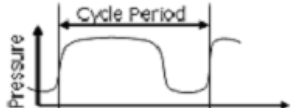
Table 5 - 1 Definition of APAM variables.

Variable	Definition
Pressure Amplitude	The difference between the internal air pressures in the inflated state with that in its deflated state.
Cell Profile	This describes the arrangement of inflated air cushions among deflated air cushions along a support surface. The fraction convention used (e.g. 1:2 or 1:4) details the occurrence of a deflated cushions along a support surface e.g. 1:4 means 1 in every 4 cushions are deflated at any stage of the cycle.
Cycle time or cycle period	An interval of time full accommodating the sequence of inflation and deflation of all the air cells in the mattress.

In the case of the APAM support systems, also referred to as active therapy support surfaces, the pressure application features can be defined by a number of variables. These are discussed in a recent consensus document (Tissue Viability Society, 2010). Their combination will determine the support afforded to the subject. It was decided in the present study to focus on the influence of three of the critical parameters, as defined in Table 5-1.

Table 5 - 2 Variability of Pressure configuration with APAM support surface.

APAM variable				Represent the various states
Pressure Amplitude / mmHg mmHg (mmHg)	100 / 0	60 / 40	30 / 20	
Profile	1:2	1:4		
Cycle Period / min	3	9	15	
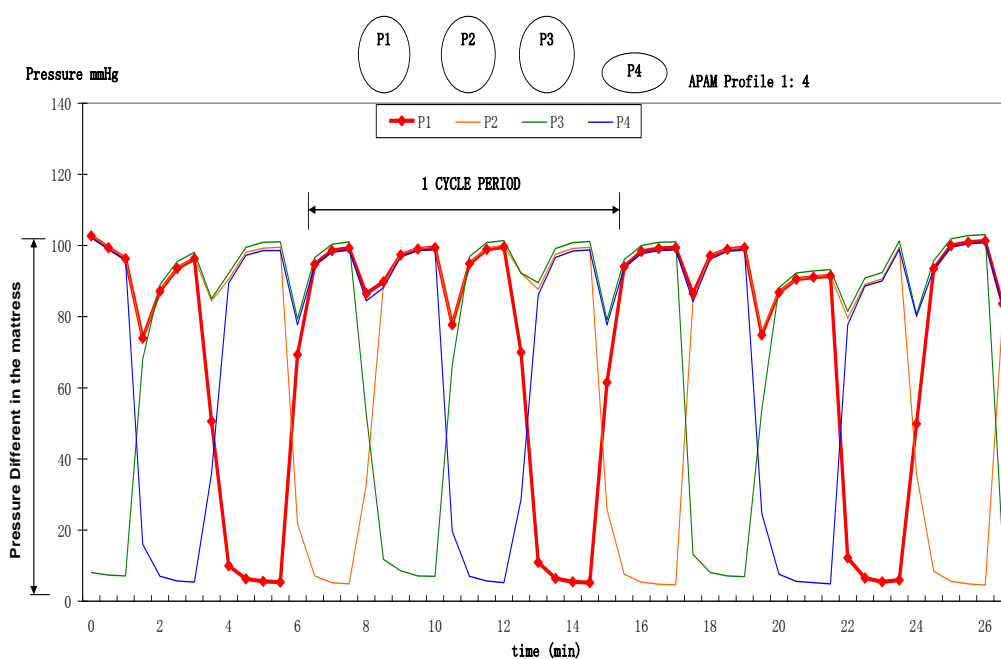
Figure 5 - 3 An example of the performance of the pressure controller in assessing the internal pressures within APAM support surface for a pressure amplitude of 100/0, a cell profile of 1:4, and a cycle time of 9 mins. P1-P4 represents the individual internal pressure values in a set of four cells.

In the previous chapter the development of a controller, this could be used in conjunction with the experimental APAM system. In particular, the performance of the controller was described in section 4.1.6. Values for the three variables were selected based on a number of factors, including compatibility with existing commercial APAM systems, as well as for practical reasons, in particular the time involved in testing each subject. Accordingly, values were assigned to each variable, as summarised in Table 5-2, and achieved by the Pneumatic Manager (section 4.1). Its performance with one such combination of variables, in terms of internal air pressures as a function of time is indicated in Figure 5-3.

5.2 Experiment Design, Subjects and Protocols

5.2.1 Design of Study

To determine the optimum pressure configuration, an array of experiments for each of the three selected APAM variables, namely pressure amplitude, cell profile and cycle period, was constructed. Their details incorporating 20 experiments per subject are specified in Table 5-3.

5.2.2 Subject Group

At the time of this study, there were no requirements in place in Queen Mary University of London for submitting a project for Ethical Approval, which involved only testing normal healthy subjects. Nonetheless before inclusion, a full description of the measurement protocols involved in the study was described to any potential subjects. It was also stated that any subject was free to withdraw, for whatever reason, at any stage of the study. The characteristics of the five healthy subjects are summarised in Table 5-4.

Table 5 - 3 Experimental matrix for each subject.

Experimental Number	Pressure Amplitude /mmHg	Cell Profile	Cycle Period /min
1-6	100 - 0	1:2 and 1:4	3, 9 and 15
7-12	60 - 40	1:2 and 1:4	3, 9 and 15
13-18	30 - 20	1:2 and 1:4	3, 9 and 15
19	Primo	N/A	N/A
20	NHS Foam	N/A	N/A

Table 5 - 4 Summary of healthy subjects included in the experimental study

	Age	Sex	Height (m)	Weight (kg)	BMI kg/m^2
Subject A	26	Male	1.72	80	27.0
Subject B	27	Male	1.75	77	25.1
Subject C	25	Male	1.72	56	18.9
Subject D	26	Female	1.64	55	20.4
Subject E	20	Male	1.81	75	22.9

5.2.3 Experimental Protocol

Both test sites were cleaned with sterile wipes, prior to application of either circular or annular sweat pads (section 5.1.2). A polypropylene plastic sheet (50 mm) of larger dimension than the sweat pad (455 SCB 50 Shorko, Courtaulds Films, Swindon, UK.) was inserted on top of the pad to minimize the loss of sweat by evaporation. The polypropylene sheet was transparent, hydrophobic in nature and thus ideally suitable as it did not react with nor retain any of the sweat collected (Shorko Films Courtaulds Films Technical report). The plastic was then sealed to the skin with 3M MicroporeTM surgical tape (Blenderm surgical tape, 3M Health Care Ltd, Loughborough U.K.). This tape is hypoallergenic and provides an optimum attachment to the moist test area during the experiment. Each labelled tube containing

both a separator and a sweat pad was weighed using an analytical balance (Ohause Balances Ltd), to an accuracy of ± 0.00017g, prior to sweat collection.

The initial phase of the experiment was carried out in a pre-heated room, which was maintained at a controlled temperature of $28 \pm 2\,°C$ and at a relative humidity of between 35 and 45%. Each subject underwent an acclimatisation period of 20 mins in the room to ensure that a steady sweat rate had been attained. Each subject then adopted a seating position on a standard chair and two pre-weighed sweat pads were attached to the pre-cleaned skin above the sacrum and heel. In both cases there was no contact between the support surface and either of the two experimental sites. This constituted the position of the subject during both the unloaded phase and subsequent reperfusion phase. During the former, the support surface was actuated with Pneumatic Manager. Thereafter, each subject was carefully positioned supine on the mattress, covered by the array of pressure measuring cells (section 5.1.1), as illustrated in Figure 5 - 4. During this loaded period, the transcutaneous gas levels and the internal pressure were monitored, along with the temperature and humidity under the sacrum and heel.

Thus each subject was subjected to the three phases, namely unloaded, loaded and reperfusion, each of which lasted 30 mins. After the completion of each phase, the individual existing sweat pads were carefully removed from each of the experimental sites and placed in their corresponding tubes using tweezers. They were then replaced with a fresh pad, a procedure which took approximately 40 seconds. Thus, a total of six sweat samples were collected from each subject.

After the prescribed period each pad was removed and sealed in a pre-weighed bottle, which was re-weighed to obtain the net sweat rate by gravimetric difference.

An overview of the experimental protocol lasting approximately 120 minutes is shown schematically in Figure 5 - 5.

Figure 5 - 4 Images showing a subject lying prone on the APAM support with measurement sensors attached.

Set up environment:
Temperature is controlled with 28 ±2 ℃

15 min

Subject acclimatised

30 min

Circular sweat pad attached to both sacrum and heel
Start sweat measurement (unload)

40 min

Transcutaneous Gas Electrode re-membraned

Support surfaces was setup with pneumatic manager

45 min

Equilibration period:

60 min

Sweat pad removed and i) annular pad attached to sacrum; ii) circular pad attached to heel

Subject positioned supine on mattress - humidity sensor located under test area

First scan of interface pressure

T_cPO_2 and T_cPCO_2 monitored during loading of sacrum

Second scan of interface pressure

90 min

Subjects lifted from the support surface and humidity sensor removed

Second sweat pad (load) removed, and fresh circular sweat pads to sacrum and heel

Transcutaneous electrode removed

Sweat pads removed

120 min

Unloaded

Loaded

Reperfusion

TOTAL TIME: 2 hours

Figure 5 - 5 Schematic detailing the timelines of the experimental protocols adopted for each measurement session.

117

5.3 Analysis of Data

5.3.1 Interface Pressure

For each test condition maximum pressure values were recorded for each of the two experimental sites. For each condition, a mean $\pm$ SD was estimated across the subject group.

5.3.2 Sweat

Sweat rate is the amount of sweat collected per minute of the collection period and can be calculated from the equation below:

$$Sweat \ rate \ mL/\min/m^2 = \frac{Sweat \ Weight \ /mg}{Collection \ Period \ /\min} \times \frac{1000}{Area \ of \ sweat \ pad \ /m^2}$$

Equation 5-1

5.3.3 Transcutaneous Oxygen and Carbon Dioxide Levels

Transcutaneous gas levels were continuously monitored during the loaded period of each test condition (Table 5-2) and displayed on a graphical output. In order to quantify T_cPO_2 and T_cPCO_2 response, the temporal raw data was processed to extract a number of selected parameters.

Oxygen tension

The oxygen values readings were normalised to initial unloading values and a parameter defined as oxygen debt in T_cPO_2 was derived, which was identical to that adopted in a previous study (Rithalia and Gonsalkorale, 2000). This parameter, as indicated in diagrammatic form in Figure 5-6, is calculated from the following equation:

$$\text{Oxygen debt} = \text{Shaded area B} - \text{Shaded area A} \qquad \textit{Equation 5 - 2}$$
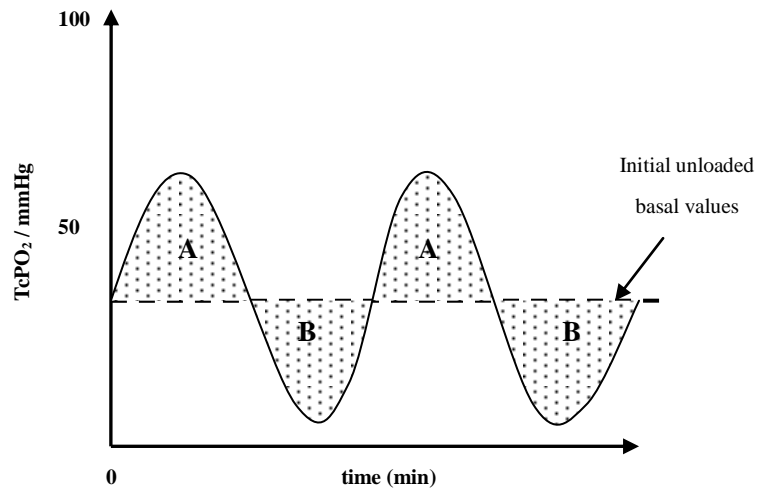
Figure 5 - 6 Diagrammatic representation of the derived parameter for oxygen debt, which represents the changes in T_cPO_2 during the monitoring period. The shaded area, A, represents the area above unloaded basal value, and the area B, the area below it.

Carbon dioxide tension

There are a series of responses predicted from the monitoring of T_cPCO_2 with time, as indicated in Figure 5-7, and previously reported from work in the host laboratory (Knight et al., 2001). It was noted that three distinct responses were apparent under a variety of controlled pressure profiles with the APAM support surface, which are conveniently listed as:

- **Mode 1** – a minimal change in T_cPCO_2 from basal values of approximately 45 mmHg (6.0 kPa),

- **Mode 2** – a distinct perturbation in T_cPCO_2 response, which appeared to be associated with the APAM cycles period in the mattress, with T_cPO_2 values exceeding 70 mmHg (9.3 kPa),

- **Mode 3** – a decrease in T_cPCO_2 over monitoring period from basal values to approximately 30 mmHg (4.0 kPa).
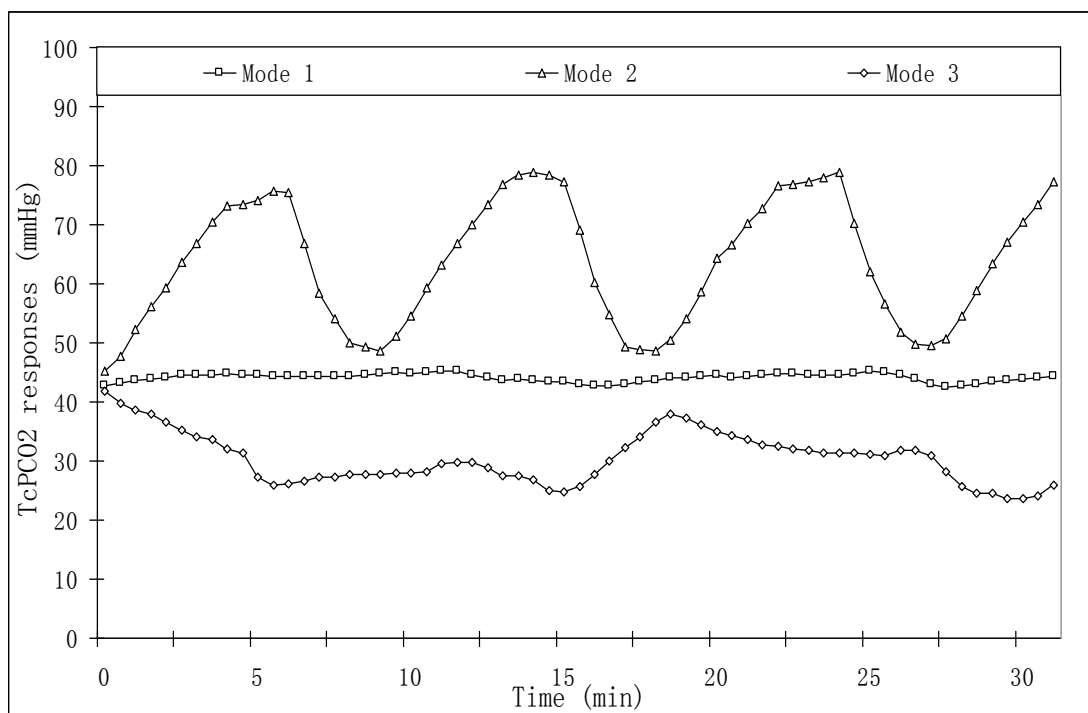
Figure 5 - 7 Typical transcutaneous carbon dioxide tension responses measured at the sacrum

To further quantify the carbon dioxide responses, an alternative parameter was selected, as previously described (Knight et al., 2001), specifically for the Mode 2 response (Figure 5-7). The area is estimated as the integration of the carbon dioxide values above the initial unloaded T_cPCO_2 level over the monitoring period, as illustrated in Figure 5-8. The parameter is thus calculated from the following equation:

$$\text{Shaded area (A)} = [T_cPCO_{2\,(test)} - T_cPCO_{2\,(basal)}] \times time \qquad \textit{Equation 5-3}$$
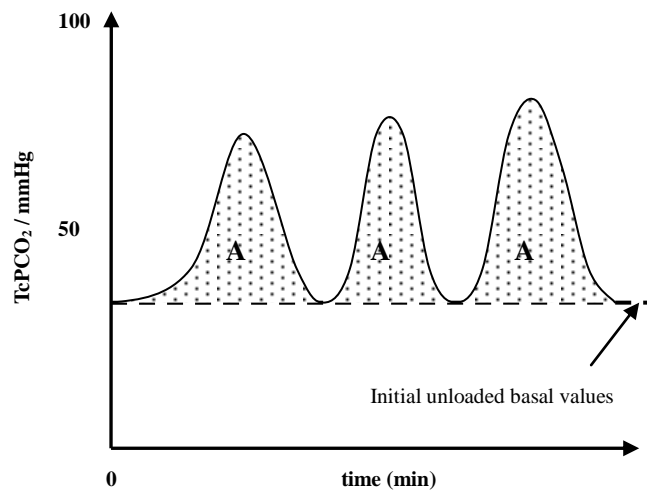
Figure 5 - 8 Diagrammatic representation of the derived parameters for describing carbon dioxide tension. The shaded area, A, represents the area above the unloaded basal value.

5.4 Results

5.4.1 Interface Pressure

The mean values of the sacral and heel interface pressures for each subject subjected to the 18 test conditions are presented in Figure 5-9. Superimposed on the graphs are the group means ± standard deviations for the data associated with the three different pressure amplitudes prescribed for APAM support surface. There are clear variations between subjects for each test condition, although no obvious trends for each subject. However, for the sacral pressures, the group means are highest for 100/0 mmHg and lowest for 30/20 mmHg, with a reduction of 33.8%, such that the latter values were similar to those measured with the Continuous low pressure mattress. A similar trend was observed for the group means of the heel pressures, although there were less marked differences between pressure amplitudes. In all cases, the NHS foam mattress produced the highest mean heel pressures of 69.8 ± 46.1 mmHg. Close examination of the data revealed few trends in the values of sacral or heel pressures when considering the influences of either cell profile or cycle times of the APAM.

5.4.2 Transcutaneous Oxygen and Carbon Dioxide Tension

The complete data for the 5 subjects are presented in attached CD. A typical set of data for one subject B (male, BMI = 25.1 g/m^2) is presented in Figures 5-10 and 5-12. These graphs include both the four internal pressures (P1-P4) and the transcutaneous oxygen (T_cPO_2) and carbon dioxide (T_cPCO_2) values at the sacrum over the monitoring period and mean interface pressures at both body sites. It is evident from each of the responses that after a period of time, the internal pressures stabilise at the prescribed pressure profiles and pressure amplitudes. The tissue response is varied. In some cases, the T_cPO_2 changes minimally over the period (e.g. Figure 5-12 c); in other cases, the T_cPCO_2 fluctuates at a similar period to the internal mattress pressures (e.g. Figure 5-10 a, b). In a few cases, the T_cPO_2 is depressed for a large proportion of the monitoring period (e.g. Figure 5-10 c). The latter case is often associated with an increase in T_cPCO_2 levels above the range 35-45 mmHg (4.7 - 6.0 kPa) considered to be normal in the unloaded state (Bogie et al., 1995; Knight et al., 2001). This response generally occurred with the pressure amplitude of 100/0 mmHg (Figure 5-10).

The corresponding data for the humidity and temperature levels at both body sites for this subject are presented in Figures 5-13 to 5-15. The data is fairly consistent across the test conditions. In terms of relative humidity, the values start at between 20 - 40% RH, increases dramatically as the mattress reaches steady state, followed by a slower increase. With many conditions, values reach 100% RH at the sacrum, whereas the humidity values at the heel more generally attain values of between 60 and 80% RH. In a similar manner, the temperatures at both sacrum and heel increase dramatically and then slowly reach a steady state value of between 33^oC and 36^oC.
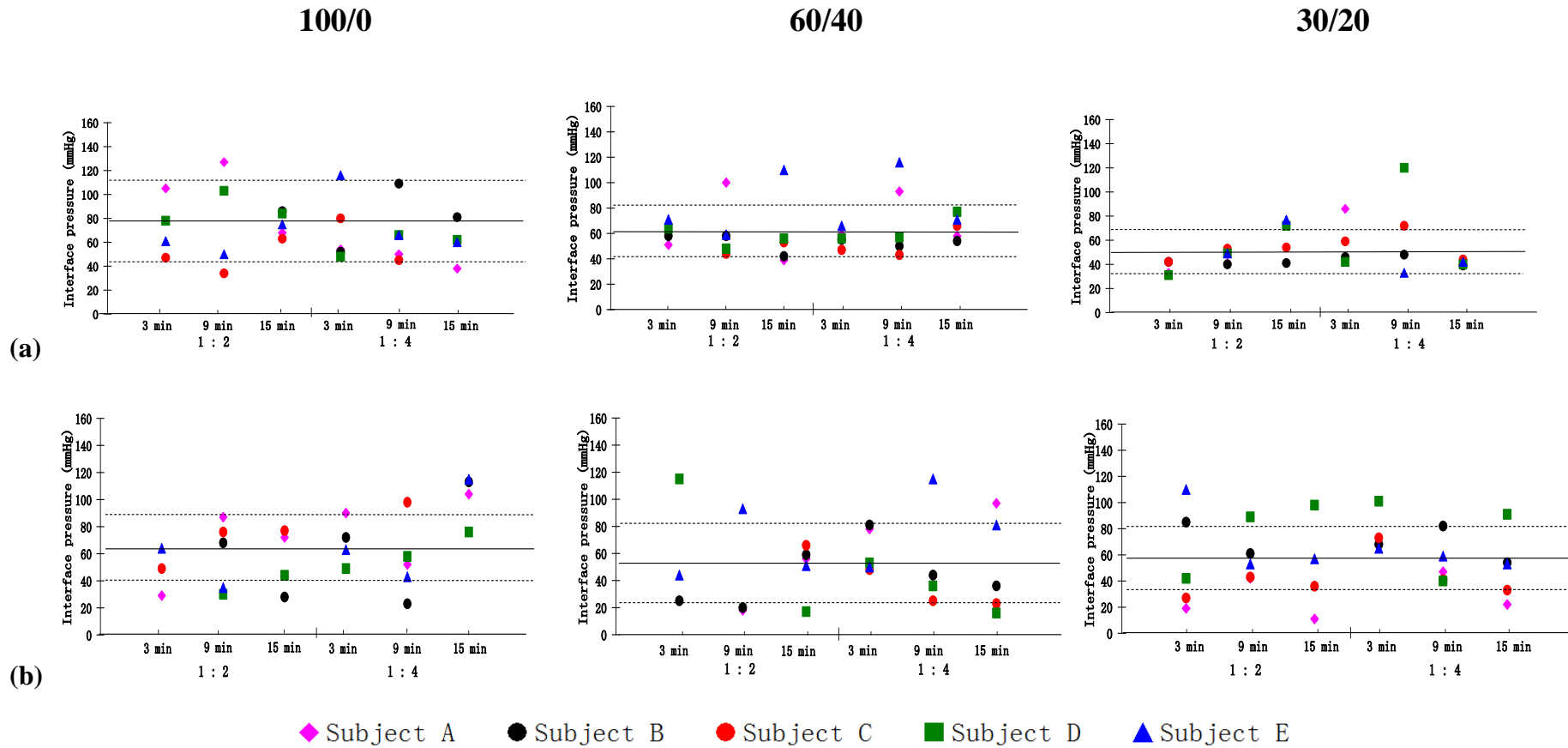
Figure 5 - 9 Distribution of interface pressure at the sacrum and heel for the 18 test conditions associated with the APAM surface. Horizontal line and dashed lines represent mean and standard deviation respectively.

a)   sacrum, a mean value of NHS mattress is 60.2 ± 46.1 mmHg, and 50 ± 17.4 mmHg with Continuous Low Pressure air mattress.

b)   heel, a mean value of NHS mattress is 69.8 ± 44.1 mmHg, and 54 ± 30.5 mmHg with Continuous Low Pressure air mattress.

_100/0_   **1:2**   **1:4**
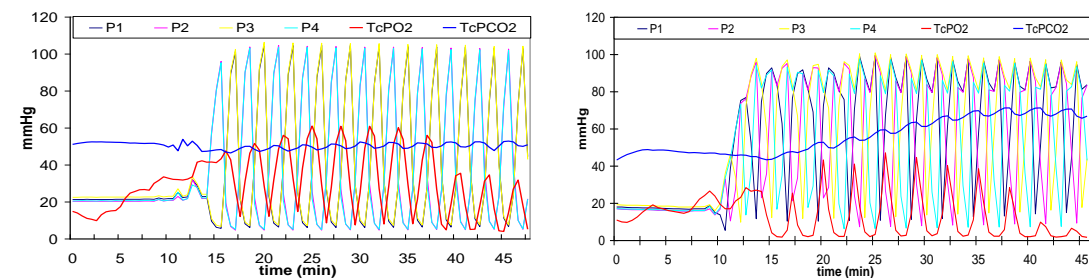
(a) 3 min
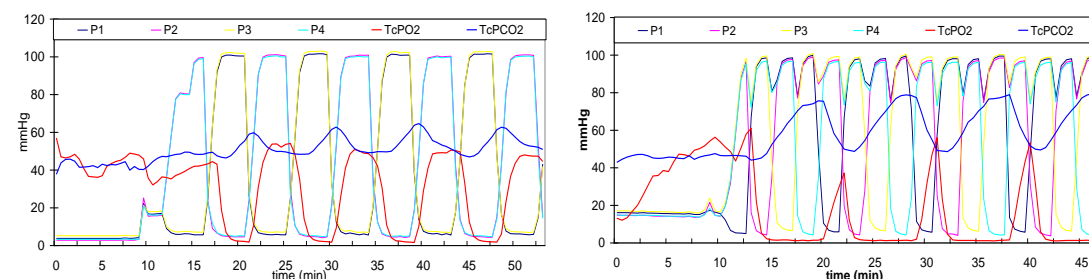
(b) 9 min
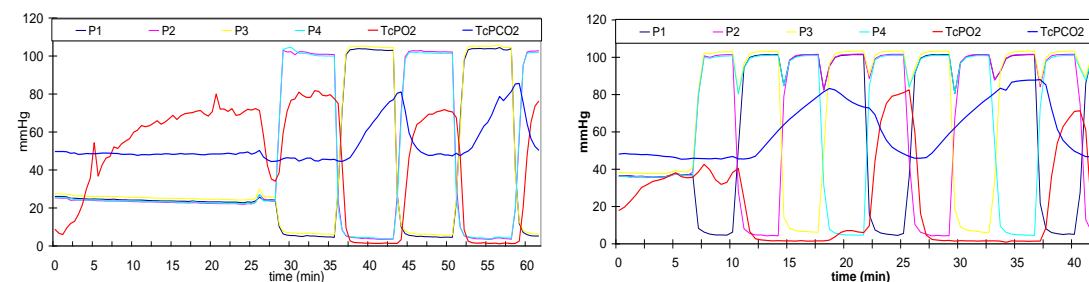
(c) 15 min

	Sacrum mmHg		Heel mmHg	
	First scan	**Second scan**	**First scan**	**Second scan**
3 min, 1:2	120	198*	125	73
3 min, 1:4	52	42	72	87
9 min, 1:2	116	246*	68	57
9 min, 1:4	109	108	23	47
15 min, 1:2	86	143	28	46
15 min, 1:4	81	69	113	155

Figure 5 - 10 A complete set of data incorporating six combinations of profile and cycle period for subject B (male, BMI = 25.1 kg/m^2) with a pressure signature of 100/0 mmHg. P1 – P4 indicate individual air cell in sets of 4. T_cPO_2 and T_cPCO_2 are corresponding gas tensions over the monitoring period. The corresponding interface pressure was show in Table.

 * Abnormal high maximum pressures – these should be ignored.

60/40   1:2   1:4
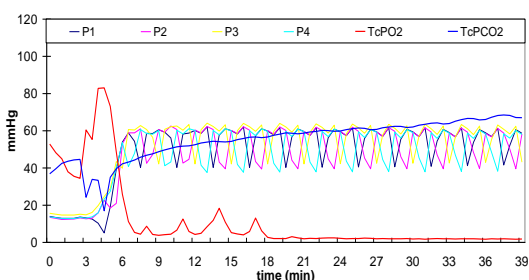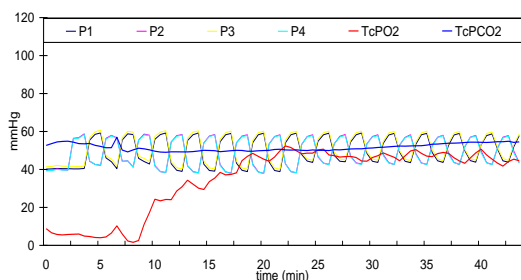
(a) 3 min
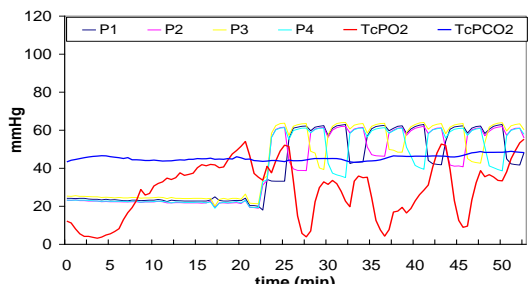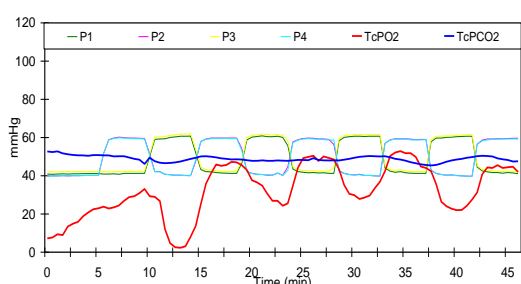
(b) 9 min
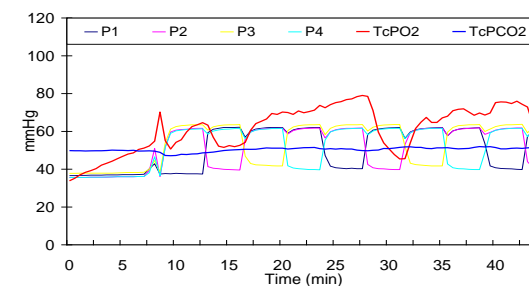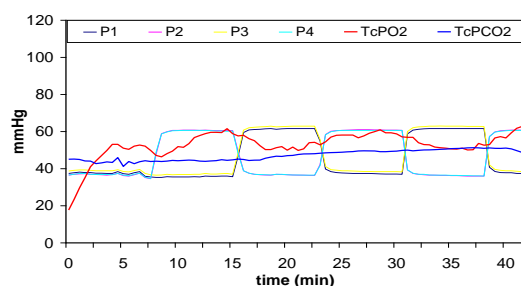
(c) 15 min

	Sacrum mmHg		Heel mmHg	
	First scan	**Second scan**	**First scan**	**Second scan**
3 min, 1:2	58	64	25	17
3 min, 1:4	55	57	81	80
9 min, 1:2	58	81	20	14
9 min, 1:4	50	72	44	64
15 min, 1:2	42	48	59	46
15 min, 1:4	54	52	36	45

Figure 5 - 11 A complete set of data incorporating six combinations of profile and cycle period for subject B (male, BMI = 25.1 kg/m^2) with a pressure signature of 60/40 mmHg. P1 – P4 indicate individual air cell in sets of 4. T_cPO_2 and T_cPCO_2 are corresponding gas tensions over the monitoring period. The corresponding interface pressure was show in Table.

_30/20_   **1:2**   **1:4**
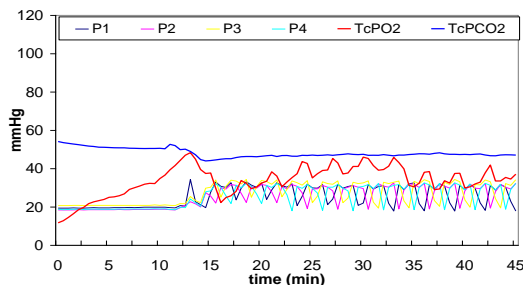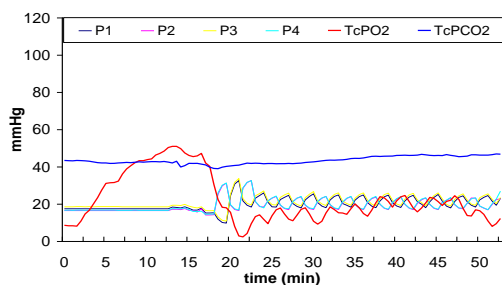
(a) 3 min
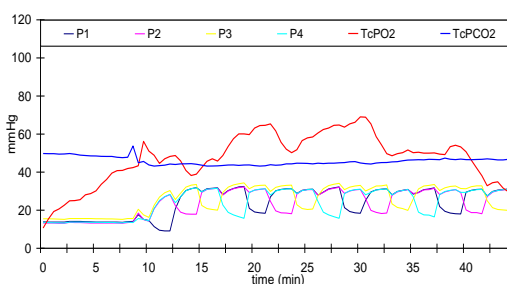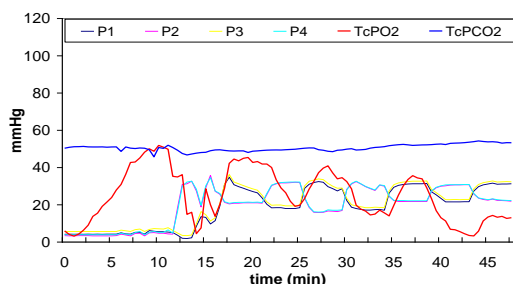
(b) 9 min
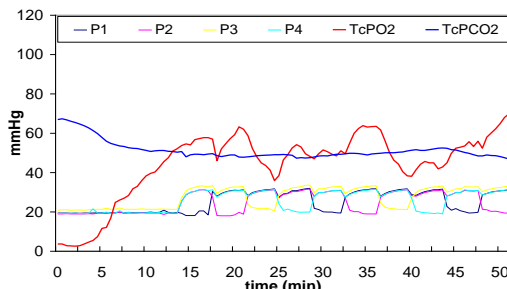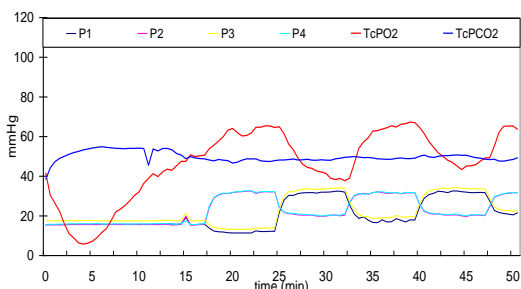
(c) 15 min

	Sacrum mmHg		Heel mmHg	
	First scan	Second scan	First scan	Second scan
3 min, 1:2	42	x	85	x
3 min, 1:4	46	56	68	85
9 min, 1:2	40	36	61	27
9 min, 1:4	48	60	82	74
15 min, 1:2	41	49	137	163
15 min, 1:4	39	41	54	79

Figure 5 - 12 A complete set of data incorporating six combinations of profile and cycle period for subject B (male, BMI = 25.1 kg/m^2) with a pressure signature of 30/20 mmHg. P1 – P4 indicate individual air cell in sets of 4. T$_c$PO$_2$ and T$_c$PCO$_2$ are corresponding gas tensions over the monitoring period. The corresponding interface pressure was show in Table.

x   Missing data

100/0　　　　　　**1:2**　　　　　　　　　　　　**1:4**
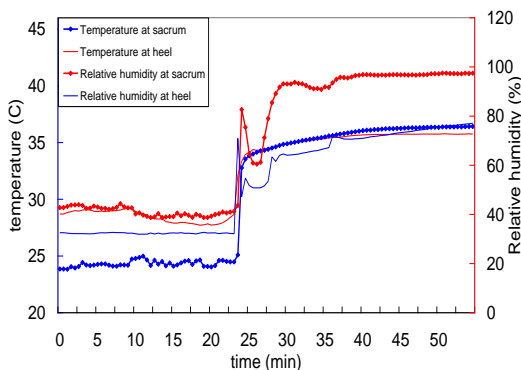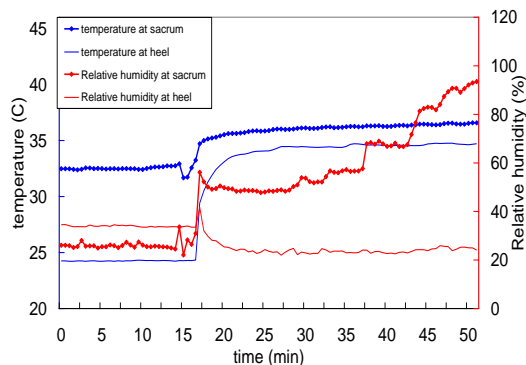
(a) 3 min
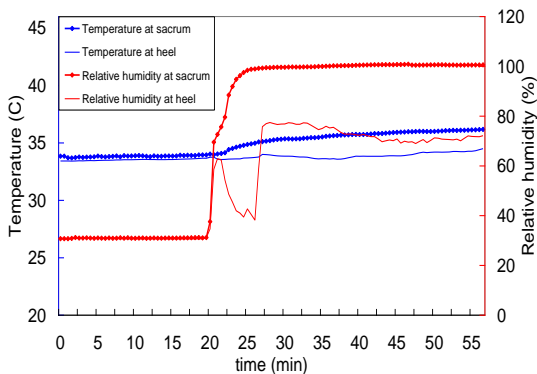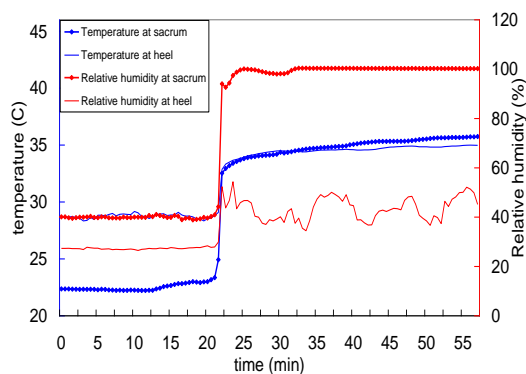
(b) 9 min
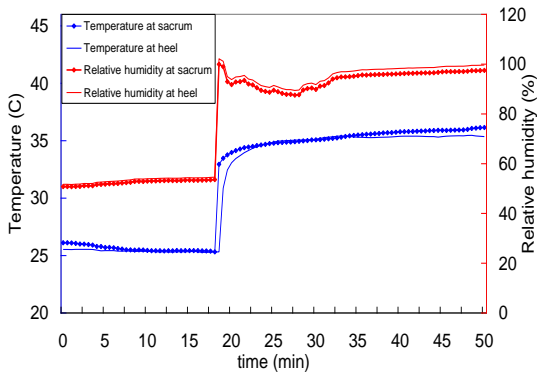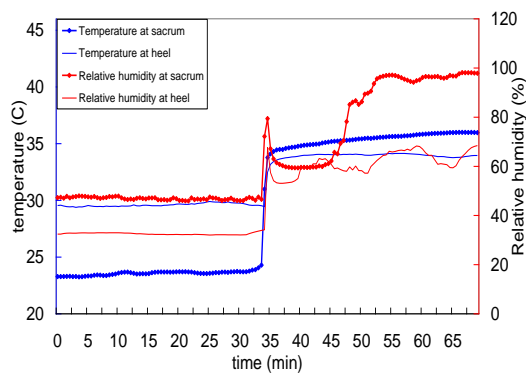
(c) 15 min

Figure 5 - 13 A complete set of data incorporating six combinations of profile and cycle period for subject B (male, BMI = 25.1 kg/m^2) with a pressure signature of 100/0 mmHg. Interface temperature and relative humidity was measured from sacrum and heel over the monitoring period.

_60/40_　　　　　　**1:2**　　　　　　　　　　　　**1:4**
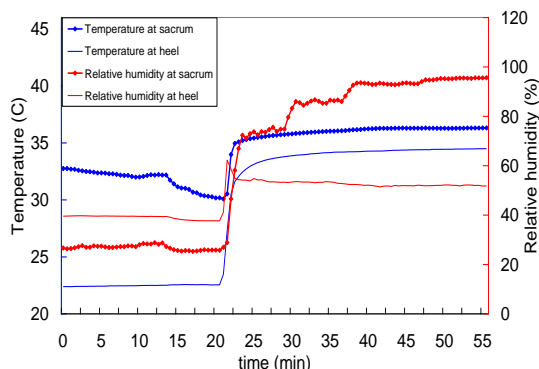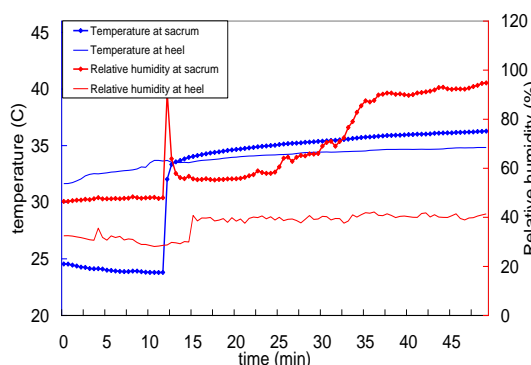
(a) 3 min
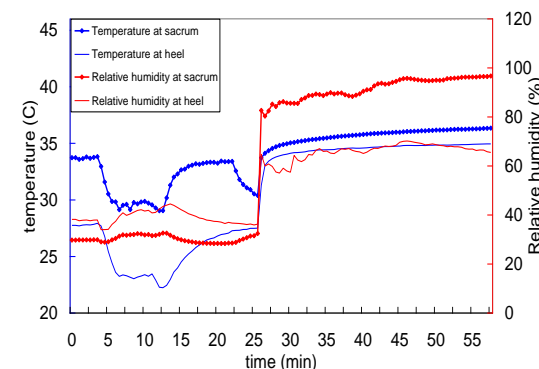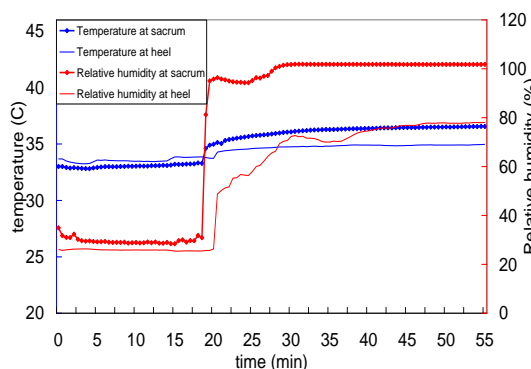
(b) 9 min
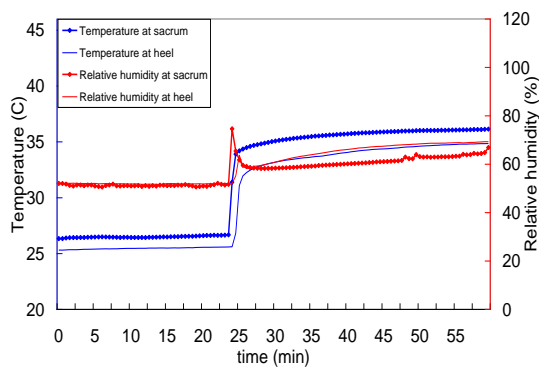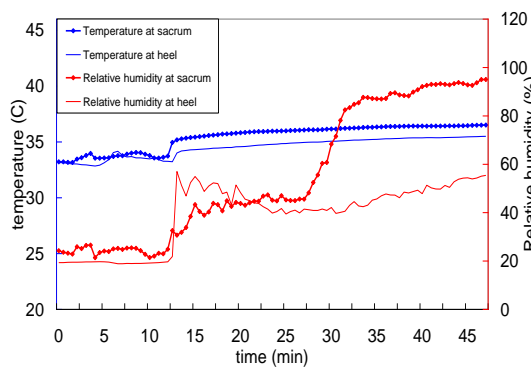
(c) 15 min

Figure 5 - 14 A complete set of data incorporating six combinations of profile and cycle period for subject B (male, BMI = 25.1 kg/m^2) with a pressure signature of 60/40 mmHg. Interface temperature and relative humidity was measured from sacrum and heel over the monitoring period.

_30/20_   **1:2**   **1:4**
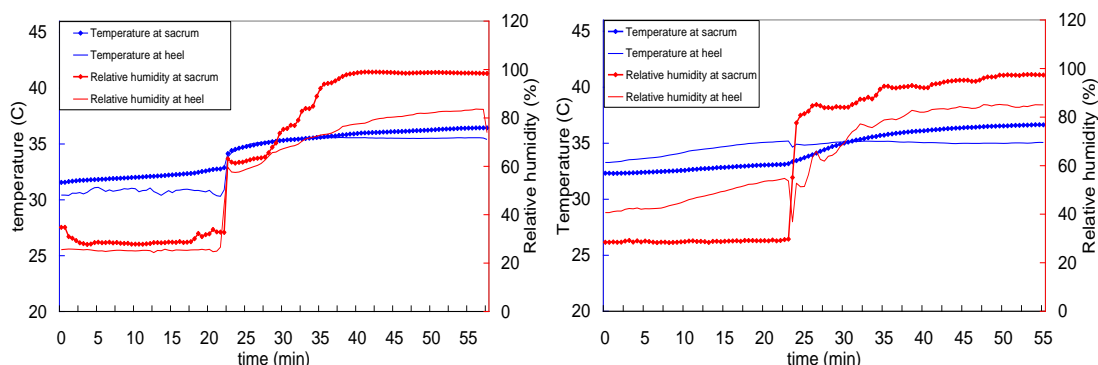
(a) 3 min
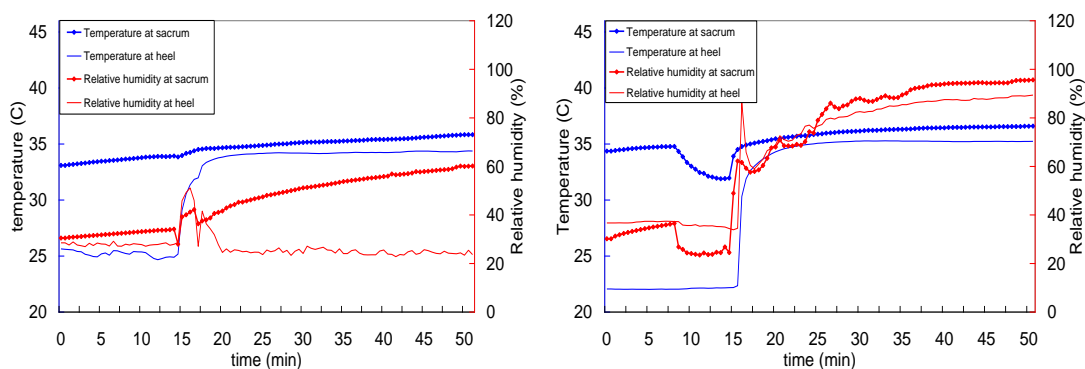
(b) 9 min
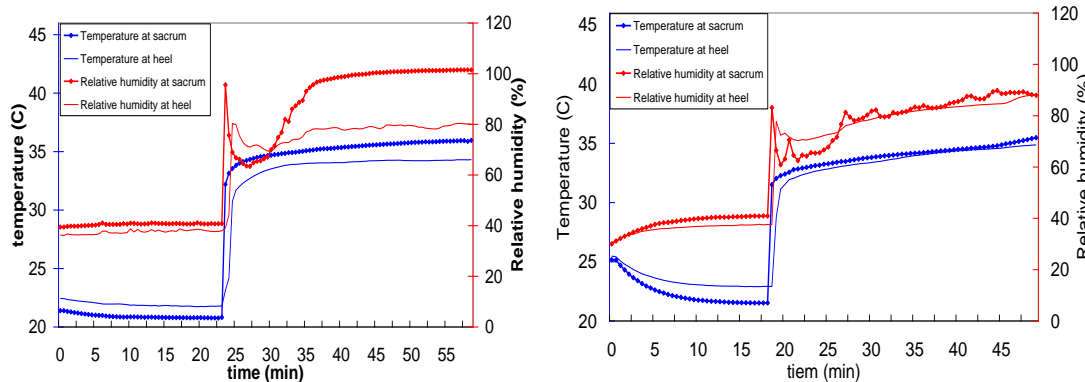
(c) 15 min

Figure 5 - 15 A complete set of data incorporating six combinations of profile and cycle period for subject B (male, BMI = 25.1 kg/m^2) with a pressure signature of 30/20 mmHg. Interface temperature and relative humidity was measured from sacrum and heel over the monitoring period.

Oxygen tension

The subject data sets were pooled to produce the parameter of oxygen debt (Figure 5-6), for all the test conditions associated with the APAM support surface. A summary of the results, as presented in Figure 5-16, reveals considerable variation at each test condition. However, trends indicate the lowest mean values associated with the pressure amplitude of 60/40 mmHg. The effects of cycle period were inconsistent, with an increasing trend for oxygen debt at a pressure amplitude of 100/0 mmHg and a decreasing trend with cycle period at 30/20 mmHg.
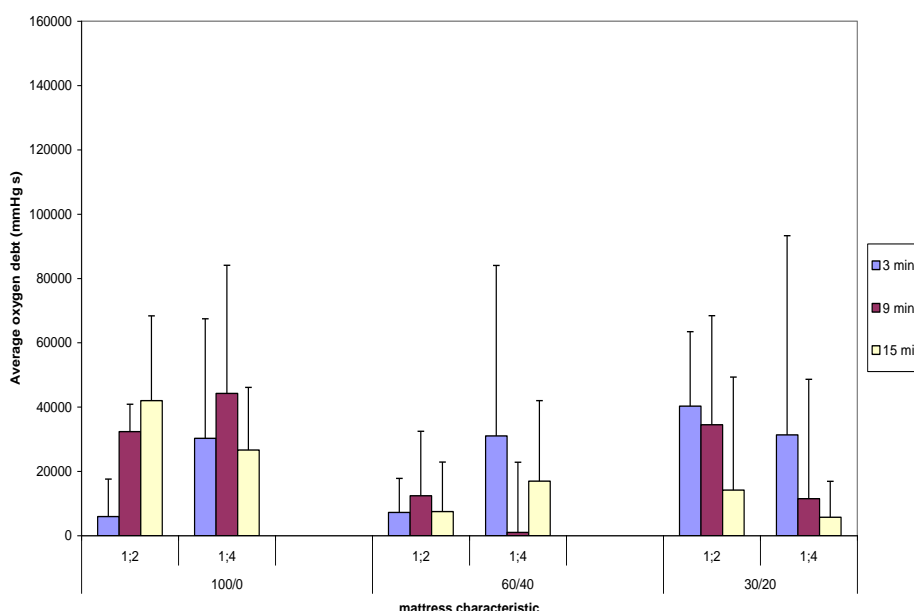
Figure 5 - 16 Mean values (+ standard deviation) of the parameter for oxygen debt estimated for all subjects in the test conditions associated the APAM surface.

Carbon dioxide tension

The carbon dioxide data was categorised into 3 responses (Figure 5-7) and a summary of these with respect to pressure amplitudes in presented in Figure 5-17. It is evident that for pressure amplitudes of both 60/40 mmHg and 30/20 mmHg, 90% of the response were Mode 1 i.e. minimal change with time from unloaded basal levels. By contrast, with a pressure amplitude of 100/0 mmHg, There were equal proportion of

responses, approximately 45%, associated with both Modes 1 and 2. The latter response suggests an elevation of T_cPCO_2 values for significant proportion of the monitoring period.

The subject data sets were pooled to produce the parameter for elevated T_cPCO_2 values (Figure 5-8), for all the test conditions associated with the APAM support surface. A summary of the results, as presented in Figure 5-18, reveals considerable variation of the group means of this parameter at each test condition. Nonetheless the results indicate that the largest mean values of the excess carbon dioxide parameters are associated with a pressure amplitude of 100/0 mmHg.
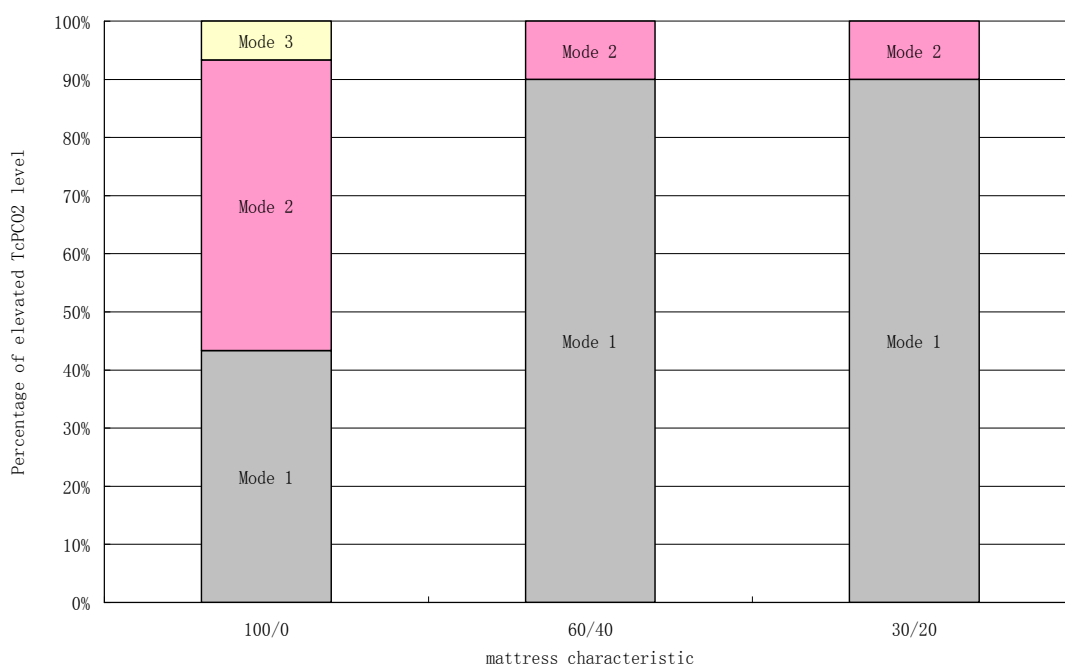
Figure 5 - 17 Proportion of response classifications for T_cPCO_2 levels, for all subjects with respect to pressure amplitude in the APAM surface.
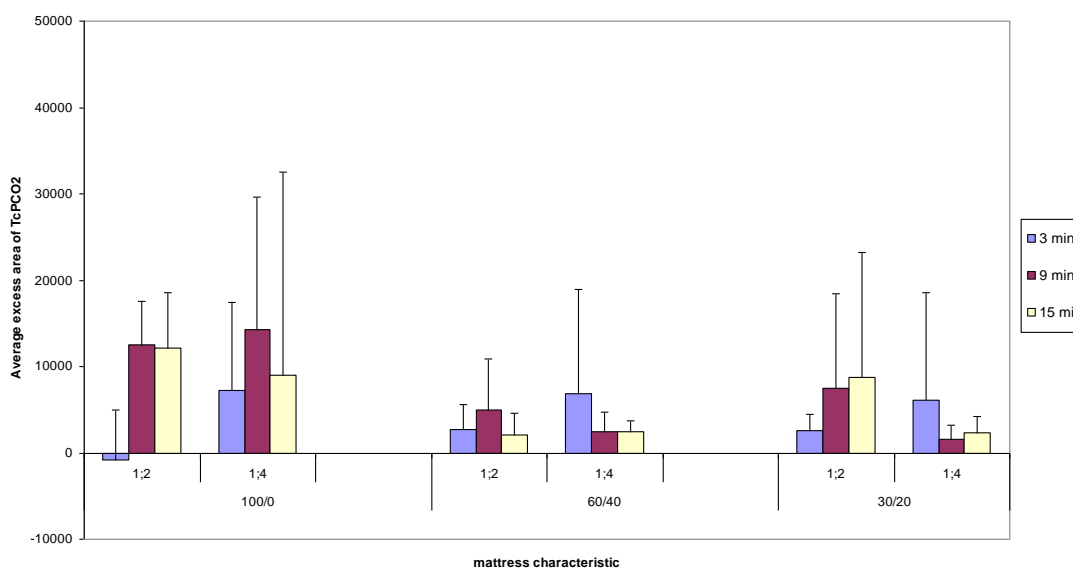
Figure 5 - 18 Mean values (+ standard deviation) of the parameter for elevated carbon dioxide level estimated for all subjects in the test conditions associated the APAM surface.

5.4.3 Inter-relationships Between the Output Paramters

The relationship between the area parameters for both oxygen (Figure 5-6) and carbon dioxide (Figure 5-8) is presented in terms of the combined tests in Figure 5-19. In addition, this relationship is examined for results classified in terms of cycle period (Figure 5-20), pressure amplitude (Figure 5-21) and pressure profile (Figure 5-22).

In terms of the combined data, a linear relationship (r = 0.55, n = 90) was found to be highly statistically significant at the 0.001 percent level. When the data was classified, there were also positive correlations, which were statistically significant for all parameters (p<0.01 or greater), with one exception corresponding to the linear model for the cycle period of 15 minutes (p<0.05%).

Given the nature of the data associated with T_cPCO_2, with only a small proportion of conditions demonstrating a Mode 2 response (Figure 5-17), these small changes tend to be associated with a large range of values associated with the parameter reflecting oxygen debt (Figure 5-19). Indeed this relationship reaffirms the proposition that increased level of oxygen debt can be associated with carbon dioxide levels which

exceed the normal range.

The complete set of sweat data for each subject is in attached CD**.** The mean values are indicated in units of mL/min/m^2 for the three phases with respect to the APAM support surface and the CLP/NHS mattresses in Figure 5-23 and Figure 5-24, respectively. Close examination of the data reveal some distinct trends, namely:

- The highest sweat rate at the sacrum corresponded to the loaded phase, with mean sweat rates exceeding 1.0 mL/min/m^2 for 18 out of the 20 test conditions,

- The sacral sweat rates were consistently higher than those at the heel,

- The sweat rates associated with the reperfusion phase were generally similar to those measured in the unloaded basal phase. This was true for 16 out of 20 test conditions.

By contrast, there were no obvious trends associated with

- Cycle profile at each of the pressure amplitudes

- Cycle period at each of the pressure amplitudes
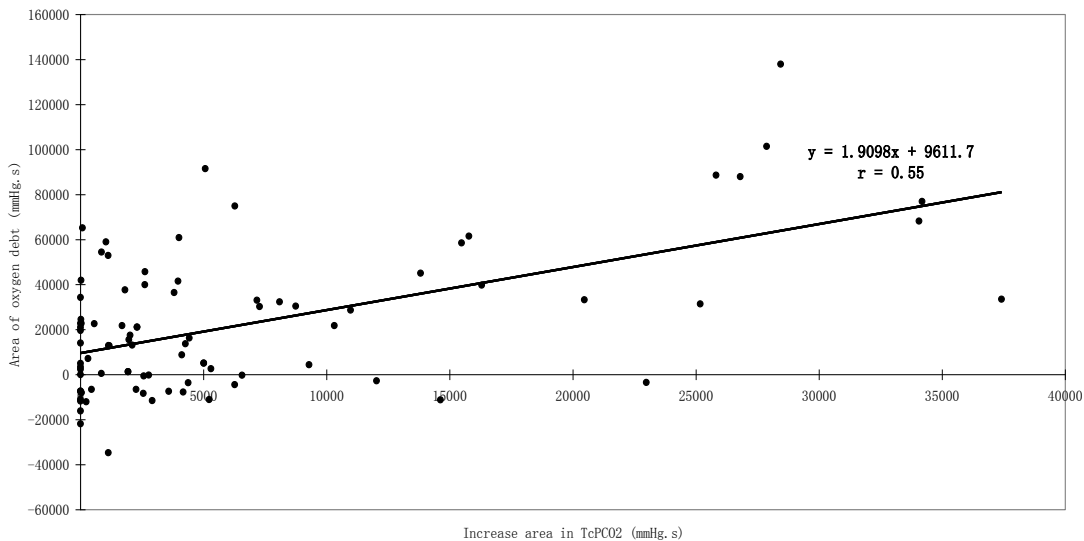
Figure 5 - 19 The relationship between the area for increase T_cPCO_2 and oxygen debt at all APAMs variable, Modes 1 and 2 only recorded in this graph.
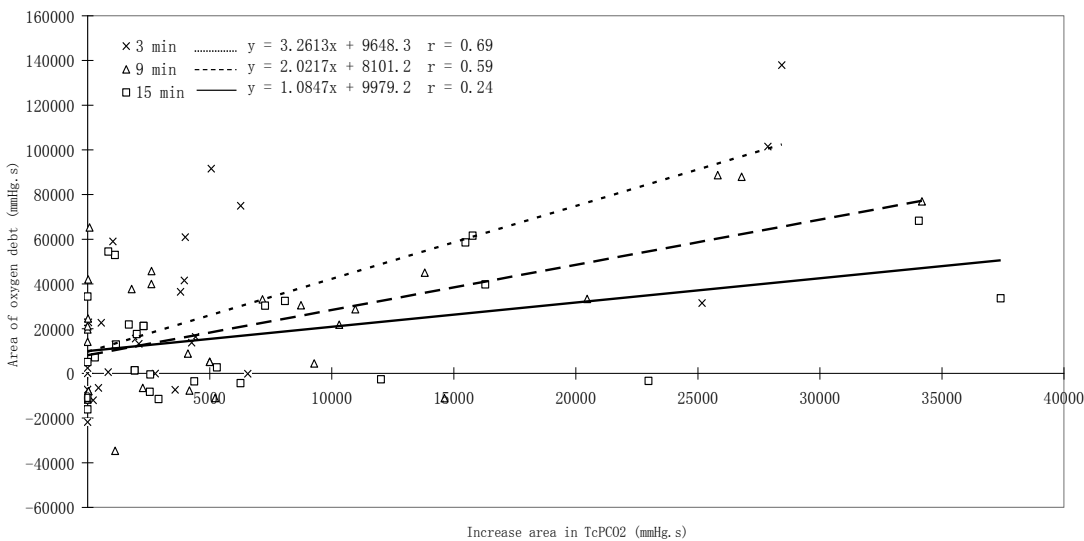
Figure 5 - 20 The relationship between the area for increase T_cPCO_2 and oxygen debt at different cycle period of mattress (3 min, 9 min, 15 min), Modes 1 and 2 only recorded in this graph.
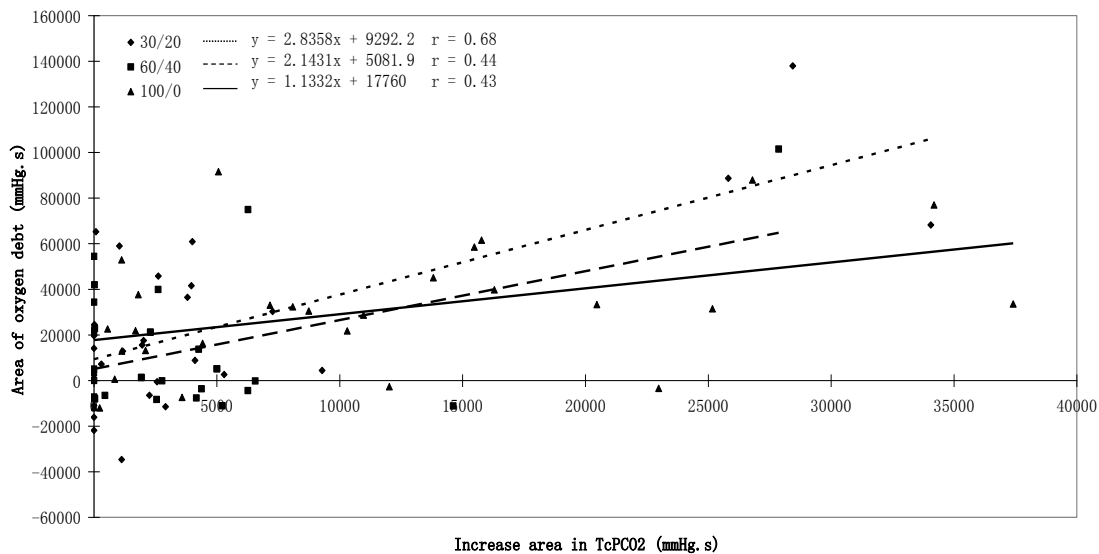
Figure 5 - 21 The relationship between the area for increase T_cPCO_2 and oxygen debt at different internal pressure (30/20, 60/40, 100/0), Modes 1 and 2 only recorded in this graph.
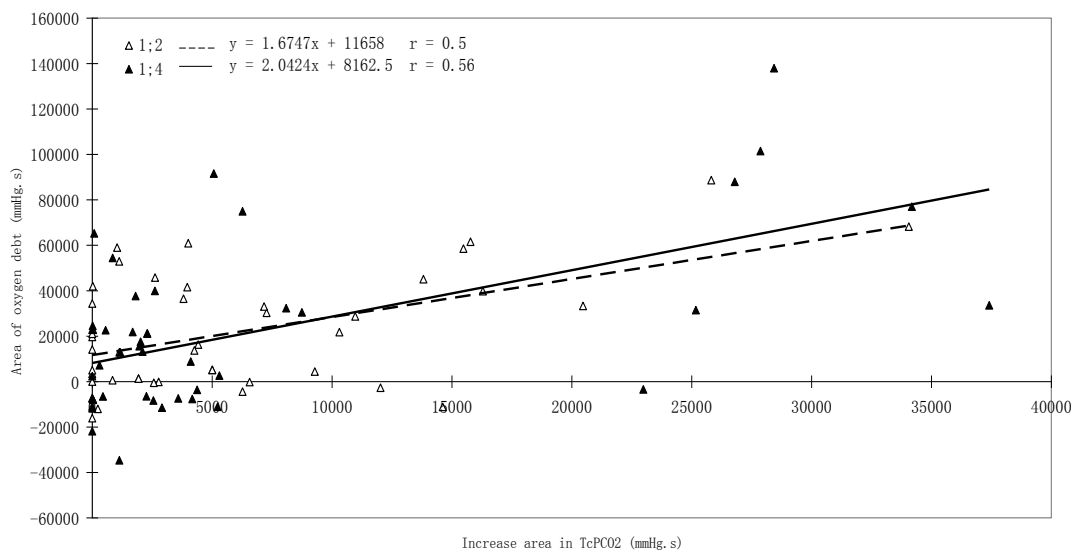
Figure 5 - 22 The relationship between the area for increase T_cPCO_2 and oxygen debt at different mattress profile (1 : 2 and 1 : 4), Modes 1 and 2 only recorded in this graph.

135

100/0   **60/40**   **30/20**

1:2

1:4
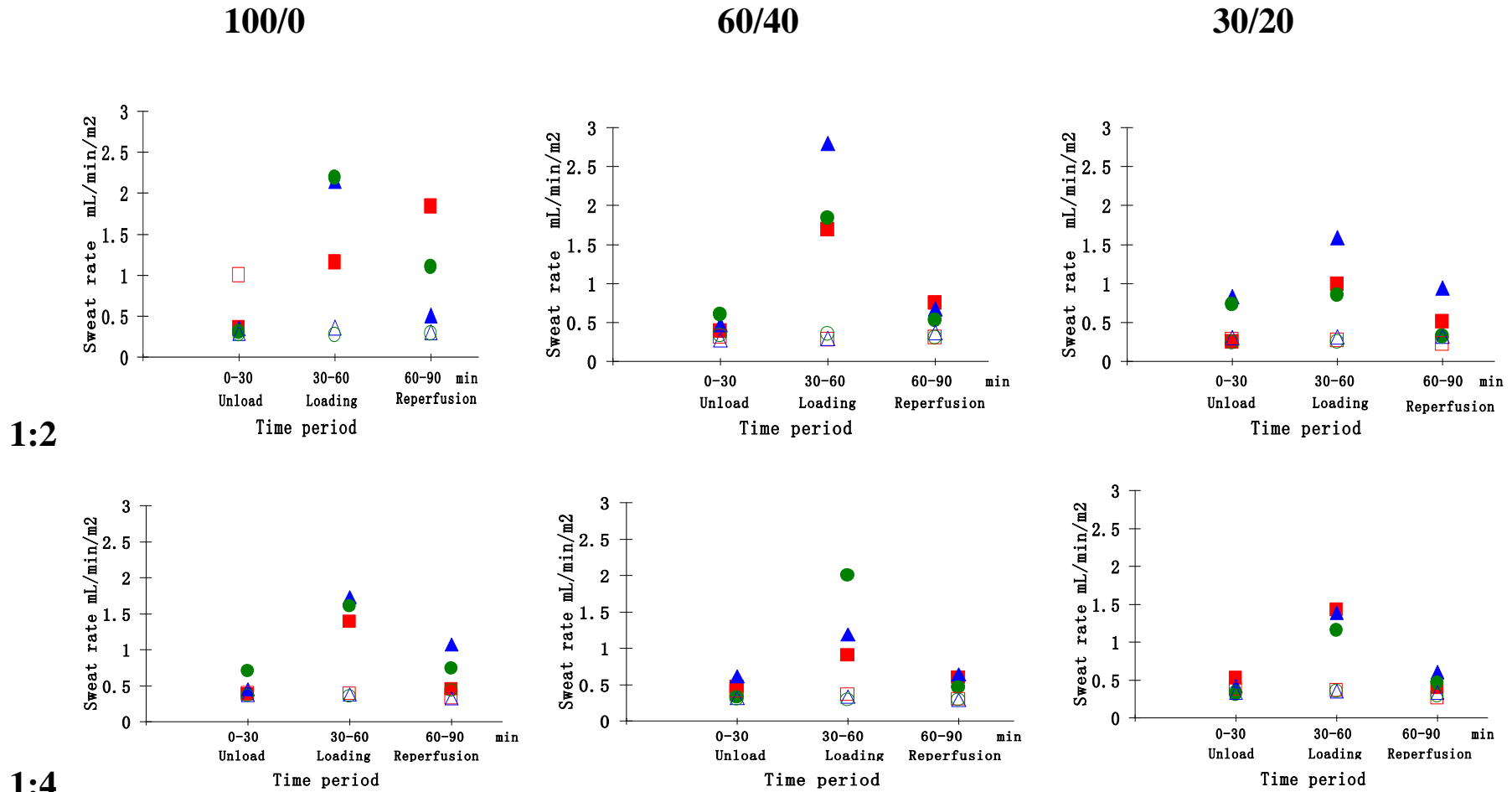
Figure 5 - 23 The mean of sweat rate versus combinations of profile and cycle period with a pressure signature of 100/0 mmHg, 60/40 mmHg, and 30/20 mmHg. The sweat rates measured for 3, 9 and 15 mins at the sacrum (■;▲;●), and the heel (□;△;○), respectively.
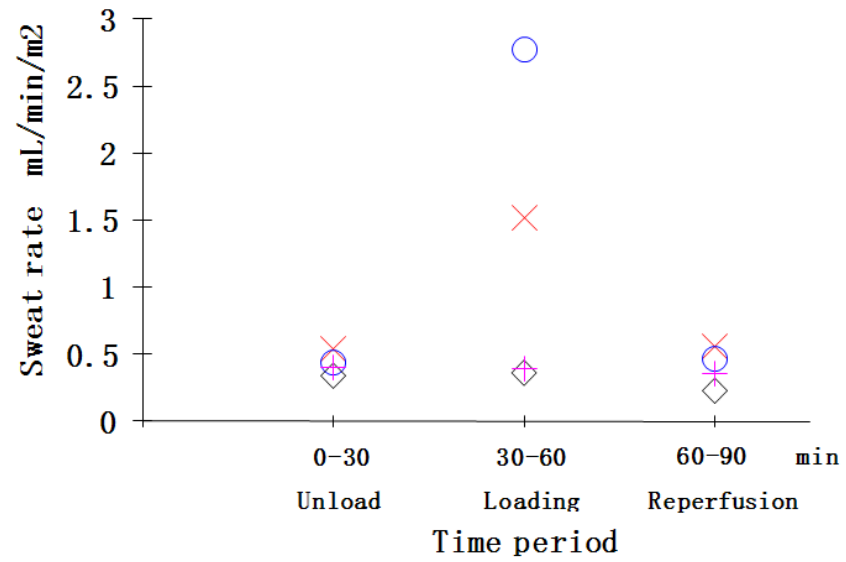
Figure 5 - 24 The sweat rate versus Standard NHS mattress and Continuous Low Pressure air mattress (Primo). The sweat rate measured at sacrum (○ ; ✕), and the heel (◇ ; ✛).

5.4.4 Performance on Continuous Low Pressure and NHS mattresses

Transcutaneous oxygen and carbon dioxide monitoring were also performed at the sacrum on both the Continuous Low Pressure (Primo^{TM}) and NHS mattresses. Interface pressures were recorded before and after the test period. The data for each volunteer is presented in Figures 5-25 and 5-26.

There are clear inter-subject variations with respect to T_cPO_2 response, as illustrated in Figure 5-25 (left) and Figure 5-26 (left). In some cases, the T_cPO_2 levels remained fairly high throughout the test period (e.g subject D and E on the Continuous Low Pressure air mattress). By contracts, some T_cPO_2 levels were considerably lower throughout the test period (e.g subjects B and E on the NHS mattress). However this latter response appeared to be independent of the measured interface pressure for the subjects.

The corresponding T_cPCO_2 response is illustrated in Figure 5-25 (right) and Figure 5-26 (right). For all subjects, the T_cPO_2 levels remained within the normal range of 35-45 mmHg (4.7 – 6.0 kPa), as previously defined (Bogie et al., 1995; Knight et al., 2001), despite the differences in interface pressures between subjects. These trends were similar for both Continuous Low Pressure and NHS mattresses.
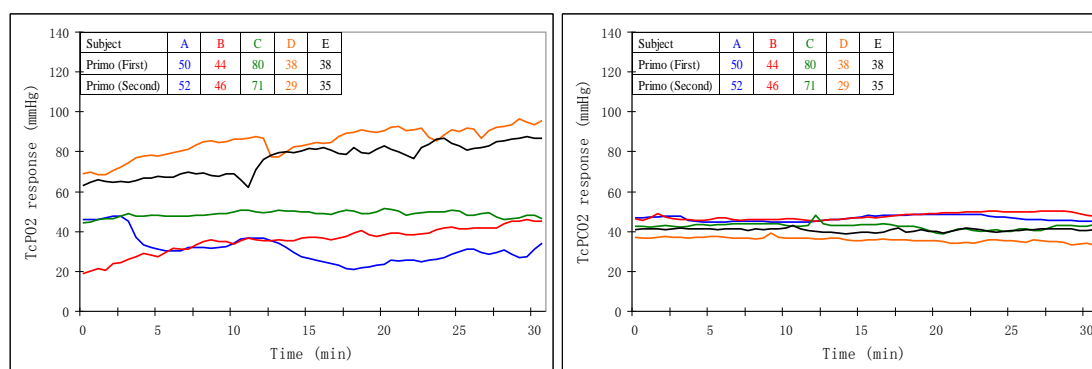
Figure 5 - 25 Both $T_c PO_2$ and T_cPCO_2 responses at sacral site of all subjects supported at Continuous Low Pressure air mattress, the interface pressure is also indicated.
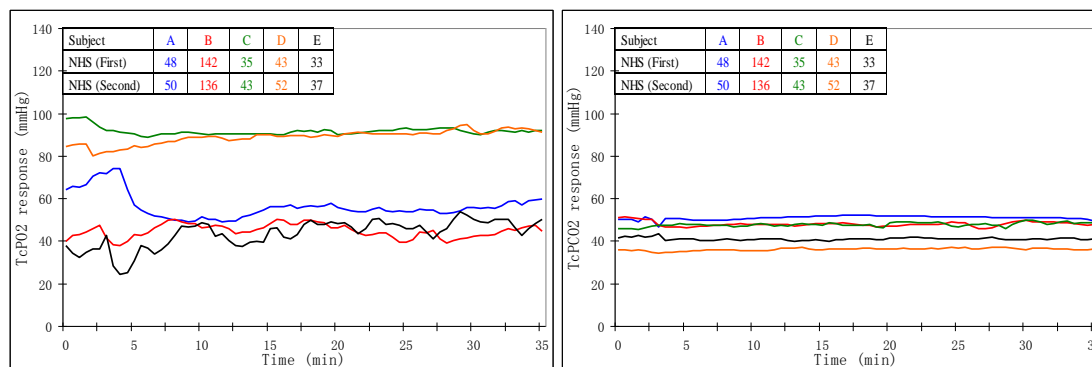
Figure 5 - 26 Both $T_c PO_2$ and $T_c PCO_2$ responses at sacral site of all subjects supported at NHS mattress, the interface pressure is also indicated.

5.5 Discussion

This chapter describes the design of an array of experiments to investigate the effects of prescribed internal pressures within an APAM support surface on the tissue viability of five healthy subjects supported in a supine position for a minimum of 30 minutes. The Pneumatic Manager proved successful in controlling three important parameters, namely pressure difference/amplitude, profile and cycle period, associated with the pressure configuration within the APAM. This enabled the experimental array of tests to be formulated (Table 5-2). It is worth noting that for the 1:4 profile for the maximum pressure decreased by a small magnitude transiently during the inflation phase, for each of the separate internal pressure measurements (Figure 5-3). Nonetheless, this was a consistent feature and enabled valid comparisons of effects of different pressure amplitudes at this pressure profile. This feature was not observed for the 1:2 profile. A series of measurements were conducted to assess either the microenvironment at the subject support interface, namely interface pressure, temperature or humidity, or tissue viability, in terms of sweat content and transcutaneous levels of oxygen and carbon dioxide. The former set of measurements revealed enhanced levels of humidity often reaching 100% RH, particularly under the supported sacrum, for a significant proportion of the monitoring period. This was associated with enhanced temperature values at the sacral region, often reaching $35^{o}C$ (e.gFigure 5-14). These increases in humidity and temperature were associated with

139

major increases in the sweat rates observed during the loaded period for all the configurations of the APAM system (Figure 5-23), as well as the Primo and NHS mattress (Figure 5-24). With respect to the microclimate at the heel, changes were less significant and this was reflected in loaded sweat rates, which were not different from those measured during both the unloaded and reperfusion periods. It should be noted that the magnitude of sweat rate was several fold-higher than that previously reported using the same collection technique (Polliack et al., 1997). However the present study collected sweat for much shorter periods of time i.e. 30 minutes compared to 8 - 14 hours, at the sacrum as opposed to the ischium. Nonetheless similar to that study was the increase in sweat rate in the loaded phase, even though other studies reported an opposing effect.

In previous studies, the constituents of sweat were analysed in a Clinical Biochemistry Department in Oxford, in particular the measurement of sweat lactate and urea (Polliack et al., 1997; Knight et al., 2001) and sweat purines (Bader et al., 2005). They generally revealed an increase in these sweat constituents which returned at different rates to basal levels during the subsequent reperfusion period. However in the present work, the equivalent measurements were not undertaken due to the accessibility and costs associated with the analytical techniques.

Interface pressure measurements were performed on two occasions, at the end of the acclimatisation period and immediately after the test period (Figure 5-5). There were clear variations between subjects. When pooled, however, the results revealed highest mean interface pressures at both sacrum and heel, when the pressure amplitude was 100/0 mmHg (Figure 5-9). Indeed, these high values even exceeded the comparable values measured with the standard NHS mattress at both body sites. By contrast the configurations associated with the other two pressure amplitudes, yielded lower mean interface pressures at both sacrum and heel, more equivalent to those values measured with Continuous Low pressure air mattress.

As was discussed in Chapter 3, a number of researchers have used transcutaneous gas measurements to estimate the viability of loaded tissues for both able-boded and debilitated individuals. Although the techniques necessitate an elevated electrode temperature of 44^oC, it is generally accepted that temporal monitoring of T_cPO_2 and T_cPCO_2 reflect relative changes in the tissue viability. In addition, changes in the gas tensions have been shown to correlate with parameters associated with collection of sweat samples at sites overlying bony prominences (Knight et al., 2001). The present findings reveal a number of different responses dependent on the internal characteristics of the mattress and, to a lesser extent, on the individual subject. However, for the most part, the T_cPO_2 levels either remained fairly stable during the loaded period or fluctuated at a periodicity equivalent to the cycle period of the APAM system. In both cases, the T_cPCO_2 levels remained within the normal basal range. By contrast, in some cases, there was a significant compromise to the T_cPO_2 levels during the loaded period, which was often associated with an increase in T_cPCO_2 levels. These cases generally, but not inclusively, coincided with an internal pressure amplitude of 100/0 mmHg. This is reflected in the pooled data for the parameters associated with oxygen debt (Figure 5-16) and elevated carbon dioxide levels (Figures 5-17 and 5-18). However, it is important to note that oxygen debt per se does not reflect continued compromise to tissue viability. Indeed it has been previously reported that it is only when the oxygen reduction reaches a threshold level is there an increase in carbon dioxide levels within the loaded tissues (Knight et al., 2001). The present results indicate such a relationship for both pooled data (Figure 5 - 19) and when the data is divided into different parameters associated with the internal mattress characteristics (Figures 5-20 to 5-22).

Certain questions were not addressed in the present study. For example, the study only employed a small group of subjects. Nonetheless, the inter-subject variability was clearly evident. As an example, a range of responses were demonstrated even on the static CLP and NHS mattress (Figures 5-25 and 5-26). Such differences might only be

amplified when the effect of a prescribed signature within an APAM system is tested on a mixed group of subjects, considered to be at risk of developing pressure ulcers.

In addition, this group of subject only included young healthy volunteers. Thus the effectiveness of the prescribed internal pressure within the mattress for bed-bound subjects, who may be particularly susceptible to soft tissue breakdown, needs to be investigated. This would elucidate whether the prescribed intermittent form of pressure relief provided by the mattress is sufficient to maintain viability of tissues compromised by intrinsic factors.

To conclude, the approach adopted indicates that the internal pressures of the mattress will influence both the microclimate of the support interface as well as the viability of the loaded soft tissues.

Chapter 6.

Physiological Response of Sacral Tissues on a Self-Adjusting Alternating Low Pressure Mattress

Pressure ulcers tend to form in specific areas overlying bony prominences, where a given interface pressure will produce concentrated levels of enhanced tissue compression. Indeed, various studies consistently highlight the sacrum as one of the most common anatomical location for pressure ulcers to develop (Le et al., 1984).

Internal pressure characteristics may be either initially prescribed for all subjects, the results of which are detailed in the previous chapter, or adjusted for each subject. The latter approach was adopted in the present chapter. This was facilitated by the use of a Self-Adjusting Alternating Low Pressure sensor (SAALP^{TM}), which was designed to be used in conjunction with a prototype alternating pressure air mattress. Based on subject morphology, the internal sensor controls the alternating low pressure signature, in terms of internal pressures and cycle time.

The present chapter examines the performance of the prototype mattress, with particular reference to assessing the interface conditions with healthy subjects of various morphologies positioned supine on an articulated bed at a range of backrest angles. In particular, the study is designed to evaluate whether the prototype mattress can maintain healthy tissue viability, in terms of transcutaneous gas tensions, over a monitoring period of at least 30 minutes.

6.1 Experimental Materials & Methods

There are many instances where impaired mobility can lead to increased susceptibility to pressure ulceration. This could include patient suffering from paralysis, locomotor disorders or musculoskeletal fractures. In addition for some conditions, such as Pulmonary Heart Disease, patients need a hoist bed frame to be moved. With such an arrangement, interface pressure, shear forces and friction will be different to a horizontal static position. In order to investigate the effects of the sensor performance (internal peak pressures and cycle time) at different orientations, the surface prototype was placed on an articulated hospital bed at a range of head of bed (HOB) angles up to 60°.

6.1.1 Characterization Support Surfaces

SAALP is a mattress replacement system designed to provide an automatic adjustment of the supporting pressure in both the alternating pressure (AP) and continuous low pressure (CP) sections of the mattress.

The prototype support mattress (PAM, HillRom, France), hereafter referred to as the mattress, was divided into four sections, as indicated in the schematic in Figure 6-1. These four sections are:

• A carved foam accommodating the heel region (pale blue section in Figure 6-1),

• 3 rows of air cells coincident with the lower limb region – under continuous pressure (CP) control,

• 8 rows of air cells accommodating the sacral region – under alternating pressure (AP) control (as indicated in yellow and blue rows),

• 9 rows of air cells accommodating the upper torso – under CP control.
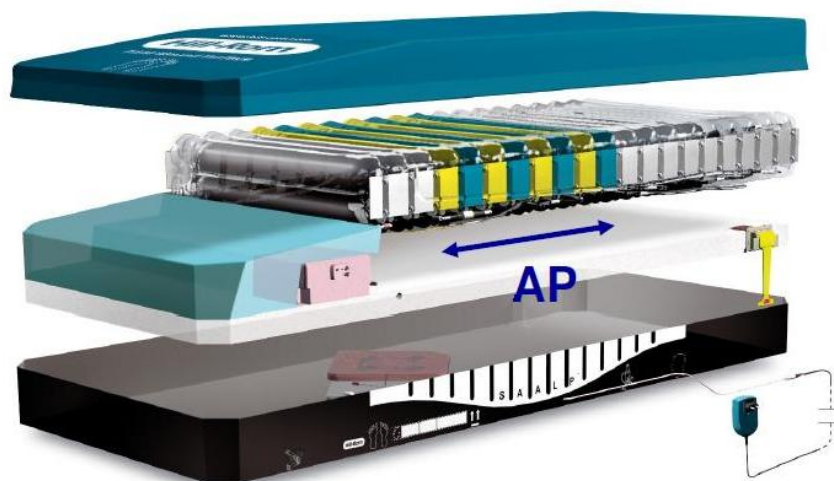
Figure 6 - 1 Schematic of the prototype mattress. Arrow indicates the sacrum section incorporating 8 air cells exposed to alternating internal pressures.

The internal pressure within the air cell of the sacral region (AP region) is adjusted automatically and in real-time in order to match the individual subject's weight, shape and position on the mattress. In addition, the duration of the pressure cycle depends on the subject's morphology and position. The control mode is based on the use of a new patented automatic sensing technology (SAALP^{TM}, HillRom, France) which, according to the subject morphology and position, adjusts both the alternating pressure signature in the sacral section and the continuous low pressures in the upper torso and the lower limb sections. The mattress was placed on an articulated hospital bed (AVG 800 frame, HillRom, France) with a head of bed (HOB) adjustment.

6.1.2 Experimental Procedure

Phase I Tests

All tests were performed in a quiet side room off the Biomechanical Performance Laboratory, which was maintained at a temperature of 26 ± 2 ^{o}C and at a relative humidity of between 35-45%. Before the test period each subject was required to sit on a high stool and two trancutaneous gas electrodes (Model 841, Radiometer, Denmark), which were set at 44° C for both calibration and test measurement, were attached to the mid-region of the sacrum and the right scapula. During an

acclimatisation period of 15 - 20 minutes, in which the trancutaneous gas values attained unloaded basal values, the mattress was activated with, for the initial measurement session, the HOB set at 0 degree. At the end of the period, the subjects were requested to gently position themselves centrally onto the mattress surface in a comfortable, supine position. The surface was covered with a thin polymer sheet incorporating a 96 cells array of air sacs (described in Figure 3-3) attached to a Pressure Monitoring system (Talley Mark Ⅲ, Talley Medical Group, Romsey, UK). The output of the internal air pressures were monitored to assess the time at which the sensor had adjusted to a steady state. This was demonstrated by repeatable levels of intermittent pressure in the sacral section of the mattress in the AP mode, which was generally achieved within 3 and 12 minutes of the subject lying on the mattress. The interface pressures were then recorded across the 96 cells array. The mean values at each cell position were subsequently estimated from approximately 5 complete scans, lasting approximately 6 minutes.

The internal pressures were recorded continuously throughout the test period on both the alternating (AP) and continuous (CP) sections of the mattress. For the AP section, the maximum and minimum internal pressures were recorded and the cycle time was estimated.

The transcutaneous oxygen tensions (T_cPO_2) were recorded continuously throughout the test period from the two electrodes. The transcutaneous carbon dioxide tensions (T_cPCO_2) were only recorded from the sacral location.

At the end of the test period, which lasted up to 60 minutes, the measurement of interface pressures was repeated. All outputs were processed using appropriate software associated with a PC. For the three subsequent measurement sessions, each subject was tested at HOB angles of 30, 45 and 60 degrees.

Phase II Tests

In some of the subjects tested in phase I, it was evident that a stable system, as defined by a repeatable alternating pressure signature, was not always achievable in the AP section of the mattress within a 15 minutes period. Accordingly the methodology was adapted in Phase II (11 subjects, Table 6-1) to include two revised protocols to accommodate.

1. Subject alignment on the surface - the subject's hip was aligned with the triangle indicated on the bed frame. This ensured both consistent subject placement and optimal performance of the SAALP^{TM} sensor in terms of individual subject characteristics, which is illustrated in Figure 6-2.

2. Steady state phase – data was collected initially for at least 4 AP cycles to ensure a uniform pressure signature was achieved, in terms of magnitude and cycle time.

Figure 6 - 2 Images showing left, the Transcutaneous gas sensor attached to sacrum and right scapula; right image show a subject lying supine on the SAALP support surface with measurement sensors attached at a HOB angle of 30 degree.

6.2 Experimental Strategy

6.2.1 Experimental Array

Potential participants were chosen from healthy volunteers who were above 18 years of age, and exclusion criteria were applied to any potential subject with a history of

chronic skin disease, such as psoriasis. The subjects, who fulfilled these requirements for inclusion, as stated in the advertisement, were identified as a participant(s) in the study. Before inclusion, an information sheet, as detailed in Appendix C-3 was made available to clarify the measurement protocols involved in the experimental study. In addition, the principal experimenter was also available to answer any further issues raised by the volunteers. The project was approved by the Queen Mary University of London (QMUL) Local Ethics Committee (Ref No. QMREC2009/43). Consent was obtained for each subject before testing. Both the information sheet and consent form are included in Appendix C-3 and C-4. An overview of the complete test protocol is provided in Figure 6-3.
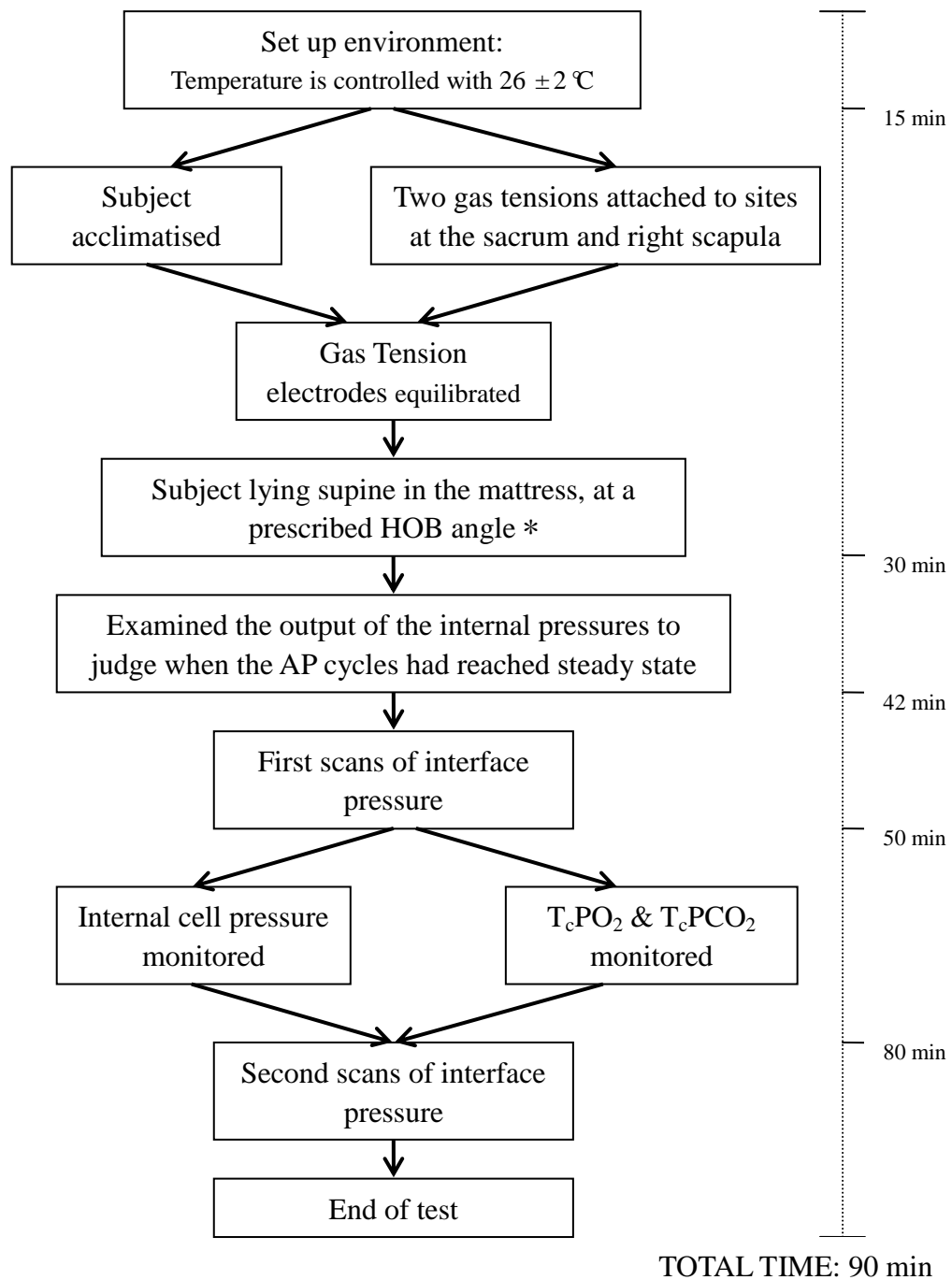
* **HOB angles presented at 0 °, 30 °, 45 °and 60 °**

Figure 6 - 3 Flow diagram indicating the timelines for the experimental protocols for measuring the combined transcutaneous gas tensions, internal pressures and interface pressures.

6.3 Result

Table 6 - 1 summarises the anthropometry of the human volunteers recruited into the study, involving 12 healthy subjects. It should be noted that five subjects, A-D and F, were included in both phase I and phase II tests. This provided some indication of the effects of positioning and the measurement repeatability on the developed test protocols. Particular attention was paid to subject L, with a body weight of 170 kg, which is in excess of the SAALP^{TM} sensor working limit (130 kg) according to the recommendations of the manufacturers.

Table 6 - 1 Summary of volunteer characteristics

Phase		Sex	Age	Height (m)	Weight (kg)	BMI (kg/m^2)
I and II	Subject A	M	28	1.76	80	25.8
I and II	Subject B	F	27	1.64	53	19.7
I and II	Subject C	M	27	1.74	70	23.1
I and II	Subject D	M	28	1.92	105	28.5
I	Subject E	M	27	1.70	75	26.0
I and II	Subject F	M	26	1.83	71	21.2
II	Subject G	F	27	1.64	60	22.3
II	Subject H	F	26	1.68	65	23.0
II	Subject I	F	30	1.64	76	28.3
II	Subject J	F	26	1.65	52	19.1
II	Subject K	M	24	1.92	115	31.2
II	Subject L	M	33	2.00	170	42.5
Range			24-33	1.64-2.00	52-170	19.1 - 42.5

6.3.1 Internal Characteristics of the Mattress

A steady state was achieved in the internal state of the mattress in over 85% of the total number of tests (phase I and II). In these cases, the maximum and minimum pressures in the AP section and continuous pressures recorded in the CP sections were

constantly maintained by the SAALP™ sensor. These results were examined in terms of the BMI of individual subjects at both phase I and II respectively, as shown in Figure 6-4.

With respect to the Phase I results (the left hand side of Figure 6-4), there were few obvious differences in the maximum internal pressures for either AP or CP sections with BMI values. For example, values ranged from 12 to 24 mmHg, in the sacral region with a HOB angle of 0 degree. Indeed close examination of the data revealed that in most cases these internal pressure were lowest at a HOB angle of 0 degree. The minimum internal pressure were generally 2 - 3 mmHg, although higher values up to 16 mmHg were measured with a few subjects supported at elevated HOB angles (Figure 6-4 b, left side). By contrast, when the maximum internal pressures in the sacral section were examined for all phase II subjects, they varied dependent on the BMI of the individual, as illustrated in Figure 6-4 a, right side. The findings suggest a gradual increase in internal pressure with BMI for all HOB angles. However, this increase was particularly marked at HOB angles of 30 degree and above, with internal pressure values exceeding of 25 mmHg for subject with a BMI of 28.3 kg/m^2 and above. Similar trends were evident in the maximum internal pressure of the CP sections (Figure 6-4 c, right side). It should also be noted that the sensor was not able to stabilise the pressure cycle for the two subjects with the highest BMI when supported with a HOB angle of 60 degree. The corresponding values for all phase II subjects at the minimum pressures of the AP cycles showed no remarkable trends with values ranging from 1.9 - 3.9 mmHg, independent of BMI values, as illustrated in Figure 6-4 b, right side. The data for Phase II test alone may be alternatively presented in graphical form with statistical analysis, using a linear regression analysis. As can be seen in Figure 6-5, the linear models were statistically significant at the 1 per cent level for all four HOB angles. It is evident that the internal pressures increased more rapidly with BMI at higher HOB angles, as reflected in the slopes of the linear models.
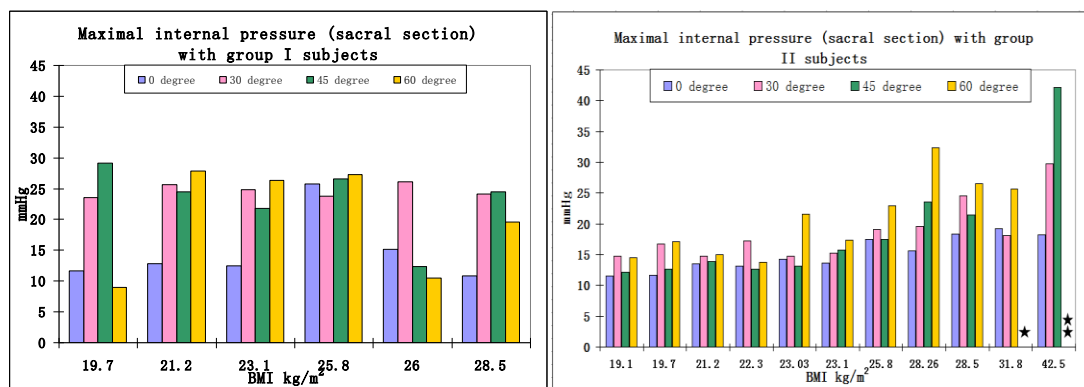
(a)
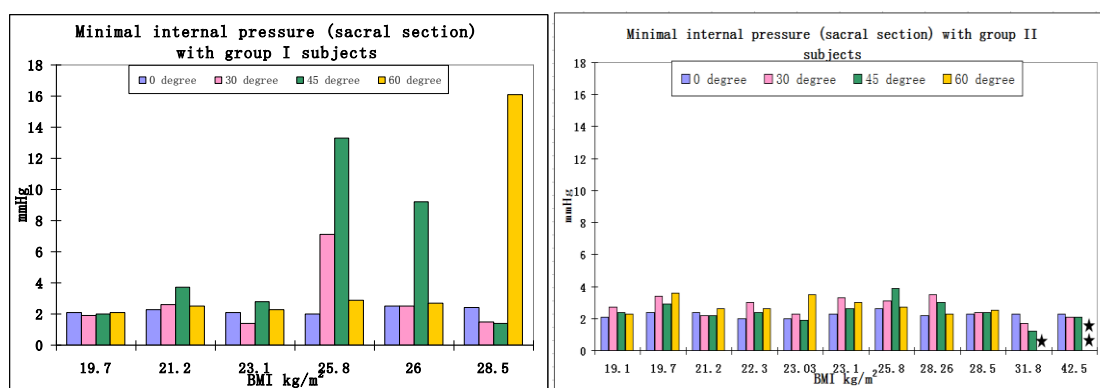
(b)
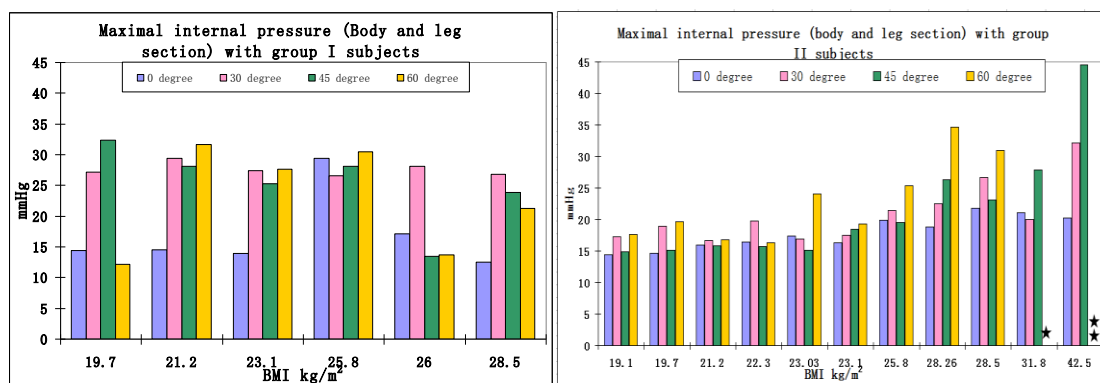
(c)

Figure 6 - 4 The relationship between maximal (a) and minimal (b) internal pressures (AP) and maximal internal pressure (CP, (c)) versus Body mass index (BMI) of subjects supported at various degrees of HOB in Phase I (left) and Phase II (right).

★ **The control system for SAALP was not stable, as defined by an irregular CP cycle**

★ **Incomplete data**

Maximal internal pressure (sacrum) with group II
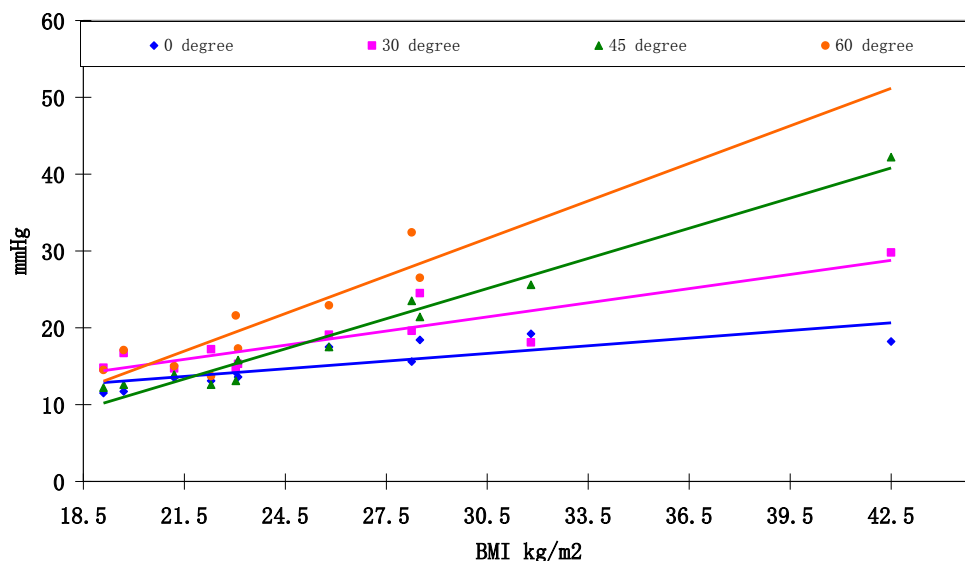
HOB angle	Linear model	r	P
0 degree	y = 0.332x + 6.526	0.80	< 0.01
30 degree	y = 0.615 x + 2.662	0.88	< 0.01
45 degree	y = 1.308x − 14.803	0.98	< 0.01
60 degree	y = 1.629x − 18.081	0.88	< 0.01

Figure 6 - 5 Statistical analysis of effects of maximal internal pressure (AP) on BMI in Phase II test. Table indicates results of linear regression.
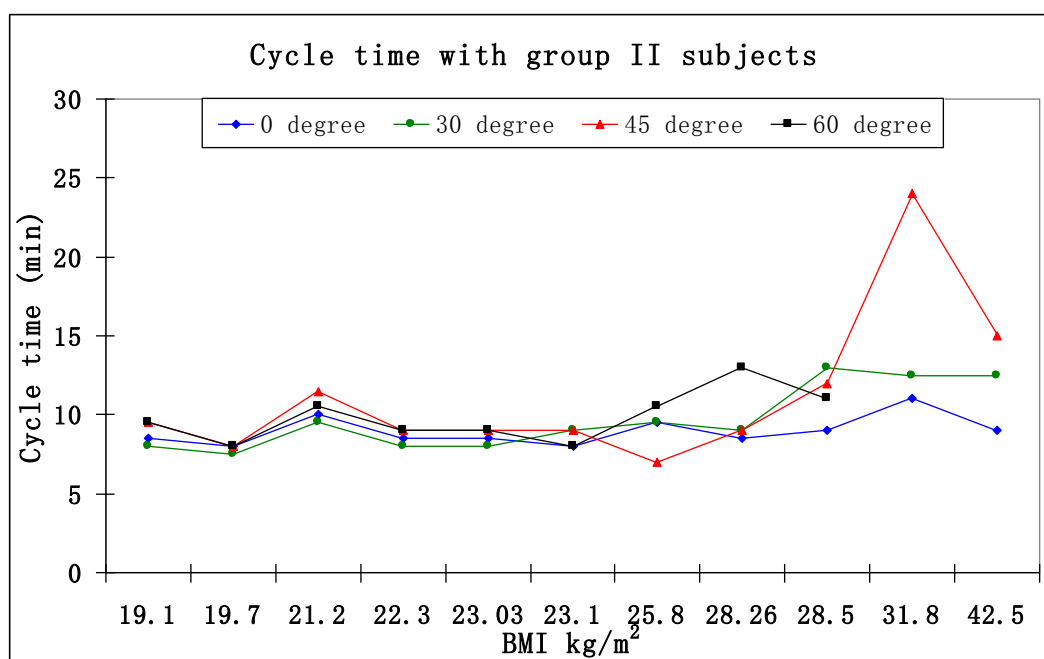
Figure 6 - 6 The relationship between cycle time in the alternating section of the mattress and BMI for each subjects tested in phase II tests only, with different Head of Bed angle.

153

The corresponding cycle time for each condition in phase II tests only is presented in Figure 6-6. There are few trends for BMI values up to 25.8 kg/m^2, with cycle times of between 7 and 11 minutes for each of the HOB angles. However, for subjects with higher BMI values, the time for the AP cycle in the sacral region could exceed 15 minutes. It is also worth noting that for these subjects a steady-state cycle period in the sacral region was not achievable with a HOB angle of 60 degree.

The complete data from the SAALP support surface is presented in Appendix C-1, indicating the internal state of the mattress for all subjects in Phase I and II tests, respectively.

6.3.2 Tissue Viability of Soft Tissue under Prolonged Loading

A. Repeatability of data

For all Phase I and Phase II tests (17 in total), complete data for transcutaneous gas tensions and associated interface pressures were collected, and details included in the attached CD.

Five subjects were tested in both phases I and II. Although there were some differences in the test protocols, as described in section 6.1.2, the measurement protocols for transcutaneous gas and interface pressures were identical. There was considerable consistency in the repeat measurements for transcutaneous gas tensions, as exemplified with one subject (Figure 6-7). For example, in both sets of measurements at the four HOB angles, the sacral T_cPO_2 was similar to the corresponding scapular values, and demonstrated adequate tissue viability, in terms of T_cPO_2 values, even at a HOB angle of 60 degree.

However with some subjects there were differences in the repeat measurements, in terms of both internal mattress characteristics and the tissue response for corresponding HOB angles. This is indicated by close examination of Table C-1-1 and C-1-2 in Appendix C and, more specifically in Figure 6-8. In the latter, it can be seen
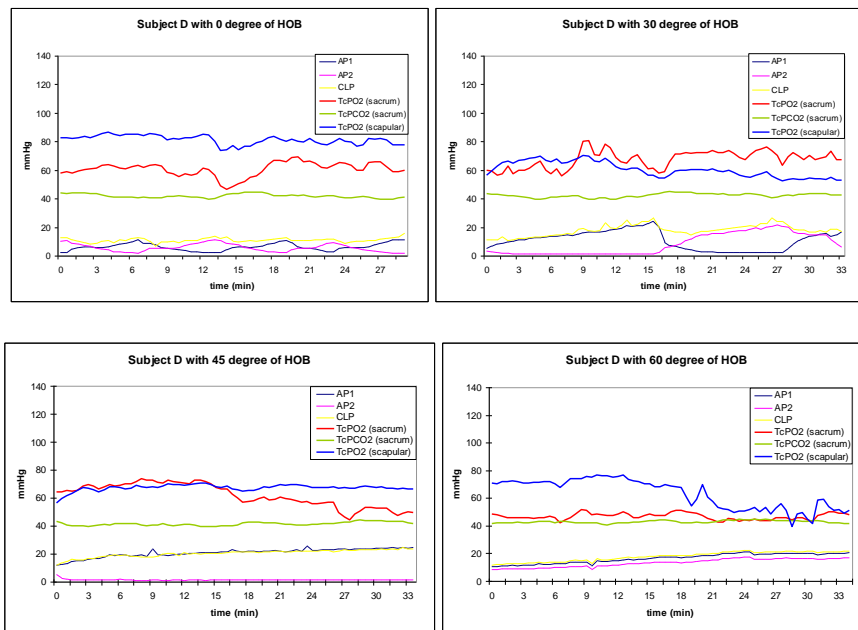
(a)
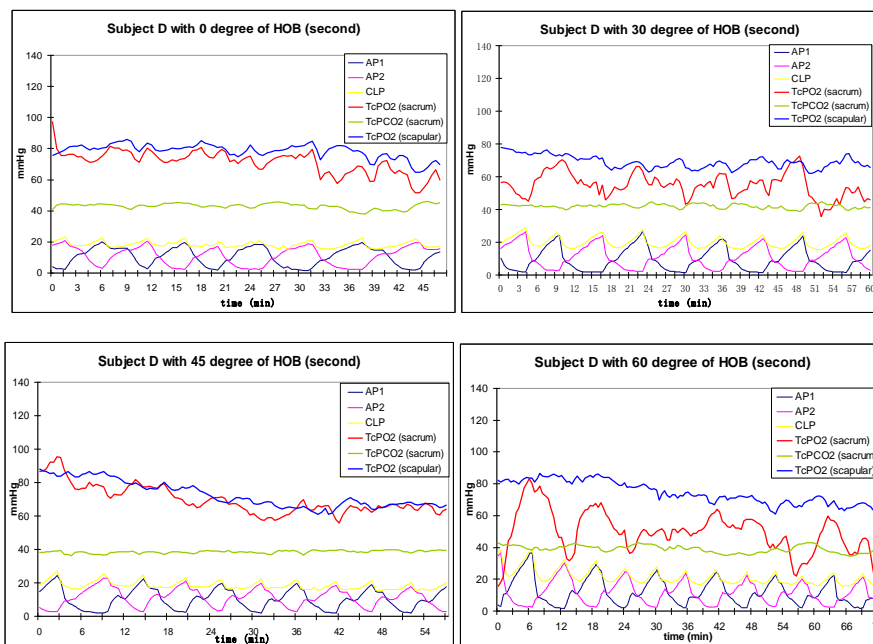
(b)

Figure 6 - 7 The T_cPO_2 response for Subject D (BMI of 28.5 kg/m^2) supported at various degrees of HOB when assessed in Phase I (a) and Phase Ⅱ (b). In addition, the T_cPCO_2 values at the sacrum are shown, and the corresponding internal pressures for each test condition.

(a)

(b)

Figure 6 - 8 The T_cPO_2 response for Subject F (BMI of 21.2 kg/m^2) supported at various degrees of HOB when assessed in Phase I (a) and Phase II (b). In addition, the T_cPCO_2 values at the sacrum are shown, and the corresponding internal pressures for each test condition.

that a periodic internal mattress state was achieved at all HOB angles and a cycle period was estimated. This indicated the importance of the modified protocols introducing in Phase II tests at Figure 6-8, b. In Phase II, the test period was prolonged to obtain a steady state phase, which is defined by at least 4 AP cycles whose profiles, in terms of both magnitude and cycle time, are relatively uniform.

B. Transcutaneous oxygen tensions

Close examination of the data enabled the categorization of a number of characteristic responses. In many cases, the sacral T_cPO_2 levels were of similar magnitude to those at the scapula, for all four HOB angles. This was associated with maximum interface pressures, which generally did not exceed 51 mmHg (6.8 kPa), such a response, which is illustrated in Figure 6-9, was evident in over 40% of the total number of responses. By contrast other responses demonstrated distinct perturbations in the sacral T_cPO_2 levels, which appeared to be associated with the AP profile within the mattress. In most cases, this mechanism ensured that the T_cPO_2 levels remained relatively high for a significant proportion of the support period. Examples are indicated in Figure 6-10 (a-c), which demonstrates one subject supported at HOB angle of between 0 and 45 degrees. However, the response of the same subject appeared to be relatively compromised at the HOB angle of 60 degree (Figure 6-10 d). These series of responses were associated with interface pressures which generally did not exceed 65 mmHg (8.7 kPa).

In some subjects, the sacral T_cPO_2 decreased markedly at elevated HOB angles, associated with an increase in interface pressure. In particular at an HOB angle of 60 degree, the T_cPO_2 levels were relatively low compared to both the sacral levels at an HOB of 0 degree and the equivalent T_cPO_2 levels at the scapular. This response is illustrated in Figures 6-10 and 6-11 and was associated with a range of elevated interface pressures in the sacral region.

	Maximum Interface Pressures (mmHg)		Maximum Interface Pressures (mmHg)	
	Sacrum		Scapular	
	First scan	Second scan	First scan	Second scan
Subject I with 0°	37	34	23	22
Subject I with 30°	39	38	32	29
Subject I with 45°	46	36	34	25
Subject I with 60°	51	51	34	34
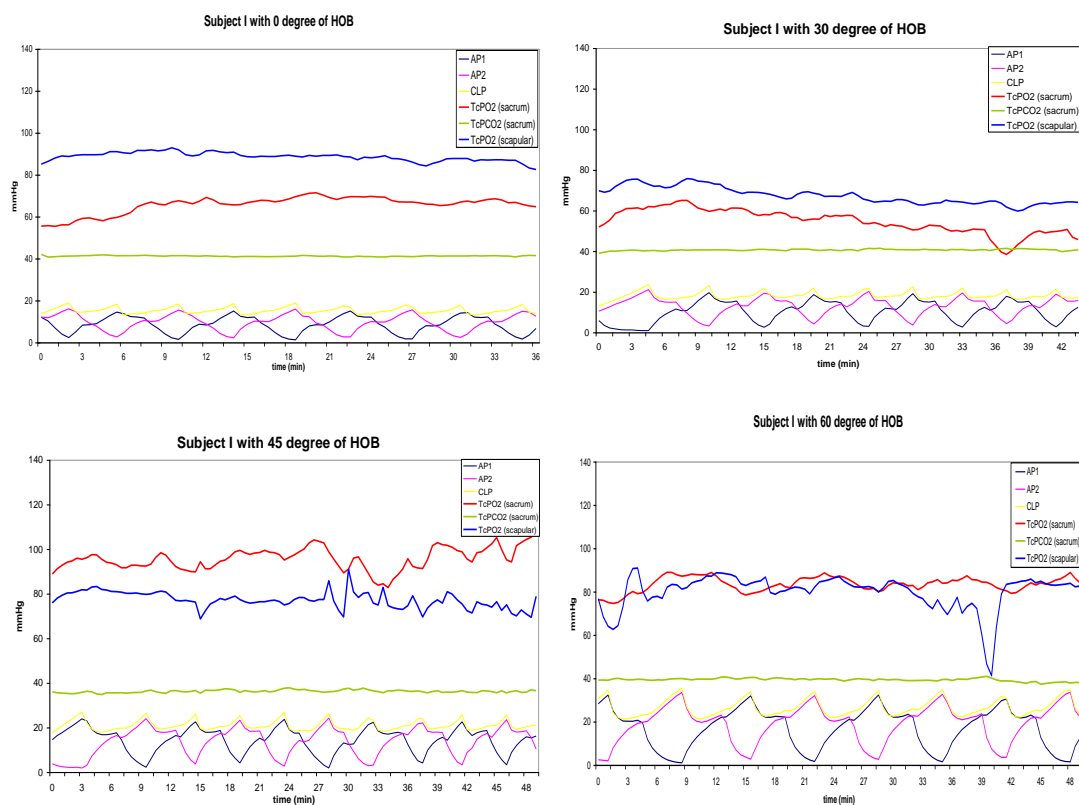
Figure 6 - 9 A complete set of data incorporating four combinations of various Head of Bed angles for subject I (Female, BMI = 28.3 kg/m^2) with a self adjusted pressure profile. AP1 and AP2 indicate individual air cell with alternating low pressure in sacral section. CLP indicated internal pressure at continuous low pressures sections. The T_cPO_2 is corresponding to gas tensions at both sacral and scapular sites over the monitoring period. The T_cPCO_2 response is only recorded from sacral location. The corresponding interface pressure was show in below.

	Maximum Interface Pressures (mmHg)		Maximum Interface Pressures (mmHg)	
	Sacrum		Scapular	
	First scan	Second scan	First scan	Second scan
Subject J with 0°	58	51	23	27
Subject J with 30°	34	37	23	24
Subject J with 45°	58	59	23	26
Subject J with 60°	62	65	22	23
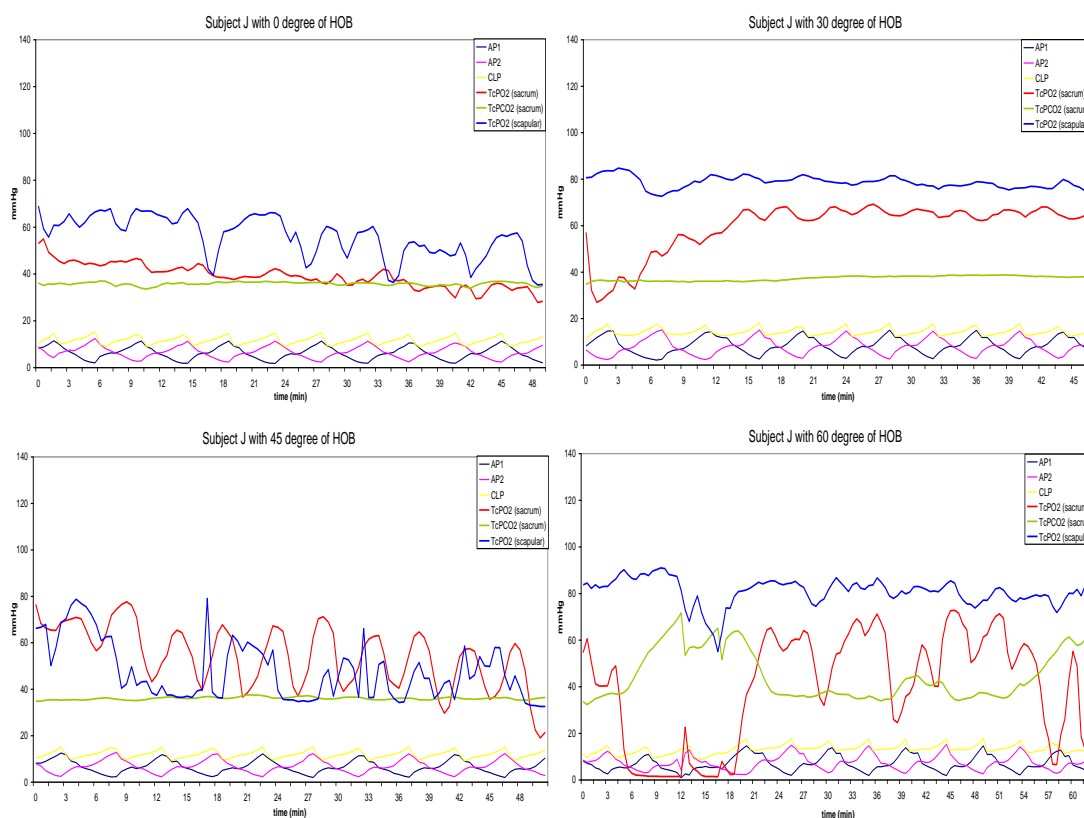
Figure 6 - 10 A complete set of data for each of the four Head of Bed angles tested with subject J (Female, BMI = 19.1 kg/m^2) lying on the prototype mattress. AP1 and AP2 indicate individual air internal pressures within the sacral section and CLP indicated the corresponding internal pressure within the continuous low pressures sections. The T_cPO_2 levels are indicated for both sacral and scapular sites over the monitoring period, whereas the T_cPCO_2 response is only recorded from the sacral site. The corresponding interface pressures are indicated for both sites in the table above.

	Maximum Interface Pressures (mmHg)		Maximum Interface Pressures (mmHg)	
	Sacrum		Scapular	
	First scan	Second scan	First scan	Second scan
Subject H with 0°	37	37	35	39
Subject H with 30°	91	145	23	22
Subject H with 45°	65	65	41	31
Subject H with 60°	147	95	41	43
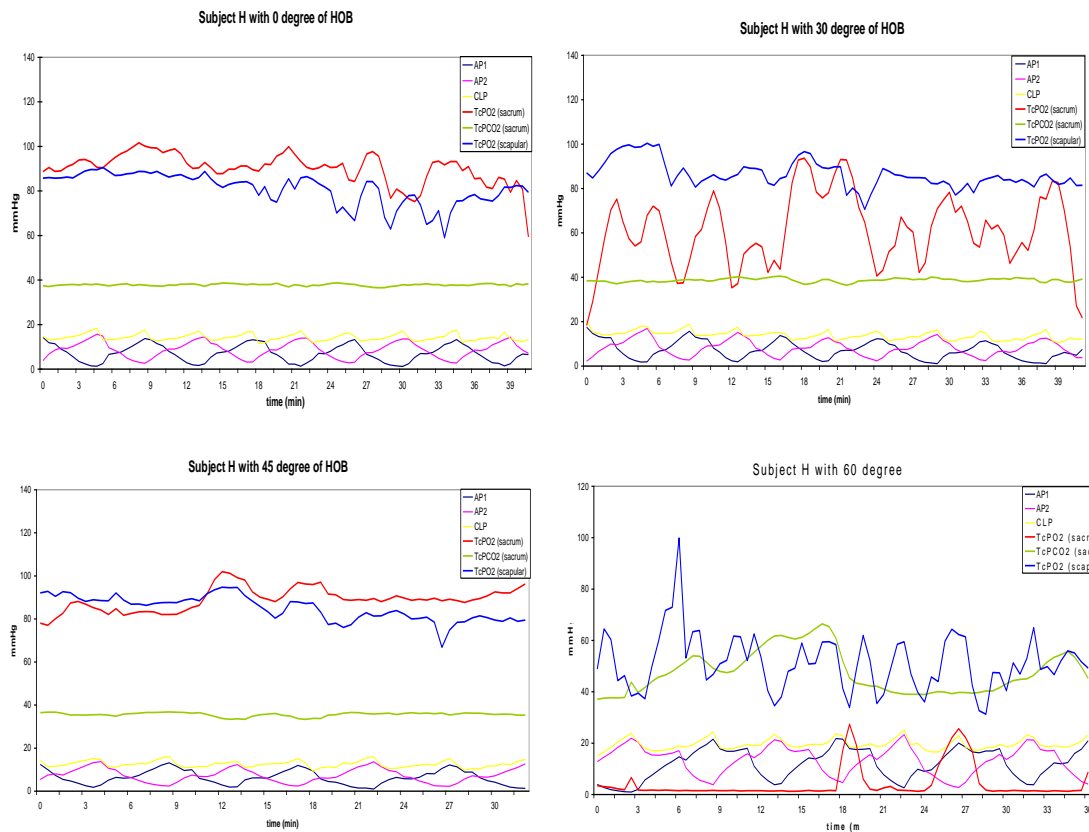
Figure 6 - 11 A complete set of data for each of the four Head of Bed angles tested with subject H (Female, BMI = 23 kg/m^2) lying on the prototype mattress. AP1 and AP2 indicate individual air internal pressures within the sacral section and CLP indicated the corresponding internal pressure within the continuous low pressures sections. The T_cPO_2 levels are indicated for both sacral and scapular sites over the monitoring period, whereas the T_cPCO_2 response is only recorded from the sacral site. The corresponding interface pressures are indicated for both sites in the table above.

C.   Transcutaneous carbon dioxide tension

In the sacral region, simultaneous measurements of transcutaneous oxygen and carbon dioxide tensions were performed. In most of the test subjects there was very little change in T_cPCO_2, as indicated in Figure 6-12 (a-d), regardless of the levels in T_cPO_2. Indeed T_cPCO_2 maintained values within a range of between 35-45 mmHg (4.7 - 6.0 kPa), generally considered to be normal (Bogie et al., 1995; Knight et al., 2001). This response was associated with interface pressures which generally did not exceed 65 mmHg (8.7 kPa).

By contrast, 4 of the subjects revealed an elevation of T_cPCO_2 values, restricted to measurement performed when the HOB was elevated to 60 degree, show in Figure 6-13 (a-d). These were all noted to be associated with T_cPO_2 values, which were largely depressed during the monitoring period.

	Maximum Interface Pressures (mmHg)		Maximum Interface Pressures (mmHg)	
	Sacrum		Scapular	
	First scan	Second scan	First scan	Second scan
Subject G with 0°	43	40	23	25
Subject G with 30°	53	50	23	26
Subject G with 45°	61	51	33	40
Subject G with 60°	66	50	26	23

(a)

(b)

(c)

(d)
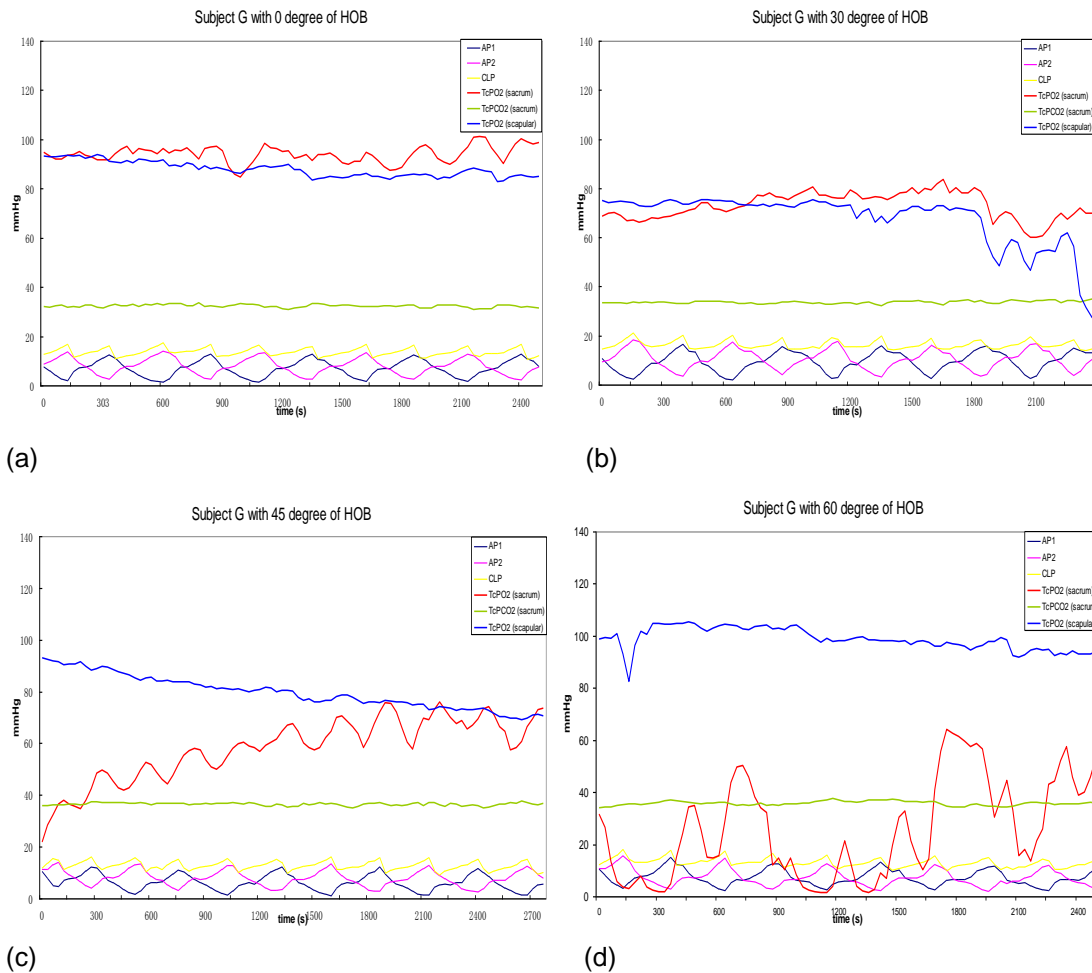
Figure 6 - 12 (a-d) Typical response of subject G (BMI of 22.3 kg/m^2), who demonstrated minimal change in T_cPCO_2 values when supported in any of the four HOB angles (as indicated with the green line). The interface pressures in the mattress are also indicated.

	Maximum Interface Pressures (mmHg)		Maximum Interface Pressures (mmHg)	
	Sacrum		Scapular	
	First scan	Second scan	First scan	Second scan
Subject A with 60°	37	36	24	26
Subject E with 60°	91	86	29	28
Subject H with 60°	147	95	41	43
Subject J with 60°	62	65	22	23

(a)

(b)

(c)

(d)
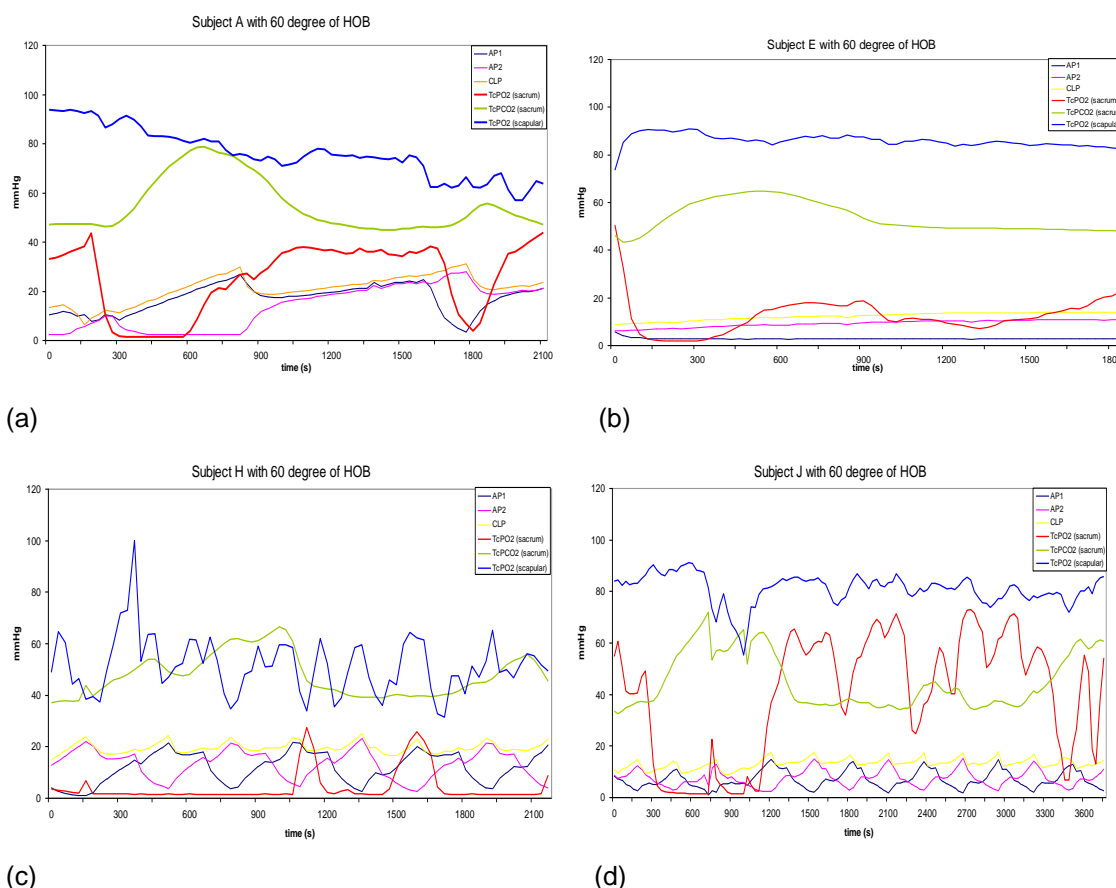
Figure 6 - 13 (a-d) Response of four subjects, who demonstrated an elevation in T_cPCO_2 values when supported at an HOB angle of 60 degrees (as indicated with the green line). The internal pressure in the mattress is also indicated.

(a) Subject A (BMI = 25.8 kg/m^2; Phase I)

(b) Subject E (BMI = 26 kg/m^2; Phase I)

(c) Subject H (BMI = 23.03 kg/m^2; Phase II)

(d) Subject J (BMI = 19.1 kg/m^2; Phase II)

163

6.4 Discussion

The developed methodology provides a well-established system of assessing the tissue viability and internal/interface conditions for volunteer subjects supported on a continuous and/or alternating air mattress system. It has been employed in the present work to evaluate physiological response of the sacrum tissue on a Self-Adjusting Alternating Low Pressure mattress supported on an articulated bed frame. The effects of the HOB angle were examined using a number of well-reported biomechanical parameters, including T_cPO_2/T_cPCO_2 levels, for a continuous period of up to 60 minutes.

This study examined the response of normal healthy subjects when positioned supine on a prototype mattress supported on an articulated bed frame at a range of Head of Bed angles up to 60 degree. A particular feature of the mattress was the incorporated Self Adjusting Low Pressure sensor (SAALP™), which adjusted the internal state of the mattress according to the morphology of the individual subject. The internal state of the mattress was monitored in terms of the maximum and minimum internal pressures and the cycle time in the AP section and the maximum internal pressures in the CP sections of the mattress.

The study incorporated a protocol which was modified from phase I tests, which indicated limit sensitivity to BMI values in terms of internal pressures in both AP and CP sections of the mattress (Figure 6-4 left). Accordingly, in phase II tests the sensor clearly adapted more efficiently to the individual morphology, matching design requirements of the manufacture. Indeed in the cases where the alternating pressure signature was stabilized, the system accommodated both higher BMI values and increased HOB angles, by increasing the internal pressure (Figure 6-4 right (a)). Identical trends were also recorded in the CP sections of the mattress (Figure 6-4, right (c)). Thus the prototype mattress with its inbuilt sensor was certainly found to be responsive to individual subject morphology. This resulted in acceptable tissue

viability levels when the bed was adjusted up to a HOB of 45 degree.

APAM systems are designed to provide intermittent pressure relief to maintain the viability of loaded tissues. This parameter was examined by monitoring the transcutaneous gas levels at the sacrum and the scapula, the latter representing a mildly loaded site in the supine position. In addition, interface pressures were measured. As indicated in section 6.3, there were distinct categories of tissue response (Figures 6-9 to 6-13).

It is evident that for many subjects, sacral T_cPO_2 and T_cPCO_2 were maintained at approximately basal levels for the 30 mins monitoring period, with associated maximum interface pressures which generally did not exceed 50 mmHg (6.67 kPa). This is illustrated in Figure 6-9 for a subject with a BMI of 19.7 kg/m^2, in which the maximum internal pressures (AP) ranged from 11.7 – 17.1 mmHg over the range of HOB angles. In other cases, the perturbations were evident in the T_cPO_2 during the monitoring period, associated with an alternating pressure signature. As indicated in Figures 6-10 and 6-12(a-c), the T_cPO_2 levels were generally maintained above 30 mmHg, a threshold value above which tissue viability is not considered to be compromised (Bogie et al., 1995). These responses from sacral tissues strongly suggest that the alternating pressure mode in the section incorporating the sacral region provides optimal support in maintaining tissue viability for most of the test subjects.

By contrast in a few cases, perturbations in T_cPO_2 consistently fell below this threshold value for T_cPO_2 (Figures 6-12 (d) and 6-13 (a-d)). These cases were generally associated with enhanced levels of T_cPCO_2 and occurred with the subjects supported at a HOB angle of 60 degree. In these cases, the pressure signature was clearly inadequate in maintaining tissue viability over the monitoring period.

The SAALP sensor appeared to adjust with BMI accordingly, even for the heavier volunteer subjects. Indeed two subjects (K and L) were included in the study, whose

BMI could be classified as obese (American Obesity Society, 2008), and their detailed results are included in Appendix C-2. It was evident that the sensor adjusted the internal pressures in the mattress accordingly with values in excess of 25 mmHg at a HOB angle of 45 degree (Figure 6-4 right, (a)). The resulting response was similar to that presented in Figure 6-10 with adequate viability over the monitoring period. However for both subjects supported at a HOB angle of 60 degree, the sensor was not able to attain a steady state pressure signature in the AP section within a cycle period of 15 minutes (Figure 6-6). These findings highlight the importance of stabilizing the AP signature for each subject if the mattress is to provide adequate support for each subject. It should be stated, however, the present work only employed normal healthy subjects and could be extended to evaluate the performance of the mattress for bed-bound subjects, who may be particularly prone to pressure ulcer development. Nonetheless the present study offers the potential for an intelligent support surface, whose internal characterises can be adjusted according to the needs of an individual morphology.

Chapter 7

Interface Climate Assessments at the Loaded Support Surface

Pressure ulcer development may in part, be related to the accumulation of heat and perspiration at the skin surface. Indeed both heat and moisture increase skin susceptibility to the damaging effects of pressure and shear, then decrease the resiliency of the epidermis to external forces (Dinsdale, 1974; Bryant, 1992; Flam et al., 1995). Therefore, both controlling the microclimate of the skin and providing a quality patient support system represent an important strategy in minimizing the risk of pressure ulcers. The main objective of the present study was to develop an experimental method which could produce reproducible results to examine interface temperature and humidity, using different mattress modes, and differing sheets, under a physical model which incorporated variable "sweat rate".

The methodology of this study was adapted from that previously reported (Figloila, 2003). However, the present work was limited to assessing the various Low Air Loss (LAL) systems. The present study was designed to compare various LAL systems with alternative pressure mattresses (APAM).

7.1 Past Relevant Study

A few studies have previously described laboratory-based tests to examine the effectiveness of moisture and temperature reduction at the patient/support interface (Nicholson et al., 1999; Reger et al., 2001; Figloila, 2003). These studies generally reported concluded that humidity and temperature can be controlled using a surface

167

which incorporates appropriate level of air flow. The details will be reviewed separately.

Nicholson et al., (1999) proposed a performance test to measure the moisture vapor and heat transport capability of various mattress support systems. The test, which was based on appropriate fabric tests used in the textile industry, develops a microenvironment of controlled humidity and temperature above a sample of fabric of a Low-air-loss cover to simulate the steady state of diffusion of moisture through the fabric at physiological conditions. The transport of moisture was measured from the controlled environment into the mattress cover. However, body weight on the mattress was not considered although it is recognised to be an important omission, as it will compresses the mattress, and thus alter its resulting performance. Hence, the findings of this study are indicative of mattress cover vapor transmissibility, not a simulation of mattress performance in a loaded clinical set-up.

Reger et al., (2001) described a test to examine mattress performance that used a water-saturated patient analog to provide moisture. The analog rests on the surface of a Low-air loss mattress (LAL). Its performance is inferred from measurements of the temperature change underneath the analog, reflecting latent energy removal for a period of up to 90 minutes. However, the study did not include an analysis of the errors involved in such complex processes and instead offers qualitative results for moisture transport capability.

By contrast, Figloila (2003) reported a reproducible controlled test methodology which could estimate the balance of moisture transported into, through, and out of a LAL mattress system. During a controlled and defined operating environment, the test system comprised of a load representing the human body controlled at a prescribed normal temperature and perspiration rate. In effect a typical support surface/patient interface microclimate was established in a laboratory setting, as shown schematically

in Figure 7-1. The input and output air flow was quantified in terms of temperature, mass flow rate and relative humidity, to gain a realistic perspective of the normal patient-mattress interface.
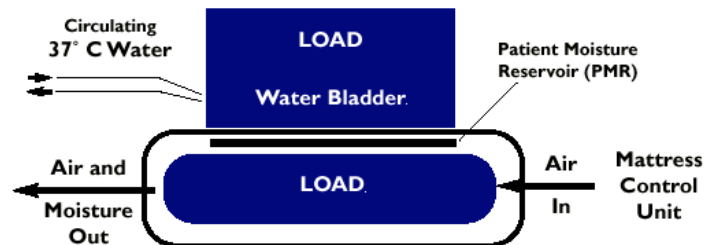
Figure 7 - 1 A schematic representation of a lab-based mattress simulation of a mattress environmental chamber (Figloila, 2003).
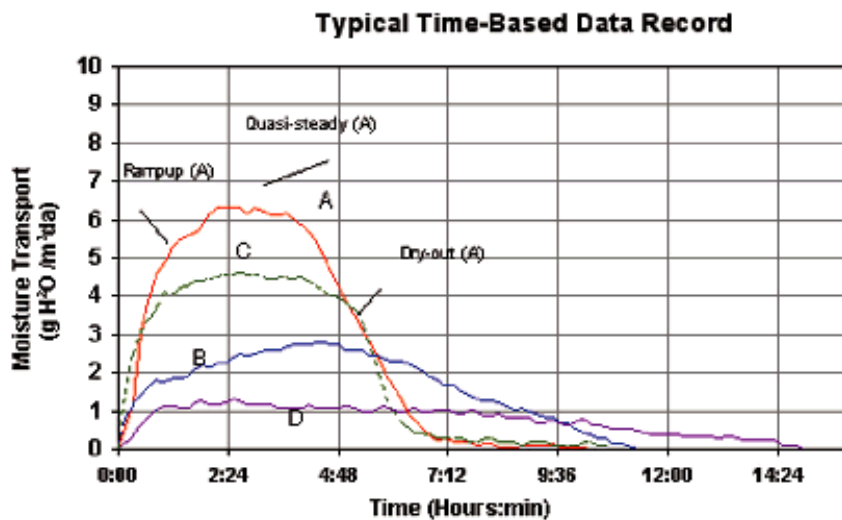
Figure 7 - 2 Temporal profile of a range of mattress systems da = dry air (Figloila, 2003).

The results, as illustrated in Figure 7-2, indicate the temporal profiles of the moisture transport for different test conditions. Moisture removal is predicted by the difference in values between airflow in and the sum of the air flow and moisture out (Figure 7-1). The dissimilar peaks in moisture transport capacities indicate the effectiveness of each of the four mattresses with "A" and "D" representing the most and least effective, respectively. Three distinct zones could be determined from the shape of each curve, which provide an overall understanding of the interface conditions during the duration of the laboratory test, namely:

1. Ramp Up – Shown as the initial increase in moisture levels of the curve, indicating the rate at which air flow attains a peak moisture transport capacity,

2. Quasi-Steady – Shown as the plateau in the curve, representing a steady state region in terms of the moisture levels,

3. Dry-Out – Shown as the decrease in moisture transport levels for each curve. This represents the desiccation of moisture from the interface of the support surface, until zero moisture transport is reached.

The system described in this study produces a useful simulation of a human sweating on a support surface. It further indicates that both temperature but, in particular, moisture can be monitored at the microenvironment interface using airflow techniques. This observation is critical if mild levels of tissue breakdown are to be avoided due to skin maceration (Allman et al., 1989; Figloila, 2003; Reger et al., 2001).

7.2 Materials & Methods

7.2.1 Design of Lab – Based Test System

The laboratory test method design is based on the principles of transport conservation. This approach requires defining a controlled environment around the test system, and representing a control volume in which inflow and outflow characteristics are monitored. Transport properties such as temperature, airflow rate, and absolute humidity levels should be monitored into and out of the control volume. The concept is that differences transport properties between inflow and outflow reflect causal effects within the control volume. In this case, humidity removed from the patient microclimate, must be either transported out of the mattress system or retained within the system. Any moisture transported out of the system will be measurable in the transport properties out of the control volume. This arrangement was used to assess the performance of the mattress system in terms of its ability to move moisture away from a patient and away from the immediate loaded mattress system environment.

7.2.1.1 Environment Control

For the purpose of measuring airflow parameters a prescribed pathway for the air flow needed to be defined and constructed. In the previous study, Figliola (2003) controlled the environment in which the experiment was set by enclosing the support surface in a vinyl 'Mattress Environment Chamber' (MEC). Air-flow was controlled and measured as it entered and left the MEC. The experiments were all maintained at a temperature 23°C +/- 1.5°C and a relative humidity of 42% +/- 4% outside the chamber in the lab. A similar method of controlling air flow and chamber environment was implemented in the present study.

7.2.1.2 Sweat Simulation and Application

A human analogue was used to simulate a sweating body. There have been several studies which have measured human sweat rates, as summarised in (Table 7-1), with all values converted into units of mL/min/m^2. A wide range of values was evident, the differences being generally due to the variations in test conditions.

For example, the high sweat rates reported by Polliack et al., (1993), were measured at the skin of the forearm when subjected to an interface pressure of 150 mmHg (20 kPa), a value considerably higher than that measured at a patient support interface, which is typically 30 - 70 mmHg. Nonetheless, these sweat rates were deemed appropriate as the "worst case scenario" for the present study.

Table 7 - 1 Comparison of sweat rates from different human studies.

Source	Conditions	Sweat rate (ml/min/m^2)
Report of the task group on reference man (1974) (quoted by Nicholson)		0.28
Polliack et al., 1993	Uniaxial loading of 150 mmHg over area of 1600mm^2 on forearm, for 30 mins at 30°C	8.30
Polliack et al., 1993	Hydrostatic Loading of 150 mmHg, over area of 1600 mm^2 on biceps for 10 mins at 30°C	7.06
Ferguson-Pell and Hagisawa, 1988	Uniaxial loading of forearms of 150 mmHg over an area of 500 mm^2	1.95
ASHRAE Handbook of Fundamentals, 1998	Inactive person over total body area of 1.8 m^2 at 37°C	0.24
Berglund, 1988		0.19
Wang, 2000	Loading at the sacrum of 80 +/-20 mmHg for 1 hour followed by 1 hour of unloading over 40mm diameter filter paper at 38°C +/- 1°C.	2.6 +/- 2.0 (ischaemia) 3.6 +/- 2.0 (reperfusion)

Moisture can be monitored using humidity sensors to gain an insight into the microclimate of the analogue mattress interface, with the sensor being introduced through the portals into the chamber. Humidity levels were measured both at the interface with the human analogue and within the chamber. This will enable direct monitoring of the moisture transport and changes in humidity at the patient support interface, using alternative mattress modes and sheets.

7.2.1.3 Temperature Simulation and Application

A few laboratory studies (Figliola 2003; Nicholson et al., 1999; Reger et al., 2001) report the use of a heat energy source to simulate human body thermal properties. Ideally the heat source should be inputted into the system at a flux representative of that of a human patient on a support surface. Furthermore, human thermoregulatory features should be conserved in the laboratory model. However, for the purpose of the current study, a heated water bladder maintained at a temperature of 37°C was deemed appropriate to reproduce the thermal environment consistent with human body temperatures.

Interface temperature measurements in previous studies, such as Reger et al., (2001), have typically utilised an array of thermistors placed at different areas of the loaded body mattress interface. This method was adopted in the present study, with the thermistors (detail show in Chapter 4) introduced through the portal on the side of the chamber to the mattress interface.

7.2.2 Test Equipment

7.2.2.1 Test Chamber

A pre-designed test chamber was created to allow a controlled atmosphere around the mattress and the human analogue, as illustrated in Figure 7-3 (left). The chamber was made of a copper frame surrounded by polyethylene sheeting, with a removable and re-sealable upper layer of polyethylene sheeting. It was designed to accommodate the test mattress. Inlet/outlet ports were installed to allow the ClinActiv mattress to connect to its external air supply and control unit, as shown in Figure 7-3 (right). In addition, extra ports were created to allow exhaust air from the controlled environment inside the chamber, as well as to allow the measurements of temperature and humidity using the probes within the chamber.

External air supply/control unit of ClinActiv mattress

Polyethylene environment chamber
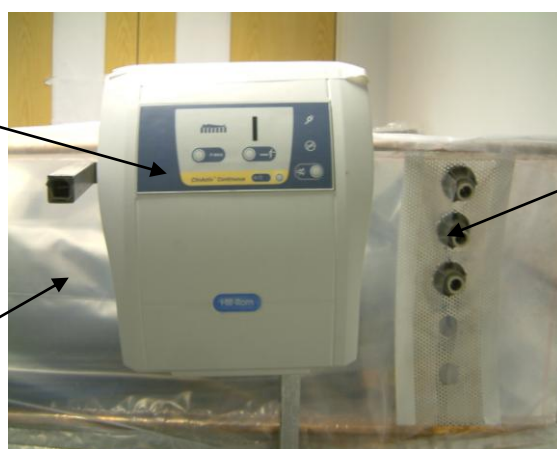
Inlet/outlet holes

Figure 7 - 3 Polyethylene environmental chamber incorporating ClinActiv mattress (above). External air supply/control unit of ClinActiv mattress and inlet/outlet holes in the side of the chamber (below).

7.2.2.2 Humidity Probes and Temperature Sensors

Figure 7-4 shows an image of the humidity and temperature sensor system, product details of which were provided in section 4.2.

Figure 7 - 4 Photo display all humidity and temperature sensor system.

One of the humidity probes was placed at the human analogue-support surface interface, as shown in Figure 7-5, while the other was placed externally within the chamber. Five temperature sensors (Table 4-5) were used, two of which were paired up with two humidity sensors, (Figure 4-9), while the other these sensors were used to monitor the interface temperatures. The arrangement is indicated in Figure 7-5.
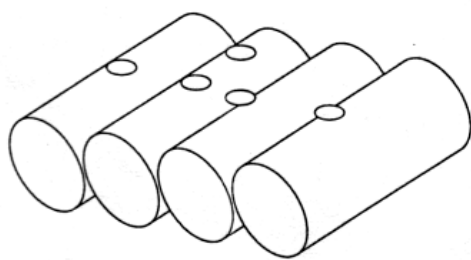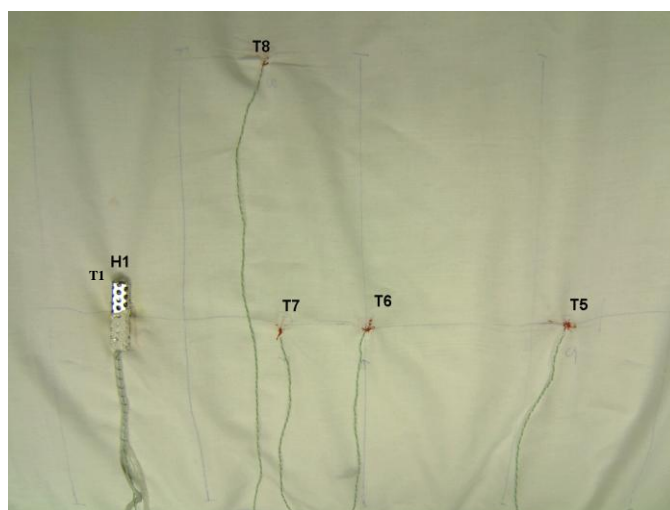
Figure 7 - 5 Placement of Temperature and Humidity Sensors at the Analogue-Support Interface over the mattress cells. An external humidity sensor (H2/T2) was also placed within the chamber.

7.2.2.3 Human Body Analogue

A medium density Polyethylene tank had been developed of external dimensions 760 x 510 x 310 mm with a full capacity of 100 litres was used as the human analogue, as shown in Figure 7-6. It was estimated that a water level of 200 mm, equivalent to 77L/77.5kg, and an empty tank mass of 20 kg over a surface area of 0.37 m^3 will establish a pressure of 18.5 mmHg (2.4 kPa). This represents a relatively low interface pressure under patients lying on a support surface. Body temperatures were simulated by maintaining the water in the tank at 37 ℃ ±1 ℃ by using 700 W fish tank heaters.

To simulate sweating, linear sections of Tygon® laboratory tubing, with an outer and inner diameter of 3.2 mm and 1.6 mm, respectively, were embedded at the base of the

tank. The tubes were maintained at a distance of 30 mm apart, with little pores of 1 mm diameter created at 30 mm intervals along the length of the tubing. A peristaltic pump (Type: ISM404B V8.01, Lsmatec SA, Labortechnik-Analytik, Figure 7-7), was used to transport the heated water up to a rate of 3 ml/min to the patient support interface. This rate is equivalent to a sweating rate of 9 ml/min/m^2.

Figure 7 - 6 Human Body analogue with an embedded sweating system made of perforated Tygon® tubing. This surface was touch at the mattress interface in experiment.

Figure 7 - 7 The peristaltic pump used to simulate sweating by delivering heated water to the body mattress interface.

7.2.2.4 Mattress System and Associated Sheets

A mattress system (ClinActive, provided by HillRom, France) was used for all the tests. It has the benefit of being able to function in either Alternating Pressure (AP) mode or a Continuous Low Pressure (CLP) mode, both of which connect with the external pump unit. This permits air to be pumped into the mattress and potentially air flow between the sheet and the mattress. There were a collection of sheets, which were provided with the mattress, the characteristics of which are summarised in Table 7-2.

Table 7 - 2 Summary of characteristics of sheets used in present study.

Colour of sheet	Grey sheet	White sheet	Blue sheet	Zephyr™ Sheet
Type of sheet	Air-Permeable,	Vapour-Permeable,	(Standard Issue) Non-Permeable, Polyurethane coating on Polyamide fabric	Vapour-Permeable, Polyurethane coating on Polyester fabric
Other info	Prototype Perforated holes at equi-distance of ≈50mm across surface of sheet	Prototype, non-waterproof	Commercial, Low Friction. Two-way stretch, breathable, bacterio-static, fungi-static, anti-microbial, waterproof	Commercial, Low friction, bacterio-static, fungi-static, anti-microbial, waterproof

7.2.3 Preliminary Test Protocol

Prior to the main experiment, an initial test was performed on a normal surface, in the absence of an air supply. This was designed to estimate the regulation of the water leakage rate in order to achieve a maximum humidity (100% RH). The test

arrangement, as illustrated in Figure 7-8, indicates the tank resting on the bedding sheet, incorporating both humidity and temperature sensors.
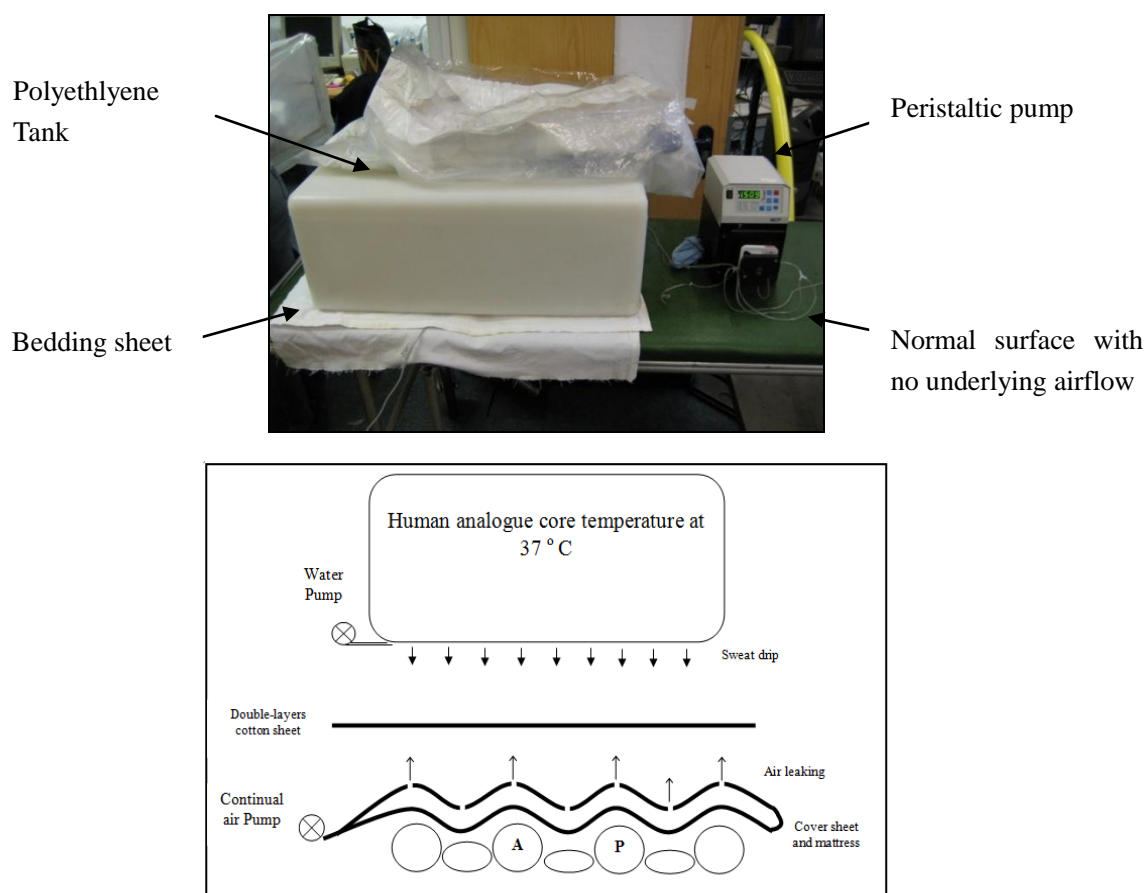
Figure 7 - 8 Pre-Test arrangement on a non-aired surface (above); and schematic diagram of the experiment under the environmental chamber (below).

7.2.4 Main Test Protocol

In the main study, all experiments were performed in the closed chamber, so as to maintain a constant environment and prevent any artefacts associated with external factors during the experiments.

A thin cotton sheet, with the strategically positioned humidity and temperature sensors was used to cover the mattress. This sheet permitted maintenance of sensor location during repeated tests, as shown in Figure 7-9.

Figure 7 - 9 Left: test arrangement of ClinActiv mattress into the environment chamber. Right: Standard cotton bedding material, doubled to protect the interface sensors.

A double sheet of standard hospital cotton bedding material was also used to cover the humidity and temperature sensors and protect them from excess moisture, as illustrated in Figure 7-9 (right). The water tank filled with 77 litres of heated water, was placed on top of the sheeting.

For each experiment, the chamber was closed and the system was allowed to run until a constant temperature at the interface was observed to be approximately 34°C, after which real-time monitoring of both humidity and temperature was then initiated, as shown in the image in Figure 7-10. The humidity and temperature of the external environment was also recorded.

Figure 7 - 10 Enclosed environmental chamber with mattress and human analogue.

The peristaltic pump was connected to the free end of the tubing and the other end was fed through the open hatch into the water in the tank. Shortly after, within 60 seconds, sweating of the Human Analogue was initiated, at one of the three prescribed sweat rates, and continued for a period of 25 minutes and then stopped. The test configuration was then allowed to continue for a further 95 minutes whilst recording humidity and temperature in real-time.

A summary of the test conditions undertaken in the main study indicated in Table 7-3. It can be seen that both low and high leaking was simulated, with flow rates of 3.0 ml/min and 1.5 ml/min, respectively. An intermediate flow rate was also used in the project.

Table 7 - 3 A summary of the test conditions undertaken in the present study.

Mattress Mode	Air low rate (equivalent sweat rate)	Grey sheet	White Sheet	Blue Sheet	Zephyr™ Sheet
CLP	3.0 ml/min (9.0 ml/min/m^2)	X	X	X	X
CLP	2.25 ml/min $(6.75 \text{ ml/min/m}^2)$	X	X		X
CLP	1.5 ml/min (4.5 ml/min/m^2)	X	X		X
AP	3.0 ml/min (9.0 ml/min/m^2)	X	X	X	X
AP	2.25 ml/min $(6.75 \text{ ml/min/m}^2)$	X	X		X
AP	1.5 ml/min (4.5 ml/min/m^2)	X	X		X

CLP – Continuous Low Pressure system; AP – Alternating Pressure system.

7.3 Results

7.3.1 Humidity Profiles

The temporal profiles of relative humidity for both CLP and AP modes of the ClinActiv Mattress for each of the four cover sheets are presented in Figure 7-11 and 7-14. It is evident that the relative humidity at the loaded interface increases with time. However there is considerable difference with reference to mattress modes and individual cover sheets. Accordingly, data is presented for each of the cover sheets separately.

Blue sheet (Table 7 - 2)

In the case of the blue sheet, only the highest sweat rate was employed, equivalent to a flow rate of 3.0 ml/min. Figure 7-11 revealed that the maximum saturation level of 100% relative humidity was reached for both modes with the blue sheet. It is worthy of note that in the initial basal value of RH was lower with the AP mode compared to the CLP, with a difference of 15% RH. The time to each saturation level was approximately 300 seconds for both AP and CLP modes.
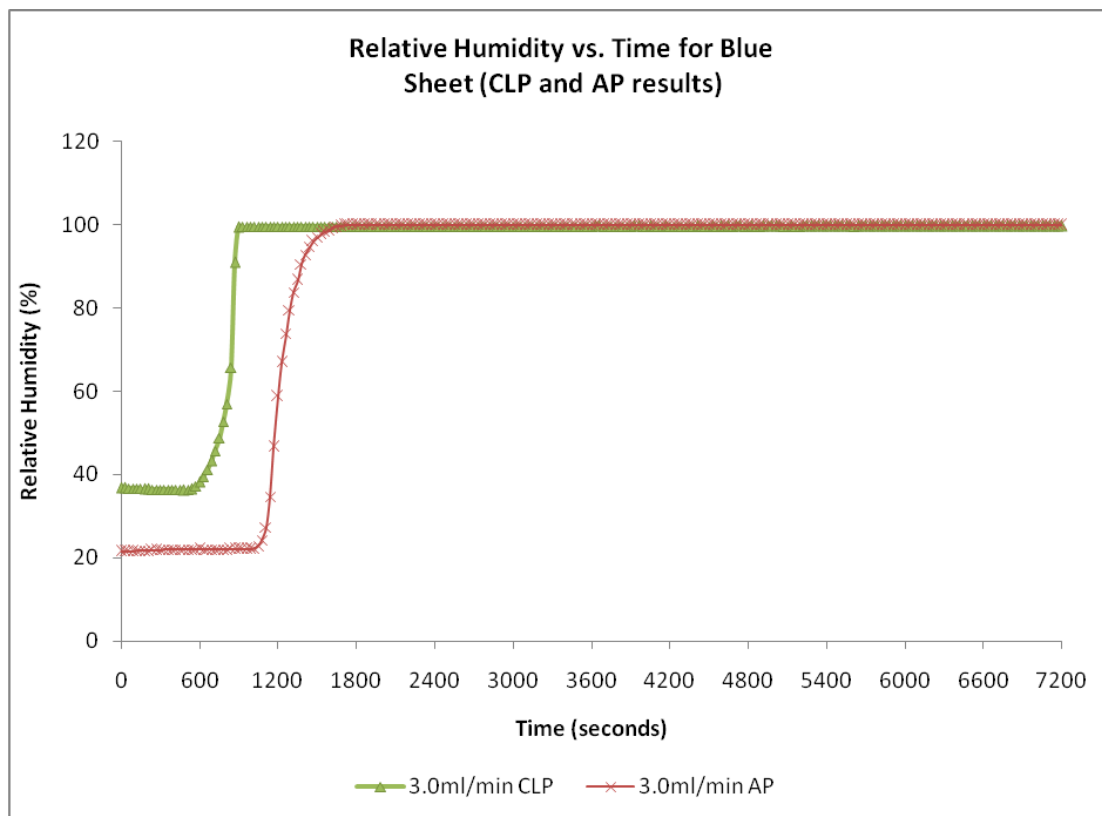
Figure 7 - 11 The temporal response of humidity at the loaded interface for the blue cover sheet at the sweat rate of 3.0 ml/min.

Grey sheet (Table 7 - 2)

Figure 7-12 illustrated the performance of the grey sheet at each of the three simulated sweat rates for both CLP and AP modes. There were clear differences between the results in terms of both final RH levels attained at the end of the monitoring period and the initial basal levels. For example, at all flow rates the basal level associated with the CLP mode was between 20 - 30% RH higher than for the AP mode. With regard to the final humidity levels, a maximum value of 100% RH was achieved for the flow rates of both 3.0 and 2.25 ml/min. the latter occurring over a shorter time period, particularly for CLP mode. By contrast at the lowest flow rate of 1.5 ml/min, the relative humidity only increased modestly over the test period. For example, in the CLP mode, it increased by approximately 22% RH over the 120 minutes test periods. The AP mode yielded a smaller increase from 26% RH to 37% RH. Close

examination revealed very small incremental perturbations in this increase associated with the operation of the mattress in alternating pressure mode.
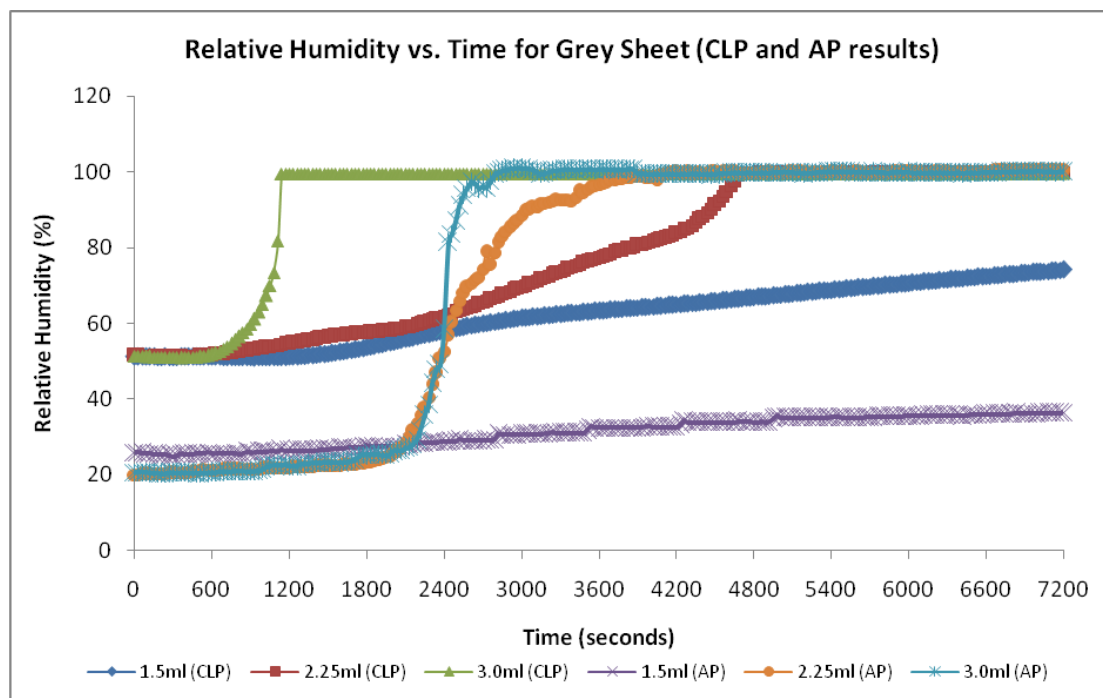
Figure 7 - 12 The temporal response of humidity at the loaded interface for the Grey Sheet at various sweat rates.

White sheet (Table 7 - 2)

Figure 7-13 illustrated the performance of the white sheet at each of the three simulated sweat rates for both CLP and AP modes. It is evident that for the highest flow rate of 3 ml/min, a maximum saturation level of 100% RH was reached for both modes very rapidly from basal levels, namely within approximately 30 minutes of the start of the monitoring period. At a flow rate of 2.25 ml/min, a relative humidity of 100% was also attained at approximately 63 and 85 minutes from the start of the monitoring period for AP and CLP modes, respectively. By contrast, at the lowest flow rate of 1.5 ml/min, there was a more gradual increase in interface humidity with time. Indeed, at the end of the monitoring period, the humidity had reached a value in excess of 95% RH (Figure 7-13).
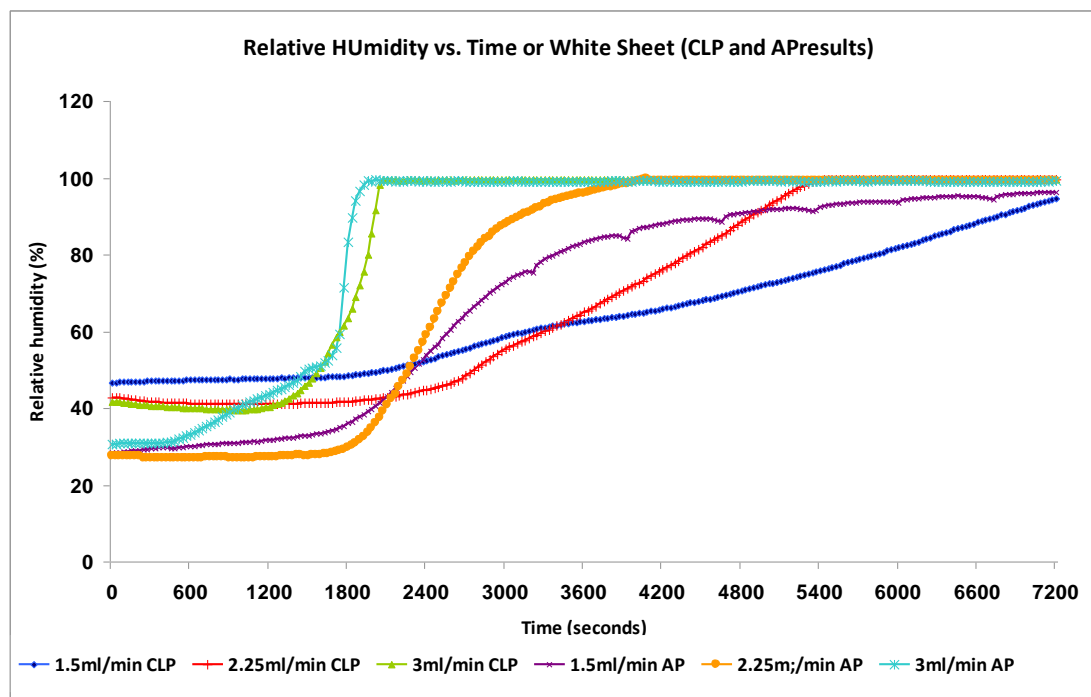
Figure 7 - 13 The temporal response of humidity at the loaded interface for the white cover sheet at various sweat rates.

$Zephyr^{TM}$ sheet (Table 7 - 2)

The performance of the $Zephyr^{TM}$ sheet in conjunction with the ClinActiv mattress is indicated in Figure 7-14. In a similar manner to the other sheet covers, at the flow rate of 3.0 m/min the interface humidity levels attained a value of 100% RH at the early stages of the monitoring period. The flow rate of 2.25 ml/min produced similar results, although the time taken to reach satiation was between 60 and 75 minutes following the start of the monitoring period. By contrast at the lowest sweat rate, the interface humidity levels increased monotonically, but at a reduced rate, reaching values of between 80% and 90% RH at the end of the 120 minutes monitoring period.
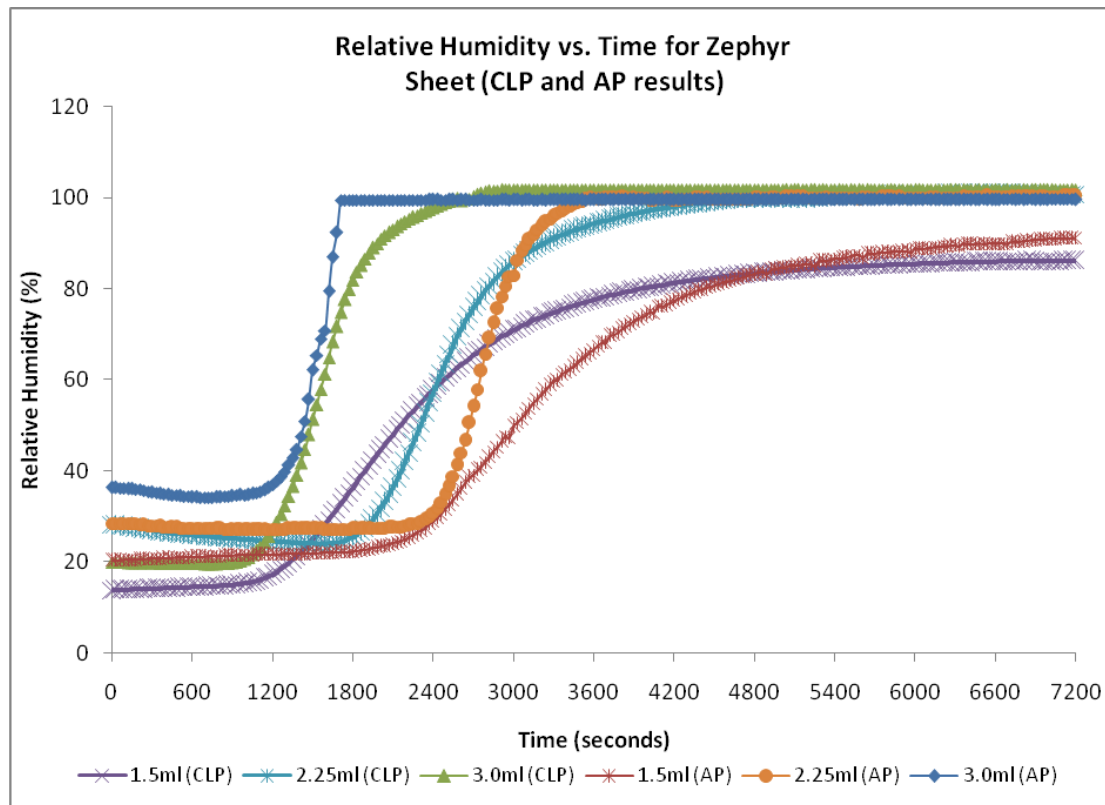
Figure 7 - 14 The temporal response of humidity at the loaded interface for the Zephyr cover sheet at various sweat rates.

7.3.2 Temperature Profiles

The temperature profile in CLP mode is similar for all cover sheets and all flow rates. The profile shows very similar characteristics on a temperature vs. time graph, e.g. the grey sheet response at 2.25 ml/min sweat rate in CLP modes is indicated in Figure 7-15. The graph shows the temperature variation over time for temperature sensors T5 to T8 (shown in Figure 7-5). All four profiles indicated an initial increase of between 1 - 2°C in the initial sweating phase, followed by a slow decline reaching a temperature of between 34 – 34.5^{o}C at the end of the 120 minutes test period.
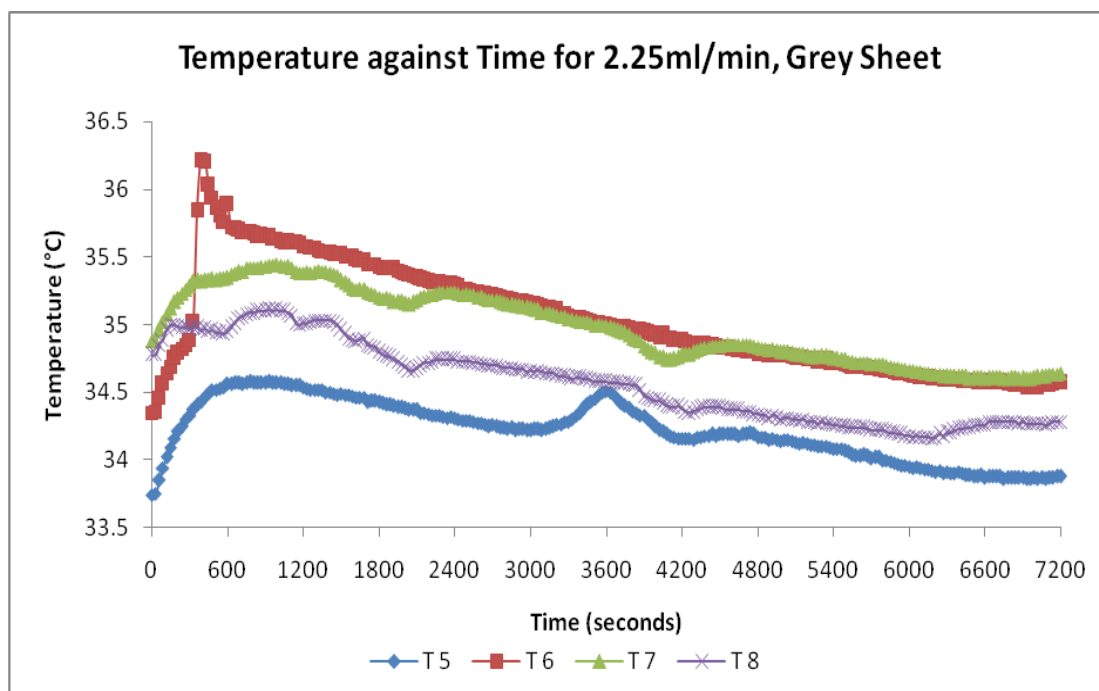
Figure 7 - 15 The temporal profile of temperatures at the loaded interface for the Grey Sheet for a volume flow rate of 2.25 ml/min over a period of 2 hours.

7.4 Discussion

Moisture and temperature are two of the critical extrinsic factors, which can cause or exacerbate tissue breakdown in the form of pressure ulcers (Flam et al., 1995). A fuller description of these parameters importance in the microclimate of the loaded body support interface was provided in section 5.1.3. The methodology developed in the present chapter provided an easy to use experimental laboratory-based system to assess the environment conditions at the interface between a simulated body and a commercial APAM mattress system. The body, which was heated to 37° C, incorporated a mechanism by which moisture could be introduced into the microenvironment to simulate thermal sweating. This arrangement enabled the study of the effects of mattress cover, mattress mode and incorporated flow rate on both interface humidity and temperature over a 120 minutes monitoring period.

One consistent finding for all sheeting materials was the rapid increase in interface humidity, as measured by the imbedded sensor, up to the maximum 100 % RH within

187

the first half of the monitoring period. This was associated with a temperature increase of less than 2° C in any of the four imbedded sensors (Figure 7-5) at the loaded interface. However, it should be recognised that these conditions are at the high range of sweat rates recorded from different human studies (Table 7-2). As a consequence the failure of the mattress system with any of the incorporated sheets to reduce the interface humidity may not be so problematic in a normal clinical setting. When the flow rate was reduced to 2.25 ml/min, the increase in interface humidity level was considerably slower, although it attained 100% RH with all covering sheets.

The results at a flow rate of 1.5 ml/min, equivalent to a sweat rate of 4 ml/min/m^2 were different to those at the other two flow rates. In particular, the interface humidity level generally did not reach 100 % RH during the monitoring period for both modes. This was noticeable for the Zephyr^{TM} cover sheet (Figure 7-14), the grey sheet (Figure 7-12) and the white sheet (Figure 7-13).

It should be noted that there will be small differences in the performance for repeated measurements performed on different occasions. This can be illustrated in Figure 7-16 in an earlier study with grey cover sheet and the Clin-Activ mattress. In the case, for a sweat rate of 1.5 ml/min. following a monotonic increase in humidity up to a level of 60% RH, there was a subsequent reduction in the latter stages of the test period in the AP mode. The corresponding responses for the CLP modes were similar for both test measurements (Figures 7-12 to 7-16). Close examination of the data, however, suggests one subtle difference, revealed in Figure 7-16, namely that in this series the initial RH value is low for CLP at a sweat rate of 2.25 ml/min. In all other cases, the AP values start at lower RH values, when compared to the CLP values.
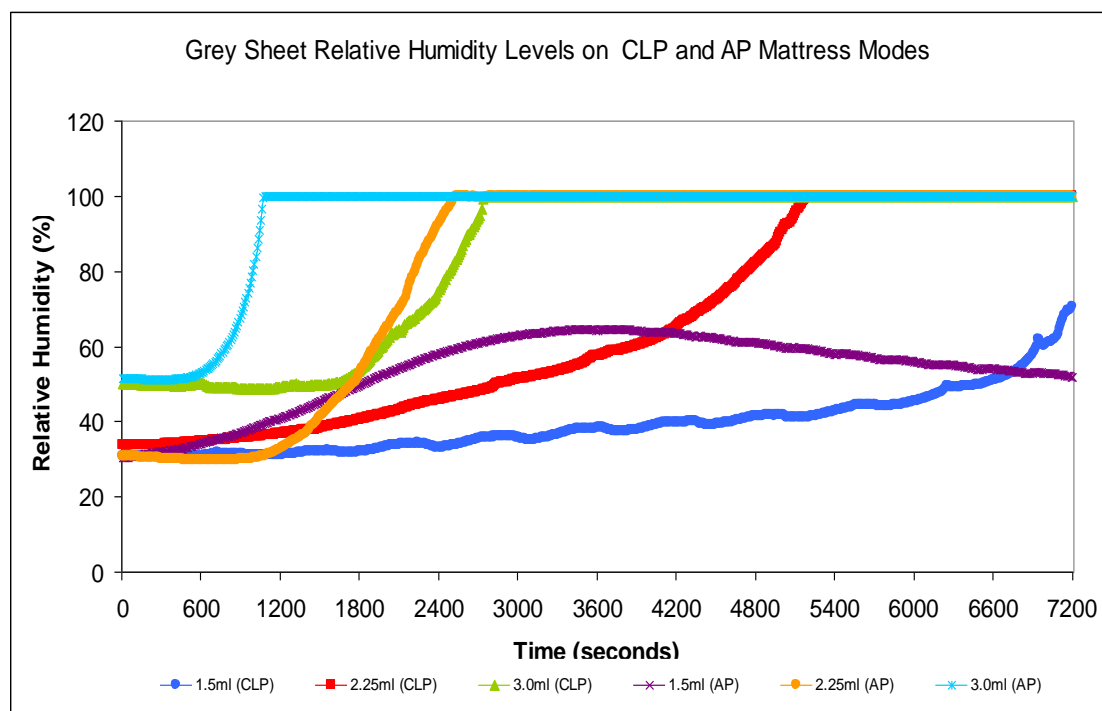
Figure 7 - 16 The temporal response of humidity at the loaded interface for the grey sheet at various sweat rates.

There were some differences in the humidity response, which could be attributed to the different modes of the mattress. These included the initial humidity levels attained during the 20 minutes sweating phase (e.g. Figures 7-11 to 7-14), as well as the rate of increase in humidity level at the interface following the low sweat rate stimulus (e.g Figures 7-12 and 7-13). Close examination of the data revealed differences in the nature of the increases between the modes, as illustrated for the grey sheet following stimulus at the lowest sweat rate (Figure 7-17). It is evident that for this section of the monitoring period, there is a smooth increase in humidity values associated with the CLP mode. By contrast, for the AP mode, there was an increase in humidity in the form of defined increments at a periodicity of approximately 650 seconds. This corresponds to measured alternating pressure period for the Clin-Active APAM of 660 seconds. Similar periodic perturbations were also evident with the temperature profiles during the monitoring period.

Other differences between modes included:

- The time taken to reach 100% RH for the high simulated sweat rates
- The increase in RH during the monitoring period

In both cases, the AP mode appeared more efficient in controlling the humidity levels at the loaded interface.
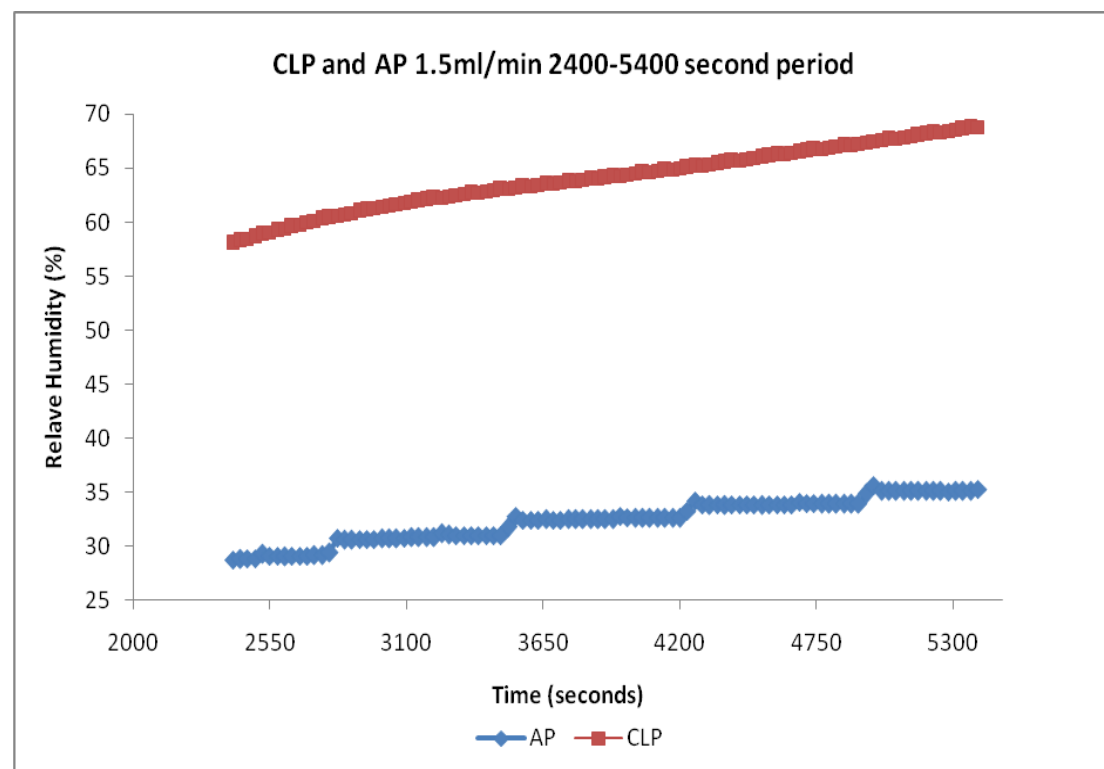
Figure 7 - 17 A magnified temporal response of humidity levels at the loaded interface, for Both CLP and AP modes, with the grey sheet at a sweat rate of 1.5ml/min.

To conclude this chapter, the experiment associated with this lab-based study has resulted in a number of highlights which are most conveniently listed:

- The experimental protocol is ideal for examining the microclimate at a loaded mattress interface,
- There was only small change in temperature for all of the test conditions,
- At the high simulated sweat rates, in excess of 2.25 ml/min, the relative humidity levels increase to 100% for all loaded test conditions,

- At the lower simulated sweat rate of 1.5 ml/min the nature of the prototype covering sheets had an effect on the interface humidity profiles,

- The Zephyr ^{TM} cover sheet (Figure 7 - 14) performed in equivalent manner to the perforated cover sheet (grey) in controlling the humidity levels at the loaded interface,

- Moisture levels at the patient support interface must be controlled to ensure tissue health and integrity.

Chapter 8.

Modeling for Interface Climate at the Loaded Support Surface

In the previous chapter, the analytical solutions for the effectiveness of moisture and temperature at patient/support interface have been given; they were used to assess the various Low Air Loss (LAL) systems and were compared with their own performance criteria. This involved the usage of a patient analog resting on the mattress surface and the mattress system. The mattress performance is inferred from measurements of the temperature drop underneath the analog, reflecting latent moisture removal for 90 minutes or less. The test offered satisfactory results providing insights into the moisture transport capability.

To understand the test in more details, this chapter describes the development of a mathematical model to evaluate the moisture vapor and heat transport capability of various mattress support systems. The model results will be examined in the light experimental data.

8.1 Problem Description

The model needs to match with the experimental set up described in the previous chapter. A schematic diagram of this with the APAM system either in continuous or alternating pressure mode is illustrated in Figures 8-1 and 8-2. Based on the thermodynamic phenomena and structure of pressure released bed, the double-layer cotton sheet can be assumed as inelastic, homogenous and isotropic porous media where each pore is regarded as being co-occupied by a fluid phase and an air phase. If

the double-layer is regarded as a unit, heat transfer can occur at three interfaces. The top interface is between the body analogue and the double-layers, the bottom interface is between the double-layers and air-permeable sheet, and the side interface is between the double-layers and its surrounding air.

The model has a number of assumptions:

1. Both the water and air permeability of the porous sheet are constant,

2. Water and air can transfer across the sheet,

3. The sheet is initially at uniform temperature and humidity,

4. The water diffuses from the top with a constant flow rate and at constant temperature,

5. The air from the bottom has a constant flow rate, temperature and humidity. The vapour is carried away to the surrounding environment at a constant temperature and humidity.

The water diffused in changes into vapour changing the local humidity; the local heat energy is increased by the input of the warm water, but is reduced by the water phase transition and the cold air inflow. In order to solve for the problem, a compartment model was employed.
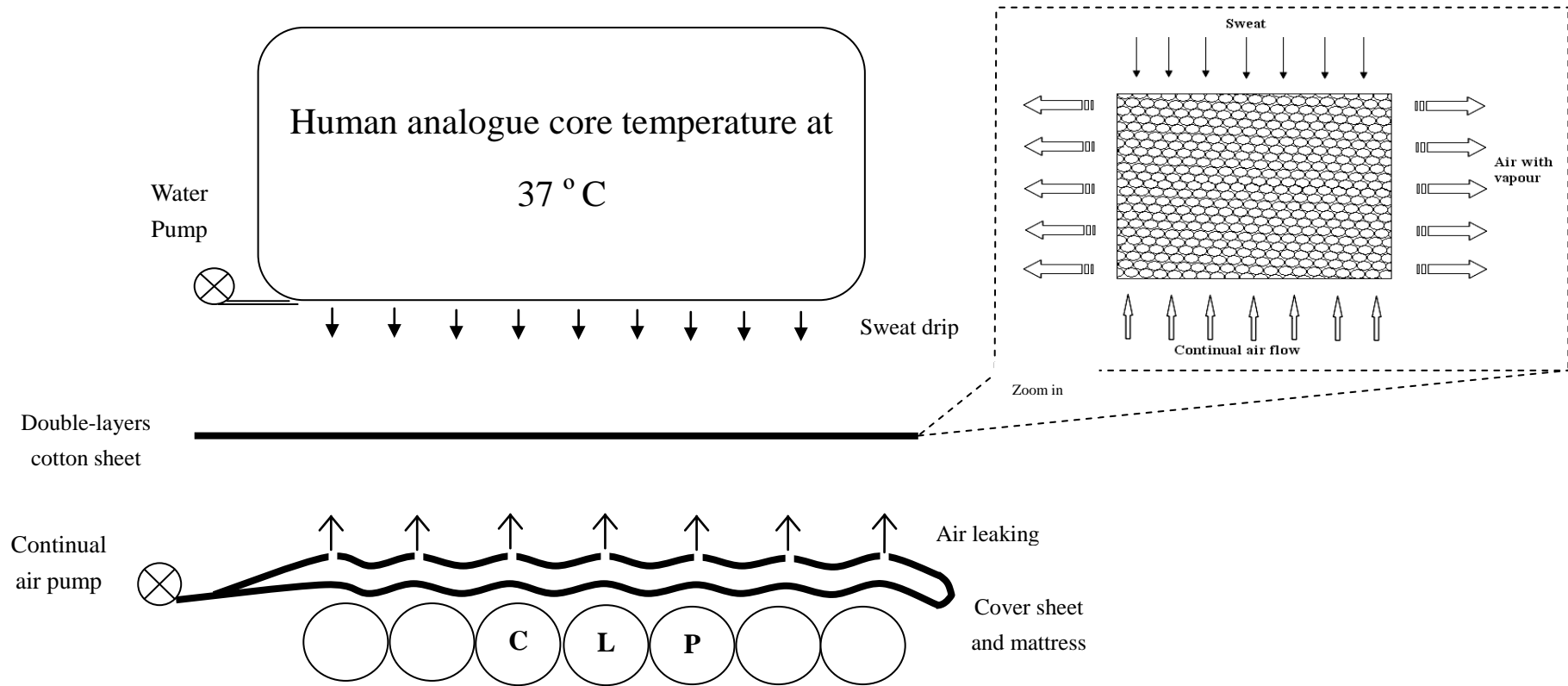
Figure 8 - 1 Schematic diagram of the experiment with continual low pressure mattress

Human analogue core temperature at

37 $^{\rm o}$ C

Water
Pump

Sweat drip

Sweat

Air with
vapour

Continual air flow

Zoom in

Double-layers
cotton sheet

Air leaking

Continual
air pump

A   P

Cover sheet
and mattress
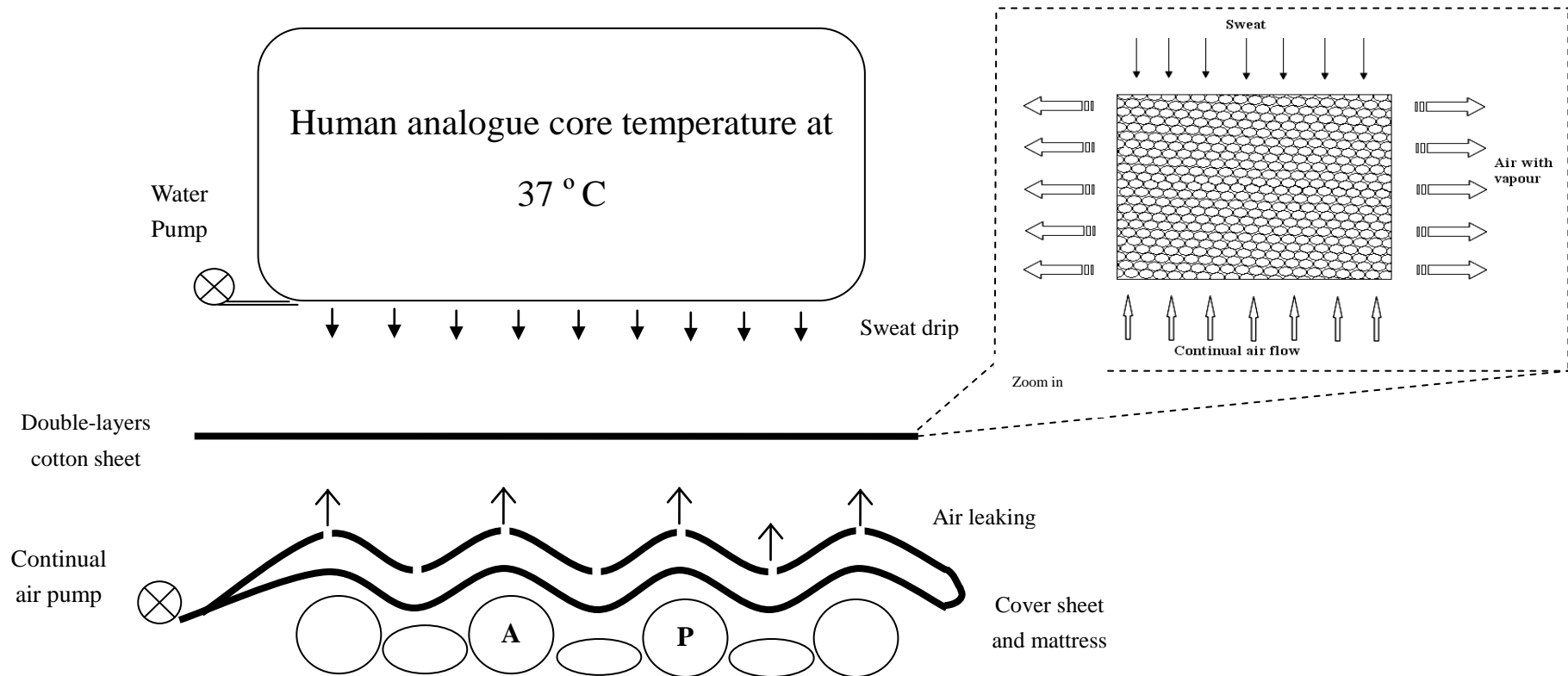
Figure 8 - 2 Schematic diagram of the experiment with alternating pressure mattress

8.2 Compartment Model

8.2.1 Introduction

A compartment model is a type of mathematical model used to describe the way materials or energies are transmitted among the *compartments* of a system. Each compartment is assumed to be a homogenous entity within which the entities being modelled are equivalent.

Compartment modeling requires the adoption of several assumptions, so that systems in physical existence can be modeled mathematically, as illustrate in Figure 8-3:

1. Instant homogeneous distribution of materials or energies within a compartment,

2. model can be thought of as the analysis of a single "compartment" *into* which some substance is flowing at a certain rate and *out of* which the same substance is flowing at some, probably different, rate.

    Rate of change of the amount of substance in the compartment   =   Input   -   Output

3. To accommodate more than one input source, a mulit-compartmental model was employed.

8.2.2 Build up of Compartments Model

The double layer cotton, with a thickness of approximately 1 mm and all contents inside is assumed to be well-mixed. The local humidity and heat transfers are only influenced by the input and output rates of substances, which are the sweat and thermal heating from top down, the relative cold and moist air supplying from bottom, and the vapour released from the side.
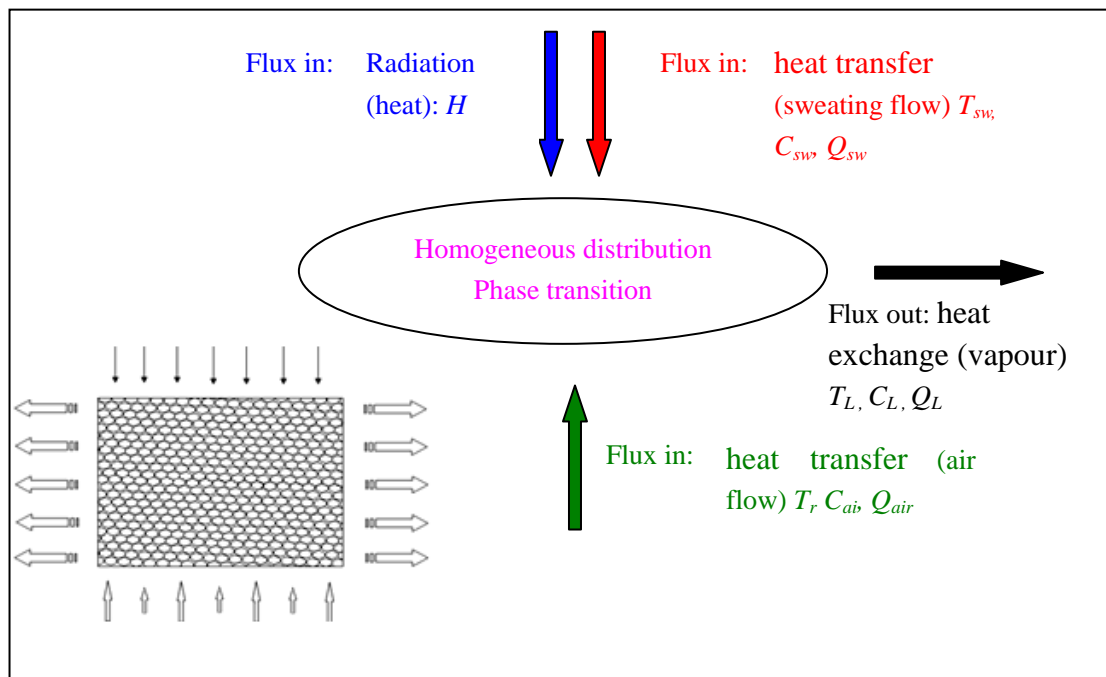
Figure 8 - 3 Schematic of the mulit - compartments model with 7 input parameters and 3 output parameters. Homogeneous distribution of vapour was assumed at inside of double layer. Two input source was included with from top to double-layers (flux in sweat and heat) and from bottom to double-layers (Flux in air). *T: Temperature; C: Specific heat capacity; Q: flow rate*

In this compartmental model, the cotton layer is the domain of interest. The upper human analogue continuously releases sweat into the domain, which is also exposed to the inflow of air at a constant temperature and flow rate. The air flux out of this domain contains moisture as the sweat evaporates in the domain. We only consider the system when it operates at steady state.

8.2.3 Thermal Equation of Each Phenomenon

Heat influx through radiation

Radiation is the energy emitted by matter in the form of electromagnetic waves (or photons) as a result of the changes in the electronic configurations of the atoms or molecules (Cengel, 2003).

In the compartment model, heat flux from the human analogue body due to temperature difference, can be described as,

$$\varepsilon \delta A_T (T_o^4 - T_L^4)$$

Equation 8-1

where:

ϵ: Emissivity of cotton, which is *0.77 at 20ᵒC*

δ: Stefan-Boltzman constant, which is *5.67 $\times 10^{-8}$ W m^{-2} K^{-4}*

A_T: Surface area of tank, given as 0.37 m^2

T_0:   Water temperature in tank, which is *37ᵒC or 310K*

T_L: Double-layers temperature, the unknown variable

Heat flux due to sweat and air inflow and outflow

The heat added to domain by the means of the sweat, in the form of warm water, is:

$$\dot{m}_{sw} C_{sw} (T_o - T_L)$$

Equation 8-2

where:

$\dot{m}_{sw}$:   Input sweating mass rate, which is approximately *400 g m^{-2} per 24 hour*s or

        4.6 $\times 10^{-6}$ kg m^{-2} S^{-1}

C_{sw}:   Specific heat of sweat (water), which is *4.1813 kJ kg^{-1} K^{-1} at 25ᵒC*

T_0:   Water temperature in tank, which is *37ᵒC or 310K*

T_L: Double-layers temperature, the unknown variable

Similarly for the air at the botton interface between the double-layer and the cover sheet, as illustrated in Figures 8-1 and 8-2. The resulting heat transfer equation is expressed as:

$$\dot{m}_{air} C_{air} (T_r - T_L)$$

Equation 8-3

where:

$\dot{m}_{air}$: Input air mass rate = density x input air flow rate, the density of 40% relative humidity at 25° C is 9.2 g/m^3 (appendix D: the absolute humidity table), dry air has a density of 1.2041 kg/m^3.

C_{air}: Specific heat of input humid air at *25°C*

T_r: Room air temperature, which is *25°C* or *298K*

T_L: Double-layers temperature, the unknown variable

For the outflow of the air and vapor mixture, the heat flux can be expressed as,

$$(\dot{m}_{sw} + \dot{m}_{a\ i})C_{m\ i}(T_L - T_r)$$

Equation 8-4

where:

$\dot{m}_{air}$: Input air mass rate = density x input air flow rate, the density of 40% relative humidity at 25° C is 9.2 g/m^3 (appendix D: the absolute humidity table), dry air has a density of 1.2041 kg/m^3.

C_{mix}: Specific heat of output humid air, where $C_{mix} = f(T_L)$

T_L: Double-layers temperature, the unknown variable

T_r: Room air temperature, which is *25°C* or *298K*

In all heat transfer equations, the specific heat capacity of humid air is expressed as:

$$C_h = 1.005 + 1.82H$$

Equation 8-5

Where: *1.005 kJ/kg k* is the heat capacity of dry air at temperature 20 ℃; *1.82 kJ/kg k* is the heat capacity of water vapor; *H* is the absolute humidity in the mixture (in *kg* water vapor per *kg* dry air), which may be derived from the experimental data reported in the previous chapter. However, *H* is directly related to temperature, where the laboratory relative humidity is approximately at 35% with room temperature *25°C*. If the relative humidity and local temperature are given, H can be defined.

$$H = \frac{vapour\ mass}{dry\ air\ mass}$$

So the specific heat can be given by

$$C_{air} = 1.005 + 1.82 * \frac{input\ vapour\ mass\ flow\ rate}{input\ dry\ air\ mass\ flow\ rate} = 1.02$$

$$C_{mix} = 1.005 + 1.82 * \frac{input\ vapour\ mass\ flow\ rate + input\ sweat\ rate}{input\ dry\ air\ mass\ flow\ rate}$$

$$= 1.04$$

Phase transition energy cost

The enthalpy is a description of thermodynamic potential of a system, which can be used to analyse the heat transfer in a quasi static process within a closed thermodynamic system under constant pressure (Schroeder, 2000). It generally represents the change in the internal system energy and work. In the current situation, all thermal phonomenas are included within a domain, and it is in a steady stage. Therefore, the change rate is between the enthalpy input and output, and should be equal to the change rate of its internal energy according to the following:

$$\frac{d\Delta H}{dt} = \frac{\delta Q}{\delta T} \qquad\qquad Equation\ 8\text{-}6$$

where:

ΔH: The change in enthalpy of the system, $kg \cdot m^2/s^2$
Q: The internal energy added to the system through heat, $kg \cdot m^2/s^2$

The formula above shows that the enthalpy of vaporization ($\Delta_v H = f(T)$) requires to transform a given quantity of a substance into a gas at its boiling point. e.g. the temperature at 25^oC is $298K$ and its co-responding molar enthalpy is $44000J/mol$. The mole mass of water is $18g/mol$, then 25^oC water vaporization enthalpy is about $2422J/g$ or $2422\ KJ/Kg$.

In the current model, all sweat influx evaporates in the steady state and the

consumed energy can be expressed as:

$$\Delta_v H \dot{m}_{sw}$$

<div align="right">Equation 8-7</div>

where:

$\Delta_v H$:   The enthalpy of vaporization, where $\Delta_v H = -45T_L + 57400$

$\dot{m}_{sw}$ Input sweating (water) mass rate, where is about *400 g m^{-2} per 24 hour*s or

4.6 ×10^{-6} kg m^{-2} S^{-1}

8.2.4 The Conservation of Energy Equations

In the steady state, sweat is completely transformed into vapour and increases the humidity of the outflow air.

The conservation of energy is:

$$\varepsilon \delta A_T (T_o^4 - T_L^4) + \dot{m}_{sw} C_{sw} (T_o - T_L) + \dot{m}_{air} C_{air} (T_r - T_L)$$
$$- (\dot{m}_{sw} + \dot{m}_{air}) C_{mix} (T_L - T_r) - \Delta_v H \dot{m}_{sw} = 0$$

<div align="right">Equation 8-8</div>

It needs to be noted that the air can only contain a certain amount of water vapour under the certain pressure and temperature. It means that the air flux can only bring away a certain amount water in the cotton layer, which is dependent on the local temperature.

So, the above equation holds under the following condition:

$\dot{m}_{sw} \le \dot{m}_{sw\_saturated}$

Once the output relative humidity exceeds the 100%, the untransformed sweat will remain and heats up the interface.

$$\varepsilon \delta A_T (T_o^4 - T_L^4) + \dot{m}_{sw} C_{sw} (T_o - T_L) + \dot{m}_{air} C_{air} (T_r - T_L) - (\dot{m}_{sw\_saturated} + \dot{m}_{air})$$
$$C_{mix} (T_L - T_r) - \Delta_v H \dot{m}_{sw\_saturated} = 0$$

$\dot{m}_{sw} = \dot{m}_{sw\_remained} + \dot{m}_{sw\_saturated}$. And, $\dot{m}_{sw\_saturated}$ can be defined as the maximum sweating rate when the output relative humidity reached 100%.

The temperature in the sheet layer, T_L can be found by solving the above equation, under following condition: the top area of the domain is *0.37 m^{-2}*, and the input sweating mass flow rate is *4.6* x *10^{-6} kg m^{-2} S^{-1}* and input air flow rate is 1.138 x 10^{-4} m^3 S^{-1}. The input air is 25°C and its relative humidity is 35%, the input air's absolute humidity is 8.05 x 10^{-3} *kg m^{-3}*. The output absolute humidity is 3.69 x 10^{-1} *kg m^{-3}*. The saturated vapour air (100% relative humidity) at *0^oC* is *4.8 g m^{-3}*, and *30.4 g m^{-3}* at *30^oC*. We note that under these conditions, the amount of the sweat can be taken by the airflow.

8.2.5 Absolute and Relative Humidity of the Air in the Outflow

The absolute humidity can be calculated as:

$$output\ absolute\ humidity = \frac{output\ vapour\ mass\ flow\ rate\ (100\%\ vaporization)*1000}{input\ air\ flow\ rate}$$

Equation 8-9

The calculation of the output relative humidity is calculated by the table of absolute humidity, an example is show in Table 8-1.

Example: if the value of T_L is 25.67^{o}C

Table 8 - 1 Part of table for absolute humidity (see detailed table in Appendix D)

Relative Humidity		30	50	%
G. Data 1 (℃)	30	9.1	15.2	g/m^3
G. Data 2 (℃)	25	6.9	11.5	g/m^3
T$_L$ (℃)	25.67	7.195	11.996	g/m^3
Output absolute humidity	9.4			g/m^3
Output relative humidity	39.186			%

$$\textit{The relative humidity} = 50\% - \frac{(50\% - 30\%)*(11.996 - 9.4)}{11.996 - 7.195} = 39.186$$

8.3 Results

In the compartment model, the sweat rate and input air flow rate directly affect the output humidity and interface temperature. In the result, various sweat rates and input air flow rates have been employed to explain the interface climate at the loaded support surface.

The sweat rate affects the output relative humidity and temperature

Figure 8-4 displays how the various sweat rates influence the output relative humidity and the interface temperature. The range of the sweat rate is between 1.71 x 10^{-11} and 2.74 x 10^{-6} kg/s. The upper limit determined by the output relative humidity, when it reaches 100%. Above this value, the system can not operate at steady state.
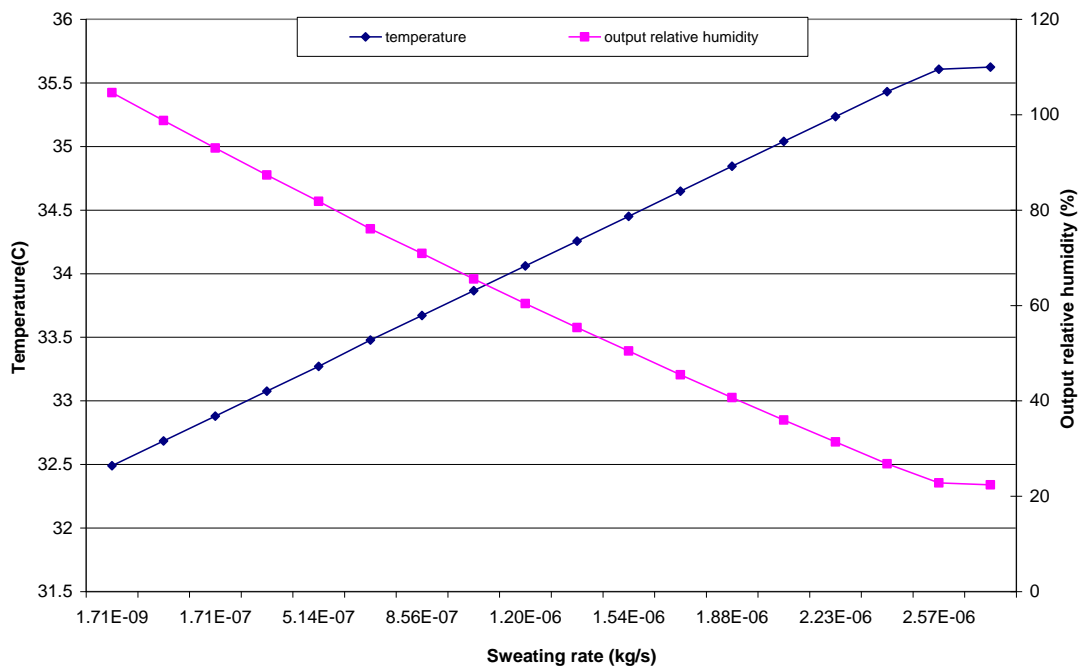
Figure 8 - 4 Effect of the sweat rate on the output relative humidity and interface temperature.

The input air flow rate affects the output humidity and the interface temperature

Input air flow is another important variable in the compartment model. In Figure 8-5, the sweat rate is fixed on the original value, the input air flows rate varies between 6.0 x 10^{-5} and 5.0 x 10^{-3} m^3/s. The limit is also determined by the relative humidity, the curve started from 100% RH, ended at 45% RH when the input air flow is 50 times more than original value. The high value of air flow is clearly hypothetical, as the mattress can never function at this high air flow rate. In Figures 8-6 and 8-7, interface temperature and the absolute humidity are given over the same range of input air flow.
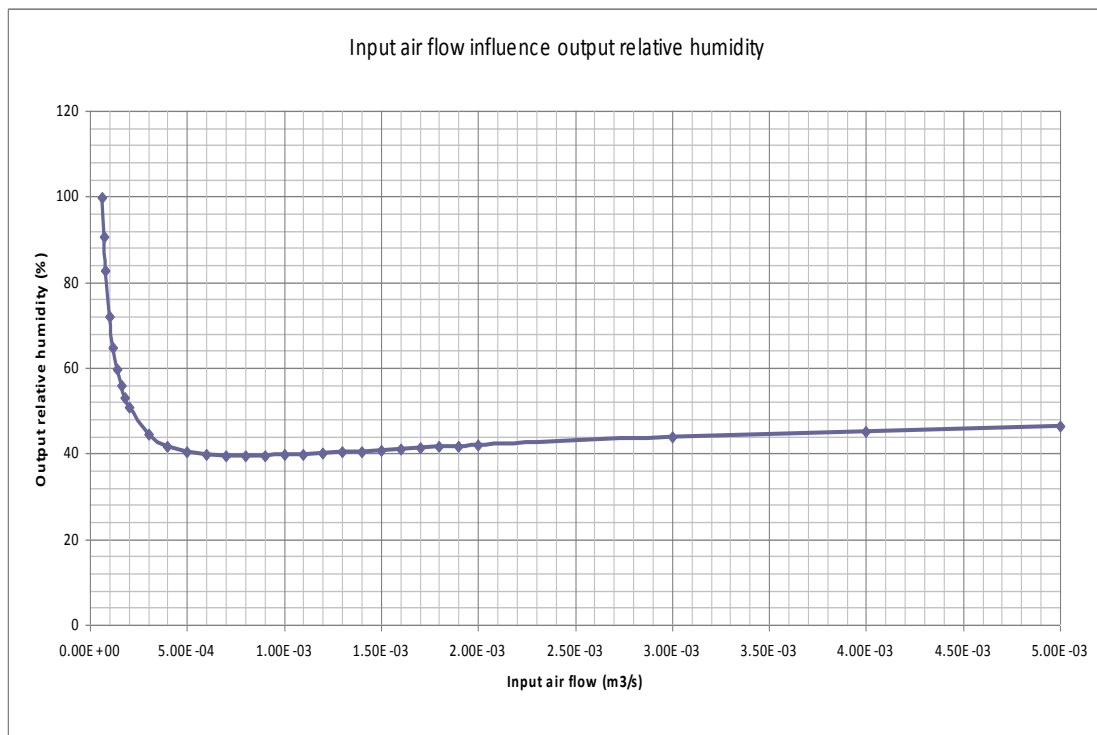
Figure 8 - 5 Various input air flows influence output relative humidity.
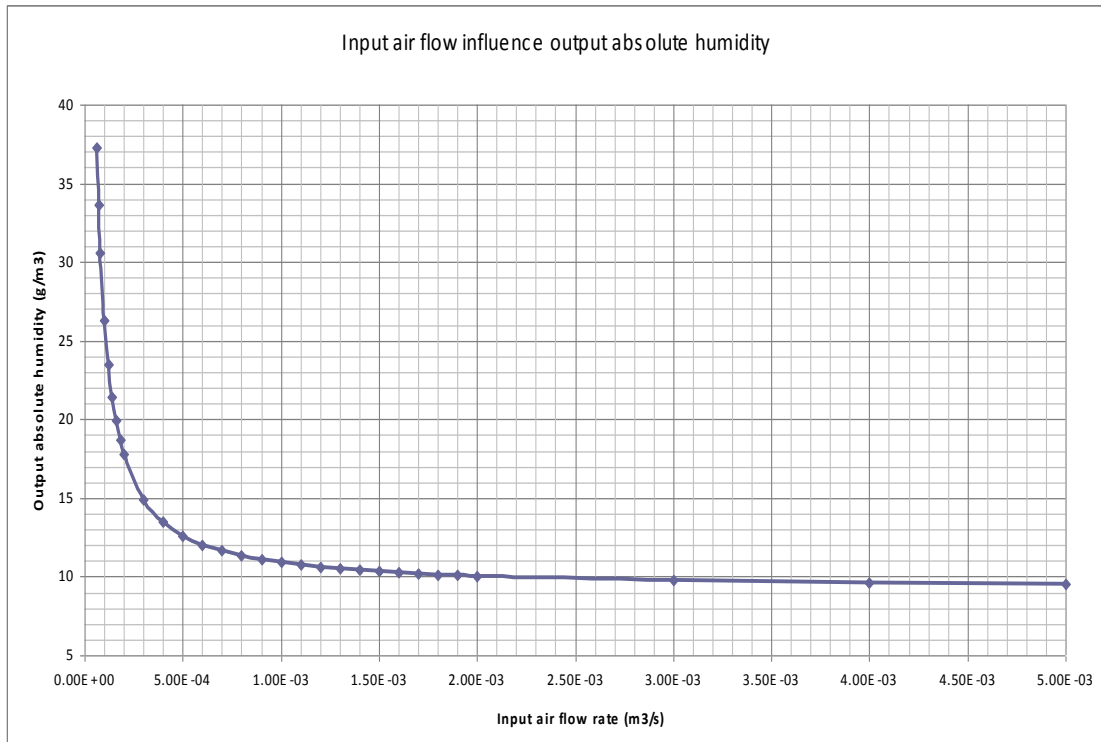
Figure 8 - 6 Various input air flow influence output absolute humidity.
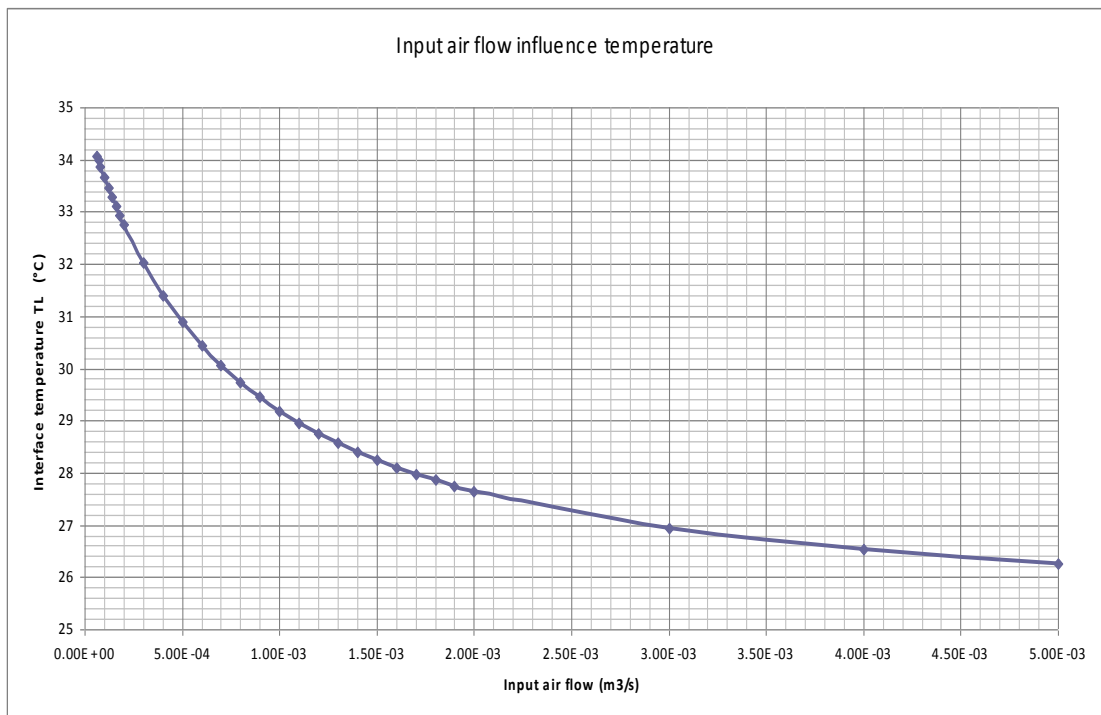
Figure 8 - 7 Various input air flow influence interface temperature.

Figures 8-8 and 8-9 show the effect of the airflow on the interface temperature and the outflow absolute humidity under different sweat rates (ranging from 0.1 times to

2 times the original value). Initial value of the air flow is determined by the relative humidity (i.e. at 100% RH).
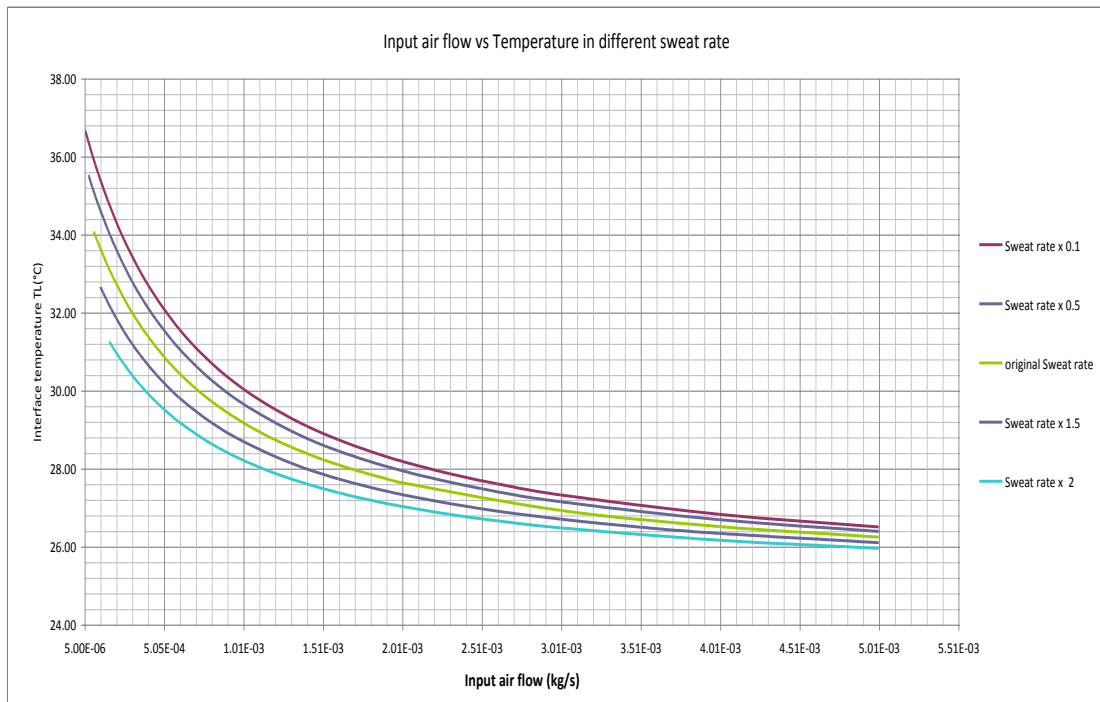
Figure 8 - 8 Input air flow vs temperature at various sweat rates.
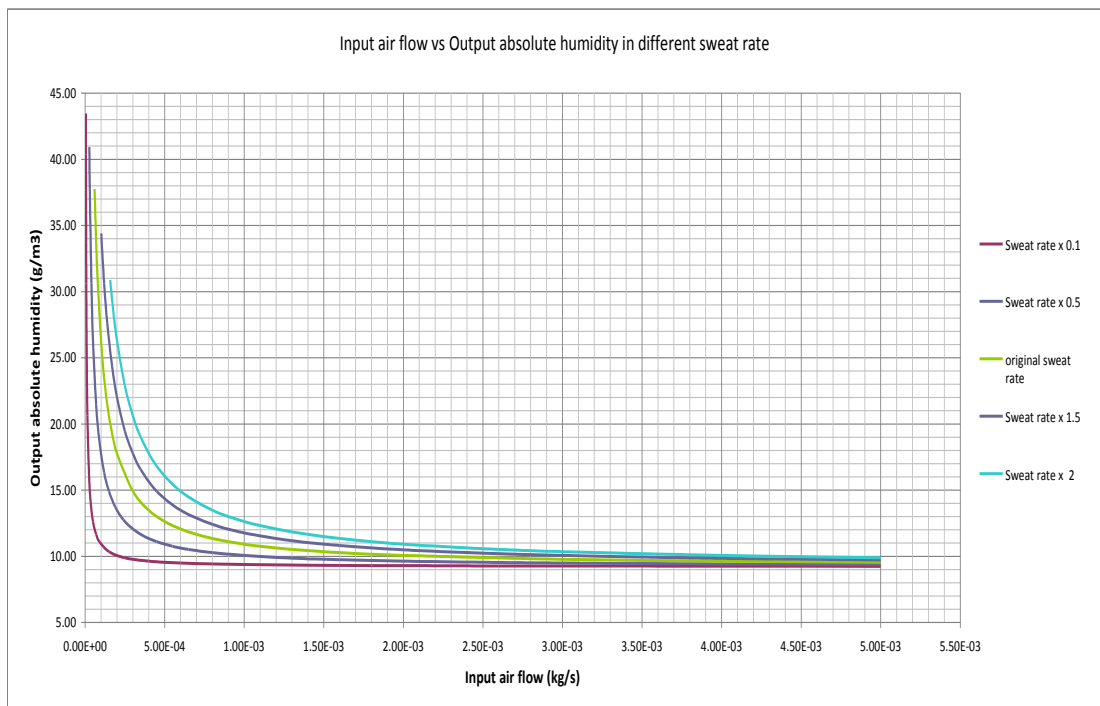
Figure 8 - 9 Input air flow vs output absolute humidity at various sweat rates.

For easy reference by user, we also present in Figures 8-10 and 8-11 the effect of the sweat rate on the output absolute humidity and temperature at different input air flow (from 0.1 times to 2 times). The relative humidity takes between 20 to 100%.
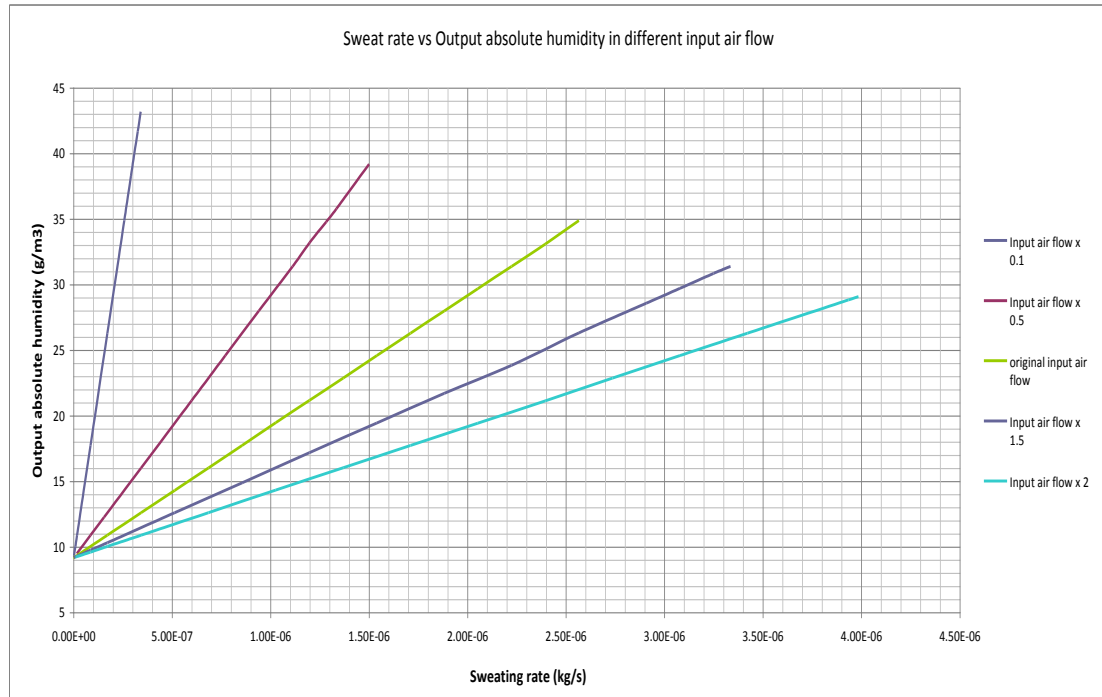
Figure 8 - 10 Effects of the sweat rate on the output absolute humidity under different air flow rates.
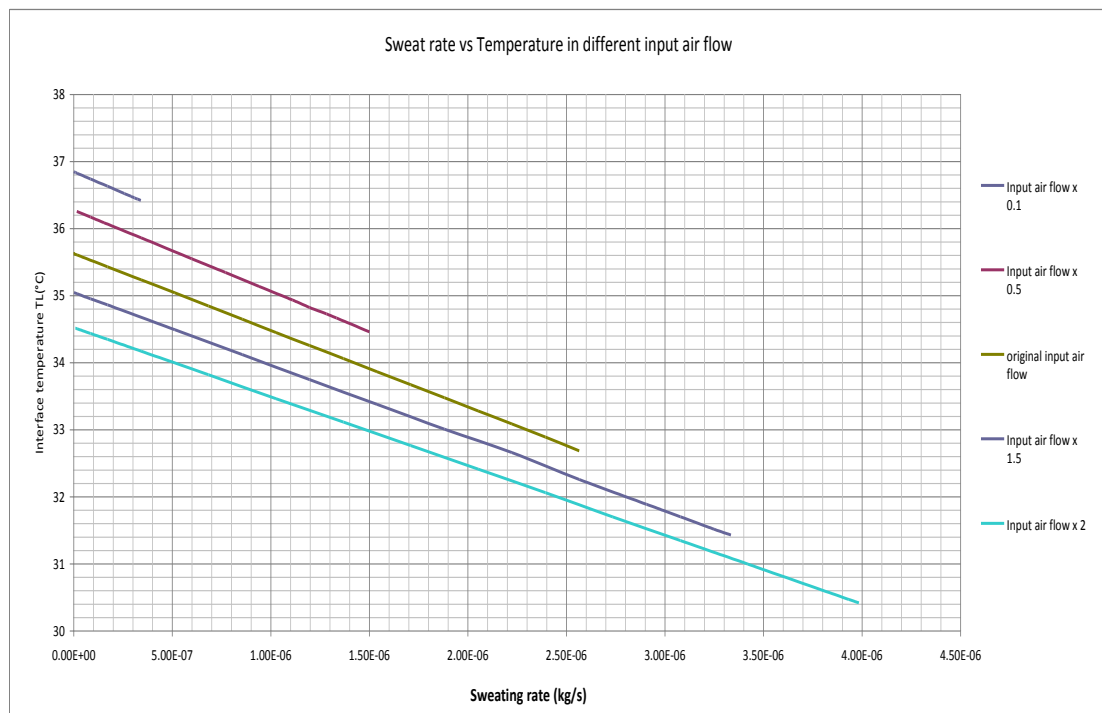
Figure 8 - 11 Effects of the sweat rate on the interface temperature under different air flow rates.

8.4 Discussion

In the compartment model, all parameters match the experiment set up. Following the original condition, the value of T_L can be calculated as 33.67 °C, If we estimate the values for the corresponding equations, we can find that:

Equation 8.1: $\varepsilon \delta A_T (T_0^4 - T_L^4) = 6.31 * 10^{-3}$

Equation 8.2: $\dot{m}_{sw} C_{sw} (T_0 - T_L) = 2.39 * 10^{-5}$

Equation 8.3: $\dot{m}_{air} C_{air} (T_r - T_L) = -1.07 * 10^{-3}$

Equation 8.4: $-(\dot{m}_{sw} + \dot{m}_{air}) C_{mix} (T_L - T_r) = -1.11 * 10^{-3}$

Equation 8.7: $-\Delta_V H \dot{m}_{sw} = -4.15 * 10^{-3}$

Compare above values, we find that:

- The value of the heat flux from sweat is much smaller than other elements, so the heat exchange due to the sweat mass flow can be ignored,

- Contribution of the sweat in heat exchange is mainly in the heat flux duo to sweat and air flow and phase transition,

- The energy associated with the phase transition is approximately 170 times greater than that associated with the sweat heat input,

- Therefore, sweat evaporation is the reason for the drop of the temperature at the interface, as showed in Figure 8-4.
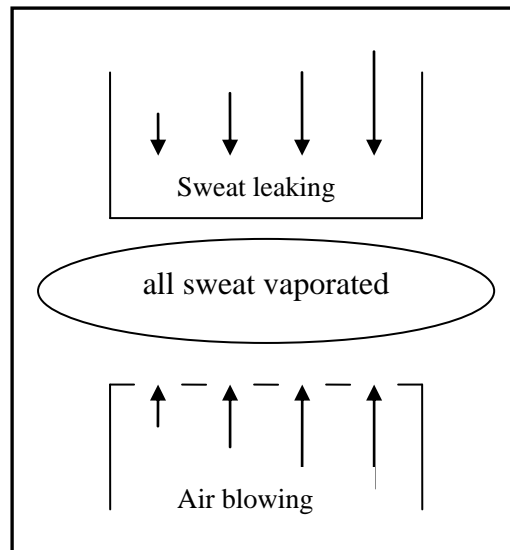
Figure 8 - 12 Schematic diagram of the various sweat rate and input air flow in compartments model

This compartment model was under the assumption of steady state equilibrium, i.e all sweat vaporated, the vapour inputs from sweat leaking and the air are well-mixed. If the input air flow is kept constant, the sweat rate increases, and more humidity can build up in central region of the interface, so output relative humidity will go up when the sweat rate increases, as displayed in Figure 8-4. Conversely, if the sweat rate is kept constantly, input air flow increases from bottom, more air blow into centre area, cool dry air takes more heat and vapour away, so relative humidity and temperature decrease when input air flow increases, as illustrated in Figures 8-5 and 8-7.

The results chapter not only shows the various input air flow graph at normal sweat rate, but also includes various input air flow at different sweat rates. Figure 8-8 compares different sweat rates in the same range of input air flow. The distributing of sweat rate is from 0.1 times to 2 times of the original sweat rate, so it is a range in ascending order by value. The result indicates that the temperature decreases while the sweat rate increase. Figure 8-9 uses the same range of input air flow and sweat rate, the output absolute humidity increase at higher sweat rate.

The last two graphs in this chapter are about various sweat rates at different input air flow. Figure 8-10 shows linear relationships between the absolute humidity and the sweat rate, and the slope of the line are greater at lower input air flow (e.g. 0.1 times the original value). The reason is that at lower air flow, a slight increase in the sweat rate will cause a significant rise in humidity. At higher air flow, it has the capacity to take more heat and vapour away.

Back to Figure 8-10, all lines start at the same level but finish at different values of the sweat rate, when 100% RH is achieved. Figure 8-13 show the relation between the maximum sweat rate (i.e. when the outflow air has 100% RH) and the input air flow rate. An almost linear relation is seen except the few initial values.
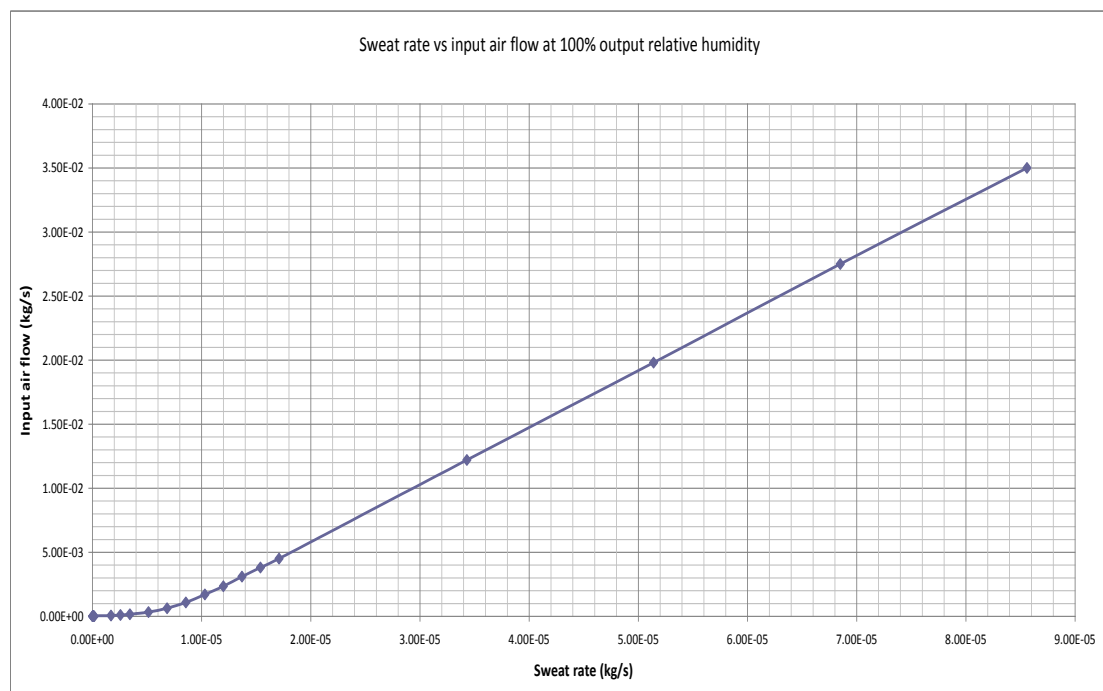
Figure 8 - 13 Sweat rate vs input air flow at 100% output relative humidity.

Chapter 9

General Discussion and Future Work

The characteristics of a patient support interface can influence the susceptibility of subjects, particularly with limited mobility and sensation, to pressure ulcer development. Accordingly, externally powered alternating pressure air mattresses (APAM) are designed to produce intermittent pressure relief and control of the interface microclimate. The primary goal of this thesis was to evaluate physical conditions at the interface and how these may be modified by proactive APAM systems.

This chapter highlights several aspects of this research which have arisen from results of studies involving predominantly experimental work with some computational modeling.

9.1 Evaluation of Physical Measurements with the APAM

9.1.1 Transcutaneous Gas Tension Measurement

Studies over the last 30 years have employed measurements of transcutaneous gas tensions, predominantly oxygen, as an objective indicator of soft tissue viability or status (Newson et al., 1981; Bogie et al., 1992; Knight et al., 2001). The technique provides continuous, non-invasive measurement of oxygen and carbon dioxide tensions within the superficial tissues. It is accepted that this technique requires elevated temperatures of between 43 ℃ and 45 ℃ to ensure maximum vasodilatation. This means that normal blood flow regulation will be altered significantly and perfusion under the electrode will be largely determined by the arterial blood pressure. Thus, although absolute gas levels will inevitably be elevated for all subjects, relative changes during different loading regiments will be of value in

assessing tissue viability (Bader, 1990).

9.1.2 Interface Pressure

Since pressure represents one of the key causative factors in the development of pressure ulcers, its measurement would seem to be appropriate, particularly as this can be achieved at the body support interface. Accordingly, there are a number of in-house and commercial systems, which have been developed to estimate the pressure distribution at the loaded interface. One such commercial system, the Talley – Oxford Pressure Monitor, was used in Chapters 5 and 6 of the present work. Pressure measurements were always performed at the sacrum, while measurements were also recorded at the heel (Chapter 5) and the scapula (Chapter 6).

It is worth mentioning that even with able-bodied subjects the pressure distribution will vary with time (Bader et al., 1986). This is due to small postural changes and the viscoelastic behaviour of both the loaded soft tissues and cushioning support materials. In addition, the use of alternating pressure air mattresses will inevitably lead to variations in interface pressures with time. For these reasons a single parameter, the mean peak value of interface pressure was estimated over a number of mattress cycles. This was recorded from either the 96 cells matrix (sacrum and scapular) or an individual 12 cells matrix (heel), as illustrated in Figure 5-2.

Results indicated that the mean peak pressures in the load bearing areas rarely exceeded 100 mmHg for any of volunteer subjects for any of the APAM test conditions. Indeed the highest pressures were recorded when the APAM system was prescribed a pressure amplitude of 100/0 mmHg (Figure 5-9). When the pressure amplitude was reduced, the mean peak pressures pooled over the normal volunteers decreased significantly. In a similar manner when the internal pressures of the APAM was adjusted by the prototype sensor in Chapter 6, the mean peak pressures rarely exceeded 60 mmHg, even when the mattress was supported at a Head-of-Bed angle of

30° or greater (Figures 6-9 and 6-10). Close examination of the data, however, failed to reveal a consistent relationship between interface pressure and specific tissue response, in terms of transcutaneous gas tensions. For example, at the prescribed pressure profiles and pressure amplitudes, the tissue response is varied, as illustrated in Figure 5-10. Both T_cPO_2 and T_cPCO_2 fluctuate at a similar period to the internal mattress pressures, and the T_cPO_2 is depressed for a large proportion of the monitoring period. In this case, it was associated with a range of interface pressure from 43 to 143 mmHg (5.7 – 19.0 kPa). Such findings reinforce the proposition that it is not the values of interface pressures per se, but their prolonged effects on the tissue viability/status which are critically important at specific body sites for an individual (Bader, 1990; colin et al., 1996; Knight et al., 2001; Goosens and Rithalia, 2009).

The limited nature of interface pressure measurements also question the value of their use in publicity material associated with commercial mattress systems. Such an approach is an undoubtedly convincing "sales pitch" to potential health care purchasers in making decisions about the most effective support surface. However, present research findings should be disseminated widely to ensure that such decisions are not made on interface pressure maps alone.

9.1.3 Sweat Analysis

Section 3.3.1 provided a critical review of the different methods available for the collection of sweat at the skin surface. In the present study, a simple filter paper collection was used in a similar manner to that previously employed in the host laboratory (Knight et al., 2001). Its main advantages compared to more sophisticated systems e.g. Macroduct[TM] (Ferguson-Pell et al., 1988) included its simplicity and its ability to ensure minimal distortion at the loaded interface. The filter paper was sealed onto the skin with a polypropylene sheet, to prevent evaporation during the collection period. However, this arrangement did not markedly change the local skin microenvironment.

Temporal studies of sweat collection suggested that a period of 20 minutes acclimatisation at a temperature of $26 \pm 2^{\circ}C$ was necessary to ensure a satisfactory sweat rate over a subsequent period of 90 minutes. This period represents the maximum allocated to the experimental protocols within chapter 5, where sweat was collected for three 30 minutes phases of unloading, loading and reperfusion. The estimated sweat rates, as indicated in Figure 5-23 and 5-24, were in general agreement with the values recorded in previous studies (Table 7-1). It is interesting to note that other studies have involved collections of up to 9 hours e.g. Taylor et al (1994). These extended periods would inevitably involve fatigue of sweat glands, a phenomenon previously reported to have been present within 3 hours of sweating (Sato, 1977).

9.1.4 Interface Climate Assessment

A detailed literature review revealed a few relevant studies, which focused on the microclimate at a loaded interface of different subject groups (Mahanty et al., 1981; Kokate et al., 1995; Patel et al., 1999). However, none of these attempted to prescribe or, more importantly, define the nature of an optimum microenvironment with the use of an analogue human body, which provided an accurate and reproducible assessment of microclimate at the interface.

The present experimental design has been based on some of the features of these previous studies. The manufactured system was instrumented with a selection of temperature and humidity sensors and test protocols developed to be used with the ClinActiv and Zephyr system. In addition, modifications were incorporated. For example, to avoid saturation of the humidity sensors, a double sheet of standard hospital cotton bedding material was used to cover the sensors, as illustrated in Figure 7-10. Its overall performance was tested using a series of prototype sheet configurations, using a carefully selected range of test protocols.

9.1.5 Internal Pressure within APAM Systems

The controller, Pneumatic Manager, was developed in order to prescribe the internal pressure configuration within an APAM system. It was designed to be a fully manipulative multi-mode system that met all of the project requirements (as detailed in Table 4-1). Accordingly the system could be manipulated to control pressure amplitude, cycle time and profile, speeds of inflation and deflation. It also enabled the APAM system to maintain a continuous low pressure mode, if required.

The system underwent some functional tests which revealed some artifacts, in the form of air leaks, which were evident when the controller was programmed for a pressure profile of 1:4 (Figure 4-8, left). These differences could be attributed to the principle underlying the controller, Pneumatic Manager, when exhibiting an equilibrating phase. Hence, in the 1:4 pressure profiles, when a cushion re-inflates from a deflated state, the solenoids permit its connection with the two other cushions which are to remain inflated during the next phase of the cycle. The difference in pressure between the two inflated and one deflated cells initiates a period in which air from the previously inflated cushions supplies the previously deflated cushion in addition to the normal air supply, until the pressures are equivalent in each cushion. This transient period is reflected in a reduction in the inflated cushion pressure. The mean pressures in the three cushions are then restored to the presented maximum pressure, as illustrated (Figure 4-8, left).

In 1:2 configurations however, the cells are either in a state of inflation or deflation. Thus the previously described phenomenon is not observed in a 1:2 alternating pressure profile (Figure 4-8, right), because there are no existing inflated cushions to equilibrate the pressure between each other.

There was also an identification of a systematic artifact in recording real time pressure. The data logger, which was connected to the pressure transducers, recorded values

which were offset by +2 mmHg. This represented a screen error due to the interface between the data logger and was accounted for in the calibration of the pressure transducers. More importantly, this did not affect the internal cushion pressures of the support surface which was verified to be the desired value, via the use of external pressure gauges.

By contrast, the provision of a prototype APAM system, with an incorporated SAALP^{TM} sensor, facilitated the control of the internal pressure characteristics based on individual morphology. The findings, as indicated Figure 6-4, demonstrated that the internal pressures within the air cells could be adjusted automatically and in real-time in order to match the individual subject's weight, shape and position on the mattress. In addition, the duration of the pressure cycle was observed to depend on subject morphology and position (Figure 6-6).

9.1.6 Critical Assessment of Computational Approach

The physical state of many patients demands the prescription of a special support surface, such as an APAM, by medical professionals. It is highly probable that such patients are going to remain bedridden either for a critical short period i.e. post operation or for an extended period of time. In either case, the microclimate at the interface between the patient and the support surface becomes a critical determinant in maintaining tissue health. Indeed, as discussed in section 2.2.l, both temperature and humidity are extrinsic factors which have been implicated in pressure ulcer development. Data from the experimental model using the body analogue demonstrated some control of the interface microclimate which was, in Chapter 8, then examined using a compartmental model. It was based on the thermal phenomena and structure of pressure released bed, to build up a compartment system. The interface-layer was regarded as a closed domain. The upper human analogue continuously releases sweat into the domain, which is also exposed to the inflow of air

at a constant temperature and flow rate. The air flux out of this domain contains moisture as the sweat can evaporate in the domain. The system eventually reaches steady state.

There is a surprising dearth in the literature examination the association of pressure ulcers with some of the well-established thermal models. Indeed the reason to use thermal models is to simplify the very complex thermal phenomena at the support interface, involving heat transfer in vapour and dry air, radiation and evaporation. The present study represents a first step in providing a complete description of the moisture vapor and heat transport capability of a range of sheet/mattress support systems, as illustrated in Figure 8-4.

An advantage of computational models is that it not only allows the inclusion of different sweat rates, to simulate sweating as measured in human studies (Table 7-1), but also allows different air flow rate to be tested without a fixed setting in terms of air flow from support interface using commercial air pressure mattresses. In concept, optimization strategies could be developed to interface with the computational model to design an optimal microclimate for each individual subject, which has excess sweating and/or episodes of incontinence or elevated body temperatures, as in pyrexia.

However, current computational models are still in their nascent stages, some approximations and assumptions were included in this modelling, and they are not yet accurate and intelligent enough to reflect a real-time change of interface humidity and temperature at experiment period. Part of what makes the model so difficult to develop is that it is computationally very difficult to describe each thermal phenomenon to perfectly simulate the experiment condition. Further, accurately specifying the parameter of the experiment and the material properties of support interface still remains a formidable challenge.

9.2 Effect of Variety Pressure Signature on Tissue Status

This thesis includes a number of studies examining the tissue viability/status on healthy volunteers supported on APAM systems. In Chapter 5 this was achieved by a custom controller, which imposed a prescribed pressure signature. Chapter 6 examined the performance of a prototype APAM incorporating a novel sensor (SAALP^{TM}), which adjusted the internal air pressure according to the characteristics of the individual volunteer. Both strategies were designed to control the volume of air and magnitude of inflation within the mattress cushions, in an attempt to provide both uniform load distribution and periodic relief/redistribution. The range of responses to these strategies is discussed in the following sections.

9.2.1 Transcutaneous Oxygen and Carbon Dioxide Tension

Tissue oxygen tension (T_cPO_2), was monitored at the sacrum of healthy volunteers in both loaded and unloaded states. This approach has been previously reported in other studies (Bader and Gant, 1988; Bader, 1990), which monitored relative changes of individuals compared with unloaded T_cPO_2 values.

The literature traditionally reports an inverse relationship between applied pressures and skin tissue oxygen tension (Seiler and Stahelin, 1979; Newson et al., 1981). Accordingly, these authors attempted to assign a threshold level of applied pressure, which would reduce T_cPO_2 tensions to zero. However, such an approach is fraught with difficulties due to the inevitable variations between individuals and tissue sites, and the physiological significance of such a threshold level has also been questioned (Spence et al., 1984). Indeed, in the present study, this approach was not possible due to the dynamic nature of the supporting pressures. However close examination of the data does suggest that the highest pressure amplitudes of 100/0 mmHg within the APAM system, generally yielded the highest interface pressures (Figure 5-9), and

indirectly periods in which the T_cPO_2 levels were low in magnitude (Figure 5-10). Similarly, in some cases, when the mattress was supported at a HOB angle of 60°, associated with elevated interface pressures at the sacrum were depressed levels of T_cPO_2 (Figure 6-10). It is interesting to note that these elevated interface pressures appeared to be independent of the internal pressures within the mattress (Figure 6-4), as controlled by the SAALP^{TM} sensor.

Tissue carbon dioxide tension, T_cPCO_2 was simultaneously monitored using the combined gas tension electrode and this measure has been proposed to reflect important information about tissue viability/status (Bader, 1990). In the present study, a number of parameters were selected to enable descriptors of the carbon dioxide tension response to applied load, as illustrated in Figures 5-7 and 5-8. The majority of findings during the loaded monitoring period indicated a Mode 1 response (Figure 5-7; 6-8b and 6-12(a-d)), namely, minimal change with time in T_cPCO_2 from unloaded basal levels. Nonetheless close examination of the data for different pressure amplitudes revealed a high proportion of Mode 2 responses (Figure 5-17) and the associated highest mean values of the excess carbon dioxide parameter (Figure 5-18) with the prescribed pressure amplitude of 100/0 mmHg (Figure 5-10). In addition, the APAM studies highlighted a strong correlation between T_cPO_2 and T_cPCO_2 and, to a lesser degree, applied pressures e.g. Figures 5-20; 5-21 and 6-13. It is interesting to note, that not all subjects demonstrated an associated increase in T_cPCO_2 levels with reduced T_cPO_2 levels. This was the case in 22% with the custom–made controller imposing the pressure profile, and 8% with the Self-Adjusting Alternating Low Pressure mattress. These findings suggest an individual capacity to prevent accumulation of T_cPCO_2, presumably by the removal of waste products even during periods of high internal pressures.

An increase in tissue levels of carbon dioxide, a metabolic waste product, could indicate stasis in blood and lymph flow which may reflect an accumulation in other

potentially harmful waste products whose presence would compromise tissue viability. Build up of carbon dioxide will also lead to a decrease in pH and the problems associated with acidosis. An elevated carbon dioxide tension is a vasodilator and can result in reduced vasomotor tone (Campbell et al., 1974).

9.2.2 Inter-relationship Between the Microenvironment at the Subject Support Interface

In chapter 5, some significant correlations were observed when the parameters associated with the transcutaneous gases, oxygen and carbon dioxide, were compared with respect to the APAM variables (Figures 5-19 to 5-22). In addition, sweat rates were estimated during identical loaded period (Figure 5-23) for which sacral gas levels were recorded. Such a combined approach, employing two distinct measurement techniques, was previously adopted in the host laboratory to assess the soft tissue response to loading. The selected gas parameters were therefore examined for each of the three APAM variables, with respect to the sweat ratios (loaded versus unloaded values). As illustrated in Figure 9-1, the resulting linear models yielded correlation coefficients ranging from 0.05 to 0.24, indicating no statistical significant ($p > 0.05$) for any of the APAM variables. This contrasts with the relationships reported in the previous study (Knight et al., 2001), and detailed in section 3.3.1. There were several differences between the two studies which may explain the contrasting results, such as the use in the present study of an alternating pressure signatory incorporating different prescribed variables and the fact that sweat metabolites were not analysed. This justifies the pooling of the data for different values of each of the three APAM variables.

Another parameter which was continuously monitored at the body-support interface was humidity, reflecting local moisture. Results indicated two distinct trends (Figures 5-13 to 5-15), dependent on whether the RH attained a value of 100% or not. It might be predicted that the level of interface moisture could be related to the sweat

collected during the monitoring period. Accordingly, the pooled subject data could be separated into two separate groups. Thus, the sweat ratios were re-examined against the two parameters related to transcutaneous gas levels. Figure 9-2 illustrates the data for the T_cPO_2 parameter (left) and T_cPCO_2 parameter (right). The trends appeared to be different, with a suggestion of an increase in sweat ratio with both gas parameters at the saturated RH and a decreasing trend at humidity levels which did not reach 100% RH. However, the linear models yielded correlation coefficients ranging from 0.19 to 0.29, none of which were statistically significant at the 5 per cent level ($p<0.05$). Clearly, the test conditions as discussed in the previous paragraph might have contributed to these findings. Further work is envisaged under more limited test conditions to examine the relationship between sweat content and interface humidity and temperature at the loaded sacrum.

(a)

(d)
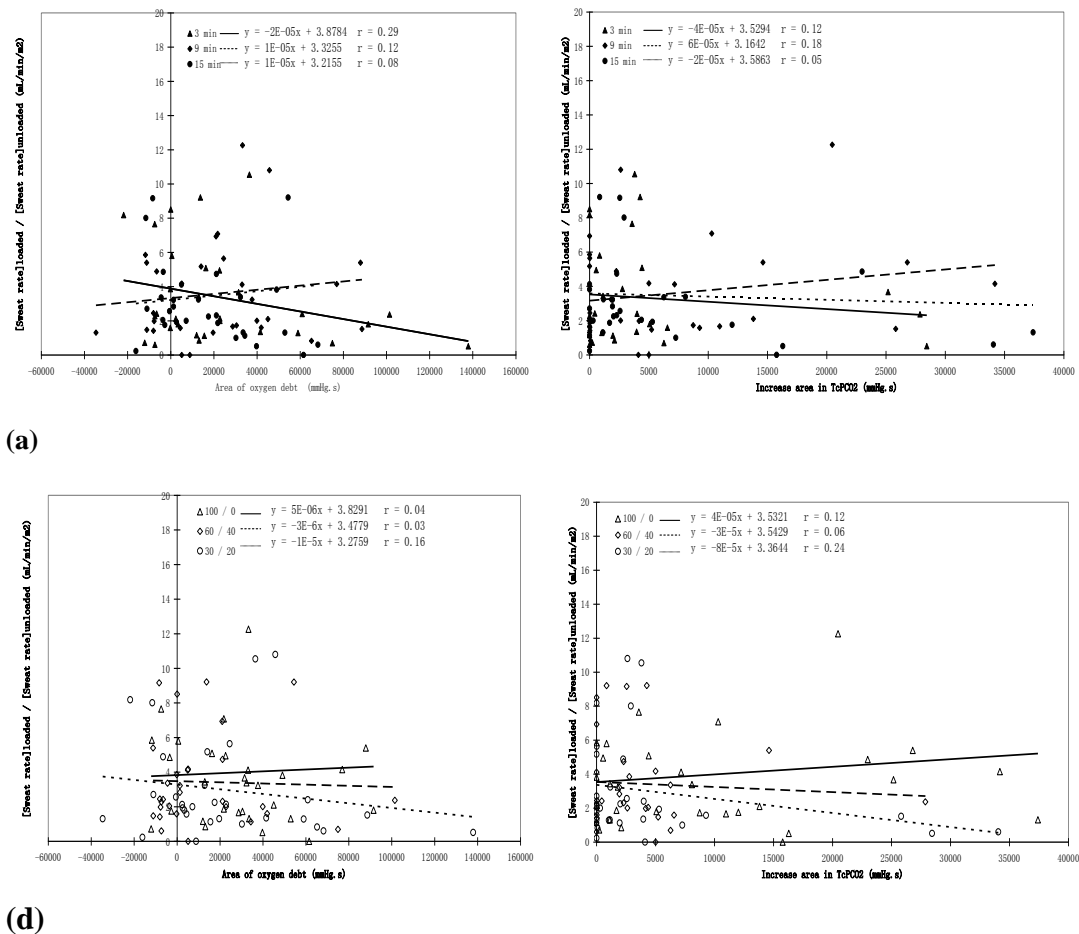
Figure 9 - 1 The relationship between the sweat ratio and response of transcutaneous gas parameters related to oxygen (left pair) and carbon dioxide (right pair). Modes 1 and 2 only recorded in this graph.

(a) Different cycle period of mattress (3 min, 9 min, 15 min)
(b) Different pressure amplitude (30/20, 60/40, 100/0)
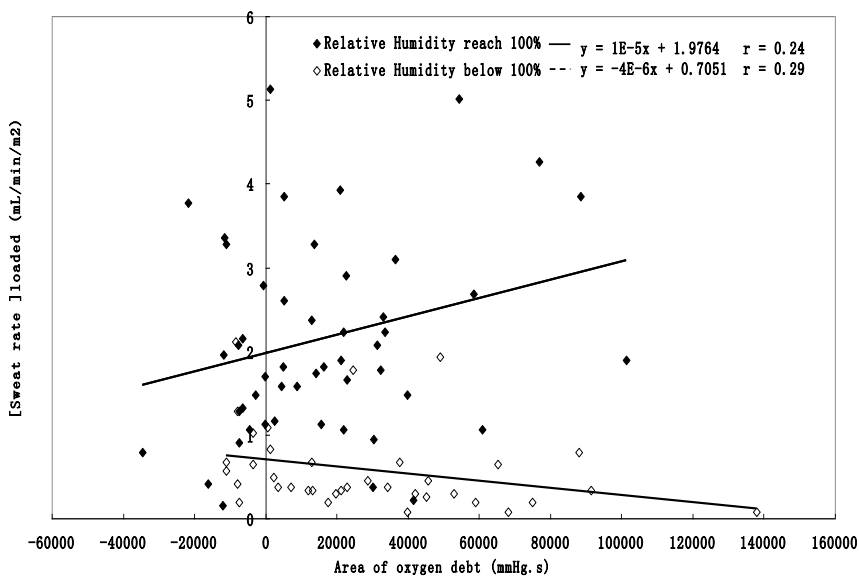
(a)
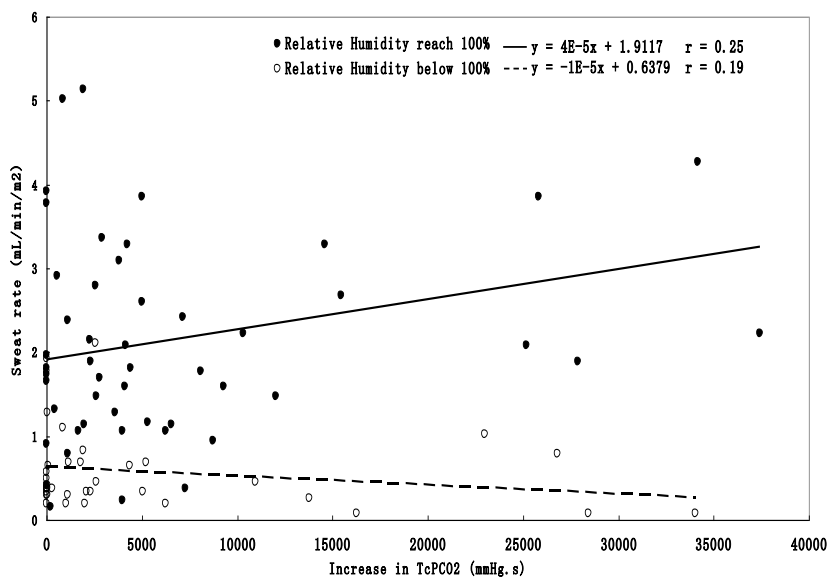
(b)

Figure 9 - 2 The relationship between the sweat ratio and response of transcutaneous gas paramters related to a) oxygen and b) carbon dioxide. The sweat ratios were separated in terms of the misture level, as separated by attaining RH level of 100% or not. Modes 1 and 2 only recorded in this graph. Pooled data for all the three variables of the APAM system.

9.3 Strategies to Prevent Pressure Ulcers

9.3.1 Personalised Support Surfaces

Pressure air mattress systems have been used for the treatment and prevention of pressure ulcers for many years. Indeed the low-air-loss mattress system was first described in the medical literature in 1971 by Scales and colleagues. Since that first description, the number of available products has increased rapidly and there are now tens of products on the market, each with slightly different features and constructions. Such support surfaces generically provide pressure reduction either by distributing body interface pressure over a large area or pressure relief via the redistribution of pressure for prescribed periods. This permits the return of blood flow to and lymph flow away from previously loaded or vulnerable tissue areas. Nonetheless, the prevalence of pressure ulcers remains unacceptably high despite the extensive efforts of providing an ideal preventative solution. This may be due to the prescribed settings of the various commercial support surfaces, which have been limited to a fixed setting in terms of pressure amplitude, pressure profile and cycle period. Accordingly, they are marketed as a "one style fits all" for subjects deemed at risk of developing a pressure ulcer. However, it is well established that such subjects vary in terms of their body weight, morphology and tissue response to loading. In the recent past, there has been a considerable drive towards personalized medicine. In the current context this is equivalent to incorporating the systematic use of information about an individual subject in selecting the optimum support characteristics. Such a simple strategy was examined in both chapter 5 and 6. In particular findings from the latter chapter revealed the potential for a single sensor (SAALP^{TM}) to adjust the internal mattress pressure. In the majority of the test conditions this provided a support, which maintained tissue viability, in term of transcutaneous gas tensions. However, there were a number of tests in which tissue viability was potentially compromised, for example, Figures 5-10 and 6-13. Thus a

more encompassing strategy for personalised support surfaces is still required. Ultimately this would incorporate the potential to change settings to accommodate any alterations in subject characteristics. This might include changes in the subject's medical and/or mental state or local changes in tissue properties due to for example, dehydration or atrophy.

In a similar manner, a personalised support could also control the microclimate at the loaded interface. The performance of such system has been examined in Chapter 7. Clearly the moisture build up, induced by simulated sweating rates, increases both the humidity and temperature levels as assessed by in-built sensors (Figure 4-5). However, in some cases, this environment could be controlled by a combination of air flow rates within the APAM system and permeable sheets. For example, by delaying the time taken to attain 100% RH at the loaded interface e.g. Figure 7-17. Such considerations are of particular relevance to subjects with a predisposition to excess sweating and/or episodes of incontinence, both of which makes the soft tissues highly susceptible to maceration and ultimate tissue breakdown.

9.3.2 Early Detection of Compromised Soft Tissues

Patient specific preventative measures will lead to a substantial reduction in the incidence of pressure ulcers, with an associated reduction in individual suffering and the financial burden on the Health Service. However this can only be achieved if objective risk assessment criteria are developed, which are more robust than the existing Nursing scales, such as the Braden and Norton. This necessitates the adoption of strategies to provide early indicators of tissue breakdown and prevent subsequent development of the condition. Both physical devices, typically transcutaneous gas tensions and Laser Doppler Fluxmetry, and biomarkers, involving sweat analysis (Bader et al., 2005) and skin markers such as the pro-inflammatory marker interleukin-la, (Bronneberg et al., 2007), provide potential screening methods for the early detection of compromised soft tissues. Ideally, these would have to be incorporated within the sheets or cushions at locations coincident with bony

225

prominences. The former strategy was described in Chapter 7 with the temperature and humidity sensors under the body analogue. This could be extended to incorporate the combined measurements of oxygen and carbon dioxide tensions, interface pressure and some of the critical biomarkers. Although the relationship between some of these parameters have been examined in the present study (e.g. Figures 5-19; 5-20; 9-1 and 9-2), this needs to be extended if a comprehensive algorithm could be developed indicating early compromise to soft tissues.

9.4 Future Work

The assessment of the status of soft tissues could be extended to include further studies involving the existing technique or other more sophisticated analysis systems.

9.4.1 Extension of Subject Groups

The techniques in this thesis have proved to be reasonably successful when applied with healthy young subjects. It is suggested that further studies should be extended and then widened to include clinical patient groups such as spinal cord injury subjects; lower limb amputees and multiple sclerosis sufferers, all of whom at risk of developing pressures ulcers.

9.4.2 Extension of Sweat Metabolite Markers

Although considered to be a potentially simple screening method, (Polliack et al., 1993 and 1997; Knight et al., 2001; Bader et al., 2005), the analysis of sweat was limited to total weight and there was no attempt at characterising its various constituents. As discussed in section 5.5 the latter analysis would have been costly to perform. However, given an extended study to analysis sweat samples collected from tissues subjected to periods of loading and reperfusion. Candidate markers would include lactate, urea and selected purines, such as uric acid and hypoxanthine, as illustrated in Figure 9-3 (Bader et al., 2005). This would also enable examining the relationship between the gas parameters and sweat metabolites.
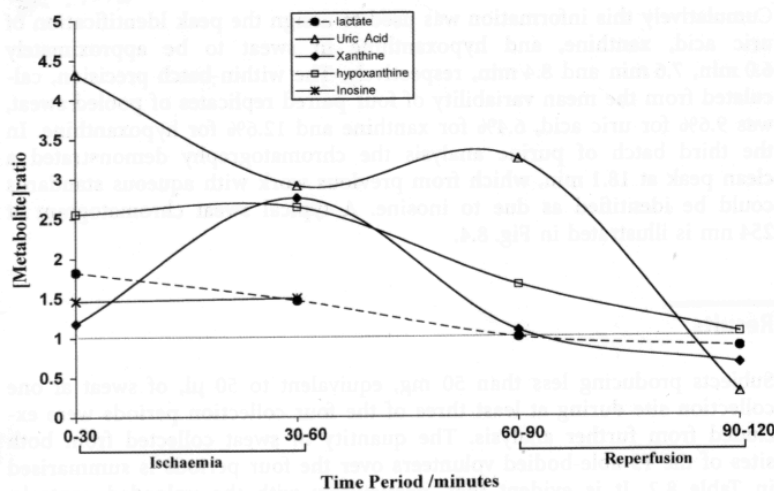
Figure 9 - 3 Median sweat metabolite concentrations for collection at two adjacent sites on the sacrum from able-bodied subjects during separate collection period (Bader et al., 2005).

9.4.3 Real Time Simulation of Interface Microclimate

One of the most obvious parameters from the work of this thesis would be the development of a continuous real time monitor of interface microclimate at subject support surface and human body analogue, the latter one then examined using a compartmental model. However, the present modeling only represents the first step in providing a complete description of the moisture vapour and heat transport capability of a range of sheet/mattress support systems, as illustrated in Figure 8-4. It is proposed that further studies should be carried out to investigate a real time simulation at the interface microclimate between the subject and the support surface. This could further elucidate that controlling the microclimate of the skin and providing a quality patient support system represent an important strategy in minimizing the risk of pressure ulcers.

9.4.4 Progressive Mobility Therapy Programmes

For many years, the plenty literature have recognised the importance of positioning techniques particularly for the prevention of tissue damage. In more recent years

however the concept of positioning has become more accepted as the potential impact becomes more deeply understood by the multidisciplinary team. Developing the techniques, protocols and tools that aid in that recovery is key to continuing to improve outcomes and Progressive Mobility is one concept that is leading to results.

Progressive Mobility is defined as a series of planned movements in a sequential manner beginning at a patient's current mobility status with a goal of returning to the patient's baseline (Vollman, 2010). These movements are administered in a step wise fashion with raising the head of the bed, passive range-of-motion, and Continuous Lateral Rotation Therapy. In this thesis was including a custom–made controller which offers a passive range-of-motion, and a prototype APAMs incorporating a SAALP^{TM} sensor, which adjusts the profile according to individual subject characteristics with raising the head of the bed. In further studies, it is planned to testing new support surface which incorporates lateral tilting mechanisms, superimposed on APAM systems, which can offer important mobilisation therapies necessary to assist patient through increasing levels of mobility from Continuous Lateral Rotation Therapy, as an added strategy for pressure relief.

Appendix A

Electrical Circuit

Electrical circuits for the controller were designed by Olav Sadoo, a Medical Engineering student at Queen Mary University. This involved electrical mains connections between the logic controller (Crouzet MILLENNIUM 2 Plus) and the four solenoid valves. Each channel port represented a switch which is controlled via the logic controller (Figure A-1). Each solenoid was inturn governed by one of these switches - in this case 3 – 6. The voltage signal representative of the measured pressure is recorded is taken from pin 2 and 3, while the input voltage of 5V is administered via pin 1 and 2 (Figure A-2).
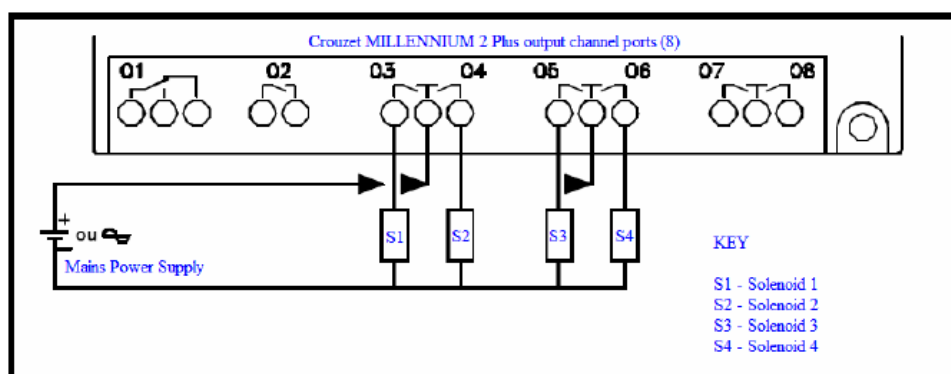
Figure A-1 Electrical mains connections between the logic controllers with the four solenoid valves.
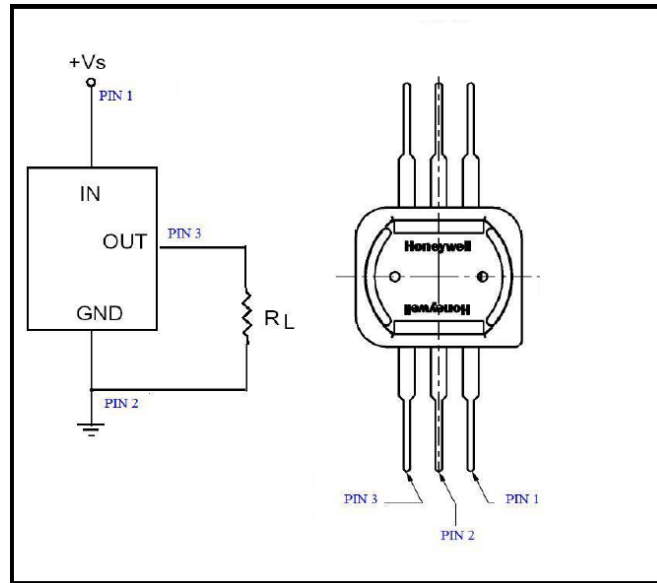
Figure A-2 Electrical connections each of the four cushion pressure sensor for the linking with the data logger.

Appendix B

B – 1: sweat collection

Sweat pad -- an annuli sweat pad with an inner and outer diameter of 16 and 45 mm, during this experiment, sweat pad is working together with fixation ring (T_cPO_2 electrode), **so working area was smaller than real pad area.**

Fixation ring

Sweat pad
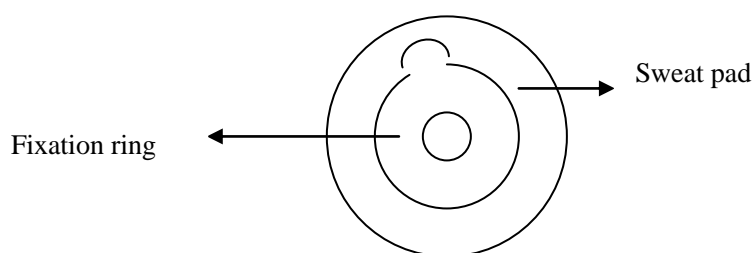
Area of circular = π * (radius of the circular)^2

Area of annuli = 3.14 * (45 / 2)^2 – 3.14 * (30 / 2)^2
$$= 1590.431 – 706.8583$$
$$= 883.5742 \text{ mm}^2$$

So: $A_{unload} = 1590$; $A_{loading} = 883$
$A_{unload} / A_{loading} = 1.8$

In order to complete *quantificative* analysis the sweat weight with same collection area, the loading sweat weight was times 1.8

For example:

	Sweat weight in the sacrum (mg)			Sweat weight in the heel (mg)		
	Unload	Loading	Reperfusion	Unload	Loading	Reperfusion
Subject A with 1:2, 3 min, 30/20	8	6	46	8	4	7
Subject A with 1:2, 3 min, 60/40	34	30	21	13	7	8

6 x 1.8 = 10.8
30 x 1.8 = 54

So new sweat weight will be

	Unload	Loading	Reperfusion	Unload	Loading	Reperfusion
Subject A with 1:2, 3 min, 30/20	8	_10.8_	46	8	4	7
Subject A with 1:2, 3 min, 60/40	34	_54_	21	13	7	8

B-2: the interface pressure table for each subject

Subject A

		Sacrum (mmHg)		Heel (mmHg)	
		First scan	Second scan	First scan	Second scan
100/0	**3 min, 1:2**	105	53	29	--
	3 min, 1:4	54	52	90	149
	9 min, 1:2	127	123	87	128
	9 min, 1:4	50	45	52	67
	15 min, 1:2	68	82	72	140
	15 min, 1:4	38	75	104	20
60/40	**3 min, 1:2**	51	74	143	80
	3 min, 1:4	59	42	78	66
	9 min, 1:2	100	90	18	14
	9 min, 1:4	93	102	43	40
	15 min, 1:2	39	50	56	63
	15 min, 1:4	58	58	97	130
3-/20	**3 min, 1:2**	33	36	19	--
	3 min, 1:4	86	71	68	59
	9 min, 1:2	41	37	42	40
	9 min, 1:4	48	56	47	49
	15 min, 1:2	41	33	11	14
	15 min, 1:4	40	46	22	46
NHS		48	50	133	111
Primo		50	52	82	71

* **Abnormal high maximum pressures – these should be ignored**

x **Missing data**

-- **Value low than 10 mmHg**

Subject B

		Sacrum (mmHg)		Heel (mmHg)	
		First scan	**Second scan**	**First scan**	**Second scan**
100/0	**3 min, 1:2**	120	198*	125	73
	3 min, 1:4	52	42	72	87
	9 min, 1:2	116	246*	68	57
	9 min, 1:4	109	108	23	47
	15 min, 1:2	86	143	28	46
	15 min, 1:4	81	69	113	155
60/40	**3 min, 1:2**	58	64	25	17
	3 min, 1:4	55	57	81	80
	9 min, 1:2	58	81	20	14
	9 min, 1:4	50	72	44	64
	15 min, 1:2	42	48	59	46
	15 min, 1:4	54	52	36	45
3-/20	**3 min, 1:2**	42	x	85	x
	3 min, 1:4	46	56	68	85
	9 min, 1:2	40	36	61	27
	9 min, 1:4	48	60	82	74
	15 min, 1:2	41	49	137	163
	15 min, 1:4	39	41	54	79
NHS		142	136	20	21
Primo		44	46	69	68

*   Abnormal high maximum pressures – these should be ignored

x   Missing data

--   Value low than 10 mmHg

Subject C

		Sacrum (mmHg)		Heel (mmHg)	
		First scan	**Second scan**	**First scan**	**Second scan**
100/0	**3 min, 1:2**	47	65	49	105
	3 min, 1:4	63	63	77	64
	9 min, 1:2	34	92	76	22
	9 min, 1:4	80	63	--	--
	15 min, 1:2	124	58	72	59
	15 min, 1:4	45	43	98	97
60/40	**3 min, 1:2**	x	x	x	x
	3 min, 1:4	47	59	48	43
	9 min, 1:2	44	50	--	39
	9 min, 1:4	43	32	25	55
	15 min, 1:2	53	60	66	53
	15 min, 1:4	66	58	23	34
3-/20	**3 min, 1:2**	42	50	27	37
	3 min, 1:4	59	76	73	53
	9 min, 1:2	53	48	43	50
	9 min, 1:4	72	63	41	40
	15 min, 1:2	54	49	36	41
	15 min, 1:4	44	39	33	32
NHS		35	43	37	56
Primo		80	71	27	26

*   Abnormal high maximum pressures – these should be ignored

x   Missing data

--   Value low than 10 mmHg

Subject D

		Sacrum (mmHg)		Heel (mmHg)	
		First scan	**Second scan**	**First scan**	**Second scan**
100/0	**3 min, 1:2**	78	x	138	x
	3 min, 1:4	84	64	44	98
	9 min, 1:2	103	43	30	17
	9 min, 1:4	48	52	49	17
	15 min, 1:2	62	70	76	--
	15 min, 1:4	66	62	58	78
60/40	**3 min, 1:2**	64	50	115	16
	3 min, 1:4	56	53	53	49
	9 min, 1:2	48	33	--	25
	9 min, 1:4	57	59	36	21
	15 min, 1:2	56	84	17	10
	15 min, 1:4	77	74	16	20
3-/20	**3 min, 1:2**	31	39	42	37
	3 min, 1:4	42	36	101	101
	9 min, 1:2	49	43	89	66
	9 min, 1:4	120	106	40	34
	15 min, 1:2	72	73	98	42
	15 min, 1:4	40	40	91	47
NHS		43	52	74	77
Primo		38	29	61	56

*   Abnormal high maximum pressures – these should be ignored

x   Missing data

--   Value low than 10 mmHg

Subject E

		Sacrum (mmHg)		Heel (mmHg)	
		First scan	**Second scan**	**First scan**	**Second scan**
100/0	**3 min, 1:2**	61	76	64	154
	3 min, 1:4	116	x	63	x
	9 min, 1:2	50	152	35	51
	9 min, 1:4	66	88	43	25
	15 min, 1:2	75	126	130	59
	15 min, 1:4	60	50	115	155
60/40	**3 min, 1:2**	71	92	44	59
	3 min, 1:4	66	96	50	90
	9 min, 1:2	59	59	93	85
	9 min, 1:4	116	144	115	94
	15 min, 1:2	110	116	51	62
	15 min, 1:4	71	62	81	94
3-/20	**3 min, 1:2**	224*	206*	110	96
	3 min, 1:4	164*	192*	65	51
	9 min, 1:2	49	41	53	48
	9 min, 1:4	33	34	59	38
	15 min, 1:2	77	38	57	54
	15 min, 1:4	42	35	53	90
NHS		33	37	85	93
Primo		38	35	86	77

*   Abnormal high maximum pressures – these should be ignored

x   Missing data

--   Value low than 10 mmHg

Appendix C

C – 1: Internal pressure

Table C-1-1 Both the Internal pressures and Cycle times of mattress with Phase 1 group.

		Internal pressure with different of HOB in Phase 1 group			
		AP part (sacrum)			CLP part (scapular)
	Degree of HOB	Max internal Pressure (mmHg)	Min internal Pressure (mmHg)	Cycle Time (min)	Max internal Pressure (mmHg)
Subject A	0 °	25.8	2.0	8.5 - 19	29.37
	30 °	23.8	7.1	3–5.5	26.57
	45 °	26.6	13.3	N/A	28.1
	60 °	27.3	2.9	4.5–12	30.43
Subject B	0 °	11.6	2.1	8	14.39
	30 °	23.5	1.9	15	27.12
	45 °	29.2	2.0	7	32.33
	60 °	9	2.1	N/A	12.2
Subject C	0 °	12.5	2.1	9.5	13.97
	30 °	24.8	1.4	8	27.38
	45 °	21.8	2.8	N/A	25.23
	60 °	26.4	2.3	N/A	27.6
Subject D	0 °	10.9	2.4	5.5	12.57
	30 °	24.1	1.5	13.5	26.76
	45 °	24,5	1.4	N/A	23.8
	60 °	19.6	16.1	N/A	21.3
Subject E	0 °	15.1	2.5	5.5	17.12
	30 °	26.1	2.5	4–13.5	28.07
	45 °	12.3	9.2	N/A	13.5
	60 °	10.5	2.7	N/A	13.73
Subject F	0 °	12.8	2.3	7.5	14.47
	30 °	25.7	2.6	3.5 - 12	29.37
	45 °	24.5	3.7	N/A	28.06
	60 °	27.9	2.5	N/A	31.62

Table C-1-2 Both the Internal pressures & Cycle times in Phase II group.

		Compare internal pressure with different of HOB in Phase II group			
		AP part (sacrum)			CLP part (scapular)
	Degree of HOB	Max internal pressure (mmHg)	Min internal pressure (mmHg)	Cycle Time (min)	Max internal Pressure (mmHg)
Subject A (second)	0 °	17.5	2.6	9.5	19.9
	30 °	19.1	3.1	9.5	21.4
	45 °	17.5	3.9	7	19.5
	60 °	22.9	2.7	10.5	25.3
Subject B (second)	0 °	11.7	2.4	8	14.7
	30 °	16.7	3.4	7.5	18.9
	45 °	12.6	2.9	8	15.1
	60 °	17.1	3.6	8	19.6
Subject C (second)	0 °	13.6	2.3	8	16.3
	30 °	15.3	3.3	9	17.5
	45 °	15.8	2.6	9	18.5
	60 °	17.3	3	8	19.3
Subject D (second)	0 °	18.4	2.3	9	21.8
	30 °	24.5	2.4	13	26.7
	45 °	21.4	2.4	12	23.1
	60 °	26.5	2.5	11	30.9
Subject F (second)	0 °	13.5	2.4	10	15.9
	30 °	14.7	2.2	9.5	16.7
	45 °	13.9	2.2	11.5	15.8
	60 °	15	2.6	10.5	16.8

		Compare internal pressure with different of HOB in Phase II group			
		AP part (sacrum)			CLP part (scapular)
	Degree of HOB	Max internal pressure (mmHg)	Min internal pressure (mmHg)	Cycle Time (min)	Max internal Pressure (mmHg)
Subject G	0 °	13.1	2.0	8.5	16.4
	30 °	17.2	3.0	8	19.8
	45 °	12.6	2.4	9	15.7
	60 °	13.7	2.6	9	16.3
Subject H	0 °	14.2	2.0	8.5	17.4
	30 °	14.8	2.3	8	16.9
	45 °	13.1	1.9	9	15.1
	60 °	21.6	3.5	9	24.1
Subject I	0 °	15.6	2.2	8.5	18.8
	30 °	19.6	3.5	9	22.5
	45 °	23.5	3.0	9	26.3
	60 °	32.4	2.3	13	34.6
Subject J	0 °	11.5	2.1	8.5	14.4
	30 °	14.8	2.7	8	17.3
	45 °	12.2	2.4	9.5	14.9
	60 °	14.5	2.3	9.5	17.6
Subject K	0 °	19.2	2.3	11	21.1
	30 °	18.1	1.7	12.5	20
	45 °	25.6	1.2	24	27.8
	60 °	N/A	N/A	N/A	N/A
Subject L	0 °	18.2	2.27	9	20.2
	30 °	29.8	2.1	12.5	32.1
	45 °	42.2	2.1	15	44.5

C – 2: T_CPO_2 response

Subject K
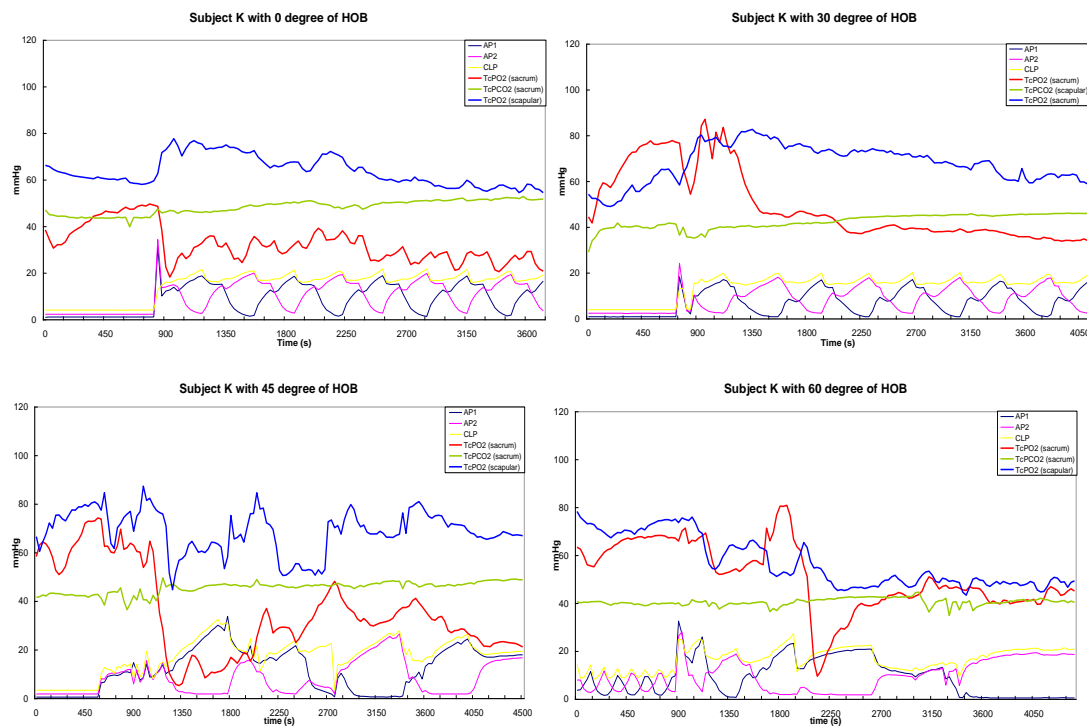
Figure C-2-1: The T_cPO_2 response at both the sacral and scapular locations of Subject K supported at various degrees of HOB when assessed in phase II tests. It was evident that the alternating mode in the mattress was not functional for subject K, at a HOB angle of 60 degrees (Figure bottom left).

Subject L
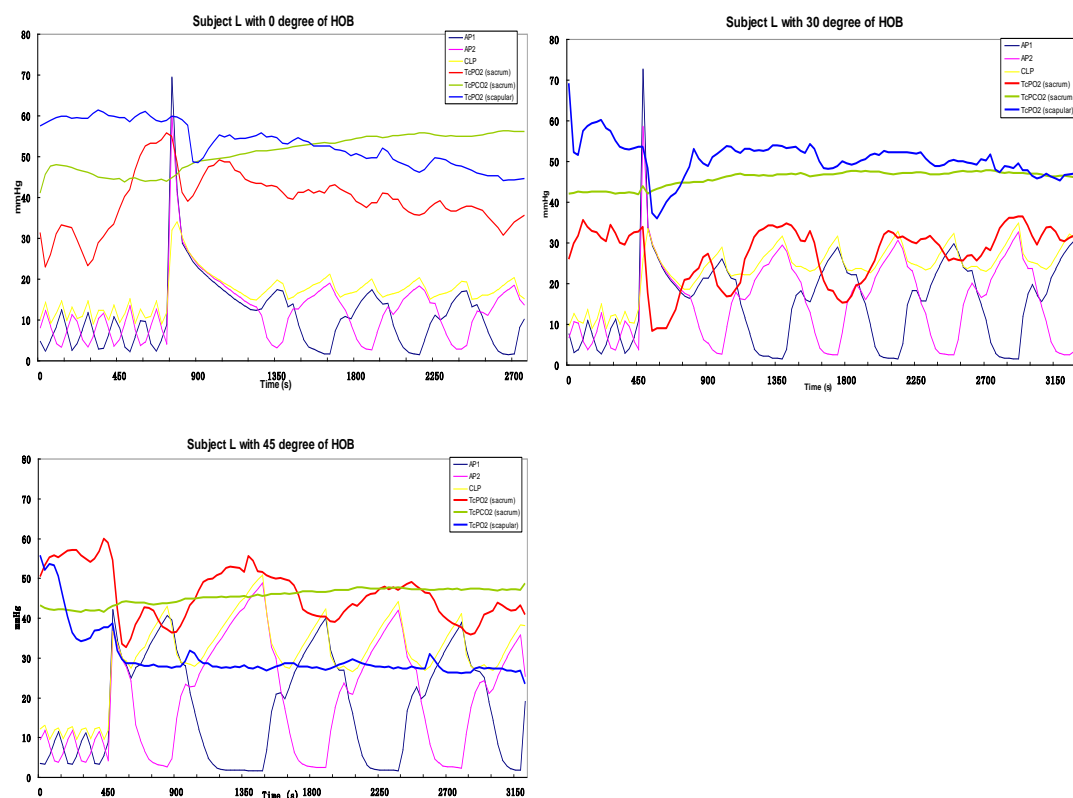
Figure C-2-2: The T_cPO_2 response at both the sacral and scapular locations of Subject L supported at various degrees of HOB when assessed in phase II tests. The test at a 60 degree HOB was not performed.

C – 3:

Information sheet

Research study [Establishing design features of pressure air mattress to minimize risk of pressure ulcer development]

We would like to invite you to be part of this research project, if you would like to. You should only agree to take part if you want to it is entirely up to you. If you choose not to take part there won't be any disadvantages for you and you will hear no more about it.

Please read the following information carefully before you decide to take part; this will tell you why the research is being done and what you will be asked to do if you take part. Please ask if there is anything that is not clear or if you would like more information.

If you decide to take part you will be asked to sign the attached form to say that you agree.

You are still free to withdraw at any time without giving a reason.

Details of study:
Pressure ulcers, also known as pressure sores or bed sores, occur in areas which are loaded for long periods of time. This may occur either when individuals lie down or sit in static positions. This condition can be prevented provided that pressure is relieved regularly by a special dynamic mattress or support surface.

Study volunteers:
Any subjects who have a history of chronic skin disease, such as psoriasis, will not be included in the study.

Aim and method of the study:
The study aims to optimise the performance of support surfaces to prevent the development of pressure ulcers. Therefore interface pressure will be measured at two locations when subjects lie in different support surfaces. In addition, local levels of oxygen and carbon dioxide measured by a device at the skin surface will be carried out which provides an indication of tissue viability.

Each subject will arrive in the test room wearing loose clothing. The experimenter will then carefully clean two test sites with sterile wipes. The two areas will be the sacral region, which is in the small of the back, and the scapular, which is under one of the shoulder blades. The experimenter will then attach sensors with double-sided tape to each test site. The complete procedure involves 4 experiments, each of which will take up to 90 minutes. Experiments will be performed on separate days, agreeable

to each participant. The procedure will not cause any pain and discomfort.

The study protocol will be performed on two types of support surface: a standard hospital mattress and an alternating pressure mattress on a stable bed frame, with head of bed angle at 0 °(horizontal position), 30 °, 45 °and 60 °.

Contact for further Information
It is up to you if you wish to take part or not. If you do decide to take part you will be given this information sheet to keep and then be asked to sign a consent form. If you do decide to take part you will still be free to withdraw at any time, without giving a reason.

Contact Details

-Prof. Dan Bader (Professor of Medical Engineering), School of Engineering and Material Science (D.L.Bader@qmul.ac.uk)

-Chanyuan Chai (PhD student), School of Engineering and Material Science (c.y.chai@qmul.ac.uk)

C– 4:

<u>Consent form</u>

Please complete this form after you have read the Information Sheet and listened to an explanation about the research and had the opportunity to ask any further questions.

Title of Study: _____

Queen Mary Research Ethics Committee Ref: _____

← •   Thank you for considering taking part in this research. The person organizing the research must explain the project to you before you agree to take part.

← •   If you have any questions arising from the Information Sheet or explanation already given to you, please ask the researcher before you decide whether to join in. You will be given a copy of this Consent Form to keep and refer to at any time.

← •   *I understand that if I decide at any other time during the research that I no longer wish to participate in this project, I can notify the researchers involved and be withdrawn from it immediately.*

← •   *I consent to the processing of my personal information for the purposes of this research study. I understand that such information will be treated as strictly confidential and handled in accordance with the provisions of the Data Protection Act 1998.*

Participant's Statement:

I _____ agree that the research project named above has been explained to me to my satisfaction and I agree to take part in the study. I have read both the notes written above and the Information Sheet about the project, and understand what the research study involves.

Signed: Date:

Investigator's Statement:

I _____ confirm that I have carefully explained the nature, demands and any foreseeable risks (where applicable) of the proposed research to the volunteer

Appendix D

The absolute humidity table

Relative humidity	10%	20%	30%	40%	50%	60%	70%	80%	90%	100%
50°C	8.3	16.6	24.9	33.2	41.5	49.8	58.1	66.4	74.7	83
45°C	6.5	13.1	19.6	26.2	32.7	39.3	45.8	52.4	58.9	65.4
40°C	5.1	10.2	15.3	20.5	25.6	30.7	35.8	40.9	46	51.1
35°C	4	7.9	11.9	15.8	19.8	23.8	27.7	31.7	35.6	39.6
30°C	3	6.1	9.1	12.1	15.2	18.2	21.3	24.3	27.3	30.4
25°C	2.3	4.6	6.9	9.2	11.5	13.8	16.1	18.4	20.7	23
20°C	1.7	3.5	5.2	6.9	8.7	10.4	12.1	13.8	15.6	17.3
15°C	1.3	2.6	3.9	5.1	6.4	7.7	9	10.3	11.5	12.8
10°C	0.9	1.9	2.8	3.8	4.7	5.6	6.6	7.5	8.5	9.4
5°C	0.7	1.4	2	2.7	3.4	4.1	4.8	5.4	6.1	6.8
0°C	0.5	1	1.5	1.9	2.4	2.9	3.4	3.9	4.4	4.8
(-)5°C	0.3	0.7	1	1.4	1.7	2.1	2.4	2.7	3.1	3.4
(-)10°C	0.2	0.5	0.7	0.9	1.2	1.4	1.6	1.9	2.1	2.3
(-)15°C	0.2	0.3	0.5	0.6	0.8	1	1.1	1.3	1.5	1.6
(-)20°C	0.1	0.2	0.3	0.4	0.4	0.5	0.6	0.7	0.8	0.9
(-)25°C	0.1	0.1	0.2	0.2	0.3	0.3	0.4	0.4	0.5	0.6

- The unit of absolute humidity is $g\ m^{-3}$

References

Allen V, Ryan DW, Lomax N, Murray A (1993a) Accuracy of interface pressure measurement systems. *J Biomed End* 15:344-48.

Allen V, Ryan DW, Murray A (1993b) Repeatability of subjest/bed interface pressure measurement. *J Biomed End* 15:329-32.

Allman RM, Laprade CA, Noel LB, Walker JM, Moorer CA, Dear MR, Craig RS (1986) Pressure sores among hospitalized patients. *Ann Internal Med* 105: 337-42.

Allman RM (1989) Pressure ulcers among the elderly. *N Engl J Med* 32: 850-53.

Ankrom MA, Bennett RG, Sprigle S (2005) Pressure-related deep tissue injury under intact skin and the current pressure ulcer staging systems. *Adv Skin Wound Care* 18(1): 35-42.

Apatsidis DP, Solomonidis SE, and Michael SM (2002) Pressure distribution at the seating interface of custom-molded wheelchair seats: Effect of various materials. *Arch Phys Rehabil* 83: 1151-6.

Arao H, Obata M, Shimada T, Hagisawa S. (1998) Morphological characteristics of the dermal papillae in the development of pressure sores. *J Tissue Viability* 8(3): 17-23.

ASHRAE Standard 55-1992: "Thermal environment conditions for human occupancy". *ASHRAE , Atlanta.*

Bader DL, Gwillim J, Newson TP Harris D (1982) Pressure measurement at the patient-support interface. In: Whittle MW, Harris JDEds. Biomechanical Measurement in Orthopaedic Practice, Oxford University Press 140-45.

Bader DL, Bowker P (1983) Mechanical characteristics of skin and underlying tissues in vivo. *Biomaterials* 4: 305-08.

Bader DL, Barnhill RL, Ryan TJ (1986) Effect of externally applied skin surface forces on tissue vasculature. *Arch Phys Med Rehabil,* 67(11): 807-11.

Bader DL (1990) The recovery characteristics of soft tissues following repeated loading. *J Rehabil Res Dev* 27(2): 141-50.

Bader DL, Wang YN, Knight SL, Polliack AA, James T, Taylor R (2005) Biochemical status of soft tissues subjected to sustained pressure. In: Bader DL, Bouten CVC, Oomens CWJ Eds. Pressure Ulcer Research: Current and Future Perspectives. 161-85.

Bain DS, Scales JT, Nicholson GP (1999) A new method of assessing the mechanical properties of patient support systems (PSS) using a phantom. A preliminary communication. *Med Eng Phys* 21: 293-301.

Barbanel J, Evans JH, Funlay JB (1972) Stress-strain-time relationships for soft connective tissues. In Kenedi RM Eds Perspectives in Biomedical Engineering, Macmillan, 165-72.

Bennett L, Kavner D, Lee BY, Trainor FS (1979) Shear vs pressure as causative factors in skin blood flow occlusion. *Arch Phys Med Rehabil* 60: 309-14.

Bennett L, Lee BY (1988) Vertical shear existence in animal pressure threshold experiments. *Decubitus*, 1: 18-24.

Berglund LG (1998) Comfort and Humidity. *ASHRAE* 40(8): 35-41.

Bogie KM, Nuseibeh I, Bader DL (1995) Early progressive changes in tissue viability in the seated spinal cord injured subject. *Paraplegia* 33: 1441-1447.

Bogie KM, Nuseibeh I, Bader DL (1992) New concepts in the prevention of pressure sores. In Frankel HL. ed. Handbook of Clinical Neurology: Spinal Cord Trauma. *Elsevier Science Publishers BV* 16(61): 347-66.

Boisvert P, Nakamura K, Shimai S, Brisson GB, Tanka M (1993) A modified local sweat collector for warm and humid conditions. *European Journal of Applied Physiology & Occupational Physiology* 66: 547-51.

Bours GJ, Halfens RJ, Abu-Saad HH, Grol RT (2002) Prevention, and treatment of pressure ulcer: descriptive study in 89 institution in the Netherlands. *Res Nurs Health* 25(2): 99-100.

Bouten CVC, Lee DA, Knight MM, Bader DL (2001) Compressive deformation and damage of muscle cell sub-population in a model system. *J Biomech Eng* 29: 153-63.

Bouten CVC, Oomens CWJ, Baaijens FPT, Bader DL (2003) The aetiology of pressure sores: skin deep or muscle bound? *Archives of PhysicalMedicine and Rehabilitation* 84(4): 616-19.

Bravemann IM (1983) The role of blood vessels and lymphatics in cutaneous inflammatory processes: an overview. *Brit J Dermatol* 109: Supp 25: 89-98.

Breuls RGM, Bouten CVC, Oomens CWJ, Bader DL, Baaijens FPT (2003) Compression induced cell damage in engineered muscle tissue: an in-vitro model to study pressure ulcer aetiology. *Ann Biomed Eng* 31:1357-65.

Bryant R (1992) Acute and Chronic Wounds: Nursing Management. New York, NY: Mosby-Year Book, Inc Attention: Order Services, 11830 Westline Industrial Drive, St. Louis, MO 63146.

1-800-426-4545

Campbell EJM, Dickenson CJ, Stress JDH (1974) Clinical physiology. *Blackwell Scientific,* Oxford. 111.

Cengel YA (2003) Heat transfer: a practical Approach. 3rd edition, McGraw- Hill Book Company, New. York.

Canning, DR, Mckeon RJ, Dewitt DA, Perry G, Wujek J, Silver J (1992) l-amyloid of Alzheimer's disease induces reactive gliosis that inhibits axonal outgrowth *Exp. Neurol* 124(2):289-298

Chaplin J (1999) Pressure sore risk assessment in palliative care. *Journal of Tissue Viability.* 10(1): 27

Chen Y, DeVivo MJ, Jackson AB (2005) Pressure ulcer prevalence in people with spinal cord injury: age-period-duration effects. *Arch Phys Med Rehabil* 86: 1208-13.

Cheng GC, Loree HM, Kamm RD, Fishbein MC, Lee RT (1993) Distribution of circumferential mechanical stress in ruptured and stable atherosclerotic lesions: a structural analysis with histopathological correlation. *Circulation* 87: 1179-87.

Chow WW, Odell EI (1978) Deformations and stresses in soft body tissues of a sitting person. *Journal of Biomechanical Engineering*, 100: 79-87.

Collines KJ, Sargent F, Weiner JS (1959) Excitation and depression of eccrine sweat glands by acetylcholine, acetyl-.f-methylcholine and adrenaline *J. Physiol* 148**:**592–614.

Costanzo LS (2002) Philadelphia: Saunders, an Imprint of Elsevier Science. *Physiology*

Crenshaw RP, Vistnes LM (1989) A decade pf pressure sore research: 1977-1978. *J Rehabil Res* 26(1): 63-74

Cullum N, Nelson EA, Flemming K, Sheldon T (2001). Systematic reviews of wound care management: (5) Beds; (6) Compression; (7) Laser therapy, therapeutic ultrasound, electrotherapy and electromagnetic therapy. *Health Technology Assessment* 5.9: 1-221.

Daniel R, Priest D, Wheatley D (1981) Etiologic factors in pressure sores: an experimental model. *Archives of Physical Medicine and Rehabilitation* 62:492-98.

Daly CH (1982) Biomechanical properties of dermis. *J. Invest. Derm* 79: 17-20.

Dealey C (1993) The size of the pressure sore problem in a teaching hospital. *Journal of Advanced Nursing* 16: 663-70.

Desmond JT (2006) Biochemistry of human skin our brain on the outside. *Chem. Soc. Rev* 35: 52-67.

Dinsdale S (1974) Decubitus ulcers: role of pressure and friction in pressure sores. *Arch Phys Med Rehabil* 55:147-52.

Elizondo RS, Banerjee M, Bullard (1972) Bullard Effect of local heating and arterial occlusion on sweat electrolyte content. *J Appl Physiol* 32: 1-6.

European Pressure Ulcer Advisor Panel (2001) The prevalence of pressure ulcers in European Hospitals.

Fardinia M, Palleshi G, Lubrano G, Guilbrault G (1993) Amperometric biosensor for determination of lactate in sweat. *Analytica Chimica Acta* 278: 35-40.

Ferguson-Pell M, Hagisawa S (1995) An empirical technique to compensate for melanin when monitoring skin microcirculation using reflectance spectrophotometry. *Med Eng Phy* 7: 104-110.

Ferguson-Pell M, Hagisawa S (1988) Biochemical changes in sweat. *Journal of Rehabilitation Research & Development* 25 (3): 57-62.

Ferguson-Pell M, Hagisawa S, Palmieri VR, Cochran GV (1988) Pressure sores: a biochemical test for early detection of tissue damage. *Arch Phys Med Rehabil* 69(9):668-71.

Ferguson-Pell M, Bell F, Evans JH (1976) Interface pressure sensors; existing devices, their suitability and limitations. In: Kenedi RM, Cowden JM, Scales JT Eds Bedsore biomechanics. Macmillan, London 189-97.

Ferguson-Pell M, Reddy NP, Stewart SFC, Palmieri V, Cochran GVB (1985) Measurement of physical parameters at the patient support interface. In: Whittle M, Harris D Eds. Biomechanical Measurement in Orthopaedic Practice. Oxford University Press 133-44.

Ferguson-Pell MW, Cardi MD (1993) Prototype development and comparative evaluation of wheelchair pressure mapping system. *Assist Technol.* 5(2): 78-91.

Ferguson-Pell M (2005) Imaging Tissues for pressure Ulcer Prevention. In Bader DL, Bouten CVC, Oomens CWJ Eds, In: Pressure Ulcer Research: Current and Future Perspectives 301-15.

Figloila RS (2003) A Proposed Method for Quantifying Low-air-Loss mattress performance by moisture transport. *Ostomy/Wound Management* 49 (1): 32-42.

Fisher SV, Kosiak M (1979) Pressure distribution and skin temperature effect of the ROHO wheelchair balloon cushion. *Arch. Phys. Med. Rehabil* 60, 70-1.

Fisher SV, Szymke TE, Apte SY, Kosiak M (1978) Wheelchair cushion effect on skin temperature. *Arch Phys Med Rehabil* 59(2): 68-72.

Flam E (1987) Optimum skin aeration in pressure sore management. *Proc Annu Conf Eng Med Biol* 29: 84.

Flam E, Isayeva E, Kipervas Y, Shklyarevsky V, Raab L (1995) Skin temperature and moisture management with a low-air-loss surface. *Ostomy/Wound Management* 41(9):50-56.

Fox IH, Palella TD, Kelly WN (1987) Hyperuricemia: Amarker for cell energy crisis. *N Eng J Med* 317(2):111-112.

Fukomoto T, Tanaka T, Fujioka H, Yoshihara S, Ochi T, Kuriowa A (1988) Differences in composition of sweat induced by thermal exposure and running exercise. *Clinical Cardiology* 11: 707-709.

Gawlitta D, Li W, Oomens CWJ, Baaijens FPT, Bader DL, Bouten CVC (2007) The relative contributions of compression and hypoxia to development of muscle tissue damage: an in vitro study. *Ann Biomed Eng* 35: 273–284.

Gefen A, Levine J (2007) The false premise in measuring body-support interface pressures for preventing serious pressure ulcers. *J Med Eng Technol* 31(5):375-80.

Goossens RH, Rithalia SV (2008). Physiological response of the heel tissue on pressure relief between three alternating pressure air mattresses. *J Tissue Viability* 17(1): 10-4.

Gibson LE, Cooke RE (1959) A test for concentration of electrolytes in sweat in cystic fibrosis of the pancreas utilizing pilocarpine by iontophoresis. *Pediatrics* 23: 545-49.

Gibson T, Kenedi RM, Craik JE (1965) The mobile microarchitecture of dermal collagen. *British Journal of Surgery* 52: 764-70.

Hagisawa S, Ferguson-Pell M, Cardi M, Miller D (1994) Assessment of skin blood content and oxygenation in spinal cord injured patients during reactive hyperaemia. *Journal of Rehabilitation Research & Development* 31(1): 1-14.

Hagisawa S, Shimada T, Arao H, Asada Y (2001) Morphological architecture and distribution of blood capillaries and elastic fibres in the human skin. *J Tissue Viability* 11(2):59-63.

Hagisawa S, Shimada T (2005) Skin morphology and its mechanical properties associated with loading. In: Bader D, Bouten C, Colin D, Oomens C, Eds. Pressure UlcerResearch: Current and Future Perspectives. Berlin, Germany: Springer-Verlag 161-85.

Hampton SC (2004) Tissue Viability: The Prevention. *Treatment and Management of Wounds.* Whurr, London.

Hampson N, Piantadosi C (1988) Near infrared monitoring of human skeletal muscle during oxygenation and during forearm ischaemia. *Journal of Applied Physiology* 64(6): 2449-57

Hannon D, Quinton P (1984) Ultramicro assay of lactate by fluorescence microscopy. *Analytical Chemistry* 56: 2350-51.

Hanson R (1997) Sore points sorted. *Nursing Times* 93(7):32-34.

Herrman EC, Knapp CF, Donofrio JC, Salcido R (1999) Skin perfusion responses to surface pressure-induced ischemia: implication for the developing pressure ulcer. *J Rehabil Res* 36(2): 109-20.

Heyningen VR, Weiner JS (1952) The effect of arterial occlusion on sweat composition. *J Physiol,* 116: 404-13.

Higo M, Kamata S (1994) Inelastic electron tunneling spectroscopic study of biological compounds in human sweat adsorbed on alumina. *Analytical Chemistry* 66: 818-23.

Hill-Rom, *Product Brochures*: The Alto™; The Duo 2™; The Primo™. Hill-Rom, Pluvigner, France. 2004.

Hobson DA (2001) Principles of pressure management. Department of Rehabilitation Science and Technology, University of Pittsburgh.

Houwing R, Overgoor M, Kon M, Jansen G, Asbeck BS, Haalboom JRE (2000) Pressure-induced skin lesions in pigs: reperfusion injury and the effects of vitamin E. *J Wound Care* 9(1): 36-40.

Hunter JA, Mcvittie E and Comaish JS (1974) Light and electron microscopic studies of physical injury to the skin Friction. *Br. J. Dermatol* 90, 491-9.

Husain T (1953) An experiment study of some pressure effects on tissues with reference to the bed sore problem. *Journal of Pathology and Bacteriology* LXVI: 347-58.

Jan YK, Brienza DM, Boninger ML and Brenes G (2011) Comparison of skin perfusion response with alternating and constant pressures in people with spinal cord injury. *Spinal Cord* 49, 136-141.

Johnson AT (1991) Thermal responses: Biomechanics and exercise physiology. New York: Whiley Interscience 405-6.

Johnson AT (1991)Biomechanics and Exercise Physiology. 1st Edn. Jhn Wiley & Sons.

Kirk E, Kvorning SA (1949) Quantitative measurements of the elastic properties of the skin and subcutaneous tissue in young and old individuals. *J Gerontol* 4: 273-84.

Knight SL (1997) Non-invasive techniques for predicting tissue status during pressure induced ischaemia. D. Phil Thesis, Queen Mary University of London.

Knight SL, Taylor RP, Polliack AA, Bader DL (2001) Establishing predictive indicators for the status of soft tissues. *J Appl Physiol* 90: 2231-37.

KoKate JY, Leland KJ, Held AM, Hansen GL, Kveen GL Johnson BA, Wilke MS, Sparrow EW, Iaizzo P (1995) Temperature-modulated pressure ulcers: a porcine model. *Arch Phys Med Rehabil* 76(7):666-73.

Komives GK, Robinson S, Roberts JT (1966) Urea transfer across sweat glands. *J Appl Physiol* 21:1681-84.

Kondoh Y, Kawase M, Ohmon S (1992) D-lactate concentrations in blood, urine and sweat before and After exercise. *European Journal of Applied Physiology and Occupational Physiology* 65: 88-93.

Kosiak M (1959) Etiology and pathology of ischaemic ulcers. *Arch Phys Med Rehab* 46: 62-9.

Kosiak M (1961) Etiology of decubitus ulcers. *Arch Phys Med Rehabil* 42: 19-24.

Krouskop TA, Reddy NP, Spencer W, Secor JM (1978) Echanisms of decubitus ulcer formation. Med Hypotheses 4:37-39.

Krouskop TA (1983) A synthesis of the factors that contribute to pressure sore formation Med. *Hypoth.* 11: 255-67.

Kumar P, Clark M, editors. Clinical Medicine. 5th ed. Edinburgh: Saunders; 2002.

Labbe R, Lindsay T, Walker PM (1987) The extent and distribution of skeletal muscle necrosis after graded periods of complete ischemia. *J Vasc Surg* 6(2): 152-57.

Laccoureye O, Bernard D, de Lacharriere O, Bazin R, Brasnu D (1993) Freys syndrome analysis with Biosensor. *Archives of Otolaryngology* 119(9); 940-44.

Landis EM (1930) Micro-injection studies of capillary blood pressure in human skin. *Heart.* 18:209-28.

Le KM, Madsen BL, Barth PW (1984) An in-depth look at pressure ulcers using monolithic

silicon pressure sensors. *Plastic and Reconstructive Surgery* 74: 745-54.

Lentner C (1981) Geigy Scientific Tables, Volume 1.8th Edition, Ciba-Geigy, Basle, Switzerland.

Liao F, Garrison DW, Jan YK. (2010) Relationship between nonlinear properties of sacral skin blood flow oscillations and vasodilatory function in people at risk for pressure ulcers. *Microvascular Research*; 80(1):44-53

Lowthian P (1997) Notes on the pathogenesis of serious pressure sores. *Br J Nurs* 6(16): 907-12.

Mahanty SD, Roemer RB, Meisel H (1981) Thermal response of paraplegic skin to the application of localized pressure. *Arch Phys Med Rehabil* 62: 608-11.

Mahanty SD, Roemer RB (1979) Thermal response of skin to skin to application of localized pressure. *Arch Phys Med Rehabil* 60(12): 584-90.

Manschot J, Brakkee A (1986) The measurement and modelling of the mechanical properties of human skin in vivo. *Journal of Biomechanics* 19: 511-21.

Mayrovitz HN, Sims N, Taylor MC (2002) Sacral skin blood perfusion: a factor in pressure ulcers? *Ostomy Wound Management* 48(6): 34-8, 40-2.

McCord J (1985) Oxygen-derived free radicals in post-ischaemic tissue injury. *The new England Journal of Medicine* 312(3):159-63.

Miller GE, Seale J (1981) Lymphatic clearance during compressive loading, *Lymphology* 14:161-66.

Mitsubayashi K, Suzuki M, Tamiya E, Karube I (1994) Analysis of metabolism sweat as a measure of physical condition. *Analytica Chimica Acta* 289(1); 27-34.

Newson T, Pearcy M, Rolfe P (1981) Skin surface PO_2 measurement and the effect of externally applied pressure. *Archives of Physical Medicine and Rehabilitation* 62(8): 390-92.

Nicholson G, Scales J, Clark R, De Calcina-Goff M (1991) A method for determining the heat transfer and water vapour permeability of patient support systems. *Med Eng Phys* 21(10):701-12.

Nola GT, Vistnes LM (1980) Differential response of skin and muscle in the experimental production of pressure sores. *Plast Reconstr Surg* 60: 728-33.

NPUAP (2009). NPUAP-EPUAP Pressure Ulcer Classification System.

Omokhodion F, Howard JM (1994) Trace element in the sweat of acclimatized persons. *Cliica Chimica Acta* 231:23-28.

Parks DA, Granger DN (1988) Ischemia-reperfusion injury: a radical view. *Hepatology* 8(3): 680-2.

Parry DAD, Barnes GRG, Craig AS (1978) A comparison of the size distribution of collagen fibrils in connective tissues as a function of age and a possible relation between fibril size distribution and mechanical properties. *Proc. R. Soc. London.* 203: 305-21.

Pasyk KA, Thomas SV, Hassett CA, Cherry GW, Faller R (1989) Regional differences in capillary density of the normal human dermis. *Plast Reconstr Surg* 83(6): 939-47.

Peeters EAG, Bouten CVC, Oomens CWJ, Baaijens FPT (2003) Monitoring the biomechanical response of individual cells under compression: a new compression device. *Medical and Biological Engineering and Computing* 41: 498-503.

Peirce SM, Skalak TC, Rodeheaver GT (2000) Ischemia-reperfusion injury in chronic pressure ulcer formation: a skin model in the rat. *Wound Repair Regen* 8(1):68-76.

Pereira J M, Mansour JM, Davis BR (1991) Dynamic measurement of the viscoelastic properties of skin. *J. Biomech* 24: 157-62.

Peter E, Swain ID (1997) Evaluation of wheelchair cushions, static and dynamic. PS4, Medical Devices Agency, Department of Health

Peter E, Swain ID (1998) Evaluation of pressure relieving ward chairs. PS5, Medical Devices Agency, Department of Health

Polliack AA, Bader DL, Taylor R P (1993) Analysis of sweat during soft tissue breakdown following pressure ischemia. *J Rehabil Res* 30(2): 250-9.

Polliack AA (1994) Sweat biochemistry as an indication of the status of soft tissues subjected to mechanical loading. D. Phil Thesis, University of Oxford.

Polliack AA, Taylor RP, Bader DL (1997) Sweat analysis following pressure ischaemia in a group of debilitated subjects. *J Rehabil Res Dev* 34(3): 303-08.

Potts RO Chrisman DA, Buras EM (1983) The dynamic mechanical properties of human skin in vivo. *J Biomech Eng* 16: 365.

Pretto EA (1991) Reperfusion injury of the liver. *Transplant Proc* 23(3): 1912-14.

Randall (1947) Local sweat gland activity due to direct effects of radiant heat. *Amer J Physiol.* 150: 365-71.

Reenalda J, Geffen PV, Nederhand M, Jannink M (2009) Analysis of healthy sitting behavior: Interface pressure distribution and subcutaneous tissue oxygenation. *J Rehabil Res* 46(5): 577-786.

Reenalda J, Nederhand M, Jannink M, IJzerman M (2009) The clinical use of interface pressure to predict pressure ulcer development: A systematic review. *Assist Technol. Forthcoming*.

Reger S, Adams T, Maklebust J, Sahgal V (2001) Validation test for climate control on air-loss supports. *Arch Phys Med Rehabil* 82:597-03.

Reichel SM (1958) Shearing force as a factor in decubitus ulcer formation. *Journal of the Amer Med Association* 166: 762-63.

Reswick JB, Rojers JE (1976) Experience at rancho los amigos hospital with devices and techniques to prevent pressure sores. In: Kenedi RM, Cowden JM, Scales JT, Eds. Bedsore Biomechanics. Baltimore, University Park Press 301-10.

Rithalia SVS, Gonsalkorale M (2000) Quantification of pressure relief using interface pressure and tissue perfusion in alternating pressure air mattress. *Arch Phys Med Rehabil* 81:1364-69

Rithalia SVS（2004）Evaluation of alternating pressure air mattresses: one laboratory-based strategy. *J Tissue Viability* 14(2): 51-8.

Rushmer RE, Buettner KJ, Short JM, Odland GF (1966) The skin. *Science* 157 (747): 343-48.

Russell RC, Roth AC, Kucan JO, Zook EG（1989）Reperfusion injury and oxygen free radicals: a review. *J Reconstr Mirrosurg* 5(1): 79-84.

Salcido R, Donofrio JC, Fisher SB, LeGrand EK, Dickey K, Carney JM, Schosser R, Liang R (1994) Histopathology of pressure ulcers as a result of sequential computer-controlled pressure sessions in a fuzzy rat model. *Adv Wound Care* 7(5): 23-24, 26, 28.

Sanders JE, Goldstein BS, Leotta DF (1995) Skin response to mechanical stress: adaptation rather than breakdown a review of the literature. *J Rehabil Res Dev* 32(3):214-26.

Sanders JE, G. J., Mitchell SB, Zachariah SG (1998) Material properties of commonly-used interface materials and their static coefficients of friction with skin and socks. *J Rehabil Res Dev,* 35(2): 161-76.

Sangeorzan B, Harrington R, Wyss C, Czerniecki J, Matsen F (1989) Circulatory and mechanical response of skin to loading. *Journal of Orthopaedic Research* 7; 425-31.

Sato K, Dobson RL (1973) Glucose metabolism of the isolated eccrine sweat gland. *J Clin*

Investig 5:2166-74.

Sato K (1977) The physiology, pharmacology and biochemistry of the eccrine sweat gland. *Reviews in Physiology* 79:52-124.

Scales J (1971) Patient-support system using low-pressure air. *Lancet 2*: 885-888.

Schroeder DV (2000) An introduction to thermal physics. New York: Addison-Wesley Longman. pp: 89.

Schubert V, Fagrell B (1991) Evaluation of the dynamic cutaneous post-ischaemic hyperaemia and thermal response in elyerly subjects in an area at risk for pressure sores. *Clinical Physiology* 11: 169-182.

Schubert V, Fagrell B (1991) Post-occlusive reactive hyperaemia and thermal response in the skin microcirculation of subjects with spinal cord injury. *Scand J Rehabil Med* 23:33-45.

Schwartz IL, Thaysen JH, Dole VP (1955) Urea secretion in human sweat as a tracer for movement of sweat withi the secreting gland. *J Exp Med* 97:429-37.

Seiler W, Stahelin H (1979) Skin oxygen tension as a function of imposed skin pressure: implication for decubitus ulcer formation. *Journal of the American Geriatrics Society* XXVII (7); 289-301.

Seiler WO, Stahelin HB (1986) Recent findings on decubitus ulcer pathology: implications for care. *Geriatrics*: 41-47.

Shakespeare PG, Swain ID (1985) Skin blood flow and TcPO$_2$, measurement.

Shimada T, Morita T, Oya M (1991) Structures and architectures of lymphatic capillaries: Morphological differences from blood capillaries. *Jpn Soc Electron Microsc* 26 (1):66-71.

Silver MB (2002) Investigation of lower-limb tissue perfusion during loading. *J. Rehab Res Dev* 39; 597-608.

Smith PW, Black JM, Black SB (1999) Infected pressure ulcers in the long-term care Facililty. *Infect Control Hosp Epidemiol* 20:358-61.

Spence V, McCollom P, Walker W (1985) Comparative studies of cuaneous haemodynamics in regions of normal and reduced perfusion.

Sprigle S, Linden M, Riordan B (2003) Analysis of localized erythema using clinical indicaors and spectroscopy. *Ostomy Wound Management* 49: 42-52.

Seiler WO, Stahelin HB (1986) Recent findings on decubitus ulcer pathology: implications for care. *Geriatrics* 41: 47-50, 53-7, 60.

Steinau HU (1988) Major Limb Replantation and Postischemia Syndrome: Investigation of Acute Ischemia-induced Myopathy and Reperfusion Injury. *Springer Verlag* 9-22. 23, 26, 33.

Stekelenburg A, Oomens C, Bader D (2005) Compression-Induced Tissue Damage: Animal Models, In: Bader DL, Bouten CVC, Colin D, Oomens CWJ, Eds. Pressure UlcerResearch: Current and Future Perspectives. Berlin, Germany: Springer-Verlag 187-203.

Sugarman J (1985) The effect of different drying techniques on the surface qualities of paper. *Journal of the American Institute for Conservation* 31(2): 175-97.

Swain ID, Stacey PO, Dunford CE, Nichols R (1993) Evaluation, PS1 Foam mattress. Medical Devices Directorate, Department of Health.

Swain ID, Stacey PO, Dunford CE, Nichols R (1994) Evaluation, PS2Static overlays. Medical Devices Directorate, Department of Health.

Swain ID, Stacey PO, Dunford CE, Nichols R (1995) Evaluation, PS3 Alternating Pressure Overlays. Medical Devices Directorate, Department of Health.

Swain ID, Bader DL (2002) The Measurement of interface pressure and its role in soft tissue breakdown, *Journal of Tissue Viability* 12(4): 132-146.

Swain ID (2005) The measurement of interface pressure. In: Bader DL, Bouten CVC, Colin D, Oomens CWJ, Eds. Pressure UlcerResearch: Current and Future Perspectives. Berlin, Germany: Springer-Verlag 51-71.

Tanaka E, Uchiyama S, Nakano S (1990) Effects of calcitonin gene-related peptide and vasoactive intestinal peptide on nicotine-induced sweating in man. *J Auton Nerv Syst* 30: 265-68.

Taylor ET, Rimmer S and Dias B (1974) Ascorbic acid supplementation in the treatment of pressure sores Lancet 2: 544-6.

Taylor R, Polliack A, Bader D (1994) The analysis of metabolites in human sweat: analytical methods and potential application to investigation of pressure ischaemia in soft tissues. *Annals of Clinical Biochemistry* 31(1):18-24.

Taylor R, James T (2005) The role of oxidative stress in the development and persistence of pressure ulcers. In Bader DL, Bouten CVC, Oomens CWJ Eds. In: Pressure Ulcer Research: Current and Future Perspectives 205-232.

The Australian Wound Management Association Prentice. 2003

Torrance C (1983) Pressure Sores, Aetiology, Treatment and Prevention (London: Croom Helm)

Tortora GJ, Grabowski SR (1996) Principles of Anatomy and Physiology - 8th Edition, Harper Collins, NY.

Touche R (1993) The cost of pressure sores. Reports to the Department of Health. Department of Health. London, UK.

Unal S, Ozmen S, DemIr Y, Yavuzer R, LatIfoglu O, Atabay K, Oguz M (2001) The effect of gradually increased blood flow on ischemia-reperfusion injury. *Ann Plast Surg* 7(4): 412-6.

Vandenburgh HH, Swasdison S, Karlisch P (1991) Computeraided mechanogenesis of skeletal muscle organs from single cells in vitro. *FASEB J* 5: 2860-67.

Vanderwee K, Grypdonck M, Defloor T (2005) Effectiveness of an alternating pressure air mattress for the prevention of pressure ulcers. *Age and Ageing* 34: 261-67.

Van heyningen R, Weliner JS (1952) The effect of arterial occlusion on sweat composition. *J Physiol* 116: 404-13.

Verde T, Shepard RJ, Carey P, Moore P (1982) Sweat composition in exercise and in heat. *Journal of Applied Ohysiology* 53(6): 1540-45.

Versluysen M (1986) How elderly with femoral fractures develop pressure sores in hospital. *Br Med J* 292: 1311-13.

Vollman K (2010) Introduction to Progressive Mobility, Progressive Mobility in the Critically Ill. *Critical Care Nurse.*

Wang W, Vadgama P (2005) Microelectrodes and biocompatible sensors for skin pO2 measurement. In Bader DL, Bouten CVC, Oomens CWJ In: Pressure Ulcer Research: Current and Future Perspectives 337-52.

Wang YN (2000) The response of soft tissues to mechanical loads at different structural levels and the implications their breakdown. PhD thesis, Queen Mary University of London.

Waterlow J (1988) Tissue viability. Prevention is cheaper than cure. Nurs Times 84(25): 69-70.

Webster JG (1991) Prevention of Pressure sores. *Engineering and Clinical Aspects* 14 (5): 209.

Wheater PR, Burkitt HG, Daniels VG (1979) Functional histology. Churchill Livingstone, New York, 116-127.

Whitehouse AGR (1935) Dissolved constituents of human sweat. *Proc R SocLond B* 117:139-54.

Williams L, Wilkins (2005) Instructor's Resource CD-ROM to Accompany *Fundamentals of Nursing: The Art and Science of Nursing Care,* Fifth Edition.

Wua KS, Van Osdolb WW, Dauskardtc RH (2006) Mechanical Properties of human stratum corneum: Effects of Temperature, hydration, and chemical treatment, Biomaterials 27(1): 785-95.

Zhang M, Roberts VC (1993) The effect of shear forces externally applied to skin surface on underlying tissues. *J Biomed Eng* 15: 451-456.

Submitted Paper

Can intelligent support surfaces adjust to the BMI of individual subjects and maintain tissue viability in alternating pressure air mattresses?
Chanyuan Chai and Bader DL
Archives of Physical Medicine and Rehabilitation

Presentations at International Meetings

"Can we develop intelligent support surfaces for the individual subjects"
Chanyuan Chai and Dan Bader
In: 12th EPUAP Annual Meeting, Amsterdam, The Netherlands, September 2009

"Do intelligent surfaces maintain viability for a range of individual subjects"
Chanyuan Chai and Dan Bader
In: Australian Wound Management Conference, Perth, Australia, March 2010

"Aetiology of Pressure Ulcers – Case Studies"
Chanyuan Chai and Dan Bader
In: Workshop on the Science of Pressure Ulcers, Perth, Australia, March 2010

"The influence of internal pressures in APAM systems in maintaining tissue viability in healthy volunteers"
Chanyuan Chai and Dan Bader
In: 3rd Dutch Pressure Ulcer Conference, Kerkrade, The Netherlands, November 2010